OPTIMIZATION OF DYE-SENSITIZED SOLAR CELLS WITH POLY(1-VINYLPYRROLIDONE-CO-VINYL ACETATE) GEL POLYMER ELECTROLYTES CONTAINING BINARY SALTS AND IONIC LIQUID

NG HON MING

FACULTY OF SCIENCE
UNIVERSITY OF MALAYA
KUALA LUMPUR

2016

OPTIMIZATION OF DYE-SENSITIZED SOLAR CELLS WITH POLY(1-VINYLPYRROLIDONE-CO-VINYL ACETATE) GEL POLYMER ELECTROLYTES CONTAINING BINARY SALTS AND IONIC LIQUID

NG HON MING

THESIS SUBMITTED IN FULFILMENT OF THE REQUIREMENTS FOR THE DEGREE OF DOCTOR OF PHILOSOPHY

DEPARTMENT OF PHYSICS
FACULTY OF SCIENCE
UNIVERSITY OF MALAYA
KUALA LUMPUR

2016

UNIVERSITY OF MALAYA
ORIGINAL LITERARY WORK DECLARATION

Name of Candidate: Ng Hon Ming

Registration/Matric No: SHC120027

Name of Degree: Doctor of Philosophy

Title of Thesis:

Optimization of dye sensitized solar cells with poly(1-vinylpyrrolidone-co-vinyl acetate) gel polymer electrolytes containing binary salts and ionic liquid.

Field of Study: Advance Materials

I do solemnly and sincerely declare that:

(1) I am the sole author/writer of this Work;
(2) This Work is original;
(3) Any use of any work in which copyright exists was done by way of fair dealing and for permitted purposes and any excerpt or extract from, or reference to or reproduction of any copyright work has been disclosed expressly and sufficiently and the title of the Work and its authorship have been acknowledged in this Work;
(4) I do not have any actual knowledge nor do I ought reasonably to know that the making of this work constitutes an infringement of any copyright work;
(5) I hereby assign all and every rights in the copyright to this Work to the University of Malaya ("UM"), who henceforth shall be owner of the copyright in this Work and that any reproduction or use in any form or by any means whatsoever is prohibited without the written consent of UM having been first had and obtained;
(6) I am fully aware that if in the course of making this Work I have infringed any copyright whether intentionally or otherwise, I may be subject to legal action or any other action as may be determined by UM.

Candidate's Signature   Date:

Subscribed and solemnly declared before,

Witness's Signature   Date:

Name:

Designation:

ABSTRACT

Energy requirement has become a popular topic in almost every nation around the world. Instead of burning the depleting conventional fossils fuels as the source of energy, researchers nowadays are focusing more on developing more reliable renewable energy resources. Solar energy is one of the interesting renewable energy technology which could easily be the best choice to deal with the growing energy demand. This is because the sun energy is so abundant that it could be literally obtained anywhere on our earth. One of the promising technologies invented for the solar harvesting applications is the dye sensitized solar cells (DSSCs). These cells have the ability to surpass the leading types of solar cells which are based on silicon with a number of unique advantages that the DSSCs have. However, most of the high performance DSSCs are fabricated with liquid electrolytes and these types of DSSCs face complications in long term practical use due to the potential possibility of evaporation, leakage, desorption, photodegradation of the dye, corrosion of the platinum secondary electrode and ineffective sealing of cells. Thus, in order to overcome these drawbacks, gel polymer electrolytes (GPE) have emerged as great alternatives to replace the liquid electrolytes. Unfortunately, even with some advantages over the liquid electrolytes, GPEs are still facing serious problems on low power conversion efficiencies and poor ionic conductivity. Thus, in order to overcome these problems, we have taken several strategies to improve the ionic conductivity as well as the photovoltaic performance of these GPE-based DSSCs. In this study, we assembled dye sensitized solar cells (DSSCs) with poly(1-vinylpyrrolidone-co-vinyl acetate) (P(VP-co-VAc)) co-polymer based gel polymer electrolytes as the usage of co-polymer could increase the stability window of the GPE due to the nature of co-polymer having both amorphous phase and the crystalline phase. We also incorporate these GPEs with two types of the different salts (potassium iodide [KI] and tetrapropylammonium iodide [TPAI]) with different size in different concentration to improve the GPE for the DSSCs.

Then, 1-methyl-3-propylimidazolium iodide (MPII) ionic liquid was added in into the best binary salt system sample. Fourier transform infrared (FTIR) studies confirmed the complexation of the P(VP-co-VAc)-based gel polymer electrolytes. The effects of the incorporation of the binary salt and ionic liquid were studied. The binary salt system samples were able to achieve highest ionic conductivity and power conversion efficiency of 1.90 $\times 10^{-3}$ S cm^{-1} and 5.53%, respectively. Interestingly, upon the addition of the ionic liquid, MPII into this sample the ionic conductivity and the power conversion efficiency had increased to 4.09 $\times 10^{-3}$ S cm^{-1} and 5.94%, respectively at its optimum concentration. In order to learn more about the GPEs and DSSCs, the dielectric and electric dispersion behaviors of the GPEs were studied by dielectric relaxation spectroscopy at ambient temperature and the electrochemical impedance studies of the DSSCs were conducted. The electrocatalytic activity of the DSSC has also been investigated using Tafel polarization studies.

ABSTRAK

Keperluan tenaga telah menjadi salah satu topik yang sangat hangat di setiap negara di seluruh dunia pada masa kini Selain daripada menggunakan bahan api fosil jenis konvensional yang semakin pupus sebagai sumber tenaga, penyelidik kini memberi lebih banyak tumpuan kepada sumber tenaga yang boleh diperbaharui. Tenaga solar adalah salah satu teknologi tenaga yang boleh diperbaharui yang sedang meningkat dari segi populariti dan bakal menjadi pilihan yang terbaik untuk menangani permintaan tenaga yang semakin meningkat pada masa akan datang. Ini kerana tenaga matahari begitu banyak sehingga ia boleh diperolehi di mana-mana sahaja di bumi kita. Salah satu teknologi yang menunjukkan tanda-tanda kejayaan adalah pewarna sensitif sel solar ataupun dikenali sebagai “dye sensitized solar cells (DSSCs)”. DSSC dijangka dapat menjangkaui keupayaan sel solar jenis utama yang berasaskan silikon dengan beberapa kelebihan yang unik.Walau bagaimanapun, kebanyakan DSSC yang berprestasi tinggi adalah direka dengan elektrolit jenis cecair. DSSC jenis electrolit cecair mempunyai banyak komplikasi dalam penggunaan praktikal jangka panjang disebabkan kemungkinan potensi sejatan, kebocoran, penyaherapan, pemfotorosotaan pewarna, kakisan elektrod platinum dan kesusahan untuk mengedap sel. Untuk mengatasi kelemahan ini, gel polimer elektrolit (GPE) telah muncul sebagai alternatif yang baik untuk menggantikan elektrolit cecair. Malangnya, walaupun dengan sifat-sifat yang baik berbanding dengan liquid elektrolit, GPEs masih menghadapi masalah yang serius pada kecekapan kekonduksian ionic yang rendah dan lemah. Oleh itu, untuk mengatasi masalah ini, kami telah mengambil beberapa strategi untuk meningkatkan kekonduksian ionik serta prestasi fotovolta DSSC berasaskan GPE. Dalam kajian ini, kami menghasillkan DSSC dengan mengunakan poly(1-vinylpyrrolidone-co-vinyl acetate) (P(VP-co-VAc)) co-polimer berasaskan gel polimer elektrolit untuk meningkatkan kestabilan GPE kerana sifat co-polimer mempunyai fasa amorfus dan fasa kristal. Kami juga menggabungkan GPE ini dengan dua jenis garam yang berbeza (kalium iodide [KI] dan tetrapropylammonium iodide [TPAI]) dan mempunyai saiz yang berbeza dengan konsentrasi yang berbeza untuk meningkatkan prestasi DSSC yang berasaskan GPE. Kemudian, 1-methyl-3-propylimidazolium iodide (MPII) cecair ionik akan ditambah ke dalam sistem sampel yang terbaik. Kajian fourier transform infrared (FTIR) telah pun dijalankan untuk mengenalpasti komplesasi gel polimer elektrolit berasaskan P(VP-co-VAc). Kesan daripada penggabungan dua jenis garam dan cecair ionik telah dikaji. Sampel sistem yang mempunyai dua garam mencapai kekonduksian ionik dan kuasa penukaran fotovolta tertinggi masing masing pada 1.90 × 10^{-3} S cm^{-1} dan 5.53%. Menariknya, selepas penambahan cecair ionik, MPII ke dalam sampel ini pada kepekatan yang optimum, kekonduksian ionik dan kecekapan penukaran fotovolta telah meningkat masing-masing kepada 4.09 × 10^{-3} S cm^{-1} dan 5.94%. Untuk mengetahui lebih lanjut mengenai GPE dan DSSC yang dihasilkan, cara penyebaran dielektrik dan elektrik daripada GPEs dikaji oleh dielektrik spektroskopi pada suhu ambien dan kajian impedans elektrokimia daripada DSSCs telah dijalankan. Aktiviti electrocatalytic daripada DSSC juga telah disiasat menggunakan kajian polarisasi Tafel.

ACKNOWLEDGEMENTS

First, I would like to take this opportunity to express my profound gratitude to Prof Dr Ramesh T. Subramaniam and Dr Ramesh Kasi, for giving me opportunity to join their research group, for their invaluable advice, and constant encouragement. Without their help, guidance and encouragement, I could not have completed my study and this thesis.

I extend my heartfelt appreciation to my course mates and group member who have helped me throughout the whole PhD program. I cherish the moments that we coped with the difficulties and challenges. Besides, I would like to thank all laboratory officers who have helped me to complete this dissertation. Their assistance and understanding make it easier for me to finish the research work in time.

Furthermore, my appreciation also goes to University of Malaya as it provides the instruments, equipment, facilities and apparatus for me to complete my research work. This work was supported by the High Impact Research Grant (H-21001-F000046) from Ministry of Education, Malaysia and High Impact Research Grant (J–21002–73851) from University of Malaya. I would also like to appreciate financial support by grant No. PG034-2013A from Institute of Research Management & Monitoring (IPPP) of University of Malaya as well as the scholarship supported by the University of Malaya Fellowship Scheme (SBUM).

I would also like to express my greatest appreciation to my family who have been supporting and encouraging me through the difficulty.

TABLE OF CONTENTS

LIST OF FIGURES

LIST OF TABLES

LIST OF SYMBOLS AND ABBREVIATIONS

DSSC : Dye sensitized solar cell

PCE : Photovoltaic conversion efficiency

P(VP-co-VAc) : Poly(1-vinylpyrrolidone-co-vinyl acetate)

KI : Potassium iodide

TPAI : Tetrapropylammonium iodide

MPII : 1-methyl-3-propylimidazolium iodide

GPE : Gel polymer electrolyte

SPE : Solid polymer electrolyte

PV : Photovoltaic

TiO_2 : Titania

Pt : Platinum

CE : Counter electrode

XRD : X-ray Diffraction

TGA : Thermalgravimetric analysis

FTIR : Fourier Transform Infrared

EIS : Electrochemical Impedance Studies

η : Photovoltaic conversion efficiency

J_{sc} : Short circuit current density

V_{oc} : Open circuit voltage

FF : Fill Factor

R_b : Bulk Resistance

E_a : Activation energy

MWS : Maxwell Wagner-Sillars effects

CPE : Constant phase element

LIST OF APPENDICES

LIST OF PUBLICATIONS AND PAPERS PRESENTED

List of Publications

Ng, H. M., Ramesh, S., & Ramesh, K. (2015). Efficiency improvement by incorporating 1-methyl-3-propylimidazolium iodide ionic liquid in gel polymer electrolytes for dye-sensitized solar cells. Electrochimica Acta. doi:10.1016/j.electacta.2015.01.076

Ng, H. M., Ramesh, S., & Ramesh, K. (2015). Exploration on the P(VP-co-VAc) copolymer based gel polymer electrolytes doped with quaternary ammonium iodide salt for DSSC applications : Electrochemical behaviors and photovoltaic performances. Organic Electronics, (March). doi:10.1016/j.orgel.2015.03.020

Ramesh, S., & ***Ng, H. M.*** (2011). An investigation on PAN–PVC–LiTFSI based polymer electrolytes system. Solid State Ionics, 192(1), 2–5. doi:10.1016/j.ssi.2010.05.045

Ramesh, S., ***Ng, H. M.***, Shanti, R., & Ramesh, K. (2013). Studies on the Influence of Titania Content on the Properties of Poly(vinyl chloride) - Poly (acrylonitrile)-Based Polymer Electrolytes. Polymer-Plastics Technology and Engineering, 52(14), 1474–1481. doi:10.1080/03602559.2013.820745

List of Conferences

Ng, H. M., Ramesh, S., & Ramesh, K. (2015). Power conversion efficiency improvement of P(VP-co-VAc) based quasi-solid polymer electrolytes. Poster presented at The Energy and Materials Research Conference (EMR2015), Madrid, Spain.

Ng, H. M., Ramesh, S., & Ramesh, K. (2014). Efficiency improvement by incorporating 1-methyl-3-propylimidazolium iodide ionic liquid in gel polymer electrolytes for dye-sensitized solar cells. Poster presented at 14th International Symposium on Polymer Electrolytes (ISPE 14), Geelong, Australia.

Ng, H. M., Ramesh, S., & Ramesh, K. (2014). Effects of Al2O3 nanofiller on the ionic conductivity enhancement of solid PVC-PAN lithium based polymer electrolyte. Poster presented at 4th International Conference of Functional Materials & Devices 2013 (ICFMD 13), Penang, Malaysia.

CHAPTER 1: INTRODUCTION

1.1 Introduction of Research

With the massive increase in the world population at the beginning of 20th century, the energy demand has grown substantially and has suddenly become a huge topic of discussion in almost every nation. Humans are starting to tap fossil fuels which is the non-renewable forms of the ancient biomass such as oil, gas and coal. These fuel fossils possess very high energy density and they could also be stored and transported easily. However, humanity finally found that the dependence on the burning of the fuel fossils actually brings more harm than benefit to them and to the earth. By extracting and burning these fuel fossils, it could actually cause geopolitical tensions, environmental damage, and puts the earth climates at huge risk. There is a need to look for alternative renewable energy resources and solar energy is one of the rising renewable energy technologies and it is a very reliable choice to face the growing energy demand. The global primary energy is consumed at a rate of about 15 TW and planet earth receives about 174×10^3 TW from the solar radiation alone which is why even if we could harvest only a tiny fraction of this energy, it would be really enormous for us (Wenger, 2010). With that reason alone, it has garnered a lot of researches on solar energy in the previous decades. We should also not forget that the solar energy are an environmental friendly application. Harnessing the solar energy would not polluting the environment even though there would be emissions associated with the manufacturing, transportation and the installation of the solar cells; these emissions were almost nothing compared to the conventional burning of the fuel fossils. Thus, the solar application could be considered as an important step in the fighting of the climate crisis.

Dye sensitized solar cell (DSSC) is one of the promising solar harvesting technologies which is improving its own popularity to the top. This application was invented by B. O'regan and M. Gratzel nearly two decades ago. DSSCs just merely consist of conductive glasses with different layer of materials for anode and cathode, an organic or inorganic molecular dye and electrolyte which consist of redox couple. However, DSSCs is a strong candidate to be able to top the leading types of silicon solar cells in the upcoming years with a number of its own unique of promising abilities. DSSCs could overcome one of the huge limiting factor of the silicon based solar cells, which was the capability of working only under perfect irradiation condition. These DSSCs are able to convert sunlight even under low sunlight condition. With that reason, this technology is really suitable for those countries which are having climates that are not suitable for the silicon based technology solar cells.

As stated previously, the DSSC composed of different types of components and materials has allowed groups of researchers to allocate themselves to study the DSSCs in different directions. Researchers who come from different background could engage and study on different ingredient in different components to investigate and improve the photovoltaic performances of the DSSCs. Studies such as, synthesizing and producing new types of inorganic dyes, incorporating new types of semiconductor layers, replacing materials of the counter electrodes and introduction of new type of redox couples has been done since the first report on DSSCs. Among all of these studies, the electrolytes is where the research community concentrated on. The highest performing electrolytes used with the DSSCs up to date are the liquid electrolyte. To date, an impressive light-to-electric photovoltaic conversion efficiency (PCE) of 12% has been achieved with liquid electrolytes but problems such as long term storage is hindering further development of liquid electrolyte type of DSSCs. Due to this problem, researchers have started to work on different type of electrolytes and found that gel type of electrolytes have the potential to replace the conventional liquid type of electrolytes. There are huge amount of advantages of using gel electrolytes over the liquid electrolytes. One of it would be the shelf time storage of the gel polymer electrolytes which is much longer compared to the liquid electrolytes. Unfortunately, the PCE rate of the gel electrolytes were not even comparable due to various reasons such as gel network that are formed by the gelators hindering the movement of the mobile ions in the system. With that, a huge list of additive and materials has been proposed over the years to produce the best performing gel electrolytes but to the fact that there are still no optimum solution has been identified yet.

In this respect, we herein propose the incorporation of the co-polymer into the gel types of polymer electrolytes to take advantage of their unique properties to boost the performance of the DSSCs. We also incorporated two type of different sizes of salts together with ionic liquid into the gel polymer electrolytes. Even though there is a lot of studies on the usage of co-polymer, binary salt system and incorporation of ionic liquid in the polymer electrolytes, the combination of these three strategies are yet to be studied. In this research, poly(1-vinylpyrrolidone-co-vinyl acetate) (P(VP-co-VAc)) based gel polymer electrolytes is introduced with the incorporation of potassium iodide (KI), tetrapropylammonium iodide (TPAI) and 1-methyl-3-propylimidazolium iodide (MPII) were prepared, studied and reported.

1.2 Objectives of the Research

The aims of the research are as follows:

1. To develop P(VP-co-VAc) based gel polymer electrolytes (GPEs) which are suitable for the use of DSSCs.
2. To characterize the prepared P(VP-co-VAc) based GPEs by using various techniques such as Fourier Transform Infrared spectroscopy (FTIR), X-ray Diffraction spectroscopy (XRD) and Thermogravimetric analysis (TGA).
3. To further improve the electrical and DSSC performances of the GPEs with the addition of the dual iodide salt (KI and TPAI) and 1-methyl-3-propylimidazolium iodide (MPII) ionic liquid.

4. To investigate the electrical and DSSC performances of P(VP-co-VAc) based GPEs with the addition of single salt (KI or TPAI).

1.3 Scope of Thesis

This thesis is aimed in developing novel materials with the motivation to further enhance the energy conversion efficiency and to get a better understanding of the DSSCs which are fabricated with these new materials. It started with the assignment on the development of the highly efficient gel polymer electrolytes which are suitable to be used in the fabrication of the DSSCs. In this aspect, we have chosen P(VP-co-VAc) as our polymer backbone as using co-polymer would give us a lot of advantage in the development of the high performance gel polymer electrolytes. The copolymer itself is an insulator. Thus, two types of salt (KI and TPAI) have been chosen to be incorporated into the P(VP-co-VAc) based gel polymer electrolytes to provide the ionic conduction ability to the gel polymer electrolytes. The electrical properties, dielectric properties and other characteristics such as thermal properties, structural properties of the P(VP-co-VAc) based gel polymer electrolytes have been studied to identify more about the properties of these gel polymer electrolytes. The P(VP-co-VAc) based gel polymer electrolytes with only the single salt were also fabricated into DSSC so that the photovoltaic performances could be studied. In order to know more about electrical properties of these DSSCs, the electrochemical impedance studies on the DSSCs have been also studied. Along the way, the suitability of the MPII ionic liquid was tested with the P(VP-co-VAc)-KI system. The changes of the addition of the MPII ionic liquid on the P(VP-co-VAc) based gel polymer electrolytes would also be observed through the electrical properties, dielectric properties, thermal properties, structural properties as well as the photovoltaic performances after it has been fabricated into DSSCs.

Once the suitability of the ionic liquid has been studied, the research would proceed with one of our strategies to improve the GPEs through the incorporation of the two different sizes of salts which is the smaller KI and bulkier TPAI in the P(VP-co-VAc) based gel polymer electrolytes. The effectiveness of incorporation of binary salt with different sizes would be observed. P(VP-co-VAc) based gel polymer electrolytes with various ratio of the KI and TPAI salt would be produced and the performance of these binary salt gel polymer electrolytes would be studied. As usual, the thermal properties and structural properties would be studied in order to know more about the characteristics of the gel polymer electrolytes. The electrical properties, dielectric properties, as well as the photovoltaic performances of the DSSCs fabricated with the binary salt gel polymer electrolytes was also studied and the best sample from the binary salt GPE systems would be picked for the addition of the ionic liquid, MPII. The aim of the addition of MPII into this best performance binary salt gel polymer electrolyte sample is to further improve the electrical performing as well as the photovoltaic performances of the P(VP-co-VAc) based gel polymer electrolytes hoping that it could be good enough to perform the DSSC applications for domestic use. Besides the electrical and photovoltaic performances, other characterization as mentioned previously were also done in order to learn more on the final product of this research in this thesis, the DSSCs based on the P(VP-co-VAc)-KI-TPAI-MPII based gel polymer electrolytes.

CHAPTER 2: LITERATURE REVIEWS

2.1 Introduction of the chapter

The introduction and literature reviews on for the solar cells, dye sensitized solar cells, types of polymer electrolytes are discussed in this chapter. This chapter also discussed on the factors that could influence the performances of the gel polymer electrolytes and strategies that could be used to improve the performance of these gel polymer electrolytes.

2.2 Solar cells

Human has been using up the conventional fossil fuels that basically took more than 400 million years to form under our earth for the last few hundred years. These fossil fuels are going to get depleted soon. This is why we, as human must put up huge effort, no matter in political or technological into renewable energy resources. It is evolving as one of the most inspiring challenges faced by today's engineers and scientists towards a solar future. Even the politicians of policymakers agree that a massive redirection of energy policy is needed for our earth to survive in the coming centuries. We all know that, even if we try to reserve these fuel fossils as hard as we could, these fuel fossils are not unlimited. Sooner or later, they will all be burnt up and finished (Bella, Sacco, Pugliese, Laurenti, & Bianco, 2014).

This is why renewable energy resources are so important nowadays and one of the promising renewable energy resources is the energy system that uses the Sun's energy directly. This technology is also known as the solar energy and the devices used to harvest these solar energy are known as the solar cells. In this perspective, more than a decade ago Michael Gratzel, in his publication on Nature has quantified the enormous supply of energy that the Sun could provide to our Earth. He mentioned that about 174×10^3 TW of energy could be produced in a year and this amount is actually ten thousand times more than the energy that are being consumed by the global population now. Just by using simple calculation, he also stated that by simply covering 0.1% of our earth surface with solar cells with the efficiency of 10% would be more than enough to satisfy the energy demand for the population on our earth (O’Regan & Grätzel, 1991).

These solar cells convert the harvested sun’s energy into electricity. The sunlight basically composed of miniscule particles called photons which is radiated from the sun. As these photons hit the solar panel, they would be absorbed by the semiconducting materials, such as silicon. After that, an electron from the atom in the cell would accept the energy release from the photons. This electron would get enough energy to move from its original position to the external electrical circuit and form a “hole” that needed to be filled by another electron (Li, Wang, Kang, Wang, & Qiu, 2006).

In order to produce voltage needed to light up an external load such as an LED, electric field was needed. To create the electric field from the solar cells, p-type (positive) and n-type (negative) of semiconductors needed to be sandwiched together. The n-type silicon normally has more electrons compared to p-type which has more holes. This is why when these two semiconductors comes together, it form p-n junction which can be used to induce the electric field. The extra electrons from the n-type flows to the p-type and vacating the holes. This phenomenon creates the electric field at the surface allowing the electrons to hop from the semiconductor to the surface. These electrons would flow into the external electrical circuit and lighting up external loads. The holes that are emptied by the electrons would then wait for another new electron to vacant. (Li et al., 2006).

As seen in *Figure 2.1*, a huge amount of different solar cells has been studied in the decades. A short summarize of the solar cell types are shown below:

- **Multijunction Cells (η = 31-44%)** – This cell has layers of different technologies built inside. It can be considered the most costly solar cells and it is mostly used for research.
- **Single-Junction GaAs (η = 29-34%)** – This cell is made with Gallium-Arsenide. Due to the raw materials used are very expensive. It is only used high end applications such as satellites.
- **Crystalline Si Cells (η = 20-27%)** – This cell is made with slices of Silicon. It is the most commonly used solar cells used by humans nowadays due to its better pricing and easy to install.
- **Thin-Film Technologies (η = 13-23%)** – This cell is made by depositing a layer of high electrical performance material such as Silicon. It is much thinner and cheaper compared to other types of cells. However, it still not popular due to its low performance.
- **Emerging PV (η = 9-14%)** – This category is normally consists of the cells that are still under research. They have considerably low performance. However, these cells are getting better and better throughout the decades.

Even though, the crystalline silicon solar cell is going to be the leading solar cell technology in the coming years, the emerging type of PV cells are rising as the challenger that will be able overtake these mainstream solar panels as the leading solar technology in the coming future. One of the promising devices of the emerging types of PV is the dye sensitized solar cell (DSSC) and it is the main focus of our research.

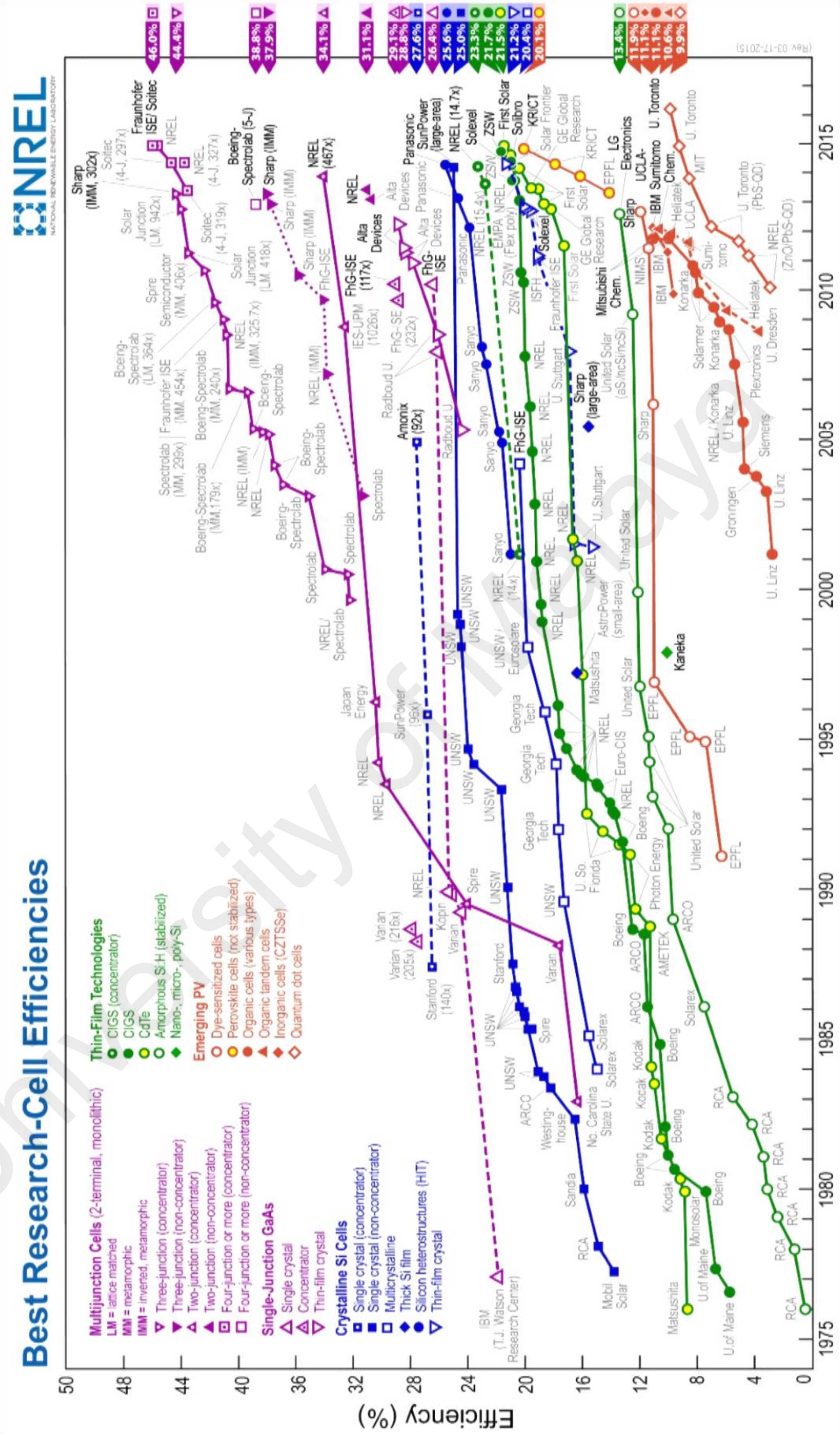

Figure 2.1: Record efficiencies for different types of solar cells in the laboratory (source: NREL)

2.3 Dye Sensitized Solar Cells

As mentioned before, to date, the photovoltaic market is still dominated by the conventional types of mainstream silicon crystalline solar panels. Even though, the prices of these silicon solar cells (cost per watt) has dropped a lot throughout the decade, they are still unable to compete to the traditional conventional grid electricity. Thus, it is important to develop photovoltaic devices which are much cheaper and with high efficiency in order to allow the global population to be able to enjoy this wonderful application with a much cheaper prices.

With this in mind, a new type of solar devices has been invented and this devices are called “dye sensitized solar cells” also known as DSSCs in short. It was first developed by O’regan and Gratzel in 1991 and their DSSC is based on nantocrystalline TiO_2 working electrodes. These DSSCs were found to have relatively high efficiency which is exceeding 11 % at full sunlight and really cost efficient. The price could be from 10 % to 20 % of the price of the mainstream silicon crystalline solar panels (O’Regan & Grätzel, 1991).

2.3.1 Benefits of using DSSCs

Being just composed of merely conductive glasses, a porous wide band gap semiconductor, a molecular dye and a redox couple, the DSSCs could make headlines as the best competitor in terms of pricing compared to the leading technology which based on silicon. This is because the materials are of low-cost materials and cheaper to manufacture. These DSSCs do not require any apparatus and can be even printed on any flexible surface. The overall peak power-production efficiency of dye-sensitized solar cells is about 11 percent, so they are the best suited to low-density applications. Though the efficiency of DSSCs is less than many of the best thin-film cells, the price-to-performance ratio obtained through these solar cells is superior to others (Rhee et al., 2014).

Unlike other thin-film cells, DSSCs were just only made of light weighted materials. However, they do not require any extra protection from the rain, trees or any other harsh objects. They were made mechanically robust and this made them easy to use and to be maintained. Besides, DSSCs also do not degrade in sunlight over a long time. This could drastically increase the lifetime of the cells and making it less frequent to be replaced (Rhee et al., 2014).

As mentioned previously, DSSCs could work under illumination below certain ranges while the other traditional cells would be failing to do so. This is because the dye used in the DSSCs can absorb diffused sunlight and fluorescent light. This characteristic helped the DSSC to be able to use in cloudy weather and low-light conditions without much impact on the power conversion efficiency. Meanwhile, DSSC can also be made in many different sizes and even bendable. This makes them to be suitable to run some small devices indoors. This could benefit a lot of countries with climates in which the silicon technology would have never been a success (Bella, Sacco, et al., 2014).

On the other hand, in the traditional cells, the electrons in the semiconductors might be pushed to conduction band mechanically as the temperature rises. This causes the silicon cells could need to have extra protection either by covering it in a glass box or other methods. This cells could get heated easily and the efficiency could be affected greatly due to the internal temperature. This situation would never occur in the DSSCs as this cells were only made with a thin layer of plastic whereas the heat could be able to radiate away easily to reduce the internal temperature. The decreasing of the temperature, in turn, increasing the power conversion efficiency of the solar cells.

2.3.2 Basic Principles of DSSCs

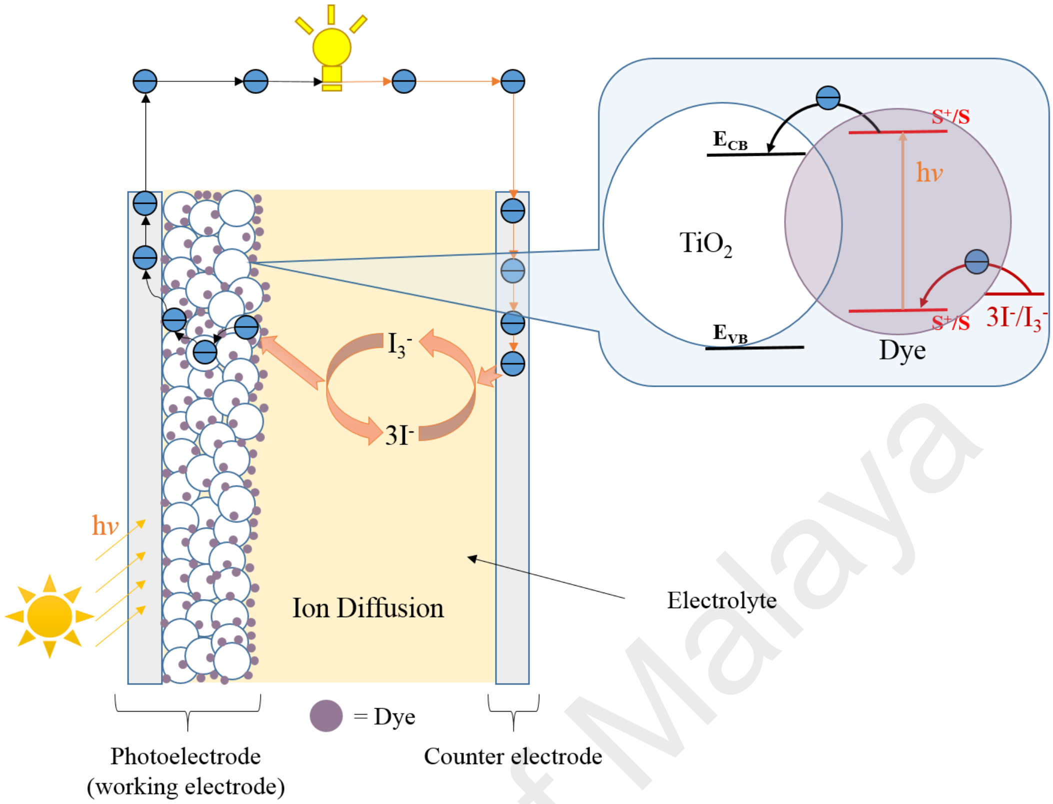

Figure 2.2: Typical structure and operation principle of a DSSC (Wei, 2011).

The typical structure and the operation principle of a DSSC is shown in *Figure 2.2*. Normally, a DSSC is made of four main elements (Wei, 2011):

- **Photoelectrode** - A thin layer of nanostructure wide band-gap semiconductor (usually TiO_2, ZnO, SnO_2, etc) coated on a conducting substrate (usually fluorine-doped tin dioxide, FTO or Indium-doped tin oxide, ITO).
- **Dye** – A monolayer of light sensitive substance which adsorbed on the surface of the semiconductor.
- **Electrolyte** – A medium which contains a redox couple (usually I^-/I_3^-).

- **Counter electrode** – A thin layer of high conductivity and catalytic activity material for the reduction of I_3^- (platinum, Pt is commonly used) coated on a conducting substrate.

Under sunlight illumination, the dyes will absorb photons or light from any light source and thus, becoming photoexcited. The adsorbed dye molecules will inject electrons into the TiO_2 working electrode and thus becoming oxidized. Then, charge separation is attained across the semiconductor interface where an electron is located in the TiO_2 and a “hole” is located in the oxidized dye molecule. The electrons will then percolate through the porous network of TiO_2 and eventually reach the back contact of the working electrode where charges are collected and charge extraction occurs. These extracted charge can then perform electrical work in the external circuit and eventually return to the counter electrode, where reduction of the redox mediator takes place. The redox couple electrolyte will complete the circuit by reducing the oxidized dye. This process occurs billions of times per second inside the cell to create an electrical current from the sunlight (Li et al., 2006).

2.3.3 The components of the DSSCs

2.3.3.1 Transparent conducting films (TCFs)

Transparent conducting films or also known as TCF is a very important component in a lot of high end technologies such as liquid crystal displays and touch screens. They are actually a very thin layer of conducting material coated on the surface of some substrates. Some examples of TCF are indium tin oxide (ITO), conducting polymer layers, carbon nanotubes, and graphene.

TCF is one of the most important components in the DSSCs. It can be made with organic and inorganic materials. However, the most popular TCF used in the DSSCs is the inorganic materials that consist of a very thin layer of transparent conducting oxide (TCO), in the form of indium tin oxide (ITO), fluorine doped tin oxide (FTO) or the doped zinc oxide (ZnO) (William, Cesar, & Johann, 1991).

2.3.3.2 The working electrodes

The working electrodes in a DSSC normally consist of a nanostructure wide band-gap semiconductor attached to a transparent conducting substrate. One of the most popular semiconductor material used is the TiO_2 which are having anatase band gap of 3.2eV. The other types of semiconductor material that can be used are ZnO, SnO_2 and NiO. The reason why TiO_2 is extensively used is that they are inexpensive, non-toxic, and it is an abundant material which can be easily obtainable. TiO_2 are also widely used in paints, sunscreens and food industries (T M W J Bandara, Svensson, Dissanayake, & Furlani, 2012).

The working electrode would have interconnected nanoparticles which is having sizes of 15-30 nm. The appearance would be in transparent or semi-opaque form with the porosity around 50%. The typical thickness for it would be around 1-15 μm. The popular deposition methods which are normally used for the thin layer preparation are screen printing and doctor blading. Both method involve the deposition of viscous colloidal TiO_2 paste onto the conducting substrate. Doctor blading is basically done with a smooth glass rod or a thin glass slides which is used to spread the viscous colloid on the conducting substrate surface to a specific thickness with the help of a tape frame and after the solvent has been evaporated, the tape would be removed. A figure of doctor blade methods is shown in Figure 2.3. Sintering would usually be performed at temperature of

450 - 500 °C after the deposition of the semiconductor materials. The high temperature would cause electrical interconnection between the nanoparticles and ultimately forms the nanostructured porous electrode. After the sintering process, the electrode would be sent for dye sensitization process where it would be performed by immersing the electrode into a dye solution for a given time (normally 24 hours) (Miao Wang, Xiao, Zhou, Li, & Lin, 2007). The reason for the working electrode to have the porous nature is that it could provide larger surface area and this would allow higher concentration of the dye to be absorbed, leading to more efficient light harvesting if you compare to those flat electrodes. A sample figure of the working electrode is shown in *Figure 2.4*.

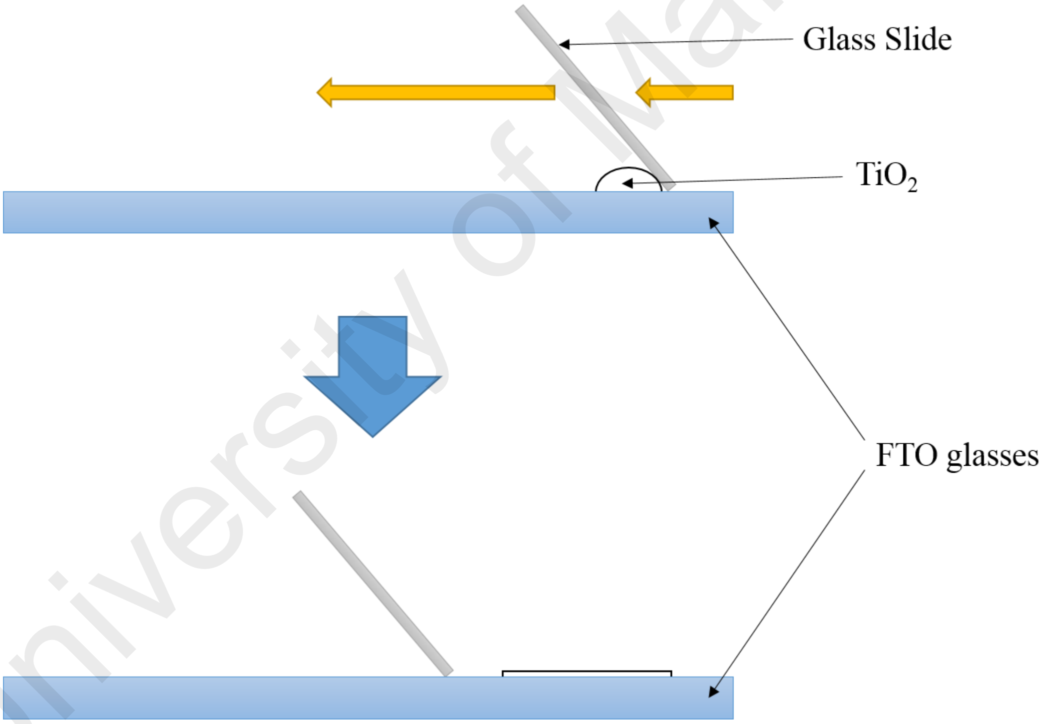

Figure 2.3: A schematic figure of the doctor blade method.

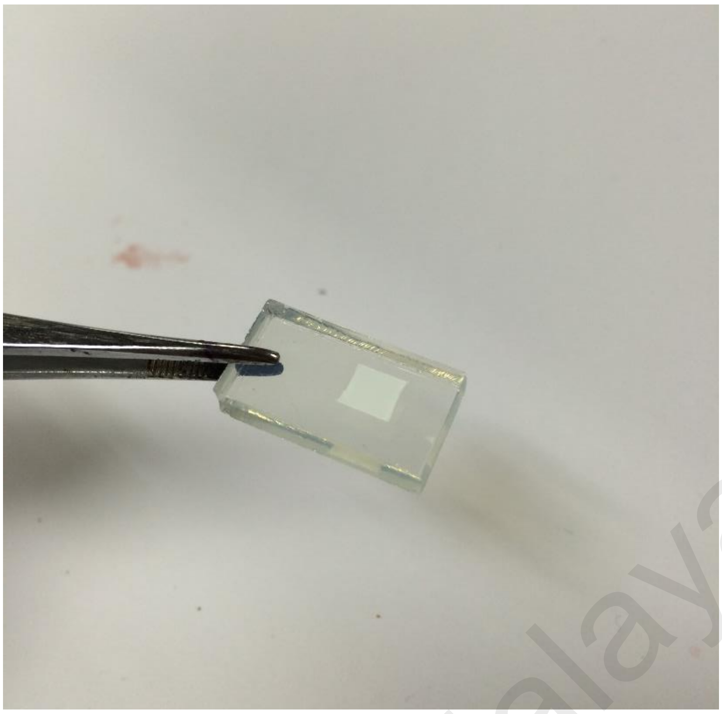

Figure 2.4: Image of a TiO_2 working photo-electrode produced in this research

2.3.3.3 The sensitizing dye

One of the most important materials in the DSSCs would be the sensitizing dye. The sensitizing dye is responsible for capturing the sunlight or proton into the DSSCs. Due to this important role, a lot of investigation has been done and a lot of effort also has been put in to create novel dyes which could lead to better efficiency of the DSSCs. Dyes used in DSSCs can be divided into two categories which is metal based complexes (inorganic) and metal-free organic dyes (Marinado, 2009).

However, the ruthenium based complexes are still preferred as they could reach around 11-12% efficiency. Some of the superior types of ruthenium dyes up to date are N3, N719 (K. Nazeeruddin et al., 1999), and Black dye (K. Nazeeruddin, Pechy, & Gratzel, 1997). N3 is the pioneering dye reported in 1993 by Nazeeruddin et al (Nazeeruddin et al., 1993). The structure of these dye are shown in *Table 2.1*.

Table 2.1: The structures of N3, N719, and Black dye.

Inorganic Dyes	Structures
N3	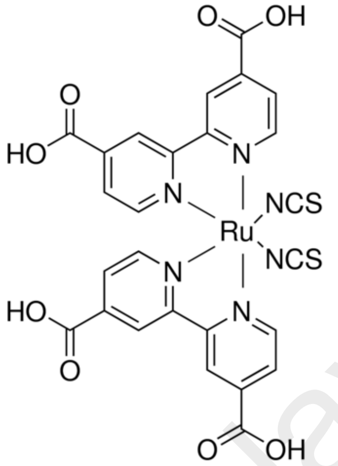
N719	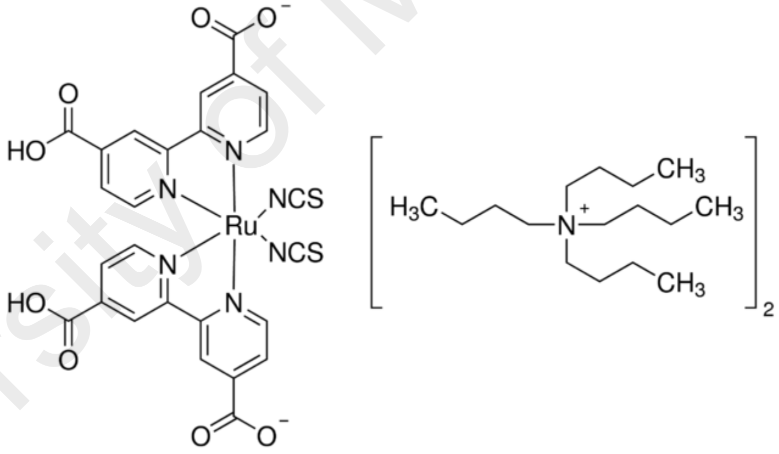
Black Dye	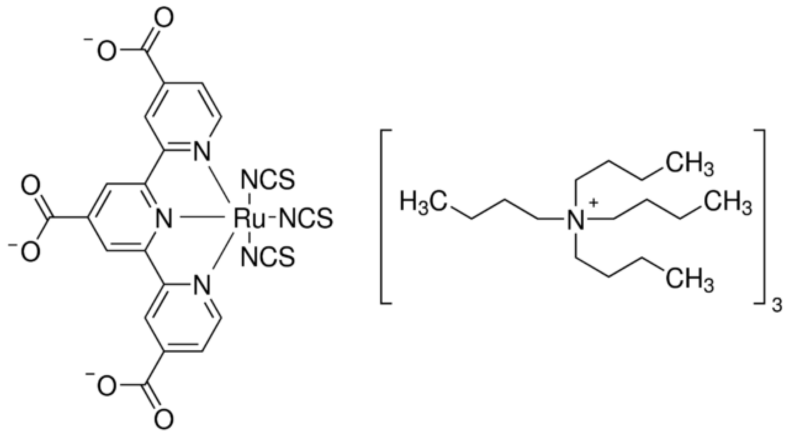

DSSCs based on organic dyes is increasing its efficiency throughout the years and getting more attention from the researchers. The main advantages of using organic dyes are that the dye structures of the organic dyes can be modified easily due to the short synthesizing routes. Moreover, they produce higher extinction coefficients compared to the inorganic dyes. This leads to the lesser amount of organic dyes needed to be used for the application of the DSSCs compared to the inorganic dyes. However, they have much narrower absorption bands compared to the inorganic dyes and this could lead to lower efficiency in the DSSCs based on organic dyes (Marinado, 2009). Some of the examples of well investigated organic dye families are triphenylamine (TPA), coumarin and indoline and the structure of these organic dye families are shown in *Table 2.2*.

Table 2.2: The structures of triphenylamine (TPA), coumarin and indoline.

Organic Dyes	Structures
Triphenylamine	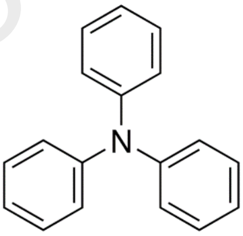
Coumarin	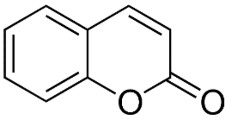
Indoline	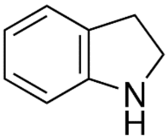

2.3.3.4 The counter electrodes

Counter electrode (CE) is another vital component in DSSCs as the counter electrode is the component that collects the electrons from the external circuit and assist in the reduction of the redox electrolyte. The main requirement for a good CE material is to have high electrocatalytic activities for a better reduction of the redox couple and having high stability. Some examples of the good CE materials are platinum (Pt), gold (Au) and silver (Ag). Pt is well known to be better in the reduction of the redox couples in liquid electrolytes while Au and Ag is better for solid state electrolytes due to the excellent ability in hole transfer. Unfortunately, these materials are really expensive due to their rare appearance. This is the reason that several materials have been studied to overcome this problem. The other materials are listed below (Ye et al., 2014):

- **Carbon materials** – These materials are cheap and giving good performances. They are also having high thermal stability and corrosion resistance.
- **Inorganic compounds** – These materials are cheap and easily obtainable. Thus, they could support very large production. However, the performance and stability of these materials are really low and need a lot of improvement. Some of the examples are CoS_2, TiC, TiN and metal oxides.
- **Conductive polymers** – These materials have high performances and very stable. Not to forget that they also have really good transparency. Some of the examples are polyaniline (PANI) and poly(3,4-ethylenedioxythiophene) (PEDOT). PEDOT is one of the most popular conductive polymers used in DSSC as the properties of PEDOT can be easily enhanced by the addition of additives. However, the price of these materials are really high and a lot of studies still need to be done to be applicable in DSSCs.

- **Composites** – These materials are composed of two or more components that could benefit each other. One of the examples is graphene-Pt/TaON/NiS2/NiO//TiN/PPy.

However, even with so many CE alternatives that can be used. In this present work, conventional type of Pt CE is used as our work is focusing more in the research of electrolytes. A figure of the platinum counter electrode used in this research is shown in *Figure 2.5.*

Figure 2.5: A figure of platinum counter electrode produced in this research.

2.3.3.5 The electrolytes

The electrolytes are also known as the redox mediator. The most successful redox mediator used up to date consists of liquid electrolytes containing redox couple such as iodide/triiodide. The diffusion of the iodide/triiodide is the process which contributes to the transportation of the charge carriers which leads to the completion of the circuit of the solar cell devices. Most of the time, the redox potential of the redox couple would dictate the electrochemical potential at the platinized counter electrode. These reactions consist of the reduction of the oxidized dye by iodide producing triiodide at the working electrode and the reduction of the triiodide producing iodide at the counter electrode.

Normally, these redox mediators are made of any kind of electrolytes which have been added with iodide salts, iodine and if necessary, some addition additives. Iodides comes in different sizes which it could provide different sizes of cations into the systems. Some examples of iodide salts are lithium iodide (LiI), sodium iodide (NaI), and tetrabutylammonium (TBAI), 4-tertbutylpyridine (4-TBP) and guanidiniumthiocyanate (GuSCN) are some of the examples of the extensively used additives in the electrolytes for the application of DSSCs (Bella, Sacco, et al., 2014). Room temperature ionic liquids (RTIL) such as 1-ethyl-3-ethylimidazolium iodide (EMII) are also added as additives in recent results as they provide good conductivity to the electrolytes. Different additives will affect the energetics of the semiconductor/dye/electrolyte interfaces. In order to have efficient dye regeneration process, a suitable redox potential in the context of DSSC is much needed and this is dictated by the success of the iodide/triiodide couple. Electrons in TiO_2 show modest electron recombination with the redox couple in comparison to many alternative charge mediators. The cause of slow electron recombination reaction are still being debated. The reasons for it might be the nature of the negative oxidized species (I_3^-) and the two electron transfer reaction of the redox reaction involving several intermediate steps.

At present, non-volatile type of redox mediator is produced and researched to avoid the leakage and the instability problems causes by liquid system. The RTILs, instead of being used as an additive are also a promising electrolyte alternatives which could provide advantages such as non-volatility, high thermal and chemical stability and excellent ionic conductivity. Unfortunately, DSSCs based on these highly viscous ionic liquids often results in mass transport limitations which could restrain the photovoltaic performance. On the other hand, solid state types of electrolyte are also getting huge amount of attention. These types of electrolyte having charge transport occurs via a hole-hopping mechanism. However, the problems of these solid state electrolytes at present are the increasing charge recombination, pore filling problems and limited charge mobility. To date, a superior or suitable type of redox mediator is yet to be found. A lot of research is still on going. The search for a superior type of redox mediator is going to be the main challenge for the future DSSC research. With that, polymer electrolytes are getting huge amount of attention nowadays because of their advantages of being flexible of going liquid, gel or even solid types of polymer electrolytes.

2.4 Polymer Electrolytes

Traditional electrolytes usually made of solvents with high dielectric constants such as ethylene carbonate, EC and ionizable species such as KOH. This mixture is usually called liquid electrolytes. Liquid electrolytes are higher in ionic conductivity but extremely inconvenient to be used due to its liquid nature. Due to this reason, Fenton et al. has produced a solid polymer electrolyte to overcome the problems of the liquid electrolytes. In 1973, they successfully dissolved alkali salts into the poly(ethylene oxide) (PEO) and the ionic conductivity of this mixture could reach 10^{-3} S cm^{-1} at the temperature above the crystalline melting temperature of PEO. A few years later, Armand and his co-workers found out the potential of this solid state electrolytes in electrochemical devices and has done a lot of studies on the solid state electrolytes. Their studies have motivated a lot of researchers to start their research on the polymer electrolytes (Fenton, Parker, & Wright, 1973). Meanwhile, DuPont has developed a perfluorosulfonated polymer in the 1960s and it was incorporated into NASA fuel cells. In the presence of water, this polymer has an ionic conductivity as high as 10^{-1} S cm^{-1}. Although, the reported conductivity values of the mentioned polymer electrolytes are significantly lower than the conductivity values of classical electrolytes, these materials could actually be used in the applications that require low currents (Hallinan & Balsara, 2013).

Polymer electrolytes are a popular class of electrolytes as they are basically safer than the classical types of electrolytes such as the $LiPF_6$/EC electrolyte. They are also compatible with applications such as fuel cell, lithium batteries, super capacitors and DSSCs. In current lithium ion battery applications, the electrolytes are basically just salts dissolved in flammable, organic solvents where simple failure of these lithium ion batteries could begin the ignition of the electrolytes. Meanwhile, higher molecular weight polymers are particularly nonvolatile and nonflammable. This could prevent lots of unnecessary accidents because of the failure of lithium battery. On the other hand, in fuel cells, reactants such as H_2 and O_2 and the products such as H_2O flow continuously past the electrodes. In this kind of systems, the use of salt free polymer electrolyte is essential.

Some of the examples of type of electrolytes with their transport coefficient are listed in *Table 2.3* (Hallinan & Balsara, 2013).

Table 2.3: Examples of selected electrolytes and polymer electrolytes with their transport coefficient (Source: Hallinan & Balsara, 2013).

Type	**Electrolytes**	***c*** **(mol liter^{-1})**	***T*** **(^{o}C)**	**σ_c (S cm^{-1})**	***D*** **(cm^2 s^{-1})**	**t^+**	**ε**
I	Aqueous liquid (H_2SO_4 in H_2O)	1.9 0.4	25	6×10^{-1} 2×10^{-1}	2×10^{-5} 2×10^{-5}	0.80 0.82	78.8
I	Organic liquid ($LiPF_6$ in EC/DMC)	1	25	1×10^{-2}	3×10^{-6}	0.38	41.8
I	Ionic liquid (ImTFSI)	4.0	80	1×10^{-2}	7×10^{-7}	0.46	-
II	Organic gel polymer ($LiClO_4$ in EC/PC + PAN)	1.5	25	2×10^{-3}	-	0.5	65.5
III	Polymer (LiTFSI in PEO)	1.5	85	1×10^{-3}	1×10^{-7}	0.41	7.5
IV	Poly(ionic liquid) (PVBnHexImTFSI)	2.0	90	4×10^{-5}	-	0	-
IV	Cross-linked polymer (PAE-XE)	0.9	85	5×10^{-6}	-	1	-
V	Aqueous polyelectrolytes (PSS + H_2O)	1.5	25	2×10^{-2}	-	1	27

These electrolytes can be defined in five types (Hallinan & Balsara, 2013):

- **Type I: classical electrolytes.** These are mixture of salts in low molecular weight solvents. Liquid electrolyte is fall in this category.
- **Type II: gel polymer electrolytes.** These electrolytes comprise a polymer network that is swollen with a classical electrolyte.
- **Type III: solid polymer electrolytes.** These are mixtures of salts in high molecular weight polymers.
- **Type IV: dry single-ion conductors.** In these electrolytes, one of the ions is covalently bound to the polymer backbone, and the polymer must participate in ion solvation.
- **Type V: solvated single-ion conductors.** These electrolytes are mixture of single ion conductors and low molecular weight solvents such as water.

Since our work is more on the polymer electrolytes studies, we will be focusing more on the gel polymer electrolytes (type II) and solid polymer electrolytes (type III).

2.4.1 Solid polymer electrolytes

Solid polymer electrolytes (SPE) has been extensively researched and applied in different types of electrochemical applications since the first discovery of the ability of the polymer polyethylene oxide to dissolve inorganic salts and they exhibit reasonable ionic conductivity. Solid polymer electrolytes are far from easy to produce compared to the traditional electrolyte. SPEs also having great flexibility that enables them to be produced in any shapes that could fit into any devices. The usage of the SPEs is also able to eliminate the usage of the separators in certain electrochemical devices which could increase their stability and safety concerns. Solid polymer electrolytes are totally free of organic solvents. Thus, it could prevent any growth of dendrites in the electrolytes which could hinder the ions mobility and decreases the performance (Fenton et al., 1973)..

The ionic conductivity of the electrolytes is very vital in many aspects when they are applied for the practical use. The total number of mobile charges and the movement of the mobile charges is determining the ionic conductivity of any SPEs. Therefore, in order to obtain a very high performance SPE, high degree of dissociations of salts and the high transference number is much needed in the SPE. The types of the transferring ions are mostly depending on the type of the electrochemical devices that it would apply on. For example, a PEO-LiI based SPE were applied into the lithium battery. The segmental motion of the polymer chains plays an important role in the mobility of the Li^+ of the system. The oxygen in the ethylene oxide of the PEO is assumed to be parts the mechanism that moves the Li^+. Thus, the Li^+ is believed to be hopping from a chain to another chain though complexations of the materials. The schematic mechanism of the common cations moving in PEO polymer matrix is shown in *Figure 2.6* (Meyer, 1998).

The glass transition temperature (T_g) of polymer matrix is often used to characterize the segmental motion of the polymer chain of the SPEs. They are also responsible for the mechanical properties. Some of the examples of polymer which has high amorphousness even at room temperature are PEO and polypropylene oxide (PPO). The low T_g they have allowed them to have comparable conductivity with some of the liquid solutions. However, these SPEs are still having problems such as complex chemistry and lack of mechanical stability and as a solution comb-type polyethers have been created. This design has made the polymer electrolytes to be able move more flexibly in the segmental motion (Lauter, Meyer, & Wegner, 1997).

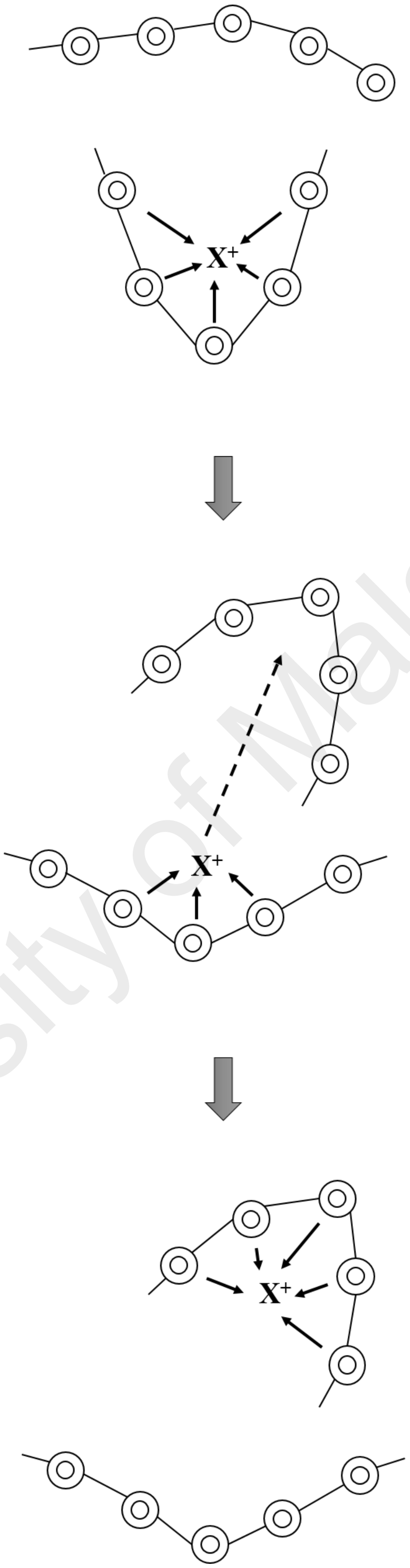

Figure 2.6: Schematic Mechanism of the cations (X^+) moving in PEO polymer matrix (Abraham, 1996)

Many types of polymers have been used to create solid polymer electrolytes. As mentioned before, PEO-based polymer electrolytes are the pioneering SPE first discovered in 1973. However, the ionic conductivity was far from satisfactory. Then, poly(acrylonitrile) (PAN) based electrolytes also emerged due to its ability to have reasonable ionic conductivity and wide electrochemical stability window. However, PAN was found to be not suitable for some electrochemical applications due to the severe passivation upon contacts with the electrodes. Other polymers that have also been extensively studied are the poly(methylmethacrylate) (PMMA) and the poly(vinylidene fluoride) (PVdF). These polymers are also demonstrated as potential host for the electrochemical applications.

Even with so many types of polymers being tested to improve the properties of the SPEs, the conductivity of these SPEs is still far from being to be able to use in practical. One of the solution is operating them at high temperature, but it is still not practical for most of the electrochemical applications especially the application of dye sensitized solar cells. Another efficient solution is the addition of ceramic fillers or ionic liquids. These additives were reported to be able to significantly improve the electrochemical properties especially the ionic conductivity. Some of the commonly used ceramic fillers are alumina (Al_2O_3), silica (SiO_2) and magnesia (MgO). Meanwhile, the examples of ionic liquids are 1-methyl-3-propylimidazolium iodide and 1-methyl-3-ethylimidazolium dicyanamide. The proposed mechanism on how the addition of the ceramic fillers can significantly reduce the possible side reactions between a conductor surface and polymer chains has been reported and shown in *Figure 2.7* (Manuel Stephan & Nahm, 2006).

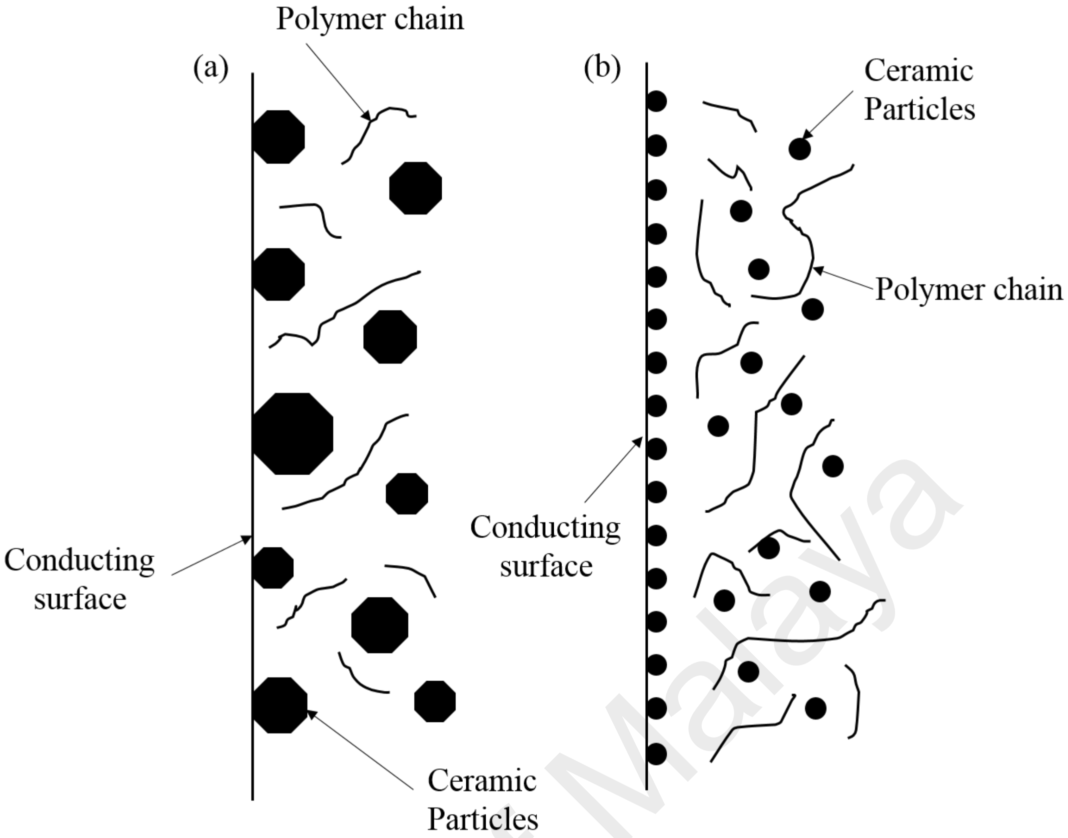

Figure 2.7: Schematic mechanism of the addition of ceramic fillers and the effect of different particles sizes, (a) macro-sized and (b) nano-sized (Abraham, 1996)

Although these SPEs are having so many superiorities, these SPEs would still be considered not having the practical advantages over the flexibility, thickness, manufacture and mechanical strength to date. Therefore, the usage of solid polymer electrolytes in the DSSCs is not so applicable yet at least up to this moment. This is the reason that, the gel polymer electrolyte are grinding their own popularity throughout the decades for the application of DSSCs.

2.4.2 Gel Polymer Electrolytes

As mentioned previously, solid polymer electrolytes (SPE) were having issue in compatibility with the electrochemical applications. Technically, liquid electrolytes are one of the best solution for this problem. However, researchers have come up with something between the liquid phase and solid phase types of electrolytes to have the benefits of both types of electrolytes. It was created by adding liquid solutions as plasticizer in the solid phase system to form gel-like structures. These gel-like structures are known as the gel polymer electrolytes (GPE). To date, the GPE has been extensively studied due to their superior properties including high ionic conductivity, electrochemical stability, safety and the tolerance against mechanical and electrical abuse. It is also reported that the use of these GPE could reduce the formation of the dendrite in electrochemical devices even though GPEs hold a huge amount of liquid solutions in their systems. Not to forget, the GPEs also have the ability to withstand the change in the volume of electrodes during any cycling. These could improve the flexibility of any cells created or designed. These GPEs also react much lesser to the electrodes of the electrochemical devices causing less corrosion and spoilage of the electrodes. These make the GPEs much more suitable type of electrolytes to be used than the liquid electrolytes due to the safety issues. Besides, the manufacturing integrity is also an advantage (Lan et al., 2008).

Similar to solid polymer electrolytes, PEO has been also extensively studied for the application of GPEs. The addition of the liquid plasticizers such as EC into the system could result in reducing the crystallinity of the PEO causing increase in polymer segmental mobility which could lead to increase in the ionic conductivity. Since the percentage of the polymer is low in the GPE system, the function of the polymer is slightly different with the SPE system. They are no longer a solvent for the salts. This polymers mostly serves to provide dimensional stability to the GPE systems. This means the interaction between the mobile charges and the oxygen or fluorine atoms are no longer necessity to form electrolytes and the pool of the choices for the polymer to be used much larger. Due to these reasons, PAN based electrolytes have been tested and studied for the application of GPE and good results have been reported for the high ionic conductivity probably due to their low crystallinity properties (Abraham, 1996b). Jayathilaka et. al. have successfully formed PAN-LiTFSI-EC-PC based GPE which has 2.50 mS cm^{-1} ionic conductivity that could be used in the electrochemical applications (Jayathilaka, Dissanayake, Albinsson, & Mellander, 2003). PMMA is also another popular polymer electrolyte which is having high ionic conductivity (Stephan & Thirunakaran, 1999). However, due to its poor mechanical strength nature, it has limited its application in GPEs. Additives such as poly(vinyl chloride) (PVC), have been used to improve the mechanical properties of PMMA based GPEs. Besides being used as additives, PVC and PVDF are also potential types of polymer which could be used for the application of GPEs. Co-polymers have started to become popular for the application of GPEs nowadays. One example of popular co-polymer is the poly(vinylfluorine-co-fluoropropylene) (PVDF-co-HFP). It is due to the reasons that the amorphous phase HFP can help to encage large amount of liquid electrolytes and the crystalline phase of PVDF can provide mechanical support as polymer matrix. Normally, those properties would not come together in normal conventional polymer such as PEO, PAN, etc (Miao et al., 2008). This is the reason that the co-polymer has been chosen as the host polymer for this research. More details on co-polymer will be discussed in *section 2.4.4.3*.

Gel polymer electrolytes were actually found to be compatible with the applications of dye sensitized solar cells. Created by trapping of liquid electrolytes in the polymer matrix, GPEs have some unique properties which fit right for the application of DSSCs. This properties includes very low evaporation rate and outstanding resistance to high temperature. Some GPEs also have sticky properties which could improve the contacts between the GPEs with the electrodes. With these features, a DSSC based on GPE would have no problems with long term stability and this literally solved a lot of problems of the liquid electrolyte based DSSCs. In order to achieve high power conversion efficiency, a high ionic conductivity electrolyte is mandatory since low ionic conductivity of an electrolyte could lower the short circuit current density (J_{sc}) of the DSSCs. Unfortunately, in this case, the ionic conductivity of the GPEs were slightly lower compared to the liquid if we compare the corresponding parameters of the GPE based DSSCs with the liquid based DSSCs. It is true that after the gelatin occurred, there would be a decrease of gas due to the comparatively lower conductivity but the open circuit voltage (V_{oc}) in this case increased because of the suppression of dark current by the polymer chains covering the surface of the TiO_2 electrode. This could result in high power conversion efficiency that were comparable or could be better than the liquid electrolytes based DSSCs (Y. Wang, 2009).

Even though GPEs are having so many advantages and even much better ionic conductivity compared to the SPEs, they are still not so applicable into the electrochemical applications yet especially in the DSSCs. The performance is still lower than those of the corresponding liquid electrolytes based DSSCs. Even though some of the polymer can gelate the liquid electrolytes properly, they still cause a lot of problems in the photovoltaic performance and stability of the DSSCs. For instance, the polymer network that form gel could have obstruct the movement of the mobile ions in the GPEs and also the gelators, in this case the polymer could have reacted with other materials like salts and additives of the GPEs. Due to these reasons, several effective strategies have been taken to improve the performances of the GPE and also the GPE based DSSCs. However, it is wiser to understand more about the factors that influence the ionic conductivity of GPE and the photovoltaic performance of their DSSCs before applying those strategies.

2.4.3 Factors influencing ionic conductivity of GPE and the photovoltaic performance of their DSSCs

2.4.3.1 Polymer concentration

The decrease in the polymer concentration is actually able to increase the ionic conductivity of the GPEs because the polymer cages trapping liquid electrolyte become larger and with more liquid electrolytes inside the GPEs, the ion can move much more faster. For the polyblend gel electrolytes based on polymers with different conductivities and viscosities, the ionic conductivity increases with the decreasing amount of the components with lower conductivity and higher viscocity under the same salt concentration. For example, the conductivity of P(MMA-co-MAA)/PEG polyblend decreased with the decreasing amount of PEG (P. J. Li et al., 2007). The reasons could be:

i. A PEG-salt complex had higher conductivity than those of P(MMA-MAA)-salt complexes under same salt concentration
ii. The decrease in viscocity with increasing amount of PEG in the system freed the segmental mobility and subsequently increased the conductivity of the system.

2.4.3.2 Different types of polymer

As discussed before, there are several types of polymers that have been used to produce many novel GPEs and already being used in DSSCs. Examples of such conventional polymers are PAN, PEO, PMMA, PVC, PVDF, etc. Because of the limitation of these conventional types of polymer in the application of GPEs, co-polymer such as P(VDF-co-HFP) and P(AN-VA) have also been used in this application as they are found to have better performances for the application of GPE based DSSCs. Other than these synthetic polymers, researchers have to use different kind of degradable polymers to form the GPEs for various types of electrochemical applications. There are also reports on natural polymers used for DSSCs has been reported. GPEs with their respective DSSCs with different materials compositions that have different electrical and photovoltaic performances is shown in *Table 2.4*.

Table 2.4: Example of photovoltaic performances of the selected DSSCs at room temperature.

GPEs	**σ (mS cm^{-1})**	**V_{oc} (V)**	**J_{sc} (mA cm^{-2})**	**FF (%)**	**η (%)**	**References**
PAN-TPAI-EC-PC	4.4	0.679	13.79	57.2	5.36	(Dissanayake et al., 2012)
(PAN-VA)-LiI-DMPII-TBP	2.7	0.802	9.77	68.0	5.27	(Xu, Tang, He, Li, & Chen, 2014)(Chen, Chang, Su, Teng, & Lee, 2014)
PEO/P(VDF-HFP)-APTS-ethanol	1.78	0.590	7.2	62.7	5.08	(Zhang et al., 2008)

2.4.3.3 The iodide salts

Without a doubt, the incorporation of salts were widely known to have played an important role in the ionic conductivity of the GPEs. Some of the examples of the salts are LiTF, LiTFSI, and LiBOB. As for the application of DSSCs, the basis for the energy conversion is the injection of the electrons from the photoexcited dye into the conduction band of the semiconductor TiO_2 on the absorption of light. The redox couple, I^-/I_3^- reduces oxidized dye and works as the charge carrier mediator to regenerate the photo-electrochemical cells. Therefore, the iodide salts such as (KI, NaI, TPAI, etc.) were proven to be giving better results in the power conversion efficiency studies. On the other hand, the addition of the iodide salts could influence the iodide ion conductivity in the gel polymer electrolyte and lead to the changes in the short circuit current density of the DSSCs. Thus, it could also influences the power conversion efficiency of the DSSCs as well (Y. Wang, 2009).

2.4.3.4 The concentration of the iodide salts.

Choosing the correct iodide salts are very important in the application of the DSSCs, suitable concentrations of the iodide salts are also equally or even more important in order to have good performance DSSCs. The number of the charge carriers increases linearly with an increase in the amount of iodide salts and then decreases after reaching optimum point of the amount of the salts that can be added. Increasing amount of salts could also lead to an increase in viscosity resulting from the bind between the metal ion and the atoms of the polymers that could leads to reduce segmental motion of the polymer chains and decreases the ionic conductivity. Moreover, the solubility of these inorganic salts is restricted by the solvents. If salt added exceed the solubility, it would separate out instead of dissolving in the system. This could result in the appearance of the crystalline phase in the GPE. With higher resistance, it could decreases the ionic conductivity of the GPEs (P. J. Li et al., 2007).

This can be explained by the pair-ions model and the phase disengagement between polymer matrix and liquid electrolyte that caused by the effect of the ions as shown in *Figure 2.8*. When a small amount of salt is added into the GPE, a homogeneous system can be formed under vigorous stirring as the state of the GPE has already been solvated. Normally in this case, the *reaction (i)* is dominant and when the amount of the salts added, it increases the charge carriers and increases the ionic conductivity value (Franck, 1960). Sodium iodide (NaI) is used as an example in this reaction as shown below:

$$(Na^+)S_n + I^- \rightarrow (Na^+)S_nI^- \qquad \text{(i)}$$

$$(Na^+)S_n + I^- \rightarrow (Na^+\,I^-)S_{n-m} + mS \qquad \text{(ii)}$$

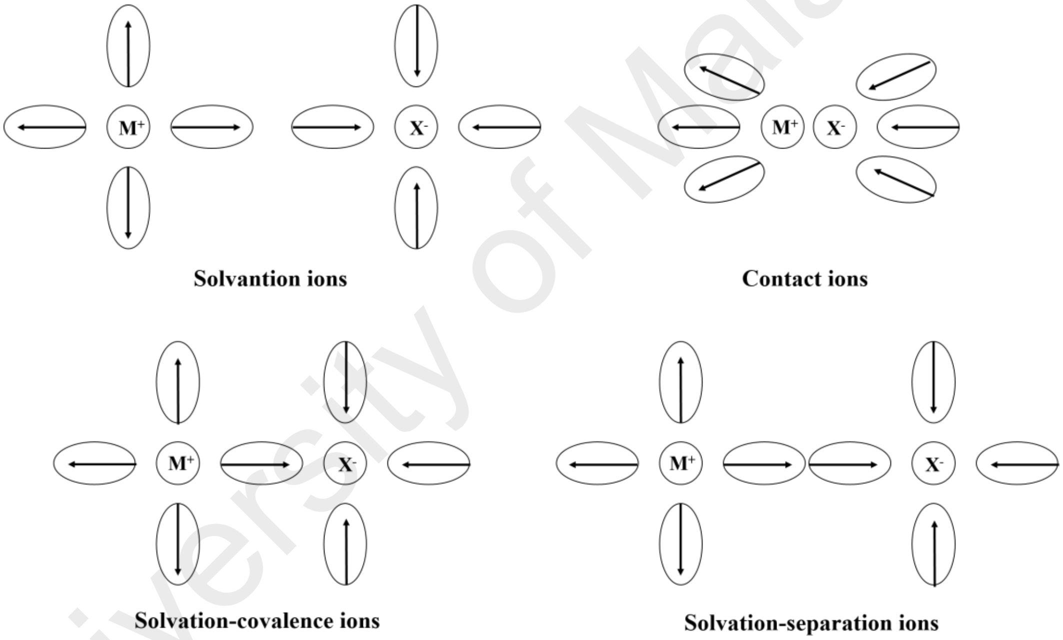

Figure 2.8: State of ions in solvent according to pair-ions model (Y. Wang, 2009).

However, when the concentration of the iodide salts is high, the state of most ions in the GPE could change from solvated ions to contact ions. In this case the dominant reactions could change from reaction (i) to reaction (ii). Contact ions are not beneficial to the GPEs as they are basically hard to move and contribute lesser to the ionic conductivity. Thus, it reduces the performances of the GPE and lead to reduced efficiency in DSSC based of that GPE (Franck, 1960). Besides, the high salts concentration in the GPE also causes shrinkage of the polymer chains and phase disengagement between the polymer and liquid electrolytes which causes many ions to remain in the liquid electrolyte rather than moving. An example of this phenomenon can be seen in poly(acrylonitrile-co-styrene)-N-methyl pyridine iodide based GPE reported by Wu et. al (J. Wu et al., 2006).

2.4.3.5 Side chains length of the organic iodide salts

The side chains length of the salts are basically very important in ionic conductivity wise. The ionic conductivity could decrease if the chain length is getting longer. This is due to the reason that longer chain length increases the viscosities, increases the van der Waals forces of attraction functioning the molecules and lowering the diffusion of the ions. As expected, the efficiency of the DSSCs based on GPEs decreases as well with the increase of the chain length of the salts added. With increasing chain length of the salts added, the electron lifetime and diffusion coefficient of the electron were reported to be increased as well. An example for the phenomenon can be seen in the PVFD-HFP based GPE which has been reported by Suryanarayanan et. al. containing different carbon chain length types of imidazolinium ionic liquid (IILs) in MPN (Suryanarayanan, Lee, Ho, Chen, & Ho, 2007). The photovoltaic performances of the DSSC based on the PVFD-HFP decreased with the increase carbon chain lengths (C3 to C7). The chemical structure of the imidazolinium ionic liquids (IILs) is show in *Figure 2.9* and *R* represents C3 to C7.

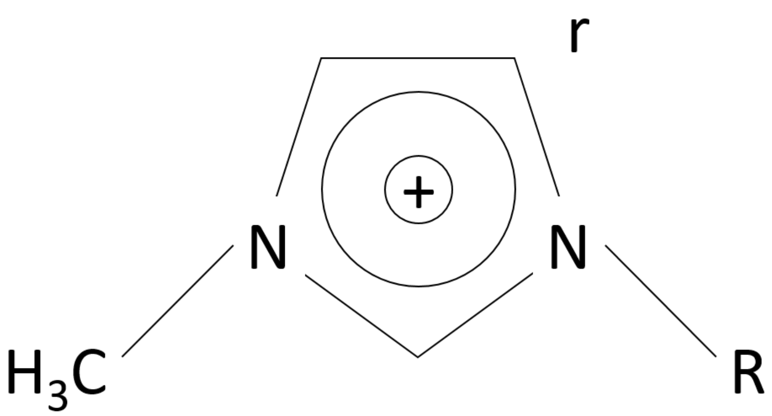

Figure 2.9: Chemical structure of imidazolinium ionic liquids (IILs).

Even though the longer side chain length of the salt could reduce the performances of the GPE and its DSSC, however, when these salt were together with each other in a binary system, especially with one shorter and another one longer chain lengths together. It could increases the ionic conductivity as well as the photovoltaic performances. It would be discussed more detail in section 2.4.4.1.

2.4.3.6 Organic solvent

Lewis acidic-basic interaction between the polymer matrix and organic solvents is what the swelling of the polymer is mainly based on. This is the reason why the solvents or even mixed solvents with different donor members could affect the liquid electrolyte absorbency. It could also determine the ionic conductivity of the GPE which causes further influences on the photovoltaic performance of the gel state DSSCs in terms of V_{oc}, J_{sc} and FF as well. Due to the more complicated factors in the GPEs, the efficiency changes with the change of the donor number of the mixed solvents would not be as regular as that the liquid based DSSCs and it is hard to be determined.

A gel polymer electrolyte with the ionic conductivity of 4.45 mS cm^{-1} have been reported by Wu et. al. by using poly(acrylic acid)-oligo-(ethylene glycol) as polymer matrix, and absorbing 30:70 of N-methyl pyrrolidone- g-butyrolactone together with 0.5 M NaI and 0.05 M $I_{2.}$ Just by incorporating another 0.4 M of the pyridine additive, gel state DSSC with power conversion efficiency of 4.74% could be obtained under normal irradiation of 100 mW cm^{-2} (AM 1.5) (J. Wu et al., 2007).

2.4.3.7 Temperature

The ionic conductivity normally increases with the increase of temperature. This has been proven many times by using the Arrhenius conductivity as shown in *Equation 2.1*.

$$\sigma = \sigma_0 \exp(-E_a/RT) \tag{2.1}$$

where E_a is the activation energy. R is the molar gas constant, A is the constant and T is the absolute temperature. This is due to the changes of conductivity depends on the thermal hopping frequency of ions when an ionic mobility process involves intermolecular ions hopping (Baskaran, Selvasekarapandian, Kuwata, Kawamura, & Hattori, 2006).

Another reason that can be used in the conductivity-temperature dependence of the GPEs is the free-volume model where it is said that the polymer matrix is amorphous and has large amounts of free-volume cages. When heat is applied, it causes more spaces and thus leads to more movable ions and a higher ionic conductivity for the GPEs. The conductivity-temperature dependence model is what that the GPE system need to be tested in order to confirm which behavior that it is following.

2.4.4 Strategies to improve the properties of the GPE and their DSSCs

As mentioned previously, although there is a huge improvement in GPEs over the SPEs in terms of performances and stability, it is found that the photovoltaic performance of the GPE based DSSCs is still lower compared to those liquid based DSSCs. Thus, several strategies need to be done in order to improve the ionic conductivity of the GPEs and thus the performances of the GPE based DSSCs.

2.4.4.1 Multiple salts system

As mentioned previously, the selection of proper metal salts for the polymer electrolytes is very important. It could be the factor of the ionic conductivity performances of a polymer electrolyte system which could directly affect the power conversion efficiency if the DSSCs as well. The different sizes of salts have their own advantages and roles to play inside the polymer electrolytes. A smaller types of metal cations could easily steer through the dye and able to intercalate in the pores of the working electrodes. Reports also show that smaller type of cations such as Li^+ or Na^+ could minimize the size of the solvated ion cloud, increasing the diffusion rate and thus, leads to higher efficiency. Meanwhile, the larger types of cations such as TBA^+ or THA^+ could help to separate the polymer chains so the mobile charges would be able to move much more freely inside the polymer matrix which could also leads to increase in ionic conductivity and power conversion efficiency(Agarwala et al., 2011).

Most of the reported DSSCs use only single ionic salt system in their polymer electrolytes with either small cations or large cations and very few have reported cases of DSSC electrolytes containing two or more different sizes of metal cations. In some of the recent studies, there are works reporting that the combination of the two different sizes of metal cations were able to enhance the power conversion efficiency compared to the single metal cation electrolytes. The aim in this strategy is to find the balance of the concentration of the different types of cations added into the system. An electrolyte with too high amount of smaller cations could have very high short circuit current density but lower open circuit voltage in their DSSC and vise versa for the electrolytes with a high concentration of large cations. Thus, having the optimum concentration of these salts could balance out each other advantages and disadvantages which could leads to an increase in the power conversion efficiency of the DSSCs(Dissanayake et al., 2012).

2.4.4.2 Addition of room temperature ionic liquid (RTIL)

Ionic liquids which is also known as the molten types of salts with temperature lower than 100^{o}C were first synthesized by Paul Walden in 1914, by neutralization of ethylamine with concentrated nitric acid to yield ethylammonium nitrate ([$EtNH_3$][NO_3]. One of the most used cations in the recent works in these few decades were first synthesized by Hussey and coworkers in 1980’s. However, these newly emerging imidazolium ionic liquids were very sensitive to water content as the moisture would reacts with it main component the chloroaluminate ($AlCl_3$). Then, in 1992, the imidazolium ILs which are stable to air and moisture were first synthesized using nitrate (NO_3), tetrafluoroborate (BF_4), and acetate (CH_3COO) anions. With the effort from these researchers, now more stable ionic liquid are becoming common in its respective field. Most of the ionic liquids nowadays were synthesized with fluorinated anions such as hexafluorophosphate (PF_6) and bis(trifluoromethylsulfonyl)imide ($N[CF_3SO_2]_2^-$ or TFSI) and these anions could hugely reduce the water solubility. However, it still needs to be noted that some of these ionic liquids still absorb moisture.

Table 2.5: Commonly used cations that comprise ionic liquids

Common cations	Structures
1-alkyl-3-methylimidazolium	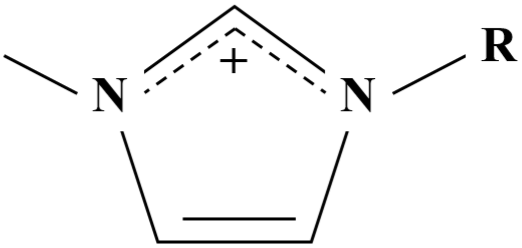
N-alkyl-N-methylpyrrolidinium	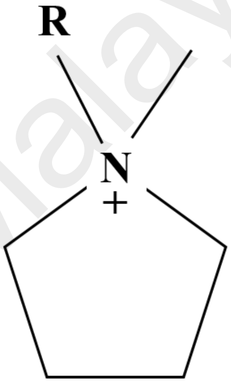
N-alkyl-pyridinium	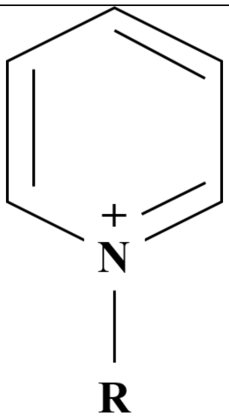
Tetraalkyl-ammonium	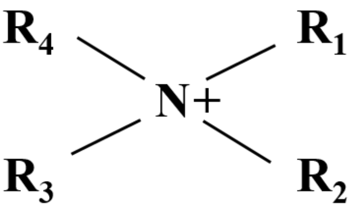

Table 2.6: Commonly used anions that comprise ionic liquids

Common anions	Structures
Hexafluorophosphate	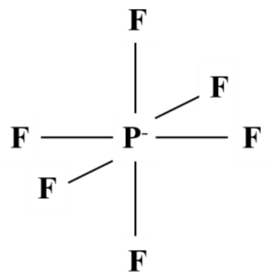
tetrafluoroborate	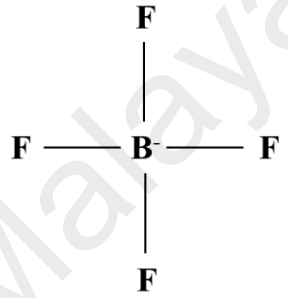 BF_4^-
Bis(trifluoromethylsulfonyl)immide	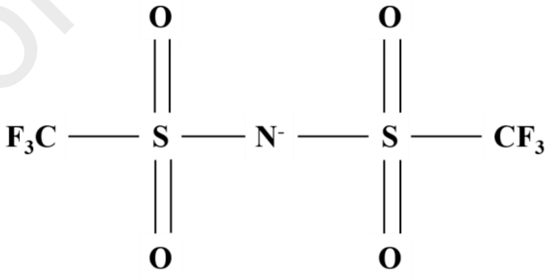 $F_3C-SO_2-N^--SO_2-CF_3$
Ethyl sulfate	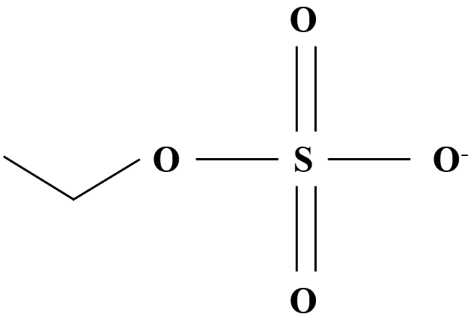
Other halogens	**Cl^-** **Br^-** **I^-**

Ionic liquids commonly have low melting points. This is mostly due to the huge size of anions that they have. These ions are huge, having highly flexible organic groups and highly delocalized charges. These attributes results in small lattice enthalpy changes for crystallization and much larger in the entropy changes for it to melt. Due to these reasons, the liquid state is preferred. Meanwhile, in the metal salts (KI or LiI), the small size of anions allows the ions to be easily packed into a crystal lattice resulting a dense charge and very strong electrostatic interactions. Thus, in this case, solid form is preferred.

A lot of work has reported that the addition of these ionic liquids into the polymer electrolytes could improve the performance of these polymer electrolytes especially in ionic conductivity. Costa et al reported that the usage of $BmImPF_6$ in PEGdME has improved their ionic conductivity from 8×10^{-6} S cm^{-1} to 3×10^{-4} S cm^{-1} (Costa et al., 2007). Improving the polymer electrolytes could lead to the enhancement of the performances of the electrochemical applications. For instance, Liew et al has reported that by using BmImBr in PVA used in the super capacitor, it has improved the voltage and the life cycle of the supercapacitor (Liew, Ramesh, & Arof, 2014). Meanwhile, incorporation of ionic liquids also found to be able to stabilize the reduction of the lithium metal in the lithium battery improving shelf lifetime and ionic conductivity. With these improvement observed in various types of electrochemical applications, we would expect that the addition of ionic liquids into our gel polymer electrolytes could help us to improve the performances of the DSSCs.

Besides having high ionic conductivity windows, ionic liquids also have much larger electrochemical window and higher thermal stability. These good attributes could be used by the researchers that would need to have their polymer electrolytes to be used at those high end situations. For instance, Nath et. al., has added ionic liquid into their polymer electrolytes to improve the thermal stability their polymer electrolytes (Nath & Kumar, 2014). Besides, there are also studies showing that by adding ionic liquids into the electrolytes, it could stabilize the reaction that happened between the electrolytes and the surface of the electrodes.

2.4.4.3 Usage of co-polymer

Homopolymer is a polymer produced by the linkage of a single monomer or a small molecule in a single polymer chain. However, when two different types of monomers comes together and join together in a single polymer chain, this polymers are usually called co-polymer. The arrangements of the monomer in the co-polymer can be made in different ways. For an example, two monomers which are named as A and B can be arranged in different ways as in the *Table 2.7*.

In alternating copolymers, it can be seen that there are two different monomers arranged themselves in an alternating manner as shown in *Table 2.7*. Meanwhile, in random copolymer, in can be observed that the monomers can be in any random positions. As in block copolymers, all of the same types of monomer would be grouped together at one side and the other monomer would be grouped at another side. As for block copolymers, it would be something like two different homopolymers connected with each others at the end of the polymer chain. An example of a very well-known block copolymer is the SBS rubber where it is used as the soles of the shoes. Graft copolymers can be produced by having chains of homopolymer grafted to the polymer chain of the other monomer. An example of the well-known graft copolymer is the high impact polystyrene (HIPS). It is a copolymer made from polystyrene as the backbone of the whole polymer and then grafted with polybutadiene as the chains. Polystyrene is normally high in mechanical strength so it would provide the material strength while the rubbery polybutadiene could help to provide some resilience to make the copolymer less brittle.

Table 2.7: The names and the structures of the arrangement of the co-polymers

Name of arrangements	**Structure of arrangements of the co-polymer**
Alternating copolymer	—A—B—A—B—A—B—A—B—
Random copolymer	—A—A—B—A—B—B—A—B—
Block copolymer	—A—A—A—A—B—B—B—B—
Graft copolymer	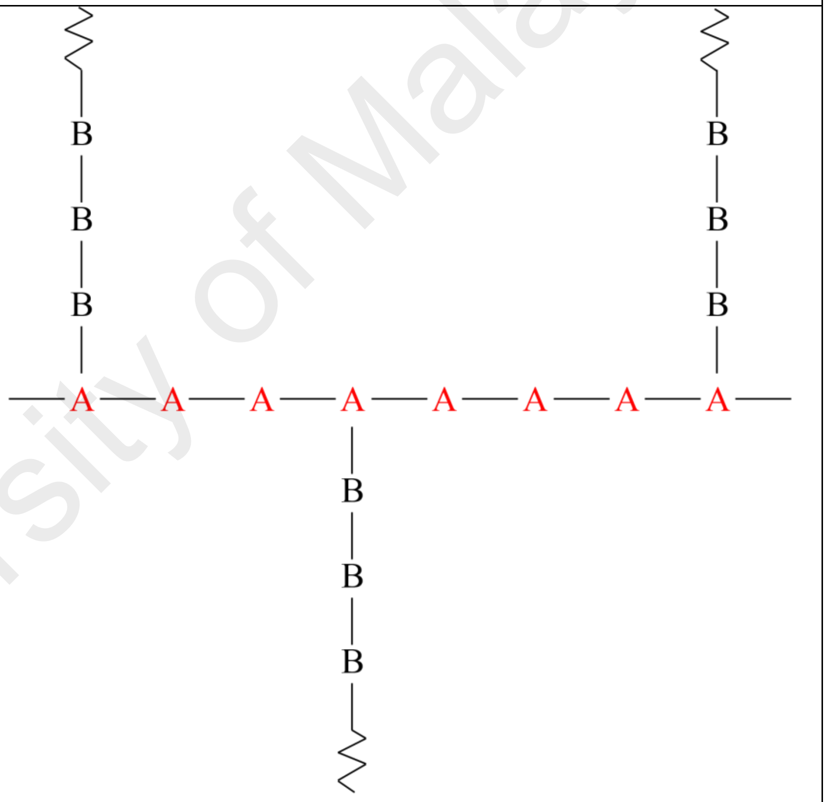

A lot of research has been done on the copolymer that were being used as the backbone of the polymer electrolytes for electrical performances. Studies show that the usage of copolymer in the polymer electrolytes show promising results. Polymer electrolyte samples which were made with copolymer were found to have high ionic conductivity, high stability, high electrochemical properties, etc (Miao et al., 2008).

In this studies, poly(1-vinylpyrrolidone-co-vinyl acetate) (P[VP-co-VAc]) has been used as the polymer backbone of the polymer electrolytes. Following is the structure of the P(VP-co-VAc) copolymer:

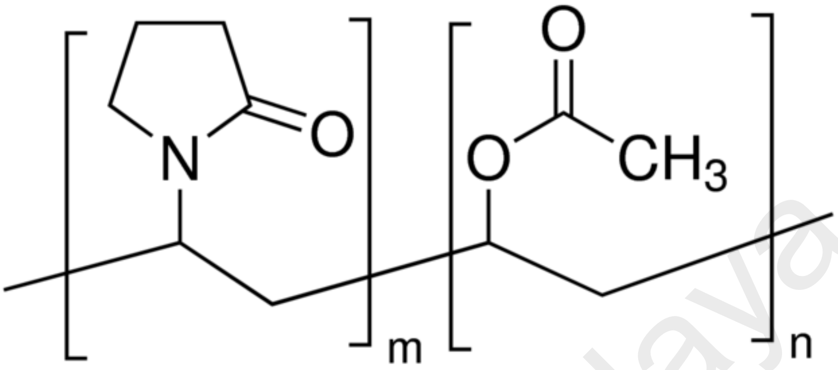

Figure 2.10: The structure of the P(VP-co-VAc) copolymer.

The crystalline PVP region of the P(VP-co-VAc) copolymer assist to improve the mechanical strengths of the gel polymer electrolytes while the amorphous PVAc region assist in improving the flow of the charged ions which could lead to improve electrical performances. Despite there is a lot of studies have been done with co-polymer in the polymer electrolytes and electrochemical fields, P(VP-co-VAc) is a co-polymer that is yet to be studied. This is the reason why we have selected this novel co-polymer as a stepping stone for better results with further improvements, in the future.

2.5 Summarize of the chapter

This chapter discussed the current literature related to solar cells, DSSCs, polymer electrolytes, solid polymer electrolytes, gel polymer electrolytes. It also discussed about the factors that could influence the ionic conductivity of GPE and the photovoltaic performance of their DSSCs as well as strategies that can be applied to overcome the weakness of the GPEs.

CHAPTER 3: METHODOLOGY

3.1 Introduction of the chapter

The material and chemical used are discussed in the first part of this chapter. Then, it proceeds with the discussion on the methodology and procedures for the polymer electrolyte preparation, dye sensitized solar cell fabrications, characterizations such as electrochemical impedance spectroscopy, structural studies, thermal studies and solar cell characterizations.

3.2 Materials

Table 3.1 shows the details of the starting materials that were used in the research.

Table 3.1: Details of the materials used in the research

	Materials	**Obtained from**
Host Polymer	Poly[1-vinylpyrrolidone-co-vinyl acetate] (P[VP-co-VAc])	Sigma-Aldrich
Inorganic Salts	Potassium iodide (KI)	Friedemann Schmidt Chemical
	Tetrapropylammonium iodide (TPAI)	Sigma-Aldrich
Ionic liquids	1-methyl-3-propylimidazolium iodide (MPII)	Sigma-Aldrich
Solvents	Ethylene carbonate (EC)	Merck
	Propylene carbonate (PC)	Merck
Redox Couple	Iodine (I_2)	Friedemann Schmidt Chemical

Table 3.1 (continued): Details of the materials used in the research

Inorganic Dye	N719 ruthenium dye (Di-tetrabutylammonium cis-bis(isothiocyanato)bis(2,2'-bipyridyl-4,4'-dicarboxylato)ruthenium(II))	Sigma-Aldrich
Semiconductor	TiO_2 P-25 and P-90	Degussa Germany

3.3 Research layouts

The research started with only the host polymer and a single salt (KI or TPAI) in order to look deeper into the compatibility of the salts with the copolymer. This was done to help us to learn more about the novel P(VP-co-VAc) copolymer in terms of electrochemical studies, ion conduction studies, molecular studies (FTIR), crystallographic studies (XRD), and thermal studies of the P(VP-co-VAc) copolymer based gel polymer electrolytes (GPE). Then, compatibility of the P(VP-co-VAc) copolymer based gel polymer electrolytes (GPE) and the ionic liquid (MPII) were tested and studied by the addition of the MPII into the best conducting samples of the P(VP-co-VAc) and KI system. This could ensure that the chosen ionic liquid works perfectly in our gel polymer electrolytes system. The characteristic of the P(VP-co-VAc), KI and MPII were studies as well. The binary salt systems of the P(VP-co-VAc) copolymer based gel polymer electrolytes (GPE) could then be started in order to look for the best ratio with the best conduction and mechanical strength. This could ensure the gel polymer electrolytes to be easily reproduce upon the addition of the ionic liquid into the system and also to make sure that the ionic conductivity will be at the best level. With the best ratio sample has been found, finally the ionic liquid, MPII would be added into the binary system. The detailed information of the prepared systems of the polymer electrolytes is shown in *Figure 3.1*.

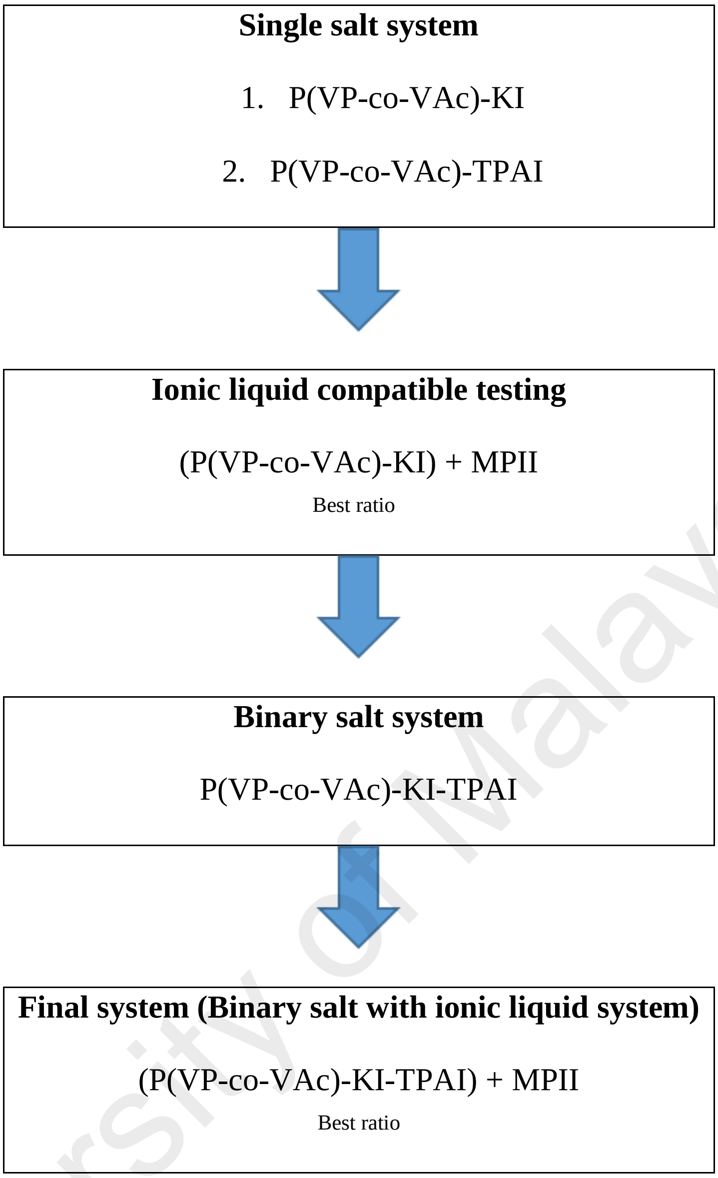

Figure 3.1: Information of the prepared system of the polymer electrolytes samples

The designation for the particular system are as following:

Table 3.2: The designation of P(VP-co-VAc)-KI gel polymer electrolyte system.

Composition						Designation
KI (wt. %)	**P(VP-co-VAc) (g)**	**KI (g)**	**I_2 (g)**	**EC (g)**	**PC (g)**	
0	5.000	0.000	0.000	1.500	1.500	**O**
10	4.423	0.500	0.077	1.500	1.500	**K10**
20	3.847	1.000	0.153	1.500	1.500	**K20**
30	3.270	1.500	0.230	1.500	1.500	**K30**
40	2.694	2.000	0.306	1.500	1.500	**K40**

Table 3.3: The designation of P(VP-co-VAc)-TPAI gel polymer electrolyte system.

Composition						Designation
TPAI (wt. %)	**P(VP-co-VAc) (g)**	**TPAI (g)**	**I_2 (g)**	**EC (g)**	**PC (g)**	
0	5.000	0.000	0.000	1.500	1.500	**O**
10	4.459	0.500	0.041	1.500	1.500	**T10**
20	3.919	1.000	0.081	1.500	1.500	**T20**
30	3.378	1.500	0.122	1.500	1.500	**T30**
40	2.838	2.000	0.162	1.500	1.500	**T40**

Table 3.4: The designation of P(VP-co-VAc)-KI-MPII gel polymer electrolyte system.

Composition							Designation
MPII (wt. %)	**P(VP-co-VAc) (g)**	**KI (g)**	**MPII (g)**	**I_2 (g)**	**EC (g)**	**PC (g)**	
0	3.270	1.500	0.000	0.230	1.500	1.500	**K30**
5	3.107	1.430	0.250	0.219	1.500	1.500	**KM5**
10	2.943	1.350	0.500	0.207	1.500	1.500	**KM10**
15	2.780	1.280	0.750	0.196	1.500	1.500	**KM15**
20	2.616	1.200	1.000	0.184	1.500	1.500	**KM20**

Table 3.5: The designation of P(VP-co-VAc)-KI-TPAI gel polymer electrolyte system.

Composition							Designation
KI:TPAI (wt. %)	**P(VP-co-VAc) (g)**	**KI (g)**	**TPAI (g)**	**I_2 (g)**	**EC (g)**	**PC (g)**	
0:30	3.378	0.000	1.500	0.122	1.500	1.500	**T30**
10:20	3.342	0.500	1.000	0.158	1.500	1.500	**KT1**
20:10	3.306	1.000	0.500	0.194	1.500	1.500	**KT2**
30:0	3.270	1.500	0.000	0.230	1.500	1.500	**K30**
0:40	2.838	0.000	2.000	0.162	1.500	1.500	**T40**
10:30	2.802	0.500	1.500	0.198	1.500	1.500	**KT3**
20:20	2.766	1.000	1.000	0.234	1.500	1.500	**KT4**
30:10	2.730	1.500	0.500	0.270	1.500	1.500	**KT5**
40:0	2.694	2.000	0.000	0.306	1.500	1.500	**K40**

Table 3.6: The designation of P(VP-co-VAc)-KI-TPAI-MPII gel polymer electrolyte system.

Composition								Designation
MPII (wt. %)	**P(VP-co-VAc) (g)**	**KI (g)**	**TPAI (g)**	**I_2 (g)**	**MPII (g)**	**EC (g)**	**PC (g)**	
0	2.730	1.500	0.500	0.270	0.000	1.500	1.500	**KT5**
5	2.594	1.430	0.475	0.257	0.250	1.500	1.500	**KTM5**
10	2.457	1.350	0.450	0.243	0.500	1.500	1.500	**KTM10**
15	2.321	1.280	0.425	0.230	0.750	1.500	1.500	**KTM15**
20	2.184	1.200	0.400	0.216	1.000	1.500	1.500	**KTM20**

3.4 Preparation of Gel Polymer Electrolytes

The materials used in the preparation of the GPEs were obtained as mentioned in *Table 3.1*. P(VP-co-VAc), TPAI and KI were vacuum dried at 50 °C for 24 hrs prior to use in order to eliminate trace amount of water in the materials. The gel polymer electrolytes with different weight percentage ratio were prepared by using the concentration data as shown in *Table 3.2* to *Table 3.6* for the five different system of gel polymer electrolytes. The weight of the solvent, PC (1.5g) and EC (1.5g) were kept unchanged with the ratio of 1:1. The weight of the I_2 was taken by keeping the iodide salts to iodine molar weight ratio as 10: 1.

The appropriate amount of salts was added and stirred in the mixture of EC and PC in a container. These mixture were then stirred for 30 minutes for complete dissolutions of the salts. After the dissolutions of the two salts, the iodine chips were added into the mixture and were stirred until the iodine chips fully dissolved. Then, appropriate amount of the P(VP-co-VAc) powder were added in batch by batch into the solutions while being stirred at 80^{o}C. The reason that P(VP-co-VAc) were added in batch by batch is to avoid overflowing of the co-polymer powder in the container and to ease the stirring process of the thick mixture. Stirring was then continued for 1 hour for complete dissolutions and homogeneity. The same procedure was carried out for the other samples with other composition of salts. The gel polymer electrolyte samples were then kept in a desiccator to eliminate unwanted traces of water caught by the gel polymer electrolytes. The gel polymer electrolytes were then analyzed using different types of instrument for different types of studies. The studies done were as following:

1. Electrochemical Impedance spectroscopy (EIS)
    a. Ionic conductivity studies
    b. Ion conduction mechanism
    c. Dielectric studies
2. Fourier Transform Infrared spectroscopy (FTIR)
3. X-ray Diffraction spectroscopy (XRD)
4. Thermogravimetric analysis (TGA)

After all the studies were conducted, the gel polymer electrolytes would be then fabricated into a DSSC and were further studied.

3.4.1 Electrochemical Impedance Spectroscopy (EIS)

The impedance spectroscopy was performed using a HIOKI 3532-50 LCR HITESTER bridge interface with a computer in order to study the electrochemical properties of the gel polymer electrolytes. Gel polymer electrolytes were sandwiched between two stainless steel electrodes which acted as blocking electrodes for the ions. Measurements were made over a frequency of 50 Hz to 1 MHz at room temperature (27 $\pm 1^{o}$C).

At every single frequency, a set of complex impedance, Z* values were obtained and from the Z* value new sets of real impedance, Z' and imaginary impedance, Z" were obtained. It was calculated by the following equations:

$$Z' = |Z(\omega)| \sin \theta \tag{3.1}$$

$$Z'' = |Z(\omega)| \cos \theta \tag{3.2}$$

The complex impedance data, Z* can be represented by its real, Z' and imaginary, Z" part by relatation:

$$Z^* = Z' - iZ'' \tag{3.3}$$

where *i* is a constant.

After obtaining all the impedance data, the complex impedance plots can be constructed. A complex impedance plots or also known as cole-cole plots are having imaginary impedance component (Z") plotted against the real impedance component (Z') at each excitation frequency. *Figure 3.2* shows a typical cole-cole plot. From the figure, it can be observed that there is spike. The intersection of the arc on the Z_{real} x-axis yield the bulk resistance value (R_b) which is a very important component to be used to calculate the ionic conductivity. The formula used to determine the ionic conductivity is as following:

$$\sigma = l / (R_b \times A) \tag{3.4}$$

where σ is the ionic conductivity (S cm^{-1}), l is the thickness of the film (cm), R_b is the bulk resistance (Ω) and A is the area of the electrode touched with the sample.

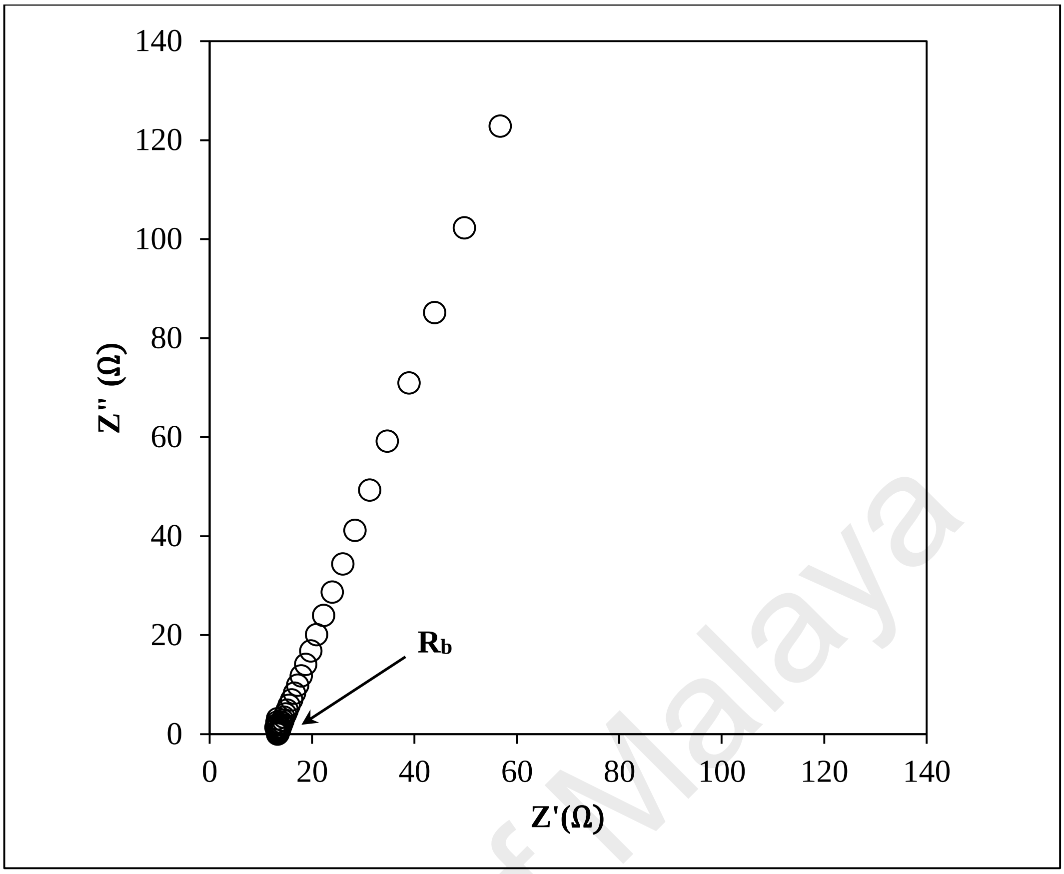

Figure 3.2: Typical cole-cole impedance plot for sample K30

The dielectric properties of all of the GPE samples were also carried out using a computer controlled HIOKI 3532-50 LCR Hi-Tester over the linear frequency *f* (*f* = ω/2π, where ω is angular frequency) range from 50 Hz to 1 MHz at room temperature (27 ± 1°C). Frequency dependent values of capacitance C_p and parallel resistance R_p of the sample holder loaded with the electrolyte sample were measured in parallel mode for the determination of the dielectric/electrical functions of the GPE samples. The frequency dependent real part Z' and imaginary part Z" of complex impedance Z*(ω) of the electrolyte films were evaluated by the following equation:

$$Z^*(\omega) = 1/Y^*(\omega) = Z' - jZ'' = R_p/(1 + (\omega C_p R_p)^2) - j[(\omega C_p R_p^2)/ (1 + (\omega C_p R_p)^2)] \quad (3.5)$$

The study of the relative permittivity, ε_r^* of the GPE samples was done to comprehend the polarization effect that happened at the electrode and electrolytes interface and the correlation between the ionic relaxation time with the ionic conductivity. The relative permittivity is the dimensionless ratio of the permittivity, ε^* over the permittivity of free space ε_0. It is also shown as a function of angular frequency where it has the real and imaginary component. The formula is shown as below [18]:

$$\varepsilon^*_r(\omega) = (\varepsilon^*(\omega)/\varepsilon_0) = \varepsilon'(\omega) - j\varepsilon''(\omega) \tag{3.6}$$

where $\varepsilon_0 = 8.854 \times 10^{-12}$ F m^{-1}, ε' is the dielectric constant, ε'' is the dielectric loss and j $=\sqrt{-1}$. The dielectric constant is the relative permittivity of a dielectric material. It is an important parameter to characterize the electrical charges capacity of a dielectric material could be attained and stored. Dielectric loss measures a dielectric material's inherent dissipation of electromagnetic energy into the movement of ions and the alignment of dipoles when the polarity of the energy field reverses rapidly. It is associated with the electrical conductivity of the materials. The dielectric constant, ε' and dielectric loss, ε'' can be calculated by following formula [19]:

$$\varepsilon^*_r = 1/j\omega C_0 Z^* \tag{3.7}$$

$$\varepsilon' - j\varepsilon'' = Z''/(\omega C_0(Z'^2 - Z''^2)) - j[Z'/(\omega C_0(Z'^2 - Z''^2))] \tag{3.8}$$

where Z^* is complex impedance, C_0 is the vacuum capacitance ($C_0 = \varepsilon_0 A/l$), l is the thickness of the GPE samples during measurements, A is the surface area contact and ω is angular frequency ($2\pi f$).

An abrupt increase in ε' and ε'' values at lower frequency side in the dielectric spectra can be observed and it is actually due to the large electrode polarization effect. This phenomenon always causes the ionic conduction relaxation to be misjudged. In order to overcome this misjudgments, modulus studies have been used and it is widely used to analyze the different relaxation phenomenon in the polymeric system and to assist in the separation of the polarization effect from the bulk relaxation phenomenon in the polymer electrolyte. Electric modulus can be defined as the reciprocal of complex relative permittivity and the inversion process able to suppress the electrode polarization effect at low frequencies and enhance small features at high frequencies as ε' contributes as the denominator to the second power in the loss function. The relationship between electric modulus, relative permittivity and impedance are given in the equation below [30]:

$$M^* = M' + jM'' = 1/\varepsilon^*_r = 1/(\varepsilon' - j\varepsilon'') = \varepsilon'/(\varepsilon'^2 + \varepsilon''^2) + \varepsilon''/(\varepsilon'^2 + \varepsilon''^2) \qquad (3.9)$$

$$M^* = j\omega C_0 Z^* = \omega C_0 Z'' + j\omega C_0 Z' \qquad (3.10)$$

3.4.2 Fourier Transform Infrared Spectroscopy (FTIR)

The fundamental vibration of the polymer electrolytes were studied using FTIR spectroscopy in the wavenumbers region between 4000 and 650 cm^{-1} at a resolution of 1 cm^{-1} using Thermo Scientific Nicolet iSIO Smart ITR machine. The basic principle behind the molecular spectroscopy is that specific molecules absorb light energy at specific wavenumber, known as their resonance frequencies.

The FTIR spectrum of a sample is collected when a beam of infrared light passed through the sample. The transmitted light could reveals how much energy was absorbed at each wavenumber. The FTIR spectrometer could assist in measuring all the wavenumbers at once. The transmittance and absorbance spectrum can be produced by the machine. These analysis on the absorption characteristics could reveal the details about the molecular structures of a sample.

3.4.3 X-ray Diffraction spectroscopy (XRD)

XRD is a rapid analytical technique usually used to identify the phase of the crystalline material and provides a lot of information regarding the dimensions of the cell unit. It could be used to identify unknown substances, by comparing diffraction data against a database which is maintained by the International Centre for Diffraction Data. Max von Laue was the person responsible in the discovery of XRD as he discovered that the crystalline substances actually act as three-dimensional diffraction grating for the X-ray wavenumbers is similar to the spacing of the planes in a crystal lattice.

The fundamental principles of X-ray Powder Diffraction (XRD) is actually not very complicated. X-ray diffraction is basically based on the constructive interference of the monochromatic X-rays and crystalline samples. A cathode ray tube is used to generate the X-rays and then the X-rays is filtered to produce monochromatic radiation and then collimated to concentrate before directed towards the samples. The interaction of the X-ray with the sample could produce constructive interference and also a diffracted ray when it has the conditions which could satisfy the Bragg's Law which is shown below:

$$n\lambda = 2d \sin\theta \qquad (3.11)$$

Bragg's Law relates the wavenumber of the electromagnetic radiation to the diffraction angle and the lattice spacing in the crystalline sample. Then, they would be detected, process, and studied. All sample would be scanned at a range of 2θ angles so all possible diffraction directions of the lattice could be attained because of the natural random orientation of the powdered material. XRD can also be used to characterize the heterogeneous mixture to determine the relative abundance of the crystalline compounds.

In this research, XRD is used to determine the crystallinity of the gel polymer electrolytes. The analysis was performed with a BTX benchtop X–ray diffractor using Cu Kα radiation wavenumber $\lambda = 1.5418$ Å for 2θ angles between 5^o to 80^o.

3.4.4 Thermogravimetric analysis (TGA)

TGA is a thermal analysis technique which is mainly used to measure the changes in the weight of a sample as a function of temperature or time. In polymer electrolyte field, TGA is commonly used to determine the degradation temperature, residual solvent levels, absorbed moisture content, and the amount of inorganic filler in the samples.

In this research, the sample is placed into a TGA sample pan holder/crucible which is made from silica. The sample pan holder would be then placed on a sensitive balance and then into the high temperature chamber. The balance would measure the initial sample weight at room temperature and then continuously monitor the changes in the sample weight as heat is gradually applied to the sample. The TGA studies was carried out on a TA Instrument Universal Analyzer 2000 with Universal V4.7A software. The sample was heated from 25^oC to 850^oC at a heating rate of 50^oC min^{-1} in a nitrogen atmosphere with a flow rate of 60 ml min^{-1}. Typical TGA curve provides information concerning the thermal stability of the initial sample, intermediate compounds and the residue if there were any of them. In addition to thermal stability, the weight losses observed in TGA can be quantified to predict the pathway of degradation or to obtain information.

3.5 Fabrication of DSSC

3.5.1 Preparation of the working electrodes

Fluorine doped tin oxide (FTO) (8 Ω cm^{-2}) conducting glasses were cleaned with distilled water and ethanol. Then, mesoporous TiO_2 layers was used as the based material of the deposition of the dye sensitizers. The fluorine-doped conducting tin oxide (FTO) glasses was coated with two layers of different types of TiO_2 (P-25 and P-90). The first layer was coated with TiO_2 (P-90) where these TiO_2 (P-90) paste was prepared by grinding TiO_2 (P-90) which was added with certain amount of nitric acid (pH=1). The mixture was grinded for 30 minutes or until it become slurry. The slurry paste will then be coated on the FTO glasses by using spin coater machine with 4 seconds of 1000 RPM and another 45 seconds of 2350 RPM. The resulting TiO_2 (P-90) coated FTO was then sintered at 450^{o}C for 30 minutes and then left to cool down to room temperature. The slurry paste of the second layer TiO_2 (P-25) was then prepared with the same method as preparing TiO_2 (P-90) but with the addition of a few drops of surfactants (Triton X-100). The second layer was then coated on the TiO_2 (P-90) coated FTO by using doctor blade method and was sintered at 450^{o}C. The thickness of the coated layers was measured with the help of a calibrated profilometer. Dye absorption was carried out by immersing the above coated FTO in ethanolic dye solution containing Ruthenium dye N719 [Di-tetrabutylammonium cis-bis(isothiocyanato)bis(2,2′-bipyridyl-4,4′-dicarboxylato) for 24 hrs prior to use.

3.5.2 Preparation of the counter electrodes

As for the Pt counter electrode, it was made from an aqueous solution containing Chloroplatinic acid solution (H_2PtCl_6) and isopropyl alcohol (C_3H_7OH) with the weight ratio of 1:1. The aqueous ($H_2PtCl_6 + C_3H_7OH$) solution was dropped on the conducting surface of the cleaned FTO substrate and air-dried. Then, the resulting mixture coated FTO was sintered with the program settings of 100°C for 5 minutes and followed by 500°C for 30 minutes. The resulting Pt coated counter electrode was then gently washed with ethanol. The same process was repeated 3 to 4 times for a thicker reflective Pt counter electrode.

3.5.3 Fabrications of the DSSCs

In this present study, the prepared gel polymer electrolytes sample, working electrodes, and counter electrodes were used for the fabrication of the DSSC. The DSSC would be assembled with the configuration shown in *Figure 3.3* and the assembled DSSC was shown in *Figure 3.4*.

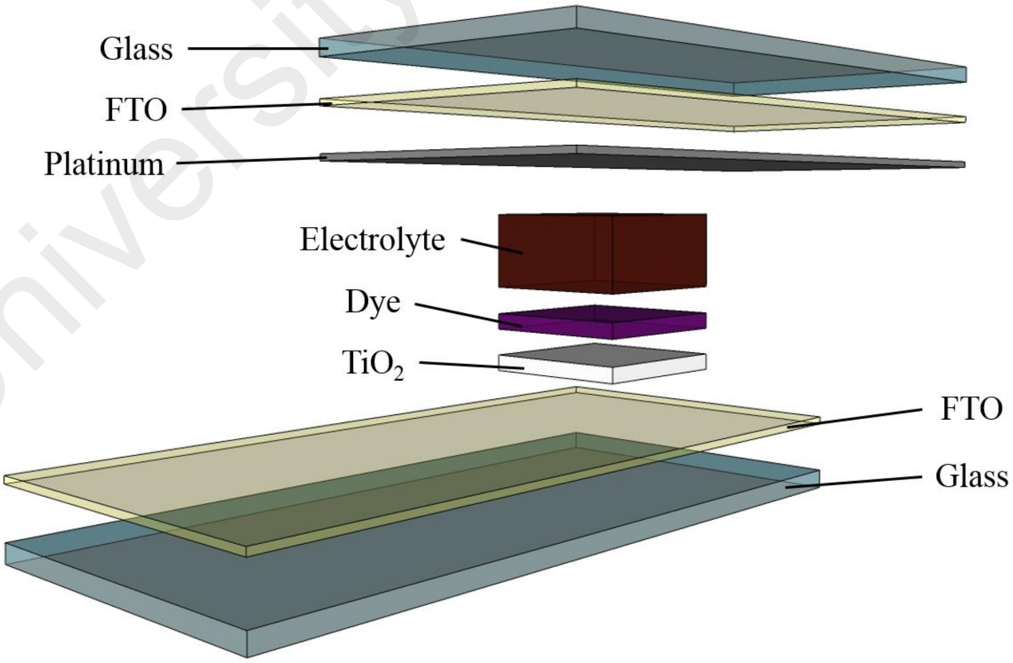

Figure 3.3: Schematic diagram of the assembled DSSCs.

Figure 3.4: A picture of the assembled DSSCs.

A small amount of gel polymer electrolytes was applied on the surface of the dye sensitized TiO_2 layer. Then, the GPE would be sandwiched together with the counter electrodes. The assembled DSSC would be then kept in position with clips. Since the polymer electrolytes is in gel form. Leakages would unlikely to happen. The DSSC would be then analyzed for photophotocurrent density-voltage (J-V) characteristics and electrochemical studies of the DSSCs with different GPE samples were measured under the illumination in the range of 20 - 100 mW cm^{-2} (P_{in} = 0.2 to 1.0) simulated sunlight from a Newport LCS-100 Series solar simulator, with a Metrohm Autolab potentiostat (PGSTAT128N). With regards to the experimental reproducibility, the J-V characteristics of the DSSCs were measured with three different replicated cells with the same composition of materials and the average values of the results were reported.

3.5.4 Photovoltaic studies

As mentioned previously, the DSSC efficiency was determined by its photophotocurrent density-voltage (J-V) characteristics under the standard illumination conditions which it the standard solar spectrum of air mass 1.5 (AM 1.5) with an intensity of 100 mW cm^{-2} which is also referred as 1 sun. The AM 1.5 spectrum corresponds to the sunlight that has passed through the atmosphere 1.5 longer than when the sun is directly overhead. Normally, the sunlight would be attenuated differently by the condition of the atmosphere on the incident radiation angle thus in the lab, the illumination conditions were provided by a calibrated lamp source from the solar simulator.

The photophotocurrent density-voltage characteristic are monitored by varying an external load which is from zero load (short-circuit condition) to infinite load (open-circuit condition). The photovoltaic performance were usually illustrated by a J-V curve which is shown in *Figure 3.5*.

The maximum power generated is when the photocurrent and the voltage is at its maximum, since the electrical power (P) is given by current density (J) times voltage (V):

$$P = JV \qquad (3.12)$$

The degree of the squared shape of the JV curve is given by the fill-factor (FF) as shown in the equation below:

$$FF = (J_{max} \times V_{max})/(J_{sc} \times V_{oc}) \qquad (3.13)$$

The DSSC efficiency is the ratio between the power generated and power of incident light as shown in equation below:

$$\eta = P_{out}/P_{in} = (J_{sc} \times V_{oc} \times FF)/P_{in} \qquad (3.14)$$

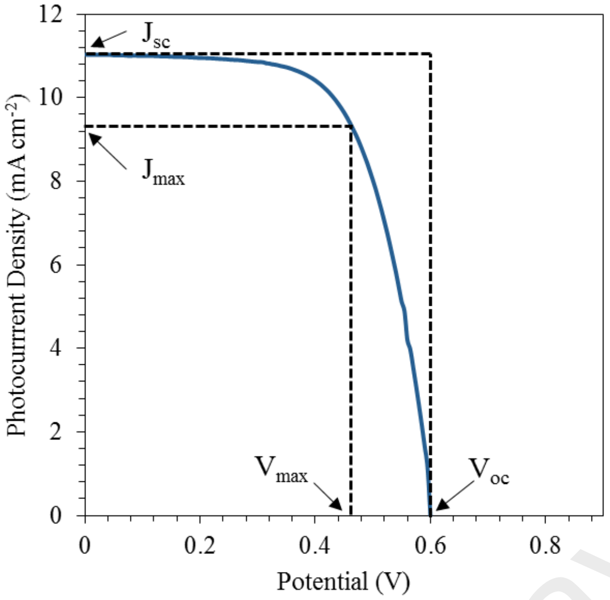

Figure 3.5: Photocurrent density-voltage characteristics of a DSSC illustrating short-circuit current density (J_{sc}), open circuit volatage (V_{oc}), current at maximum power point (J_{max}) and voltage at maximum power point (V_{max}).

3.5.5 Electrochemical studies

The electrochemical impedance spectroscopy (EIS) measurements of the DSSCs were carried out in the range of 0.1 Hz - 100 kHz and the AC potential of 10 mV was used. A potential bias equal to open circuit voltage was applied. The obtained impedance spectra were analyzed and fitted using Metrohm Autolab Nova software with appropriate equivalent circuits. Tafel polarization studies has also been studied.

3.6 Summarize of the chapter

The experimental methods including GPE preparations and designations, DSSC fabrications and related characterization are discussed in this chapter. The results and discussion will be expressed in following chapter.

CHAPTER 4: RESULTS AND DISCUSSION

4.1 Introduction of the chapter

The five P(VP-co-VAc) based gel polymer electrolytes (GPEs) systems which were analyzed using different characterizations such as EIS, FTIR, XRD, TGA and photovoltaic studies were discussed in this study.

4.2 P(VP-co-VAc)-KI Gel Polymer Electrolytes

4.2.1 Ambient Temperature-Ionic Conductivities Studies

Electrochemical impedance spectroscopy (EIS) is a useful technique that can be used to characterize the electrical or dielectric properties of the interfaces between the electronic and ionic conducting phases. The EIS also can be used to determine the dynamics of bound or mobile charges in the bulk or interfacial regions of a variety types of solid or gel conducting materials and even insulators (dielectrics) (Aravindan & Vickraman, 2007).

Polymers are normally ionic and electronic insulators. Not much different with co-polymer such as P(VP-co-VAc) that we are going to use in this research. The ionic conduction in a polymer electrolyte is basically coming from the diffusions of the ions through the free volumes. This is the reason that the inorganic salts added into the polymers to form a mixture that support ionic conduction and in our case, the salts that were used is KI and TPAI (Mishra & Rao, 1998). The differences in these salts is that they are actually different in sizes. KI is a small sized salt and TPAI is a bulky sized salt. Both of these salts will play a different role inside the polymer electrolyte to improve the ionic conductivity which is going to be explained in later chapters.

Here, we are going to look into the ionic conduction properties of the P(VP-co-VAc)-KI gel polymer electrolyte system. *Figure 4.1* and *Figure 4.2* show the complex impedance plot of sample O and all of the samples in this system, respectively.

Sample O is the sample where only the P(VP-co-VAc) is added into the EC and PC to form a gel polymer electrolyte. As seen in the impedance plot of sample O, it shows the typical impedance behavior where a semicircular region can be seen in the high frequency region followed by a spike or also known as the residual tail at low frequency. The phenomenon can be represented by a resistor where it shows that there are migration of ions occurred through the free volume matrix of the gel polymer electrolyte. It also shows that the immobile polymer chain becomes polarized in the alternating field which also can be represented by a capacitor. With the ionic migration and bulk polarization are physically in parallel, it explains why the semicircle can be observed at high frequencies (C. S. Kim & Oh, 2000).

Meanwhile, in the P(VP-co-VAc)-KI GPE samples (*Figure 4.2*). The semicircle which can be observed previously in sample O disappears in its complex impedance plots. At low frequencies, the linear region attributed to the effect of blocking electrodes and the semicircle in the high frequency is actually related to the conduction process in the bulk of the complex. With the disappearance of the semicircle, it indicates that the current carriers now are mostly ions and the total conductivity is mainly the results of the ion conduction. It is also indicating that there were very good contacts at the interface in between the electrodes and polymer electrolytes (C. S. Kim & Oh, 2000).

By using the *equation 3.4*, the bulk resistance (R_b) is obtained from each of the impedance plots and the ionic conductivity for each sample was determined. The variation of the ionic conductivity values for each sample is shown in *Figure 4.3* and the value of the ionic conductivity is shown in *Table 4.1*. Based on the results, the introduction of KI into the gel polymer electrolyte shows an increase in the ionic conductivity from 4×10^{-4} mS cm^{-1} (sample O) to 0.45 mS cm^{-1} (sample K10). Then, the ionic conductivity increases gradually up to 30 wt.% of KI salt concentration before a rapid decrease at 40 wt.% of KI salt added. The highest ionic conductivity for this system was achieved at 30 wt.% of KI, with a value of 1.72 mS cm^{-1}.

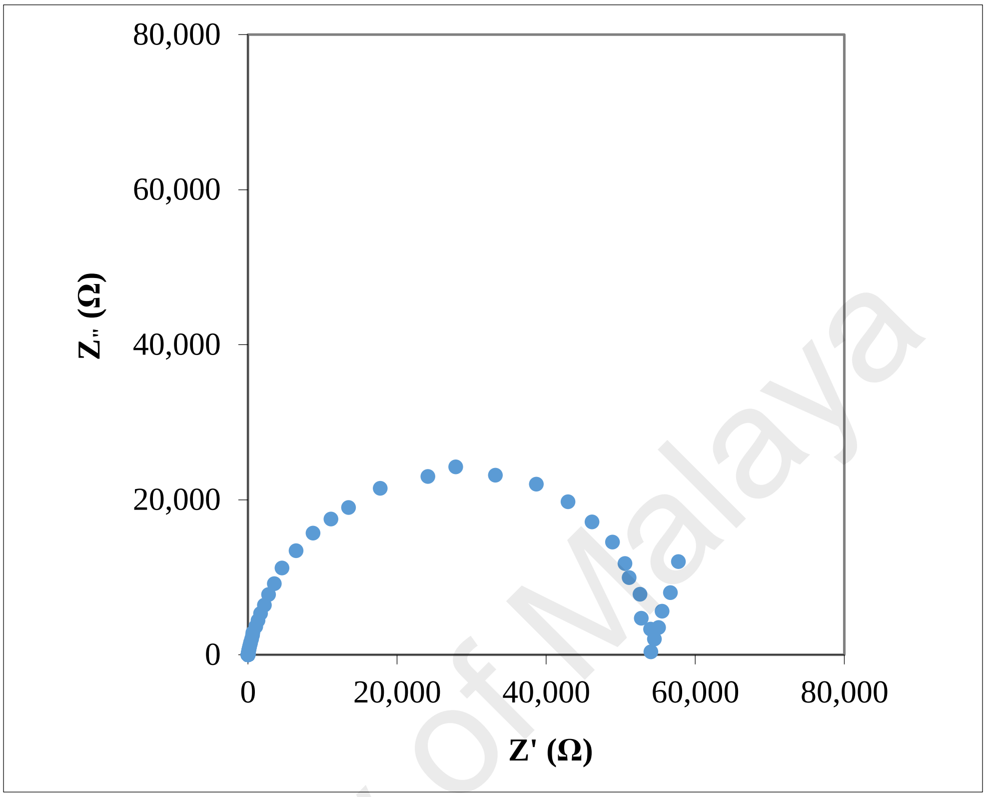

Figure 4.1: Impedance plot of sample O.

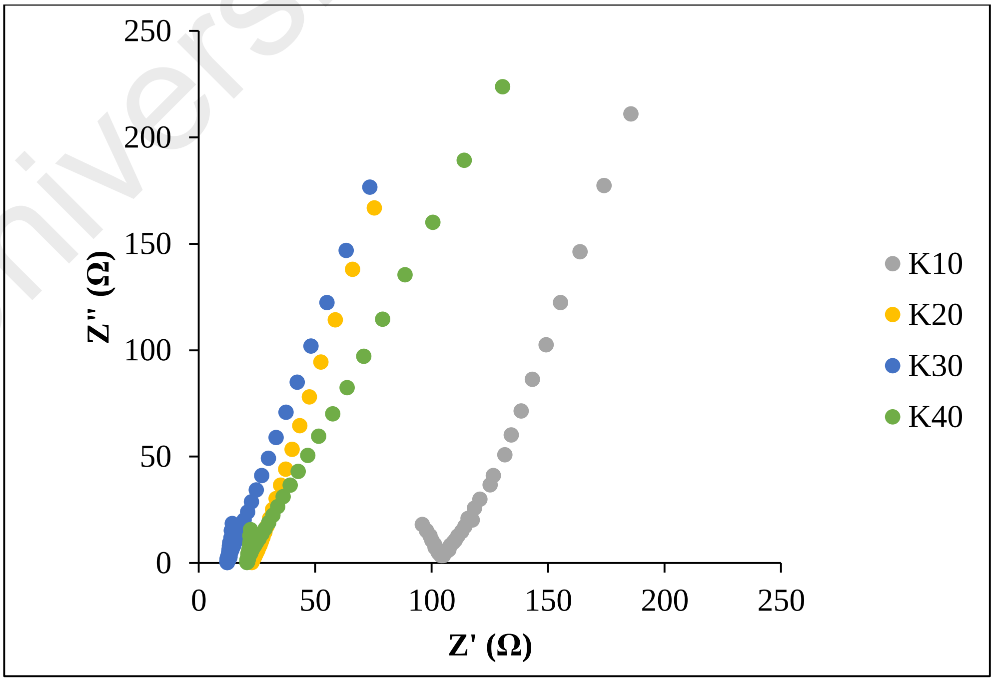

Figure 4.2: Impedance plot of P(VP-co-VAc)-KI GPE samples at room temperature.

Table 4.1: Ionic conductivity values for the P(VP-co-VAc)-KI GPE samples at room temperature.

Electrolytes	Ionic Conductivity (mS cm^{-1})
O	4×10^{-4}
K10	0.45
K20	1.08
K30	1.72
K40	1.07

The typical expression for the ionic conductivity of the homogenous polymer electrolytes given in *Equation 4.1*:

$$\sigma(T) = \Sigma(n_i q_i \mu_i) \tag{4.1}$$

where n_i is the number of mobile ions type of i, q_i is the charge of ions type of i, and μ_i is the mobility of ions type of i. From the equation, it can be observed that the number of the mobile ions and the mobility of these ions is controlling the trend of the ionic conductivity of the polymer electrolytes. Normally, at lower amount of salts, the ionic conductivity was dictated by the quantity of the mobile ions generated but when it reaches the certain optimum point, it changes to another phenomenon (Ramesh, Liew, & Arof, 2011). The ionic conductivity at this point was dependent on to the mobility of the ions and the ionic conduction pathways. The increment of the ionic conductivity observed in *Figure 4.3* is due to the increase in number of charge carriers generated by KI salt. KI salts provide K^+ and I^- ions. When the concentration of these charge carriers is increasing, it reduces the salvation of the K^+ cations and thus, it encourages the decoupling of the ions. The ionic conductivity starts to decrease after 30 wt.% of KI added into the system. This point can be determined as the optimum threshold for the GPEs to fully utilize the mobile charge carriers generated by the KI salt (Ravi, Bhavani, Kiran Kumar, & Narasimaha Rao, 2013). Beyond this point, there would be a lot of excess mobile charge carriers and it would cause agglomeration between then excess mobiles charge carriers.

The excess charge carriers could form ion pairs, in which could disturb the movement of the mobile charge carriers. When this mobile charge carriers move much slower in the polymer matrix, the ionic conductivity decreases (Woo, Majid, & Arof, 2012). Moreover, due to excess number of KI salts added into the gel polymer electrolyte, the salts tend to aggregates and form a more rigid physical appearance. Thus, it also restricting the ionic mobility.

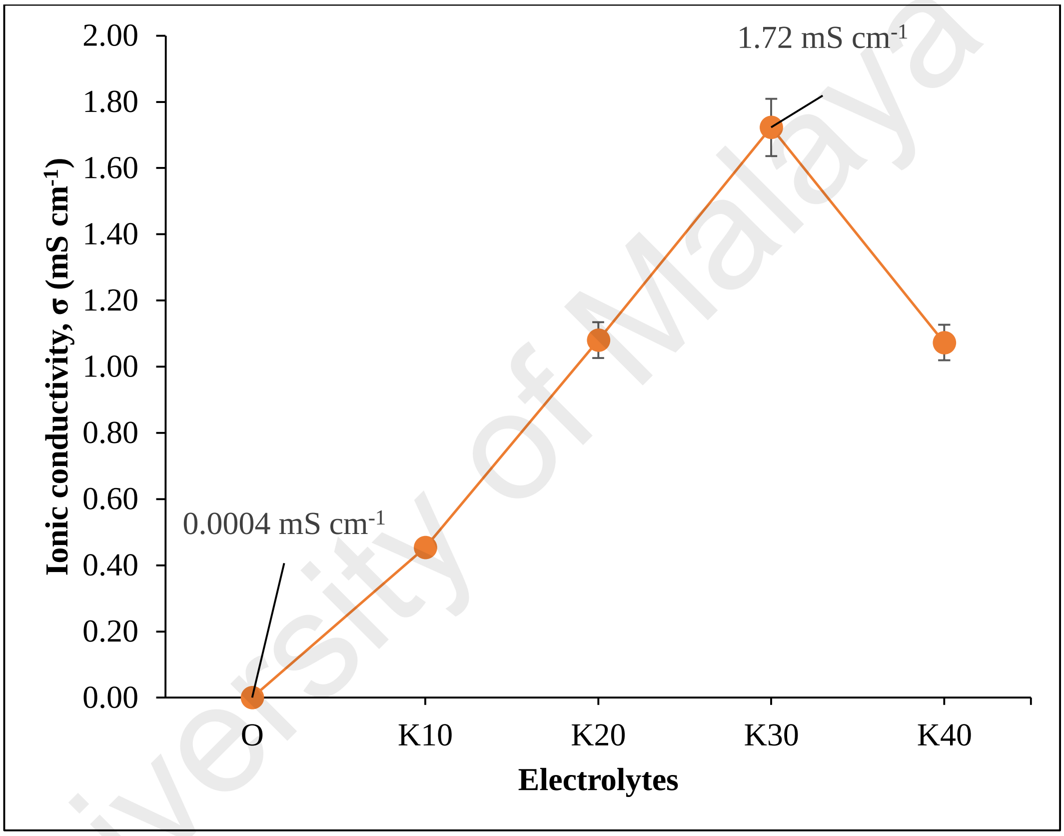

Figure 4.3: Variation of ionic conductivity of the GPE samples with different KI concentration at room temperature.

4.2.2 Temperature dependence-Ionic conductivity studies

Figure 4.4 shows the Arrhenius plot for the ionic conductivity with variation of the temperature range from 30 °C – 100 °C. The linearity of the graph reveals that the GPEs have the ionic conduction mechanism of Arrhenius theory which is represented by the *Equation 2.1* which has been mentioned previously.

By obeying the Arrhenius theory, it indicates that the mobile charge in the GPEs are hopping around the polymer matrix from its own site into neighboring vacant site. The frequency of the mobile charge hopping is expected to increase when the samples become heated due to the increasing energy supplied by the high temperature. When the frequency of mobile charge hopping increases, it basically leads to increase in the mobility of the charge carriers, and thus, it will lead to the increase of the ionic conductivity as well (Tang et al., 2012). Activation energy is defined as the minimum energy required to start a chemical reaction. In this research, it would be the energy that is required by the mobile charge to hop from one site to another site. The activation energy of a reaction is usually denoted by E_a and given in units of kilojoules per mole (kJ mol^{-1}). The E_a can be determined by calculating the slope of each respective graph. *Table 4.2* shows the calculated E_a value for different GPEs with different KI salt concentration added. K30 is having the lowest E_a which is 0.77 kJ mol^{-1}. As expected, the GPEs with lower activation energy will have higher ionic conductivity as lesser energy is required by the mobile charges to move around. Thus, the mobile charges was able to move more easily in the polymer matrix and it directly increases the ionic conductivity (Sivakumar, Subadevi, Rajendran, Wu, & Wu, 2007). The relation of the activation energy, E_a and the ionic conductivity values are shown in *Figure 4.5*.

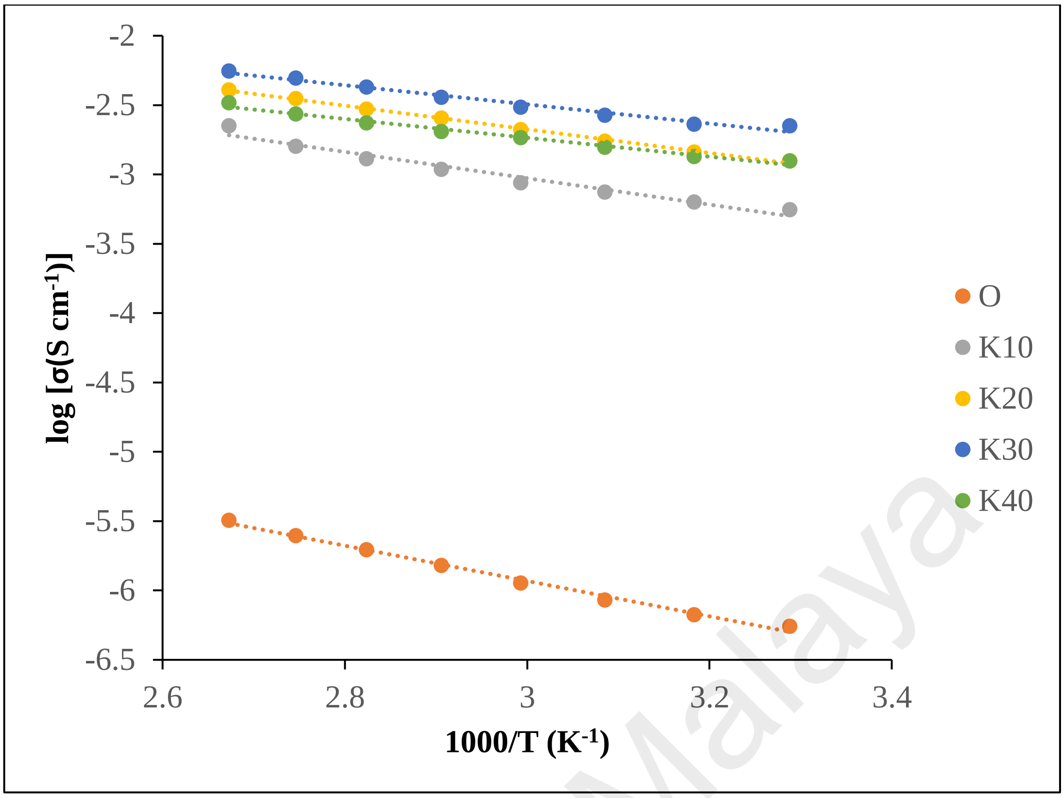

Figure 4.4: Arrhenius plots for the conductivity of the P(VP-co-VAc)-KI GPE samples with different concentration of KI.

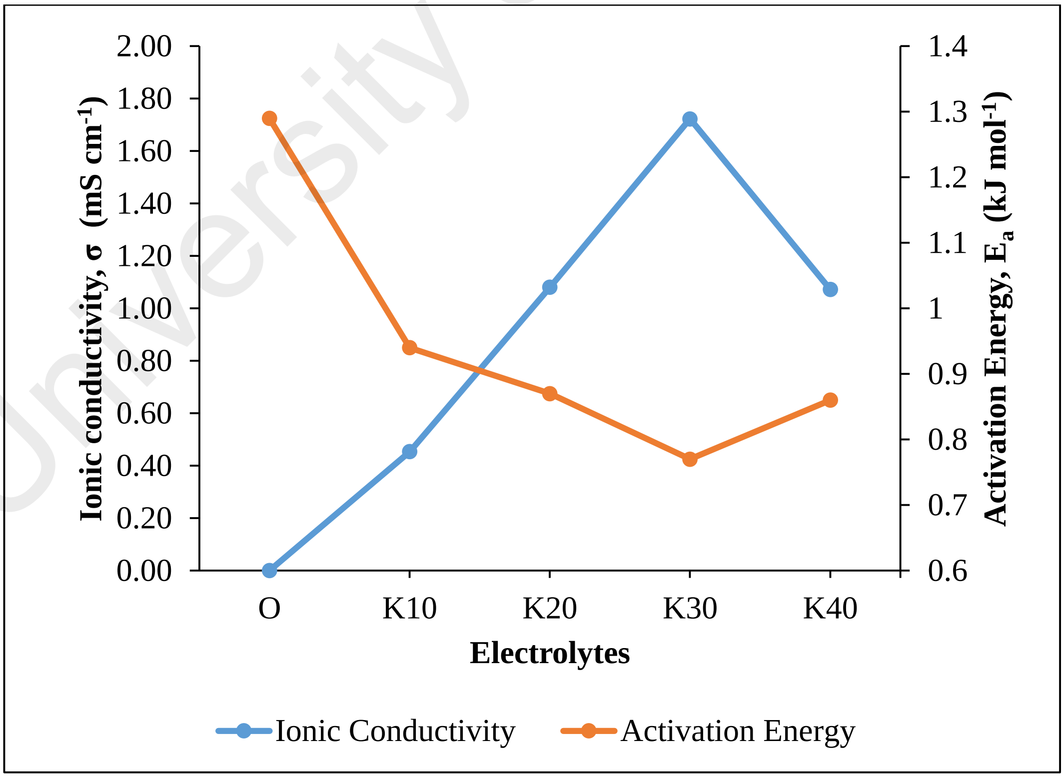

Figure 4.5: Variation of ionic conductivity and the activation energy of the P(VP-co-VAc)-KI GPE samples with different KI concentration at room temperature.

Table 4.2: The activation energy of the GPEs sample with different concentration of KI

Electrolytes	Activation Energy, E_a (kJ mol^{-1})
O	1.29
K10	0.94
K20	0.87
K30	0.77
K40	0.86

4.2.3 Dielectric Studies

4.2.3.1 Conductivity-frequency studies

The conductivity of the gel polymer electrolytes for this system was analyzed with respect to frequency in order to investigate the relaxation processes of the samples.

Figure 4.6 shows the variation of the ionic conductivity with the frequency for different KI content added into the gel polymer electrolyte samples at room temperature. In low frequency region, there is a deviation from the plateau region can be seen in figure for all of the samples. This is indicating that there are significant effect of the electrode polarization and also a proof that shows the nature variation of the ionic conductivity is similar to the universal dynamic responses which can be normally seen in disordered material like ionic conducting glasses and also conducting polymer electrolytes. Meanwhile, in high frequency region, the conductivity dispersion shows that there is a correlation between the forward and backward jumping of the charge carriers. Besides, the relaxation of the dynamic cage potential was also happening at high frequency region. According to the relaxation model, at this high frequency region, chances for the charge carriers to hop back to their initial site increases because the time needed is available and short enough for it to move. (Dillip et al., 2009).

On the other hand, the conductivity was observed to be low when the frequency is low as well and vice versa. This explains that the low frequency dispersion is due to the interfacial impedance and the space charge polarization inside the polymer electrolytes, which is also known as Maxwell Wagner-Sillars (MWS) effects. The charge at the electrode and electrolyte interface would accumulate as the frequency decreases which causes the number mobile ions to decrease. This could directly leads to the decrease of the ionic conductivity of the polymer electrolytes. Meanwhile, at higher frequency region, the mean displacement of these mobile ions decreases and the mobile ions could move better. This could directly increases the mobility of the mobile ions and as explained previously, this helps to increase the ionic conductivity as well (Dillip et al., 2009).

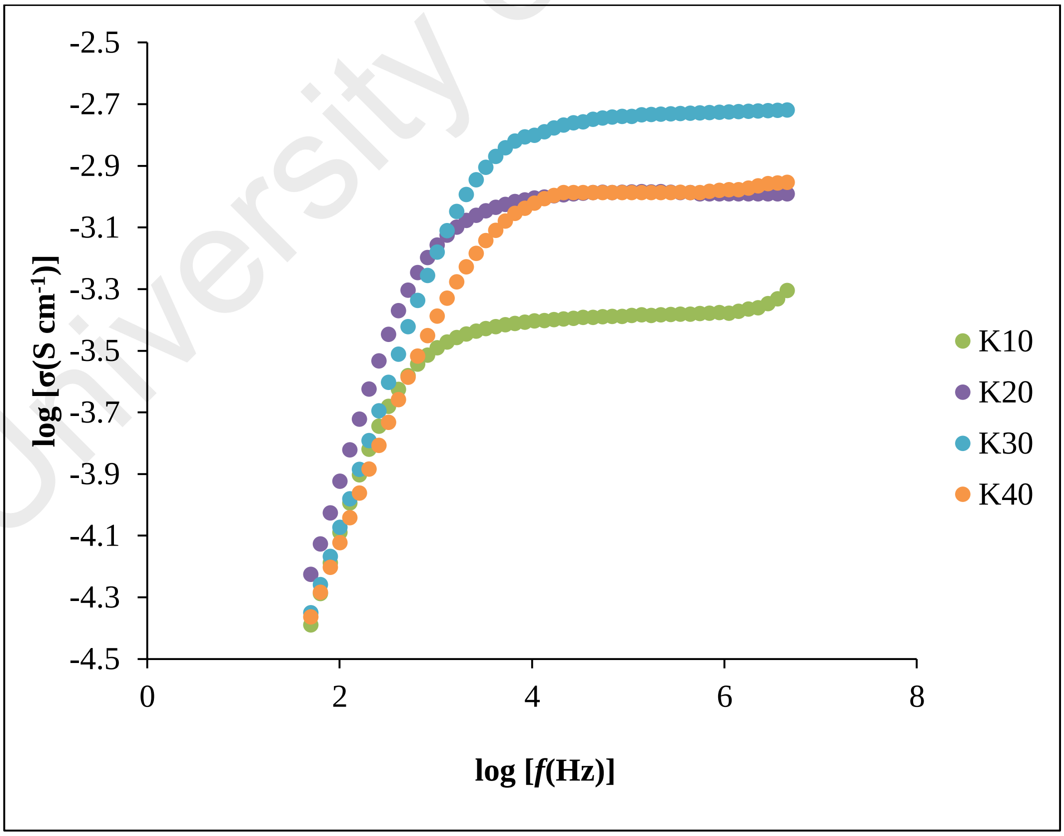

Figure 4.6: Frequency-dependent conductivity at various KI concentration of P(VP-co-VAc)-KI gel polymer electrolytes samples.

4.2.3.2 Dielectric Relaxation Studies

The polarization effect of the GPEs at the electrode and electrolytes interface and the correlation between ionic relaxation time with conductivity of the GPEs are essential to be studied in order to be able to comprehend more on the dielectric properties of the GPEs. This is the reason why the studies on the relative permittivity needed to be done on the GPE samples. The relative permittivity, ε^*_r of the system is dimensionless ratio of the permittivity, ε^* over the permittivity of free space ε_0. It is also shown as a function of angular frequency where it has the real and imaginary component. These two components are 90° out of phase. The formula are shown as below(B. Singh, Kumar, & Sekhon, 2005):

$$\varepsilon^*_r(\omega) = (\varepsilon^*(\omega)/\varepsilon_0) = \varepsilon'(\omega) - j\varepsilon''(\omega) \tag{4.2}$$

where $\varepsilon_0 = 8.854 \times 10^{-12}$ F m^{-1}, ε' is the dielectric constant, ε'' is the dielectric loss and j $= \sqrt{-1}$. Dielectric constant is a measure of polarization of the samples which linked with capacity to retain or store electric charge and also represent the amount of dipole alignment in a given volume. Dielectric loss is a measure of energy loss to move ions and align dipoles when the polarity of electric field reverses rapidly and is related to the electrical conductivity of the materials. Both ε' and ε'' can be calculated by following formula:

$$\varepsilon^*_r = 1/j\omega C_0 Z^* \tag{4.3}$$

$$\varepsilon' - j\varepsilon'' = Z''/(\omega C_0(Z'^2 - Z''^2)) - j[Z'/(\omega C_0(Z'^2 - Z''^2))] \tag{4.4}$$

where Z^* is complex impedance, C_0 is the vacuum capacitance ($C_0 = \varepsilon_0 A/d$), d is the thickness of the electrolyte film, A is the surface area contact and ω is angular frequency where $\omega = 2\pi f$.

Figure 4.7 shows the dielectric constant *ε'* versus log *f* plots of the GPE samples with different concentration of KI at room temperature. As observed, the dispersion value of *ε'* is really high at the low frequency region. This dispersion is caused by the dielectric polarization. The ions diffuse and then move around the polymer matrix under the electrical field. Unfortunately, they are blocked by the block electrolytes and they were unable to cross the electrode and electrolyte interface. It causes the ions to have hard time moving into the external circuit. Due to this reason, a hetero-charge layer was formed by the accumulated trapped ions at the interface of the electrode and electrolyte. The charge density will then increase which subsequently leads to interfacial polarization(Ramesh, Yahaya, & Arof, 2002). Meanwhile in the high frequency region, it can be seen that the dielectric constant decreases tremendously and becomes frequency independent. The charge carriers become hard to be translated and the dipoles in the polymer chain becoming hard to be oriented to the direction of the applied field at this frequency region. The periodic reversal of the electric field occurs so fast that there is almost no excess ion diffusion in the direction of the field (Jayathilaka et al., 2003).

Dielectric loss, *ε''* versus log *f* plot is presented in *Figure 4.8*. The ions and the dipoles carry the effect of inertia inside the polymer matrix. Both the ion translational diffusion and dipole orientation undergo a process of deceleration, stop and acceleration in reverse direction. This would causes internal friction to happen and these frictions produces heat, which would lead to loss of energy. A huge amount of energy would be dissipated and gone out of the phase with the electric field. As more salt is added, more charge carriers are generated and these charge carriers increase the energy dissipation rate until it reaches the optimal point at 30 wt.% of KI. The dielectric loss then reduces after the optimal point due to the re-association of the ion to become neutral pair as discussed previously (Howell & Bose, 2007).

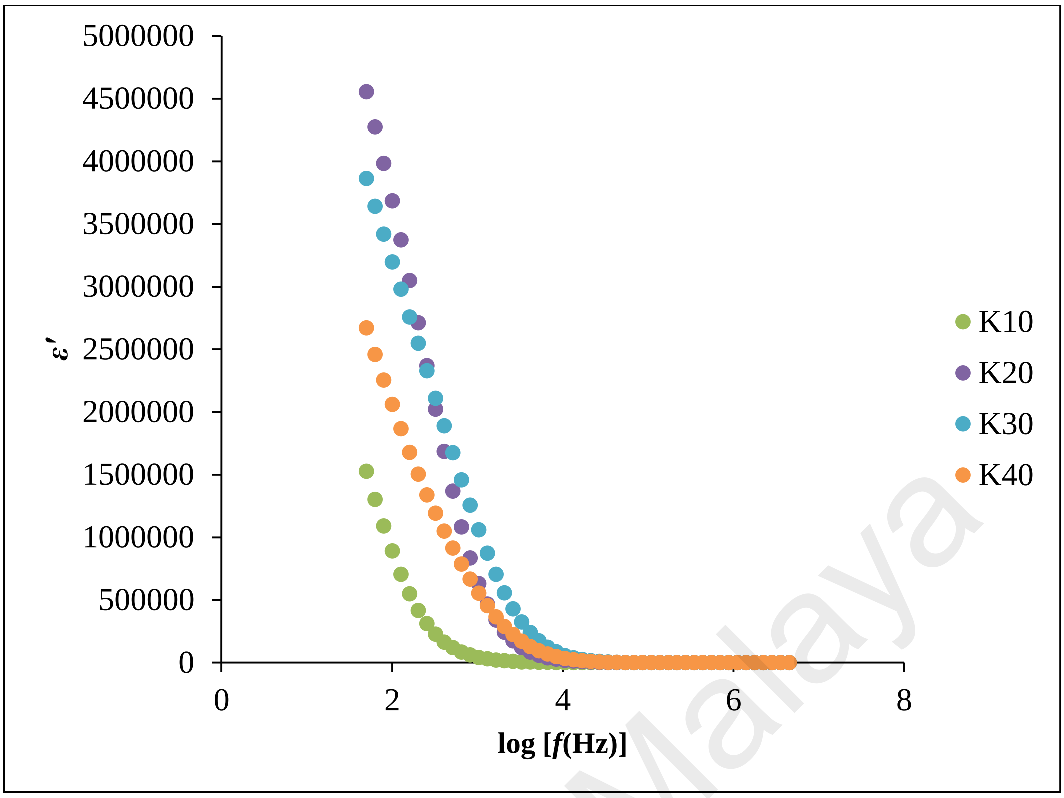

Figure 4.7: Variation of real part of dielectric constant, ε' with frequency for sample K10, K20, K30, K40

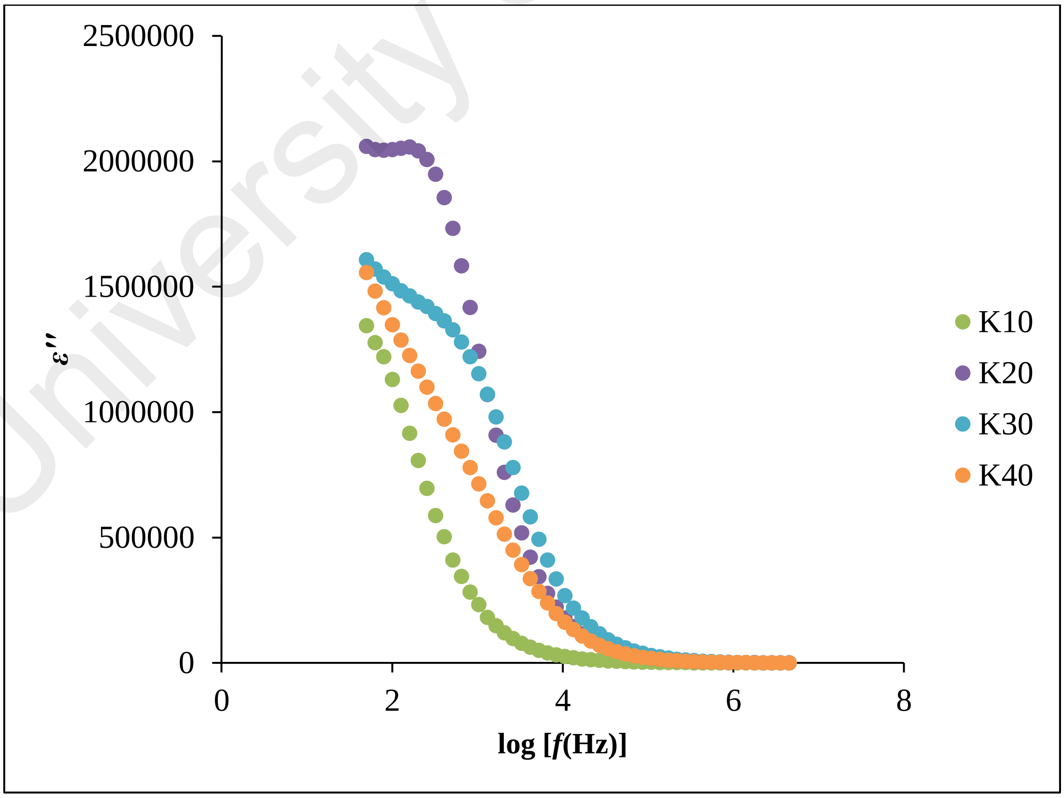

Figure 4.8: Variation of real part of dielectric loss, ε'' with frequency for sample K10, K20, K30, K40

4.2.3.3 Modulus Studies

The relationship between electric modulus, relative permittivity and impedance are given in the equation below (Avakian, Starkweather, & Kampert, 2002):

$$M^* = M' + jM'' = 1/\varepsilon^*_r = 1/(\varepsilon' - j\varepsilon'') = \varepsilon'/(\varepsilon'^2 + \varepsilon''^2) + \varepsilon''/(\varepsilon'^2 + \varepsilon''^2) \qquad (4.5)$$

$$M^* = j\omega C_0 Z^* = \omega C_0 Z'' + j\omega C_0 Z' \qquad (4.6)$$

The reciprocal of complex relative permittivity can be defined as electric modulus. Electric modulus is particularly useful to analyze the electrical relaxation processes. The inversion process is able to suppress the electrode polarization effect at low frequencies and enhance small features at high frequencies as ε' contributes as the denominator to the second power in the loss function. The variation of the real (M’) and imaginary (M”) parts of the modulus as a function of frequency are shown in *Figure 4.9* and *Figure 4.10* respectively. As observed in *Figure 4.9*, M’ of every samples was seen approaching zero at low frequency and a long tail can be seen in the figure. The long tail can be explained by the large capacitance related with the electrode polarization. This shows that the electrode polarization phenomena in these GPEs may be negligible. In the high frequency regions, a sigmoidal shape spectra is expected but in the figure, the spectra shown are shifted to the right to even higher frequency window. Thus, only the dispersion part of the electric modulus can be seen. The variation of the dispersion, as can be seen in the inset figure, shows that the dispersion are the reverse of the conductivity trend where the M’ is lower when the ionic conductivity is higher. Similar variation of the spectra for M” can be seen in *Figure 4.10*, the peaks are shifted to the higher region of the frequency with shorter relaxation time as expected as inset figure is showing the same variation of the dispersion as mentioned before as well. These spectra are expected to have a well-defined resonance peak at high frequency region. Conductivity relaxation can be explained as follows. An ion usually is able to have more than one equilibrium site of same potential energies. It can be separated by a potential barrier. By using their own natural jump frequency, these ions can move to its adjacent sites. However, when the external field is comparable to this frequency, the maximum energy was transferred. This maximum energy results in resonance effects and thus, the conductivity relaxation (Sudhakar, Selvakumar, & Bhat, 2014).

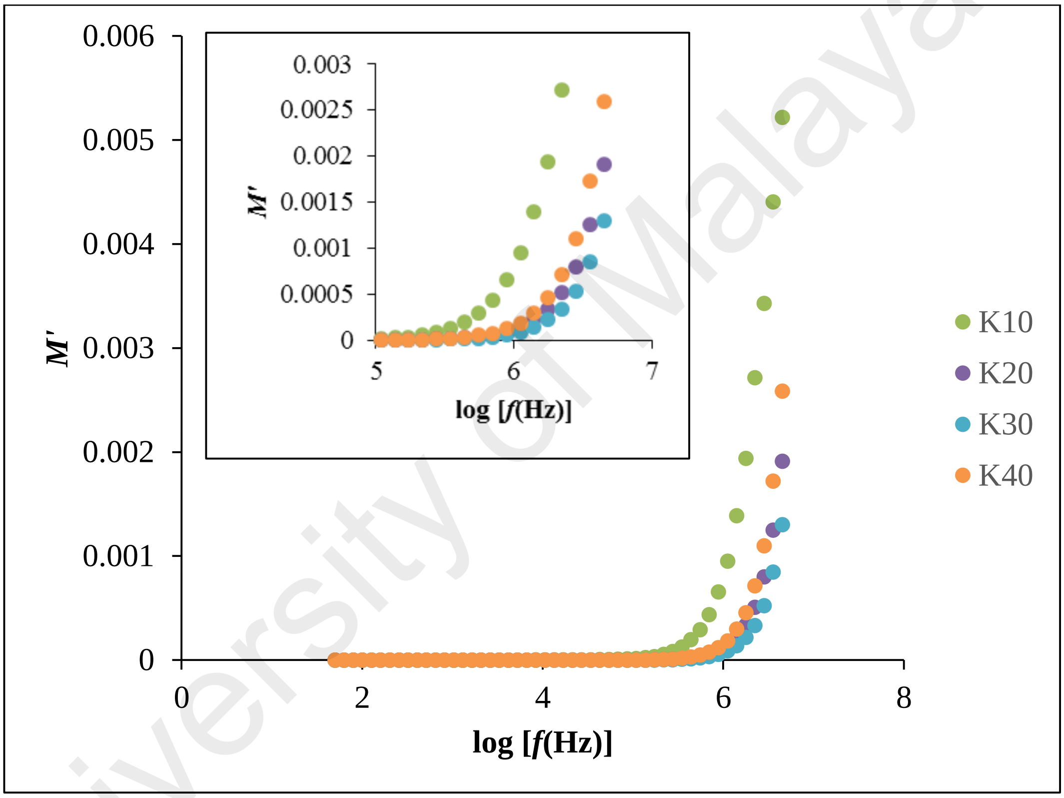

Figure 4.9: The real part of modulus, M' as a function of frequency for K10, K20, K30, and K40.

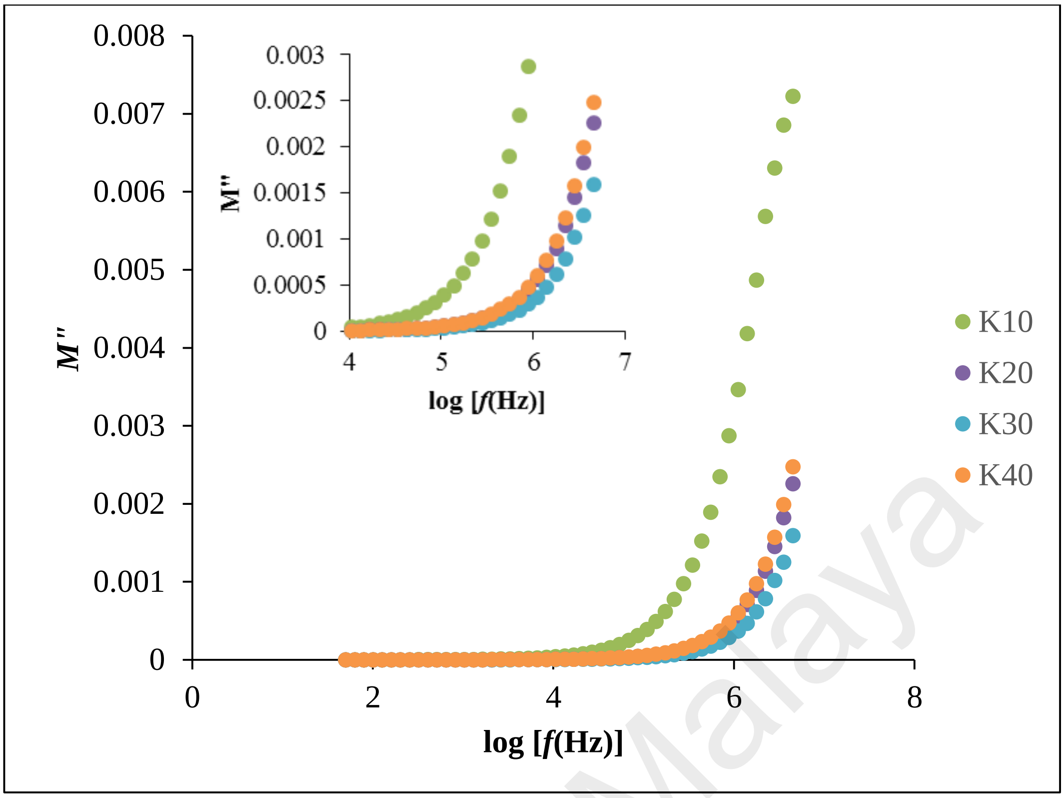

Figure 4.10: The imaginary part of modulus, M" as a function of frequency for K10, K20, K30, and K40.

4.2.4 FTIR studies

FTIR spectroscopy is a powerful diverse molecular spectroscopy and chemical analysis method used to investigate the natural molecular bonding and different functional groups which presents in the samples just be monitoring the vibrational energy levels of molecules. Different molecules would have their own unique fingerprint which can be seen in different vibrational energy levels. In this studies, the FTIR spectroscopy is used to investigate and confirm the occurrence of the degrees of co-ordination or complexation between the materials. It can be confirmed by comparing the changes that can be seen in the FTIR spectra after the addition of different materials into a certain system. The changes could also be varying with the different concentration added into the system (Selvasekarapandian, Baskaran, Kamishima, Kawamura, & Hattori, 2006).

The FTIR spectra for pure P(VP-co-VAc), pure KI, and the P(VP-co-VAc)-KI GPE samples are shown in *Figure 4.11*. The main absorption band of P(VP-co-VAc) were summarized and tabulated in *Table 4.3*. The FTIR Spectra of the carbonyl (C=O) stretching region for samples K10 to K40 are shown in *Figure 4.18(a)* and *Figure 4.18(b)***.** The strong band of C=O stretching of PVAc and PVP region was shown in the spectra in the region of 1750 cm^{-1} to 1710 cm^{-1} and 1690 cm^{-1} to 1630 cm^{-1}, respectively. It can be observed that the bands were shifted to higher wavenumber for the band in *Figure 4.12(a)*. As for the C=O stretching of PVP region (*Figure 4.12(b))*, it was observed that it is shifted to lower region with the addition of KI salts. These two occurrences show the complexation in the polymer matrix. These complexation was further proven in the XRD studies which would be shown after this. The shifting of the bands can also imply that the K$^+$ ions interact with the strong electron donor group C=O. Similar ion interactions with the carbonyl oxygen of polymers have been reported in literature (Wieczorek & Stevens, 1997).

The appearance of the band at 1230 cm^{-1} to 1260 cm^{-1} shown in *Figure 4.12(c)* corresponds to C-N stretching frequency of pure P(VP-co-VAc). It shifts to higher wavenumbers with the addition of salts. It is actually due to the interaction of I$^-$ ion from KI with the strong withdrawing character of the N atom of the C-N in the PVP chain (Ramya, Selvasekarapandian, Savitha, Hirankumar, & Angelo, 2007). The observed shift in the IR region is mostly due to the coordination of the cations and anions with the carbonyl (C=O) and N atom of C-N stretching and in this case, it can be assumed that the K$^+$ ion is able to interact with the oxygen atom of both PVP region and PVAc region while the I$^-$ ion is able to interact with the N atom of the C-N stretching in the PVP region.

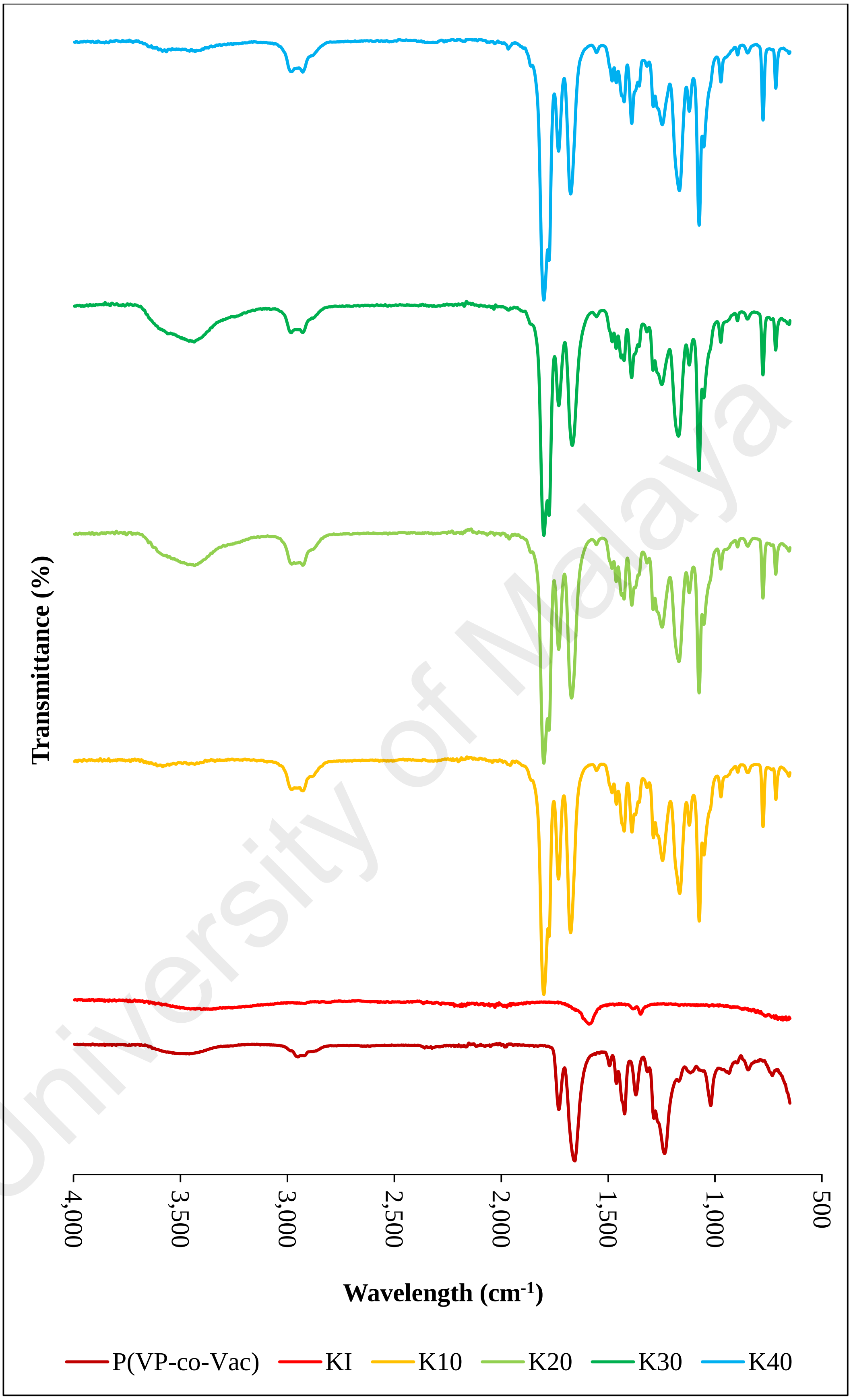

Figure 4.11: FTIR spectra for pure P(VP-co-VAc), pure KI and P(VP-co-VAc)-KI gel polymer electrolytes.

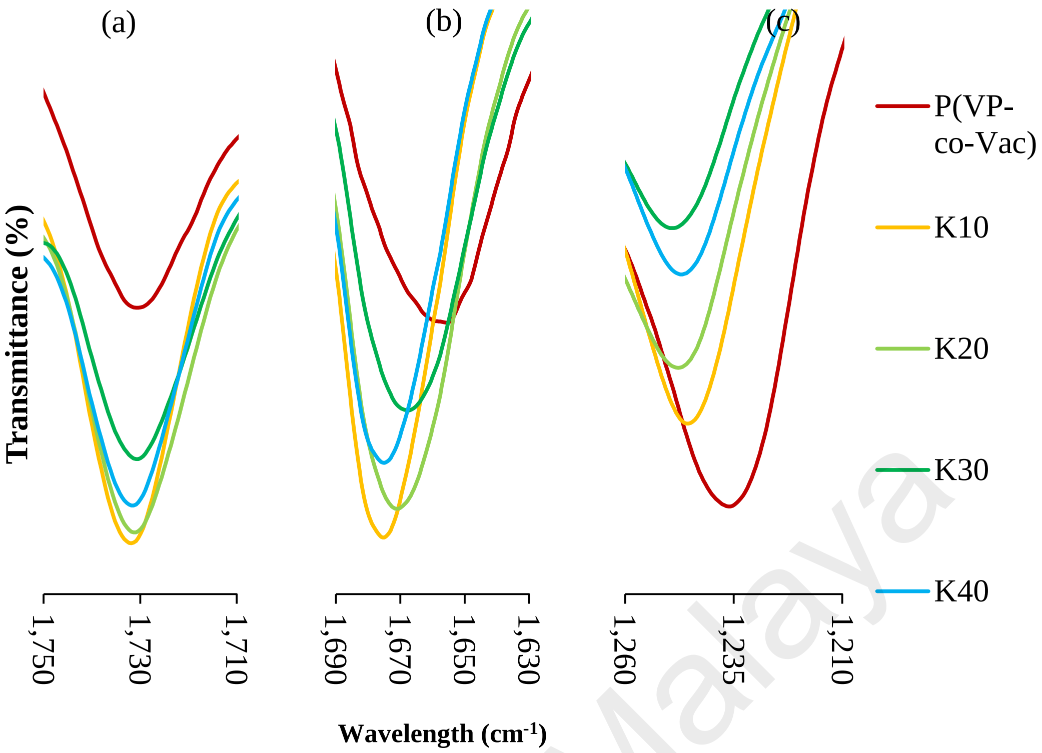

Figure 4.12: FTIR spectra in the region (a) 1750-1710 cm^{-1}, (b) 1700-1650 cm^{-1}, (c) 1260-1230 cm^{-1} for pure P(VP-co-VAc) and P(VP-co-VAc)-KI GPE samples.

Table 4.3: IR parameters for pure P(VP-co-VAc) co-polymer.

Respective bands	**Wavenumber (cm^{-1})**	**References**
O-H stretching	3600 – 3000	(Lee, Lin, Vittal, & Ho, 2011)
C-H stretching	3000 – 2800	(Lee et al., 2011)
C=O carbonyl group (PVAc)	1734	(Ulaganathan, Nithya, Rajendran, & Raghu, 2012)
C=O carbonyl group (PVP)	1677	(Ramya et al., 2007)
C-N stretching	1446	(Lee et al., 2011)
C-O-C stretching	1300 – 1000	(Kumar, Selvasekarapandian, Baskaran, Savitha, & Nithya, 2012)
C-H bending (PVAc)	1380	(Ulaganathan et al., 2012)
C-H wagging (PVAc)	775	(Ulaganathan et al., 2012)
C-H bending (PVP)	1433	(Ravi, Kiran Kumar, Madhu Mohan, & Narasimha Rao, 2014)
C-N stretching (PVP)	1247	(Ravi et al., 2011)
C-CH_2 stretching (PVP)	1171	(Ravi et al., 2011)
C-C stretching (PVP)	972	(Ravi et al., 2011)
CH_2 bending (PVP)	846	(Ramya, Selvasekarapandian, Hirankumar, Savitha, & Angelo, 2008)

4.2.5 X-ray diffraction (XRD) studies

XRD studies provides a wide range of information on crystal structure, crystal orientation, crystallinity, crystallite size and phase changes of material which are characterized by the presence of sharp diffraction rings of peaks. In amorphous materials, there is no long-range order present, however, the non-crystalline samples are characterized by one or two broad halos. For the present case, the X-ray diffraction method has been used to identify the following:

(a) Amorphous, crystalline or semicrystalline nature of material.
(b) Complexation of the samples
(c) Relative amorphicity of the films

XRD studies were performed for the pure P(VP-co-VAc), pure KI, sample O, K10, K30 and K40. The XRD patterns are shown in *Figure 4.13*. As observed, two broad characteristic peaks of P(VP-co-VAc) were obtained at angles of $2\theta = 11.9^o$ and $2\theta = 21.5^o$ which are attributed to the the overlapping of PVP and PVAc region, respectively reveal the amorphous phase of the P(VP-co-VAc) copolymer (Rajendran, Babu, & Sivakumar, 2007).

Pure KI in *Figure 4.13* illustrates sharp intense peaks at $2\theta = 26.8^o$, 34.0^o, 38.2^o and 51.9^o reveals the crystalline characteristic of the potassium iodide, KI (Rajendran et al., 2007). This crystalline peak appears to be disappeared in the P(VP-co-VAc)-KI based gel polymer electrolytes. The absence of this intense peaks actually indicates that the KI was fully complexed with the P(VP-co-VAc) copolymer. A complete dissolution could lead to a complexation between the P(VP-co-VAc) and KI and this has also been proven in the FTIR studies in *section 4.2.4* (Costa et al., 2007). The absence of the intense crystalline peaks and the appearance of the broad characteristic peaks once again show that the P(VP-co-VAc)-KI based gel polymer electrolyte were in amorphous region. The characteristic peaks found in 2θ = 21.5^o was found to be shifted to 2θ of 20.7^o for K10, to 21.0^o for K30, and to 21.2^o for K40. This shifting is also another way to confirm the complexation between the P(VP-co-VAc) and KI as it is reported by Sivakumar et. al. on their PVA-PMMA polymer and $LiBF_4$ salt (Sivakumar, Subadevi, Rajendran, Wu, & Lee, 2006). This complexation can be further confirmed based on the changes in the peak intensity of the gel polymer electrolytes. As observed in the figure, the characteristic peak intensity actually decrease upon the addition of KI up to 30 wt.% and then slightly increases at 40 wt.% of KI. It is proved that the degree of crystallinity decreases and hence increase the amorphous region in the polymer electrolytes which could leads to an increase in the ionic conductivity and in this case it is in agreement with the study of the ionic conductivity which has been discussed previously.

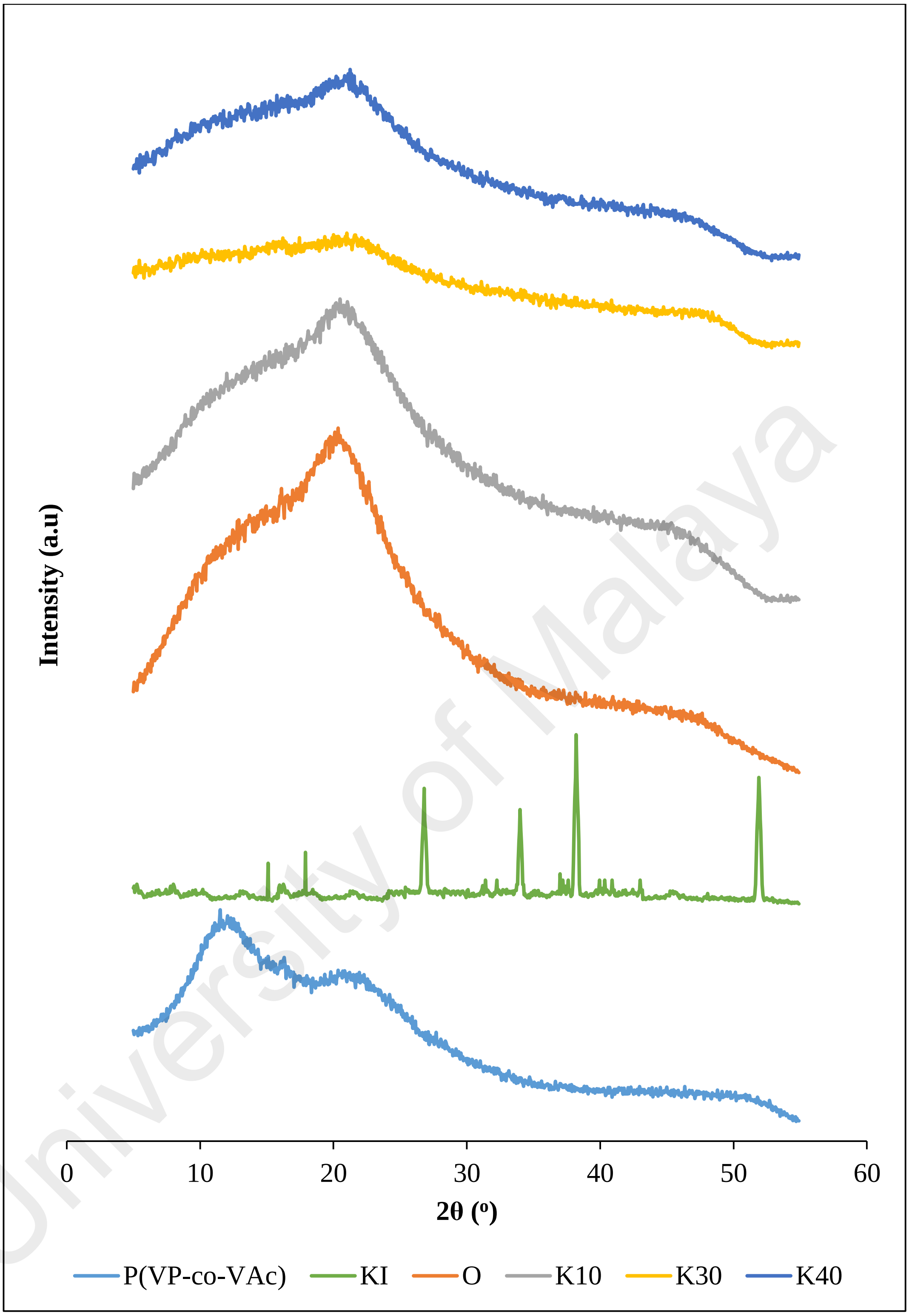

Figure 4.13: XRD patterns of the pure P(VP-co-VAc), pure KI, sample O, K10, K30 and K40.

4.2.6 Thermogravimetric analysis (TGA)

Thermogravimetric analysis (TGA) is a technique of thermal study in which changes in physical and chemical properties of samples are measured as a function of increasing temperature with constant heating rate, or as a function of time with constant temperature and/or constant mass loss. TGA is commonly used to determine the polymer degradation temperature, residual solvent levels, absorbed moisture content, and the amount of material composition inside the polymer electrolytes.

Thermogravimetric analysis of the pure P(VP-co-VAc), pure KI, sample O, K10, K20, K30, and K40 was investigated at a heating rate of 50.00 ℃/min under nitrogen atmosphere and shown in *Figure 4.14*. In every P(VP-co-VAc)-KI gel polymer electrolyte samples, 2 – 6 wt.% of small mass loss was observed in the range 30 ℃ - 100 ℃ . This was attributed to evaporation of low molecular weight substances such as the moisture adsorbed and minor impurities. Meanwhile, the mass loss that can be seen at 100 ℃ - 200 ℃ is attributed to the evaporations of the solvents EC and PC as well as the small amount of iodine added into the polymer matrix. Interestingly, in these P(VP-co-VAc)-KI GPE samples, the EC and PC were found to evaporate at temperature lower than their initial high boiling point. Similar occurrence also has been reported in previous studies (K.-S. Kim, Park, Yeon, & Lee, 2005). *Figure 4.14* shows the thermogravimetric curves of pure P(VP-co-VAc) and GPE samples and the summarized degradation temperature and weight loss are tabulated in *Table 4.4*.

Pure P(VP-co-VAc) had two stage of degradation which can be seen at T_{max1}= 300 ℃ and T_{max2} = 385 ℃. These two stages correspond to the degradation of vinyl acetate, PVAc (25.5% of weight loss) and vinylpyrrolidone, PVP (62.7% of weight loss), respectively. These results are in agreement with the literature which describes that PVAc suffers deacetylation in the temperature range 160 ℃ - 400 ℃ (Bianco et al., 2003) and that degradation of PVP occurs in the temperature range 380 ℃ - 530 ℃ (McNeill, Ahmed, & Memetea, 1995). It was observed that with the increasing amount of KI in the system, T_{max1} is decreasing. This shows that the PVAc region in the GPEs samples suffers decrease in thermal stability upon addition of salt. In contrast, it is observed that PVP region for all the GPEs are increasing in thermal stability and it can also be observed that the degradation temperature of the PVP region is increasing as more KI salts added into the polymer electrolytes. These observations can be supported by the weight loss at both regions where it can be seen that with the increasing amount of KI salt, it increases the weight loss of the PVAc region and decreases the weight loss of the PVP region. These occurrences might be due to the complexation which has occurred inside the polymer matrix as shown previously in the FTIR and XRD studies. The weight loss at 700 ℃ - 800 ℃ corresponded to the degradation of the KI (Zaccaron, Oliveira, Guiotoku, Pires, & Soldi, 2005).

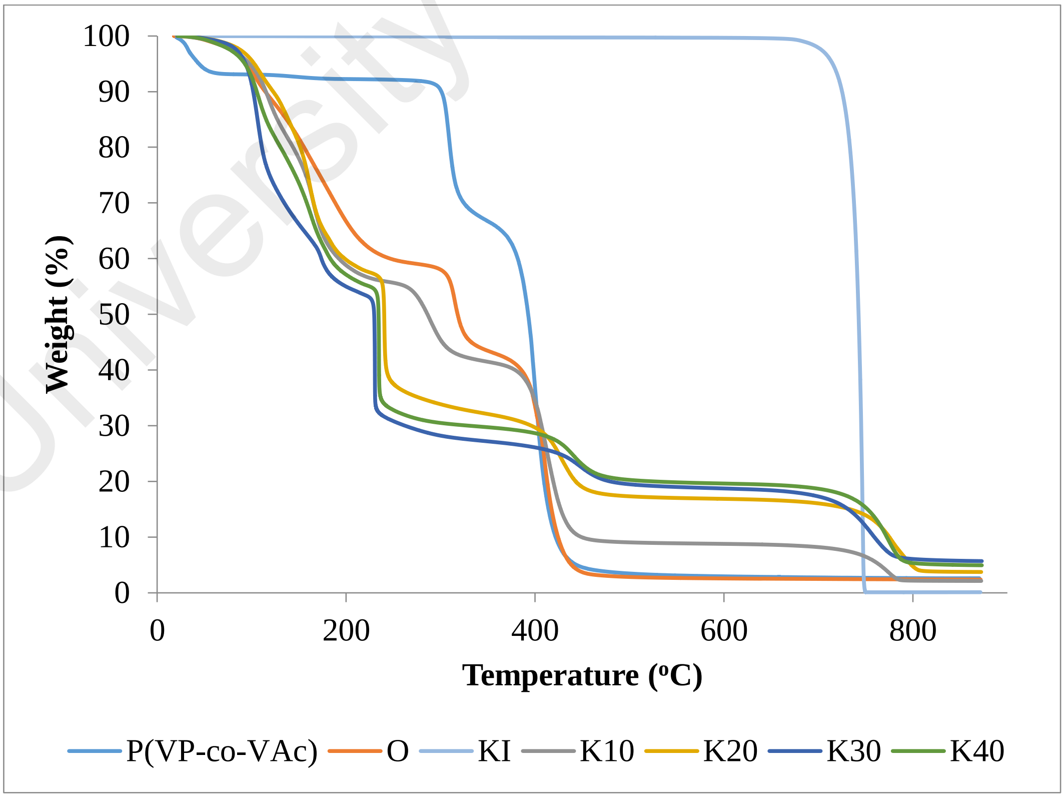

Figure 4.14: Thermogravimetric analysis of pure P(VP-co-VAc), sample O and the P(VP-co-VAc)-KI GPE samples.

Table 4.4: The degradation temperature of the pure P(VP-co-VAc), sample O and the P(VP-co-VAc)-KI GPE samples.

Samples	**T_{max1} (ºC)**	**T_{max2} (ºC)**
P(VP-co-VAc)	310	385
O	314	411
K10	287	412
K20	240	426
K30	234	440
K40	230	444

4.2.7 Photocurrent density-voltage (J-V) Characteristics

Figure 4.15 shows the photocurrent density-voltage (J-V) curves for the DSSCs with samples K10 to K40. Sample O was not tested as it is expected to have poor results because there was no iodide ions present and there is no redox couple added. The values of the open-circuit voltage (V_{oc}), short-circuit current density (J_{sc}), fill factor (FF) and conversion efficiency (η) were obtained, summarized and tabulated in *Table 4.5*. *Figure 4.16* shows the normalized variation of the normalized J_{sc}, V_{oc}, FF and photovoltaic efficiency of the GPE samples with different concentration of the KI salt added. It can be seen that the trend of the photovoltaic efficiency is similar to short-circuit current density, J_{sc}. Meanwhile, if one compared the trend of the J_{sc} with the ionic conductivity, it can be observed that the trends are similar as well. This shows that J_{sc} plays an important role in the variation of the photovoltaic performances for these GPE samples. J_{sc} value is basically directly related to the mobility of the mobile charge carriers which is similar to the ionic conducting mechanism (Cha, Lee, Kang, & Kang, 2010). The increase in the mobility of the charge carriers improves the diffusion ability of the triiodide, I_3^- and when the diffusion coefficient increases, it increases the regeneration ability of the dye molecules and thus, increases the photovoltaic performance (Lin et al., 2014). The highest photovoltaic conversion efficiency that was achieved in this system is 2.94% with J_{sc} of 8.05 mA cm^{-2}, V_{oc} of 0.58 V and fill factor of 63%. The variation of the normalized current density of the DSSC under different illumination condition were measured and shown in the inset of *Figure 4.17*. The linear shape of the curve in the figure proves that no mobile ions and electron transport occurring at the Pt and electrode interface that could represent the rate-determining steps in the photo-electrochemical process (Chiappone et al., 2014).

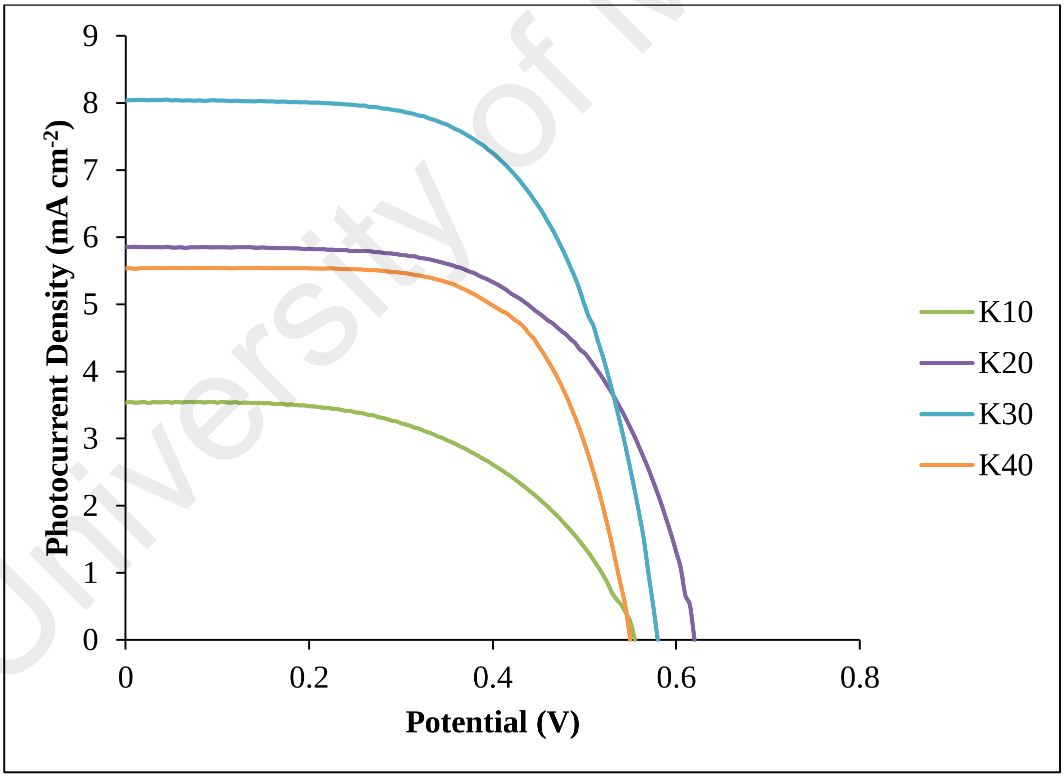

Figure 4.15: The photocurrent-photovoltage (J-V) characteristics of the GPE samples consisting of different weight percentages of KI.

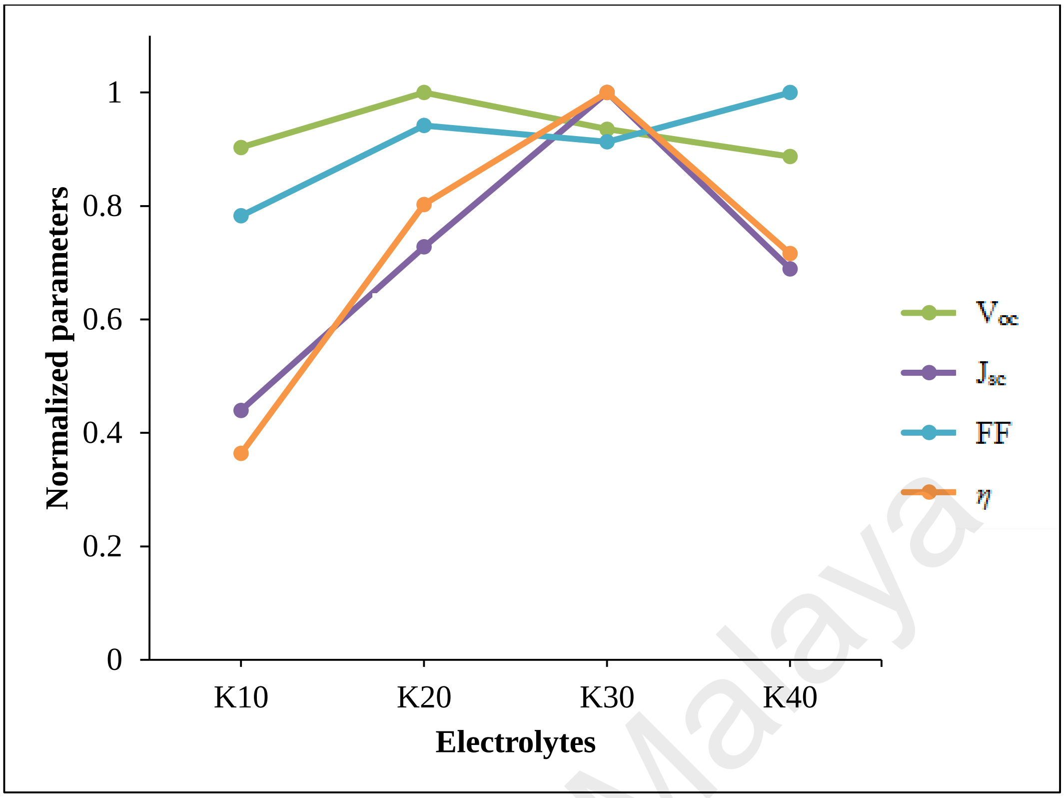

Figure 4.16: The normalization curves of the various performance parameters of the DSSCs fabricated with different P(VP-co-VAc)-KI GPE samples.

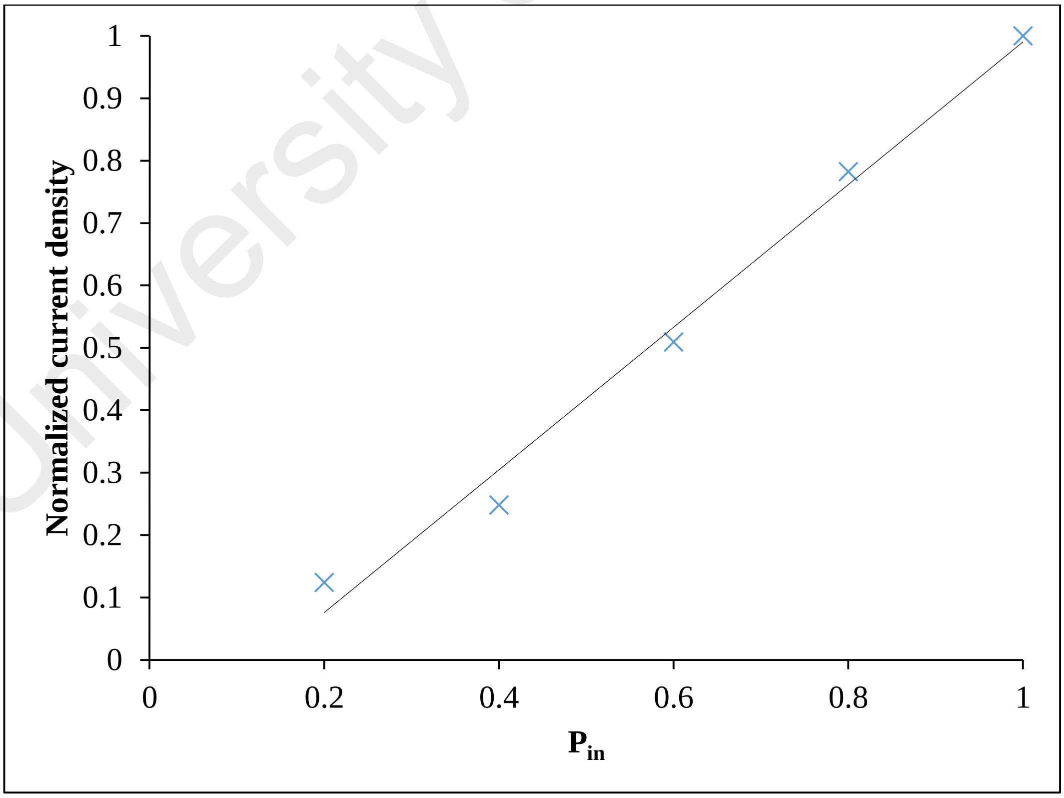

Figure 4.17: Normalized J_{sc} values plotted as a function of different light intensities (P_{in}) for sample K30.

Table 4.5: Photovoltaic parameters of the GPE samples consisted of different weight percentages of KI.

Electrolytes	V_{oc} (V)	J_{sc} (mA cm^{-2})	FF (%)	η (%)
K10	0.56	3.54	0.54	1.07
K20	0.62	5.86	0.65	2.36
K30	0.58	8.05	0.63	2.94
K40	0.55	5.55	0.69	2.11

4.2.8 EIS studies for DSSCs

In order to investigate the impedance behavior of the DSSCs fabricated with our gel polymer electrolytes, the EIS data of the DSSCs assembled with the samples from P(VP-co-VAc)-KI gel polymer electrolytes system were collected, and the results shown in *Figure 4.18(a)*. The data have been fitted and the equivalent circuits used to fit the data are depicted in *Figure 4.19*. The parameters of the equivalent circuit for both of the DSSCs were tabulated in *Table 4.6*. In *Figure 4.23(a)*, it can be seen that there are two semi circles can be observed in the EIS spectra. At the high frequency region, the first semicircle found was corresponded to the charge transfer resistance at the Pt counter electrode. Meanwhile, at middle frequency, the semicircle corresponded to the charge resistance of the charge recombination between TiO_2 conduction band and I_3^- ions at TiO_2/dye/electrolyte interface. The spike below the 5 Hz is corresponded to the Warburg parameter, Y_0 ($S^{1/2}$ Ω^{-1}) (Hieu et al., 2014). The intersection of the high frequency first semicircle and the x-axis as labeled in the figure is corresponded to the sheet resistance of the FTO substrate and it is also named as the ohmic serial resistance (R_s). Meanwhile, the first and second semicircles were named as R_{ct1} and R_{ct2}, respectively (Ke et al., 2014).

As shown in *Table 4.6*, R_{ct2} was found to be highest for sample K20 with a value of 18.7 Ω, followed by K30 and then K10 with the value of 12.4 Ω and 12.0 Ω, respectively.

The lowest value of R_{ct2} was found to be for sample K40 with the value of 11.1 Ω. The V_{oc} is reported to be related to the rate of the recombination process of the electrolytes in the DSSCs where lower charge recombination rate of the samples would lead to lower V_{oc} value. With the increase of R_{ct2}, the recombination reactions at the TiO_2/electrolyte interfaces decreases due to the electrical double layer which might have suppressed the recombination reaction between the free electron the I_3^- (Sharma, Daphnomili, Angaridis, Biswas, & Coutsolelos, 2013). This agrees well with the J-V data where sample with high R_{ct2} would have higher V_{oc}. *Figure 4.20* shows the relation between the R_{ct2} and V_{oc} of the sample and they found to have a similar trend.

On the other hand, the Bode EIS spectra of the DSSCs fabricated with the P(VP-co-VAc)-KI gel polymer electrolytes system were shown in *Figure 4.18(b)*. The important region that we were going to look into is the middle frequency region as the character frequency in this region is inversely proportional to the electron lifetime according to the EIS theory. The required time for the I_3^- reduction can be calculated with the following equation (Hoshikawa, Ikebe, Kikuchi, & Eguchi, 2006):

$$\tau = \frac{1}{f_p} \tag{4.7}$$

where f_p is the peak frequency at high frequency and τ is the characteristic time for I_3^- reduction. Normally, sample with low charge recombination rate would have higher electron lifetime and the result is in agreement with the EIS data that were collected previously.

Tafel polarization measurements were performed to explore the electrocatalytic activity and interfacial charge-transfer properties of the I^-/I_3^- redox couples on the gel polymer electrolytes. The current density (J) as a function of potential (V) for the reduction of I_3^- ions is shown in *Figure 4.21*. The diffusion coefficient (D_n) is depicted by the following equations (Mingkui Wang et al., 2009):

$$D_n = \frac{d\ j_{\lim}}{2nFC} \tag{4.8}$$

where d is the cell gap, n is the number of electrons, F is the Faraday constant and C is the initial concentration of I_3^- ions. The limited diffusion current density, J_{lim} which is dependent on the diffusion coefficient (D_n) of the I^-/I_3^- couples in electrolyte can be obtained from the intersection of the cathodic branch with the Y-axis. As observed from the Tafel curves, the J_{lim} of K30 was found to be highest following by K20, then K40 and K10. The increase in J_{lim} generically shows that there would be increase in the diffusion kinetics for I^-/I_3^- redox species in the GPEs (Mingkui Wang et al., 2009). On the other hand, the larger slope for the anodic or cathodic branch of the Tafel curve indicates the exchange current density (j_0) and it can be associated with the R_{ct2} by the following equation :

$$j_0 = \frac{RT}{nFR_{ct}} \tag{4.9}$$

where R is the universal gas constant and T is the absolute temperature. These results show that Tafel polarization studies matches well with the EIS studies. Apparently, the calculated slope for J_0 is following the trend as: K20>K30>K10>K40 which is in agreement with the previous EIS studies of the DSSCs (C. Wu et al., 2012).

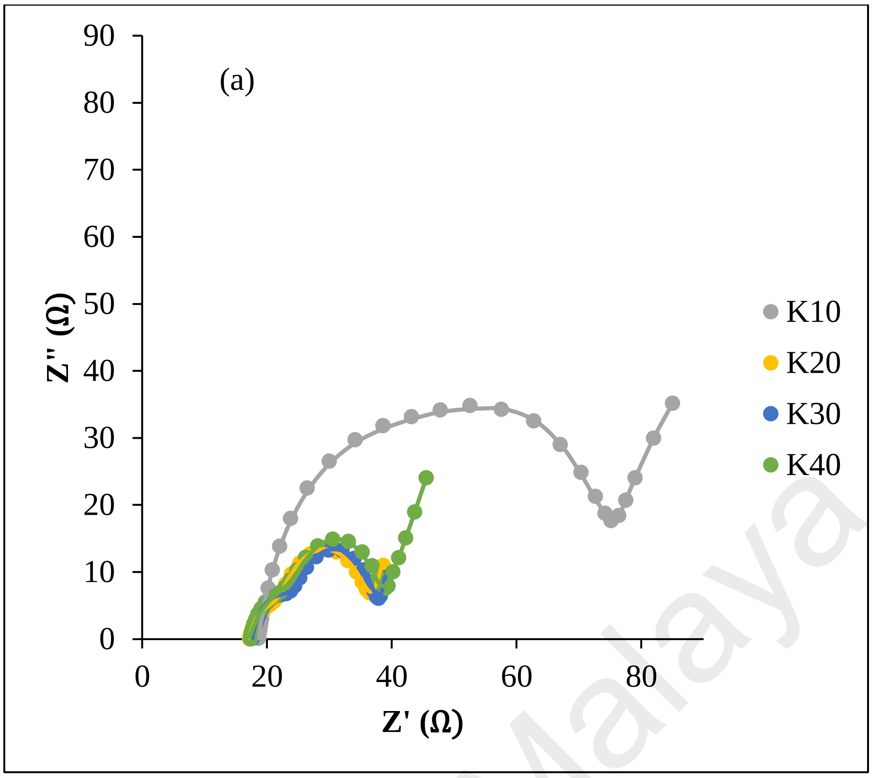

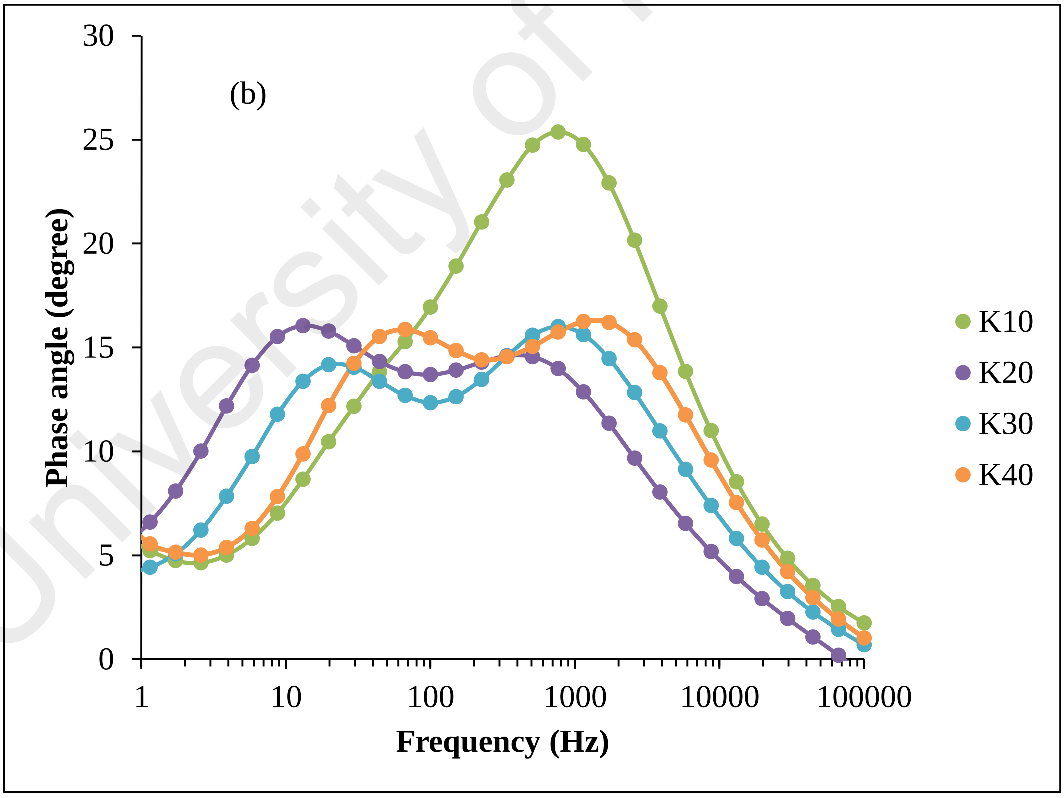

Figure 4.18: The electrochemical impedance spectra of DSSCs assembled with P(VP-co-VAc)-KI GPE samples in the forms of (a) Nyquist plots and (b) Bode phase plots (b). The spectra were measured under 100 mW cm^{-2} illuminated sunlight.

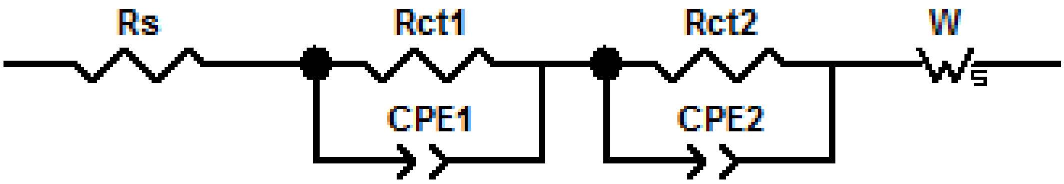

Figure 4.19: The equivalent circuits used to fit the data of the DSSCs.

Table 4.6: The parameters of the equivalent circuits used to fit the EIS impedance data of the P(VP-co-VAc)-KI based DSSCs.

Electrolytes	R_s (Ω)	R_{ct1}(Ω)	R_{ct2}(Ω)	W($S^{1/2}$ Ω^{-1})	τ (ms)
K10	16.9	11.7	12.0	0.46	42.1
K20	16.6	15.8	18.7	0.68	78.0
K30	18.0	9.2	12.4	0.80	61.7
K40	13.8	6.3	11.1	0.40	29.5

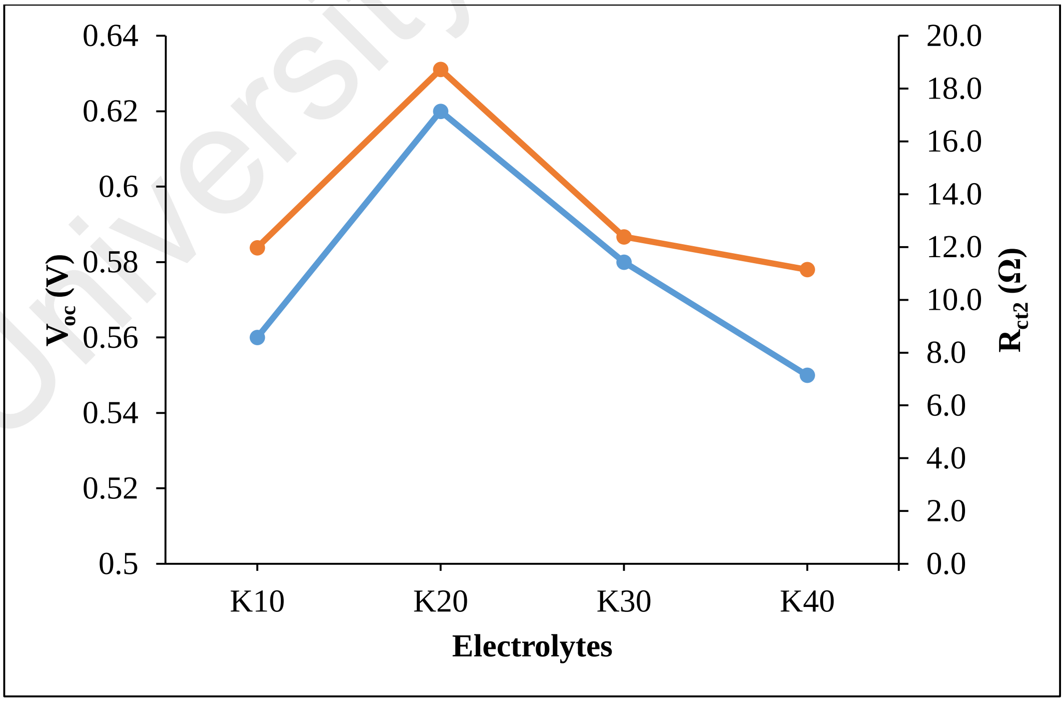

Figure 4.20: The open circuit voltage and R_{ct2} with the respect of different KI concentration in P(VP-co-VAc)-KI GPE samples.

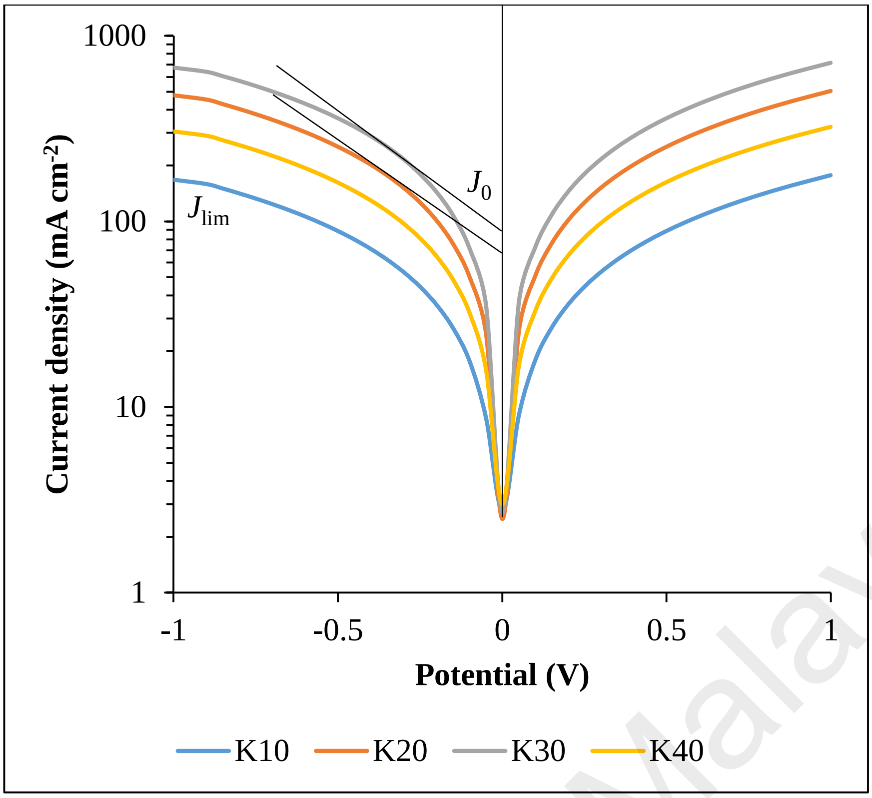

Figure 4.21: Tafel polarization curves of symmetric Pt cells with P(VP-co-VAc)-KI gel polymer electrolytes samples

4.3 P(VP-co-VAc)-TPAI Gel Polymer Electrolytes

4.3.1 Ambient Temperature-Ionic Conductivities Studies

Figure 4.22 shows the cole-cole plots of all gel polymer electrolytes samples for this system (T10-T40). These GPE samples only have a single spike type shape of curve over the entire experimental frequency range. Such behavior of Z” vs Z’ plots normally shows that the current carriers in the system are the mobile ions that were controlling the entire total electrical conductivity of these electrolytes. In addition, a single spike shape also indicates that there are formation of good contacts at the interface of the electrodes and the polymer electrolytes (Sengwa & Choudhary, 2014).

The ionic conductivity (σ) is calculated with *equation 3.4* which has been explained previously. The calculated values are shown in *Table 4.3*. The ionic conductivity with the variation of TPAI concentration is shown in *Figure 4.23*. As mentioned previously, the ionic conductivity is directly related to the number of charge carriers inside the polymer matrix. Same phenomenon can be observed in this system and it is proven in *Figure 4.7* where there is increase of the ionic conductivity when huge amounts of the mobile ions were generated by the TPAI salt (<30 wt.%). Beyond the optimum point, in this system it would be TPAI more than 30 wt.%, it can be observed that the ionic conductivity is decreases. This is due to the reason that the system just cannot utilize any of the excess mobile ions anymore beyond the maximum threshold and this excess mobile ions will start to clump together and forming neutral pairs as explained in *section 2.4.3.4*. This phenomenon hindered the mobility of the mobile charge carriers inside the polymer matrix and thus, reduces the ionic conductivity(Prasanth, Shubha, Hng, & Srinivasan, 2012). The highest ionic conductivity that could be obtained for the GPE samples is 1.60×10^{-3} S cm^{-1}.

Table 4.7: Ionic conductivity values for the P(VP-co-VAc)-TPAI GPE samples at room temperature.

Electrolytes	Ionic Conductivity (mS cm^{-1})
O	4×10^{-4}
T10	0.43
T20	0.89
T30	1.60
T40	0.86

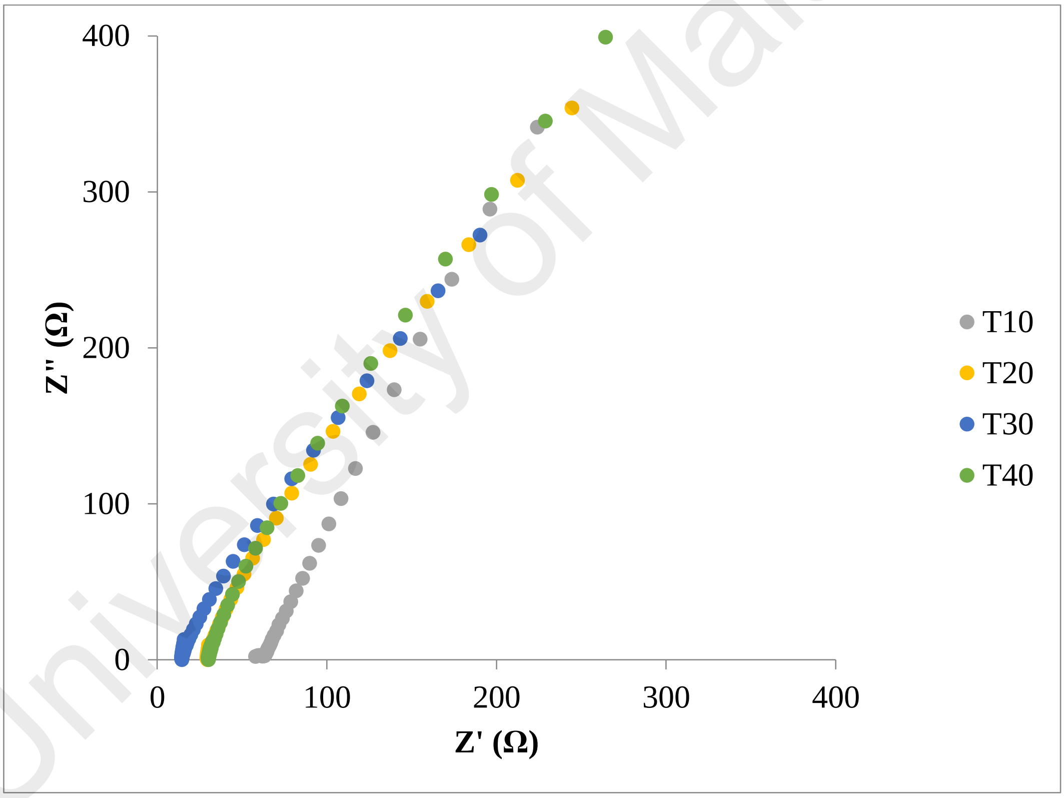

Figure 4.22: Typical complex impedance plot of P(VP-co-VAc)-TPAI GPE samples at room temperature.

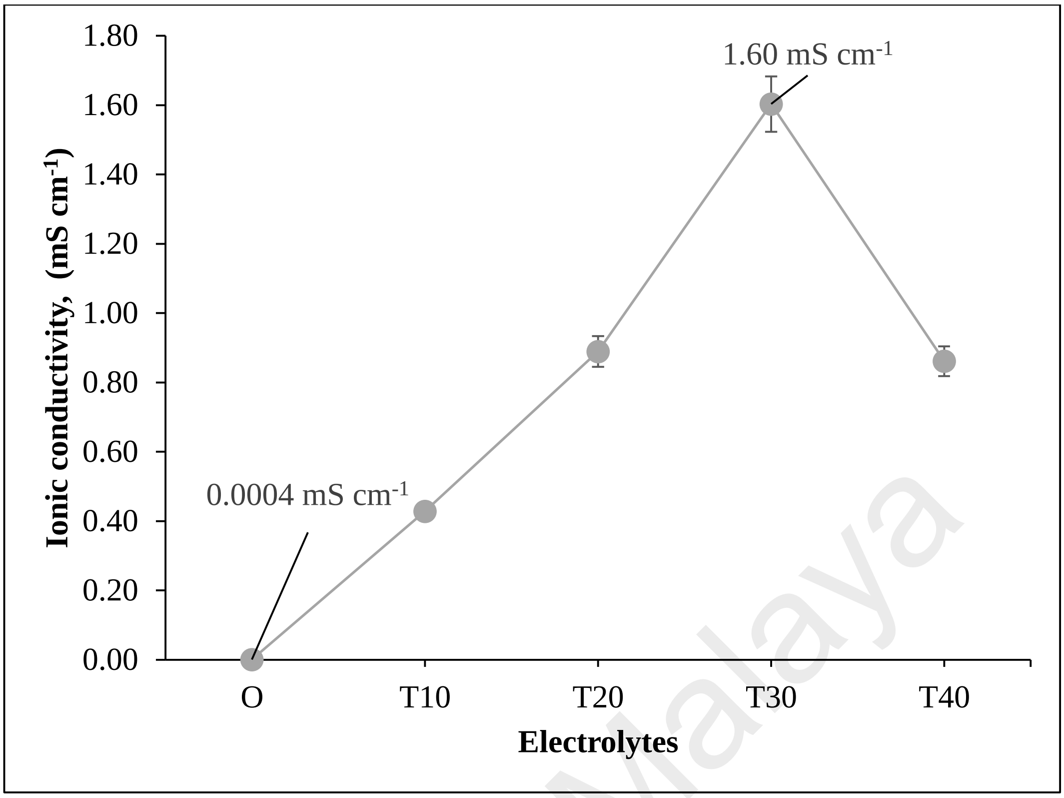

Figure 4.23: Variation of ionic conductivity of the GPE samples with different TPAI concentration at room temperature.

4.3.2 Temperature dependence-Ionic conductivity studies

The obtained ionic conductivities at different temperature for the GPE samples were plotted against temperature in the form of Arrhenius plot as shown in *Figure 4.24*. As expected from single salt system, the linearity of the shape reveal that the ionic conduction mechanism of the GPE samples obey the Arrhenius theory (Dissanayake et al., 2012).

This implies that with an increase of the temperature applied to the GPE samples, the chances of the mobile ion of the GPEs jumping into another site are increasing due to more energy being provided by the increasing temperature. The activation energy (E_a) was determined by calculating the slope of each respective graph in *Figure 4.24*. As mentioned previously, the activation energy is the minimum energy that is required by the ions to hop from one coordination to another coordination. Thus, GPEs with lower E_a

value will require lesser energy for the mobile ions to get excited and it will increase the frequency rate of ion hopping leading to higher ionic conductivity. The calculated E_a value for the samples with different concentration of the TPAI are summarized, tabulated and plotted in *Table 4.8* and *Figure 4.25* respectively. As expected, the values of the E_a and ionic conductivity have a trend of variation as explained previously where samples with lower activation energy had higher ionic conductivity(Zaccaron et al., 2005). The variation of the ionic conductivity and E_a was shown in *Figure 4.25.*

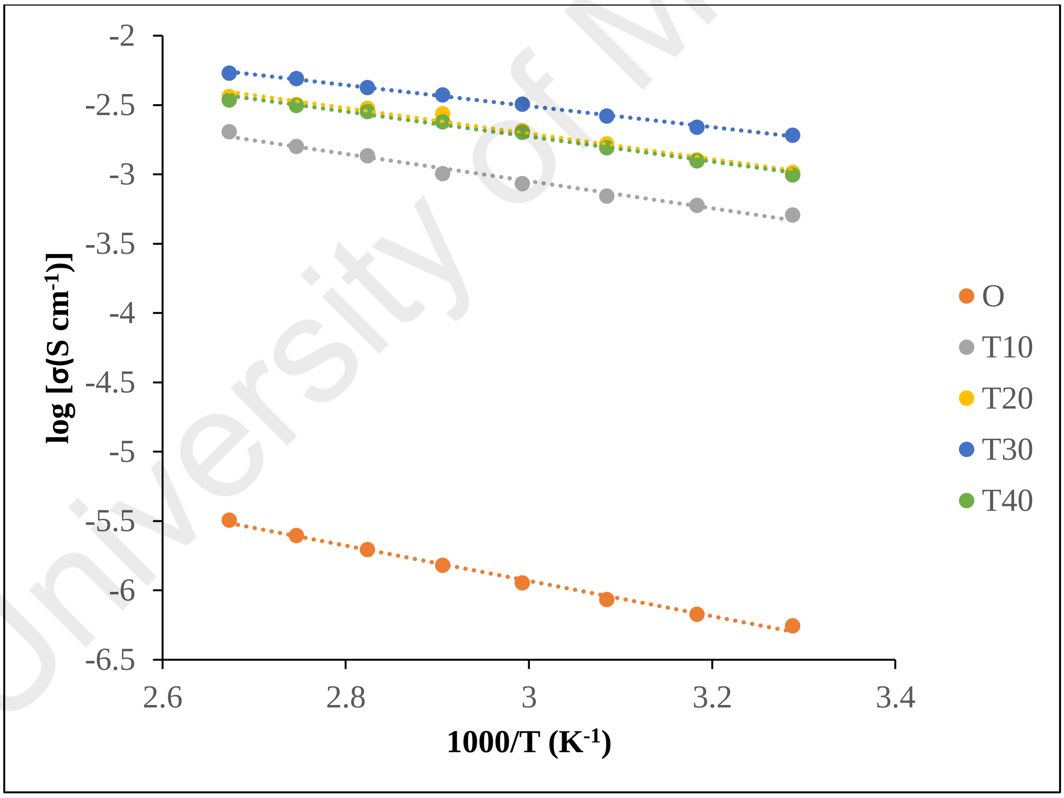

Figure 4.24: Arrhenius plots for the conductivity of the GPE samples with different concentration of TPAI.

Table 4.8: The activation energy of the GPEs sample with different concentration of TPAI

Electrolytes	E_a (kJ mol^{-1})
O	1.29
T10	0.96
T20	0.99
T30	0.65
T40	1.07

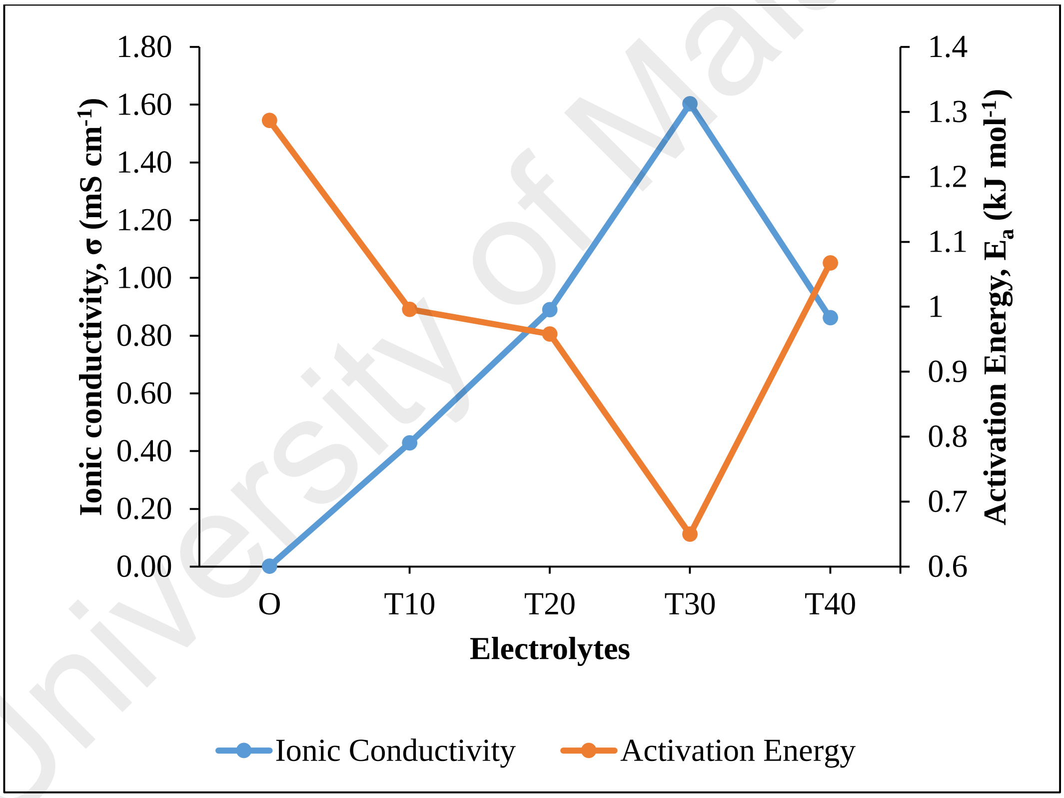

Figure 4.25: Variation of ionic conductivity and the activation energy of the P(VP-co-VAc)-TPAI GPE samples with different TPAI concentration at room temperature.

4.3.3 Dielectric Studies

4.3.3.1 Conductivity-frequency studies

The ionic conductivity of T10, T20, T30 and T40 were analyzed with the respect to frequency in order to monitor the relaxation processes of the gel polymer electrolytes with a bulkier type of salt, TPAI. The results were shown in *Figure 4.26*. Similar phenomenon can be observed compared to the KI single salt system gel polymer electrolytes. It was observed that there is also a deviation from the plateau region in the ionic conductivity in the lower frequency. This illustrates that the size of salts doesn't affects the changes of the relaxation processes of single salt system of P(VP-co-VAc) gel polymer electrolytes. The ionic conductivity is low when the frequency is low as well. They were found to be following the Maxwell Wagner-Sillars (MWS) effects. Just as mentioned previously, this is due to the interfacial impedance and the space charges polarization inside the gel polymer electrolytes. With the similar results that observed in the figure, it is also expected that the mobility of the mobile charge ions were moving effectively when high frequencies were applied (Dillip et al., 2009).

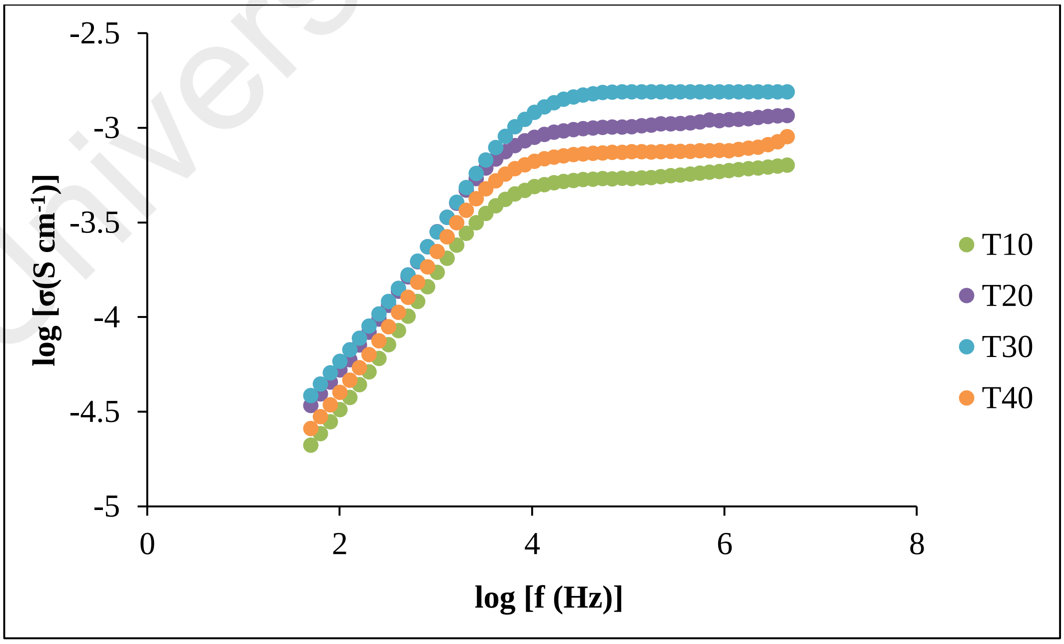

Figure 4.26: Frequency-dependent conductivity at various TPAI concentration of P(VP-co-VAc)-KI gel polymer electrolytes samples.

4.3.3.2 Dielectric Relaxation Studies

The complex permittivity which is the real part *ε'* and dielectric loss, *ε''* spectra of the GPE samples are shown in *Figure 4.27* and *Figure 4.28* respectively. The *ε'* values of the GPE samples are very large at lower frequency. This is probably caused by the dielectric polarization that happens at this frequency range. It has been explained previously, the mobile ions that usually move around in the polymer matrix under electric field are not able to cross the electrode and the electrolyte interface. It is due to the blocking electrodes that have blocked the mobile ions from moving into the external circuit which causes the mobile ions to accumulate at the interface of the electrode-electrolyte interface and form a hetero-charge layer (Raghu, Kilarkaje, Sanjeev, Nagaraja, & Devendrappa, 2014). At high frequency region, the mobile ions are facing difficulty to be able to orient themselves to the direction of the applied field and this causes a very fast periodic reversal of the electric field and leads to insufficient time for the charge to build up at the interface. Hence, the polarization due to the charge accumulation decreases leading to decrease in *ε'* (Raghu, Kilarkaje, Sanjeev, & Devendrappa, 2013). The dielectric loss, *ε''* versus the log *f* plot is presented in *Figure 4.28***.** The inflexion points that can be seen in the figure reflect that there is presence of highly complex molecular relaxation processes in the dynamical structures. The variation of the dielectric loss *ε''* for the samples at different frequency at room temperature can be seen that the *ε''* is decreasing with an increase of frequency. Inside these GPE samples, there is a lot of friction caused by the inertia motion of the mobile ions. Friction produces heat that will dissipate into loss of energy. Thus, at high frequency when the mobile ions are moving much faster, it could cause more friction and lead to decrease in the dielectric loss, *ε''* (Abo El Ata, Attia, & Meaz, 2004).

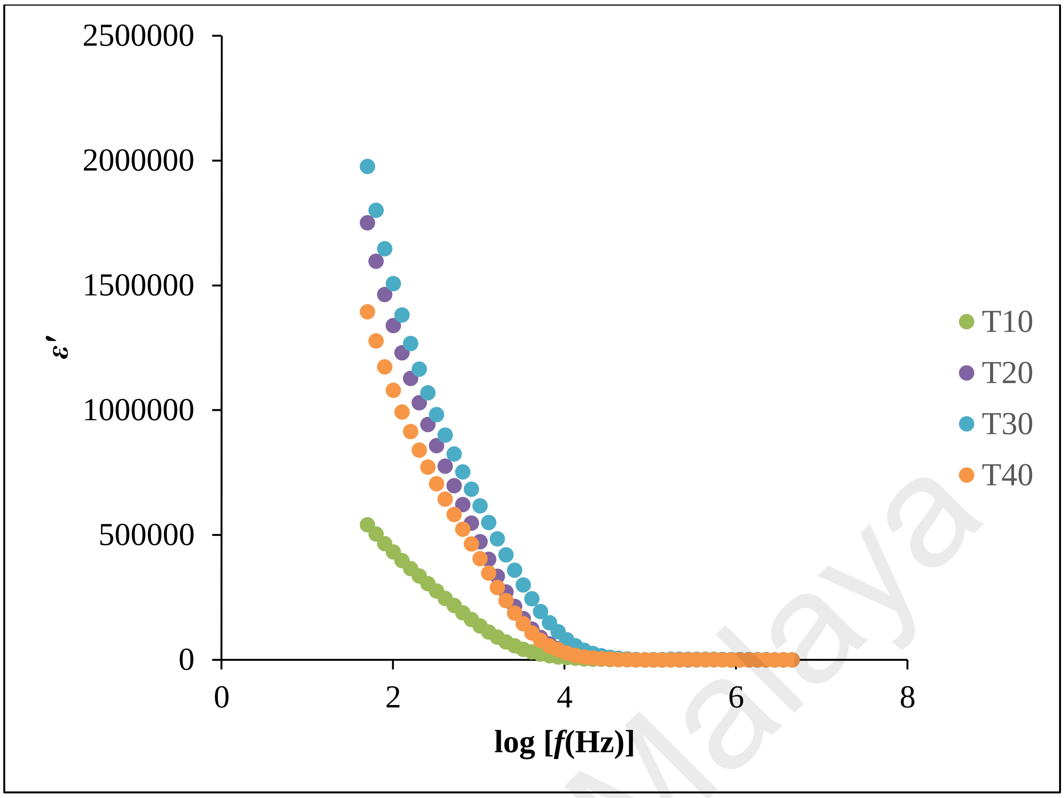

Figure 4.27: Variation of real part of dielectric constant, ε' with frequency for sample T10, T20, T30, T40

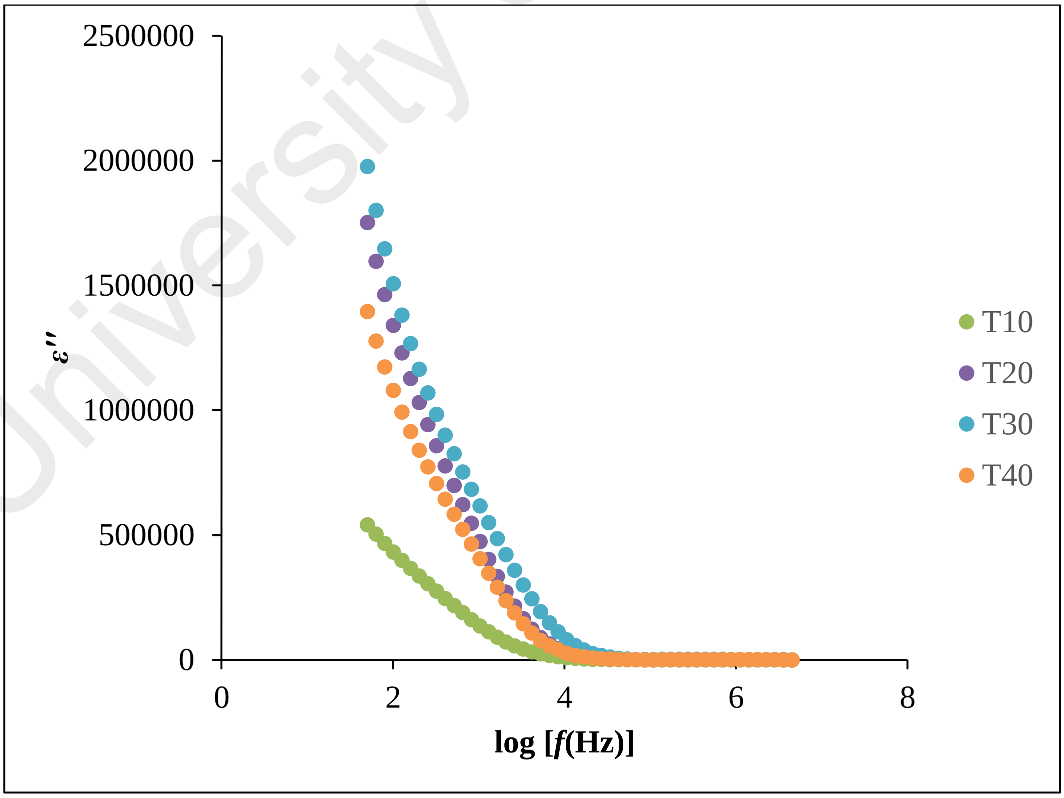

Figure 4.28: Variation of real part of dielectric loss, ε'' with frequency for sample T10, T20, T30, T40.

4.3.3.3 Modulus Studies

As observed previously, there would be an abrupt increase in *ε'* and *ε''* values at lower frequency side in the dielectric spectra which is due to the large electrode polarization effect. Modulus studies needed to be done to analyze the different relaxation phenomenon in the polymeric system and assist in the separation of the polarization effect from the bulk relaxation phenomenon in the polymer electrolyte (Ramya et al., 2008).

Real (M') and imaginary (M'') part of the modulus as a function of frequency for the GPE samples are shown in *Figure 4.29 and Figure 4.30,* respectively. From *Figure 4.29*, it is observed that the dispersion of M' takes place at higher frequency region. It approaches zero when it reaches lower frequency. This actually indicates that there is masking of the electrode polarization effect happening at the electrode-electrolyte interface. Well-defined resonance peaks are expected to be seen at the high frequency region in the spectra. It is an indication of good ionic samples that have long range of conductivity relaxation. The loss of the peaks is actually due to the limitation of range of the frequency that can be done in this experiment. Thus, only the dispersion part of the electric modulus can be seen but the trend of the variation of the dispersion that were in the inset of *Figure 4.29* shows that the peaks were shifted towards higher region of the frequency with an increase of TPAI concentration. This indicates that the relaxation time of the samples was shortened with an increase of TPAI concentration. Similar variation of the spectra for M" can be seen in the inset of *Figure 4.30* (Ramesh & Ng, 2009).

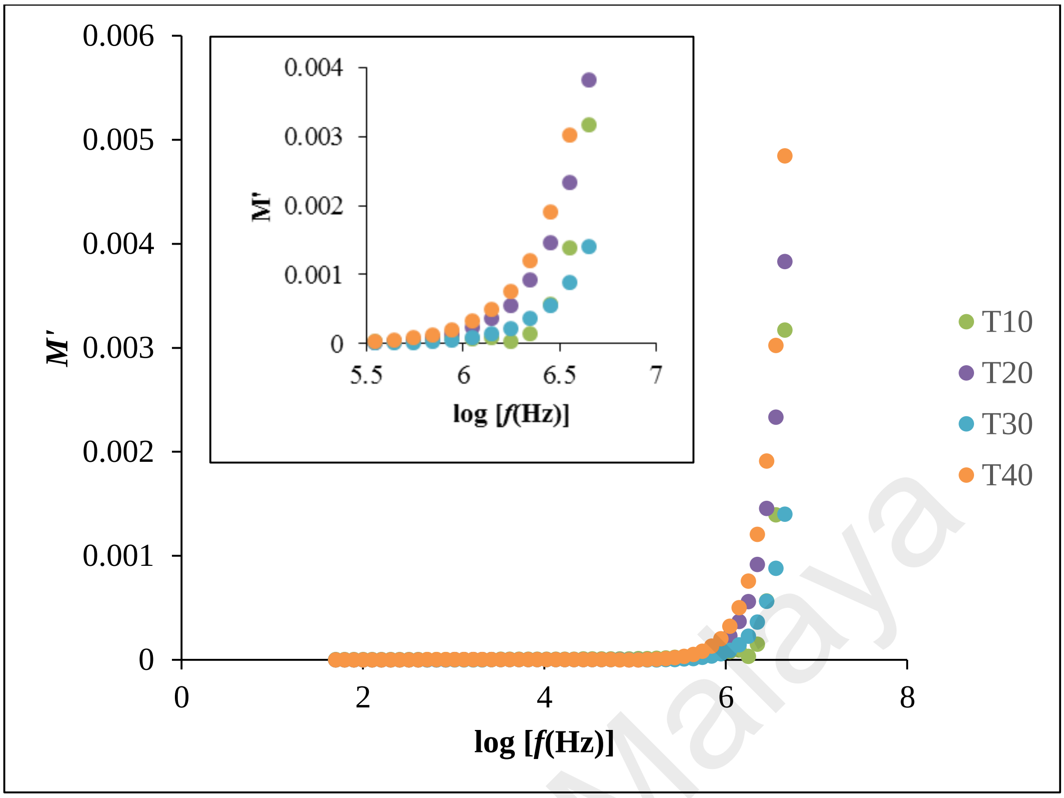

Figure 4.29: The real part of modulus, M' as a function of frequency for T10, T20, T30, and T40.

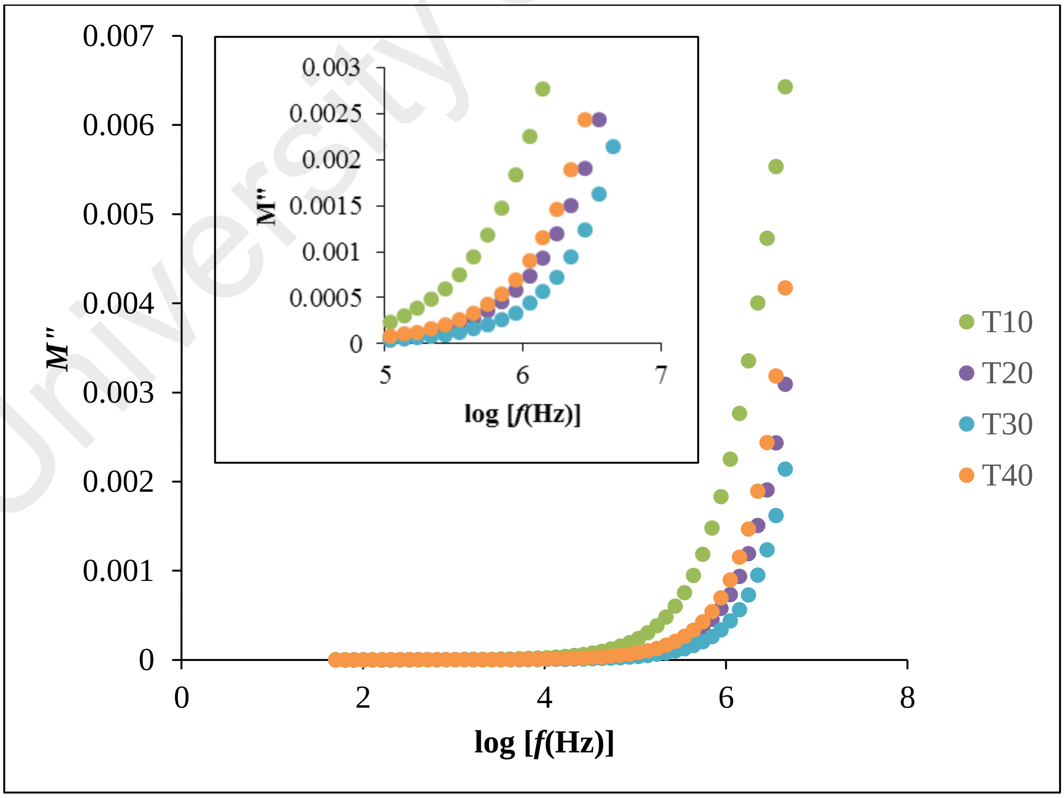

Figure 4.30: The imaginary part of modulus, M" as a function of frequency for T10, T20, T30, and T40.

4.3.4 FTIR studies

Figure 4.31 depicts the FTIR spectra of the pure P(VP-co-VAc), pure TPAI, and the GPE samples of this salt system. As shown in the previous studies, the P(VP-co-VAc)-KI system, the C=O stretching region is where it is important to be studied as it could shows us the interaction in between the TPA$^+$ ions with the strong electron donor group, the C=O bonding of the P(VP-co-VAc) copolymer. The FTIR spectra have been enlarged and the spectra for the important carbonyl stretching region for sample O and sample T10 to T40 are depicted in *Figure 4.32(a)* and *Figure 4.32(b)*. It is observed that there is shifting occurred in both of the C=O stretching peaks of the PVAc and PVP region respectively. It can be seen that in *Figure 4.32(a)*, the peaks for the PVAc region of the samples with TPAI salt were seen to be shifted to a higher wavenumber. Meanwhile, in PVP region, the peaks were seen to be shifted to the higher region after the addition of TPAI salt. This could help us to determine that the TPA$^+$ ions did interacts properly with these strong electron donor group, the stretching C=O bond (Wieczorek & Stevens, 1997). The interaction is expected to be similar with what is happening in the previous system.

Without a doubt, the interaction between anions with the C-N stretching frequency in the PVP chain of the P(VP-co-VAc) was also studied in this system as it could assist in confirming the interaction of the I$^-$ ions from the TPAI salt with the strong ion withdrawing properties of the N atom of the C-N stretching. As expected, the appearances of the peaks of the P(VP-co-VAc)-TPAI GPE samples at 1210 cm^{-1} to 1260 cm^{-1} shown in *Figure 4.32(c)* is corresponding to the C-N stretching were shifted to higher wavenumbers with the addition of TPAI salt. This shows that the same interaction is also happening in this P(VP-co-VAc)-TPAI gel polymer electrolytes system where the I$^-$ from the TPAI interacted with the strong withdrawing character of the N atom of the C-N in the PVP chain (Ramya et al., 2007). These interactions of proves the complexation occurred between the materials used in this system (Selvasekarapandian et al., 2006)..

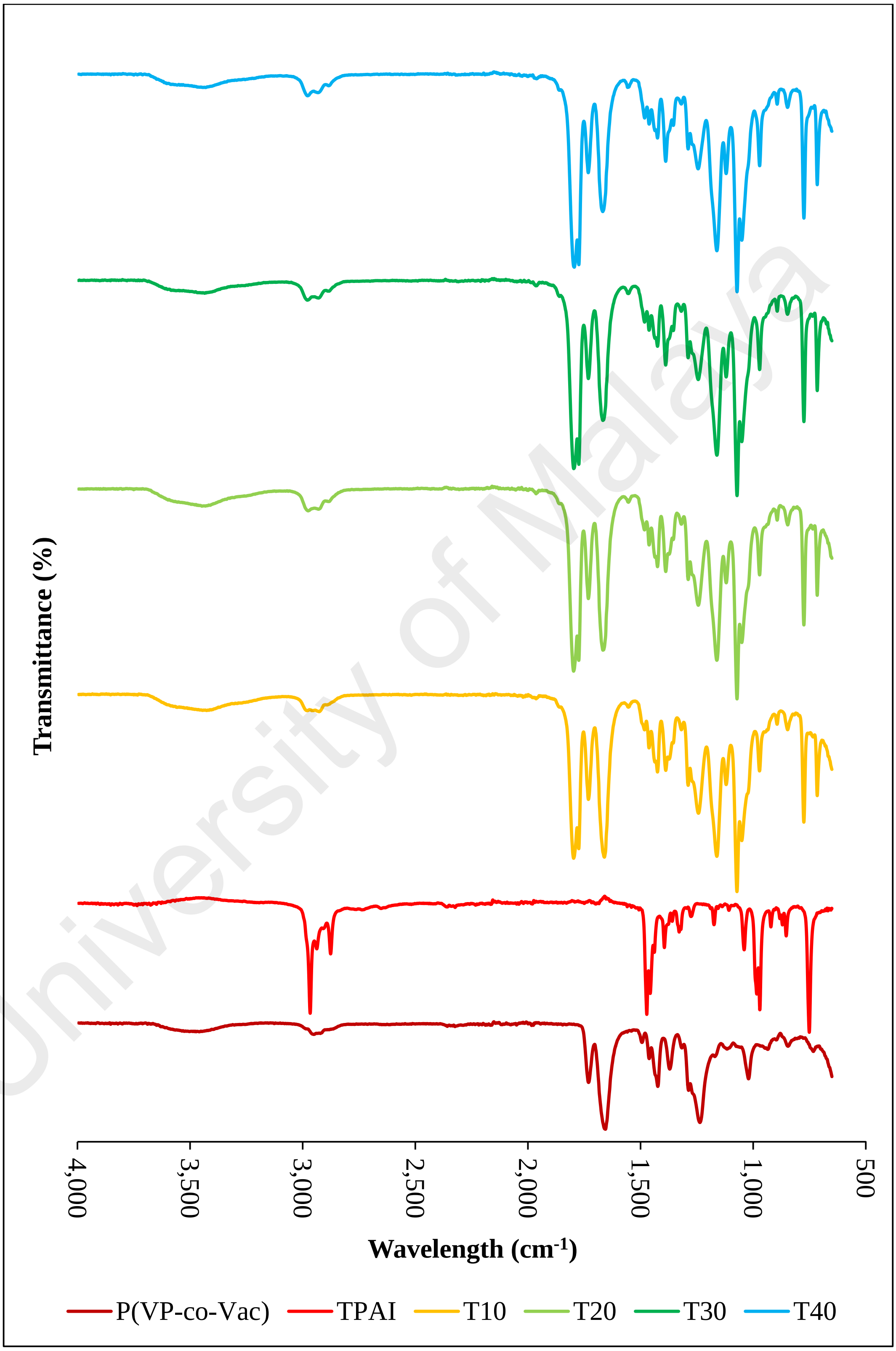

Figure 4.31: FTIR spectra for pure P(VP-co-VAc), pure TPAI and P(VP-co-VAc)-TPAI gel polymer electrolytes.

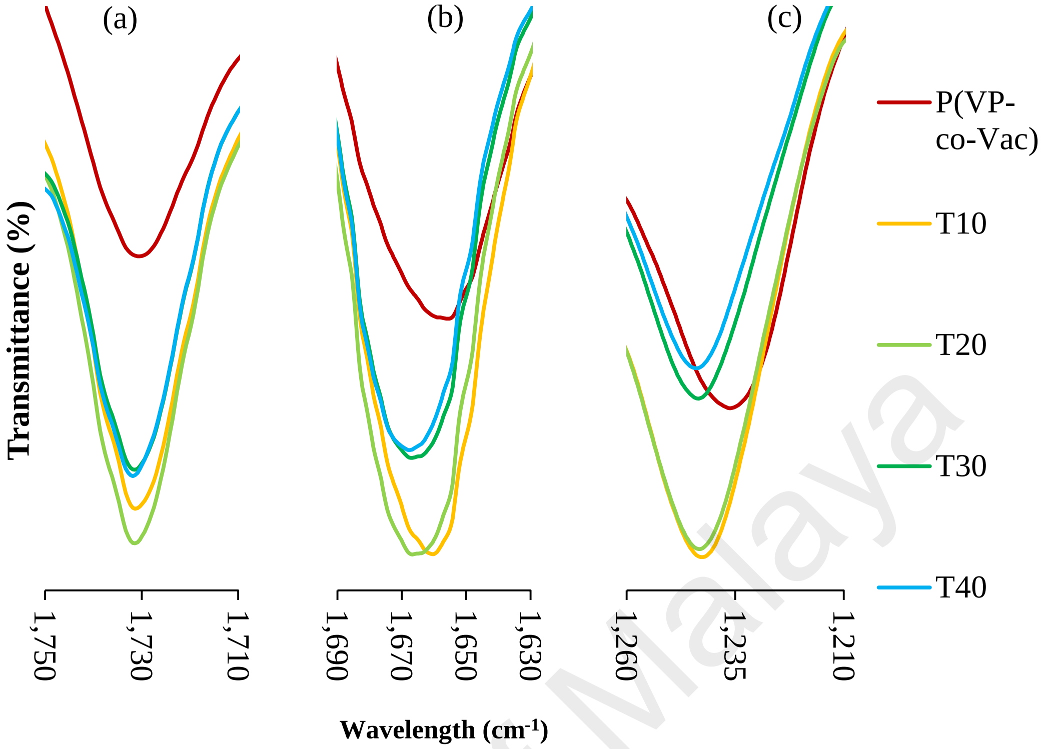

Figure 4.32: FTIR spectra in the region (a) 1750-1710 cm^{-1}, (b) 1690-1630 cm^{-1}, (c) 1260-1210 cm^{-1} for pure P(VP-co-VAc) and P(VP-co-VAc)-TPAI GPE samples.

4.3.5 X-ray diffraction (XRD) studies

XRD analysis has been performed and the respective patterns of the P(VP-co-VAc), TPAI, sample O and all of the samples in the P(VP-co-VAc)-TPAI gel polymer electrolytes system were shown in *Figure 4.33*. The sharp diffraction peaks at 2θ = 18.9°, 25.5°, 34.3° and 42.5° of the XRD pattern in pure TPAI implied the crystalline nature of the pure TPAI (Rajendran et al., 2007). All of these sharp diffraction peaks of TPAI were found to be absent in the XRD pattern of the sample T10, which is the sample where the first addition of TPAI was performed on the P(VP-co-VAc)-TPAI based gel polymer electrolytes. It indicates the TPAI salt undergoes complexation completely and there is no separated phase in the samples of the P(VP-co-VAc)-TPAI based gel polymer electrolytes system. This also proves the complete dissolution of the TPAI in the gel polymer electrolyte complexes and the formation of the complexation between the copolymer and the TPAI salt (Rajendran et al., 2007). However, these intense peaks started to reappear in sample T40 indicating that there were presence of the excessive TPAI salt inside the polymer matrix. The excess ions from the TPAI salt obstructs the initially free moving mobile charges and leads to the decreases in the ionic conductivity as shown in *section 4.3.1*.

Meanwhile, the appearance of the broad peaks in all of the samples which can be seen in XRD patterns of the samples indicate the amorphous characteristic of the P(VP-co-VAc)-TPAI based gel polymer electrolytes (Rajendran et al., 2007). The broad peaks were found to be shifted from $2\theta = 21.5^{o}$ to $2\theta = 21.1^{o}$ for T10, to $2\theta = 21.4^{o}$ for T30 and to $2\theta = 21.4^{o}$ for T40. The shift indicates the complexation that has occurred in between the copolymer and the TPAI salt. The peak which is found at $2\theta = 11.9^{o}$ in pure P(VP-co-VAc) was found to be absent in all of the P(VP-co-VAc)-TPAI based gel polymer electrolytes samples. It is this indication of the complexation occurred as well (Costa et al., 2007).

Another way to prove the complexation of the P(VP-co-VAc) and the TPAI salt is to observe the changes in the intensity. With the increase in the concentration of the TPAI, it is observed that the peaks become broader and the intensity decreases as illustrated in *Figure 4.33* but only up to sample T30 which has 30 wt.% of the TPAI. This is due to the decrease in the crystallinity of the gel polymer electrolytes induces by the TPAI salt which causes the gel polymer electrolytes to have more flexible polymer backbone. Moreover, with the increase in the flexibility of the polymer backbone the mobile charges could move even faster inside the polymer matrix (Sivakumar et al., 2006). Thus, it increases the ionic conductivity as well.

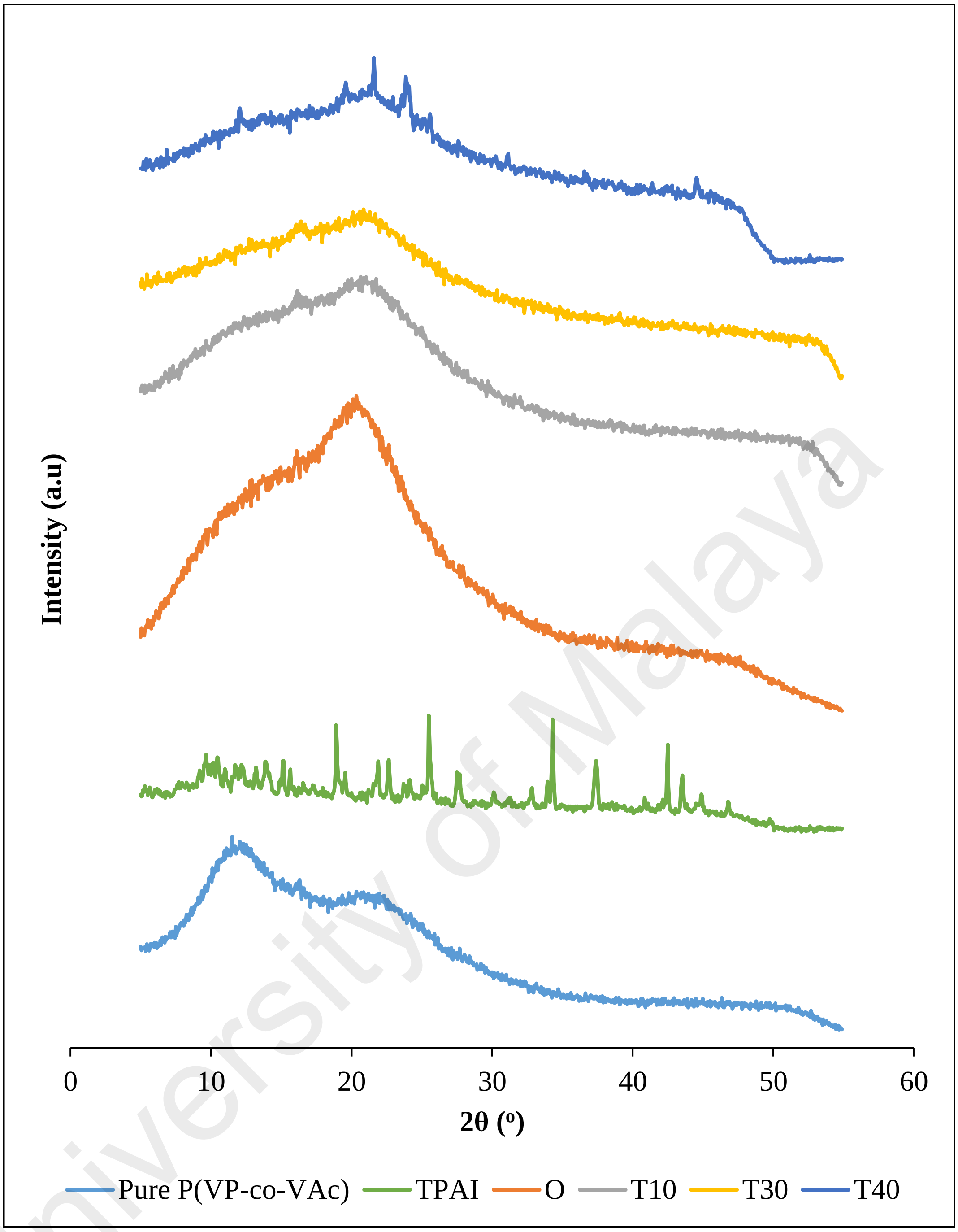

Figure 4.33: XRD patterns of the pure P(VP-co-VAc), sample O, T10, T30 and T40.

4.3.6 Thermogravimetric analysis (TGA)

The decomposition temperatures and the percentages of total weight lost of sample T10, T20, T30 and T40 obtained from TGA were listed in *Table 4.9*. The TGA curves of pure TPAI and the samples were depicted in *Figure 4.34*. As observed in every sample, it can be observed that there would be a rapid decrease in weight from 30 ℃ - 100 ℃. As explained before, this is due to the evaporation of the low molecular weight substances such as moisture adsorbed and minor impurities. Meanwhile, the mass loss at 100 ℃ - 200 ℃ is due to the evaporations of the solvents EC and PC as well as the small amount of iodine added into the polymer matrix (K.-S. Kim et al., 2005). Since the degradation properties of the P(VP-co-VAc) copolymer have been discussed previously. This section would only be focused on the changes of the thermal stability of the P(VP-co-VAc) gel polymer electrolytes which has been added with the TPAI salt. The degradation temperature of the pure TPAI was found to be at 257 ^{o}C. However, after it is added into the gel polymer electrolyte it was found that the degradation temperature increases to 300 ^{o}C and above in all of the samples where it can be seen overlapping with the degradation temperature of the PVAc region. The PVAc in the copolymer is found to have a decrease in the degradation temperature after the addition of TPAI and further reduces as more TPAI was added into the gel polymer electrolytes. Meanwhile, in this P(VP-co-VAc)-TPAI system, the PVP region reacted differently. It was found the degradation temperature of this PVP region remain the same even after a total 40 wt.% of TPAI has been added into the system. This might show that the complexation that occurred inside the polymer matrix are more to the PVAc region instead of the PVP region.

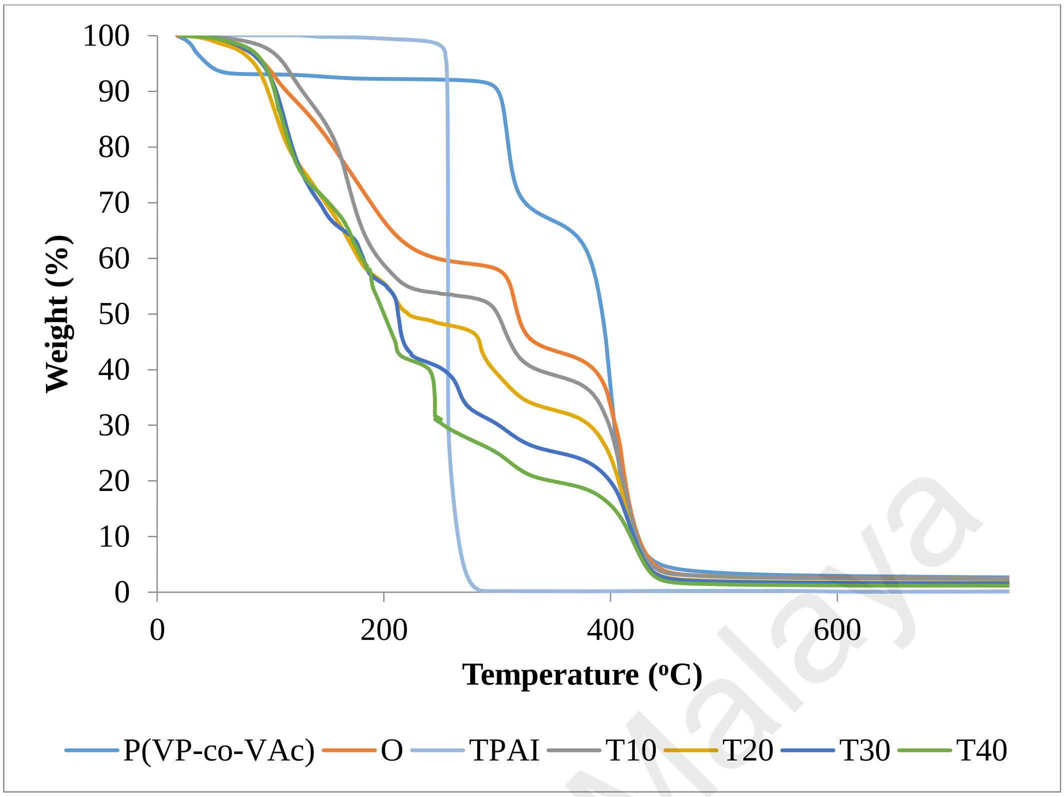

Figure 4.34: Thermogravimetric analysis of pure P(VP-co-VAc) and the P(VP-co-VAc)-TPAI GPE samples.

Table 4.9: The degradation temperature of the pure P(VP-co-VAc), sample O and the P(VP-co-VAc)-TPAI GPE samples.

Samples	**T_{max1} (°C)**	**T_{max2} (°C)**
P(VP-co-VAc)	310	385
O	314	411
T10	303	412
T20	284	412
T30	265	412
T40	245	410

4.3.7 Photocurrent density-voltage (J-V) Characteristics

The four GPE samples of this system are assembled into DSSCs and tested for the photovoltaic performances. The J-V characteristics of the P(VP-co-VAc)-TPAI based gel polymer electrolytes DSSCs are shown in *Figure 4.35* and the values of the parameters listed in *Table 4.10*. *Figure 4.36* shows variation of the normalized J_{sc}, V_{oc}, FF and photovoltaic efficiency of the P(VP-co-VAc)-TPAI GPE samples with different concentration of the TPAI salt added. At first glance, it can be noted that the photovoltaic performance is strongly influenced by the increasing amount TPAI concentration. In particular, η and J_{sc} values varied widely in the investigated domain, while the variation of FF is not much but still well appreciated. The open circuit voltage, V_{oc} instead seems not dependent on the change in the concentration as it does not change much as it was observed in *Figure 4.36.* The J_{sc} increases TPAI concentration increases and this would be explained by the increase of the iodide ion conductivity, which has been covered in the ionic conductivity section. The increase of the iodide ion conductivity increases the chances of the positive shifting into the conduction bands and thus, increases the charge injection rate which could leads to an increase of the J_{sc} (Bella, Ozzello, Sacco, Bianco, & Bongiovanni, 2014). The highest photovoltaic conversion efficiency that was achieved is 3.07 %.

The variation of the normalized current density of the DSSC under different illumination condition was measured and shown in *Figure 4.37*. The linear shape of the curve shows that there are no mobile ions and electron transport occurring at the Pt and electrode interface that could represent the rate-determining steps in the photo-electrochemical process (Chiappone et al., 2014).

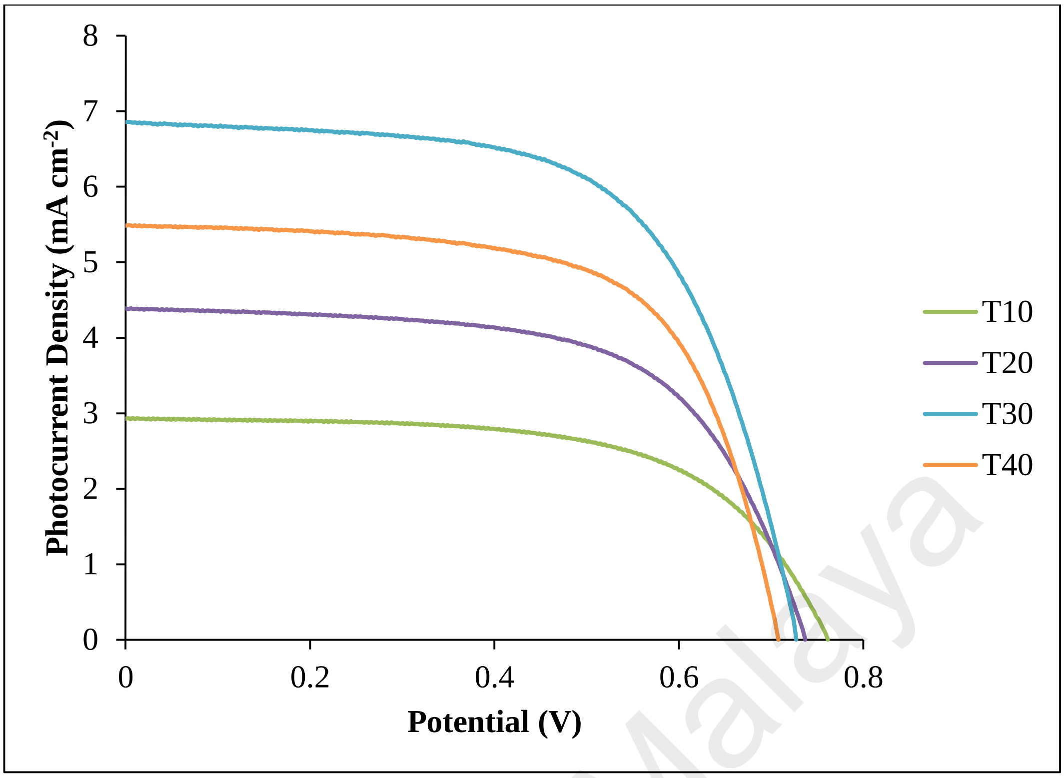

Figure 4.35: The photocurrent-photovoltage (J-V) characteristics of the GPE samples consisting of different weight percentages of TPAI.

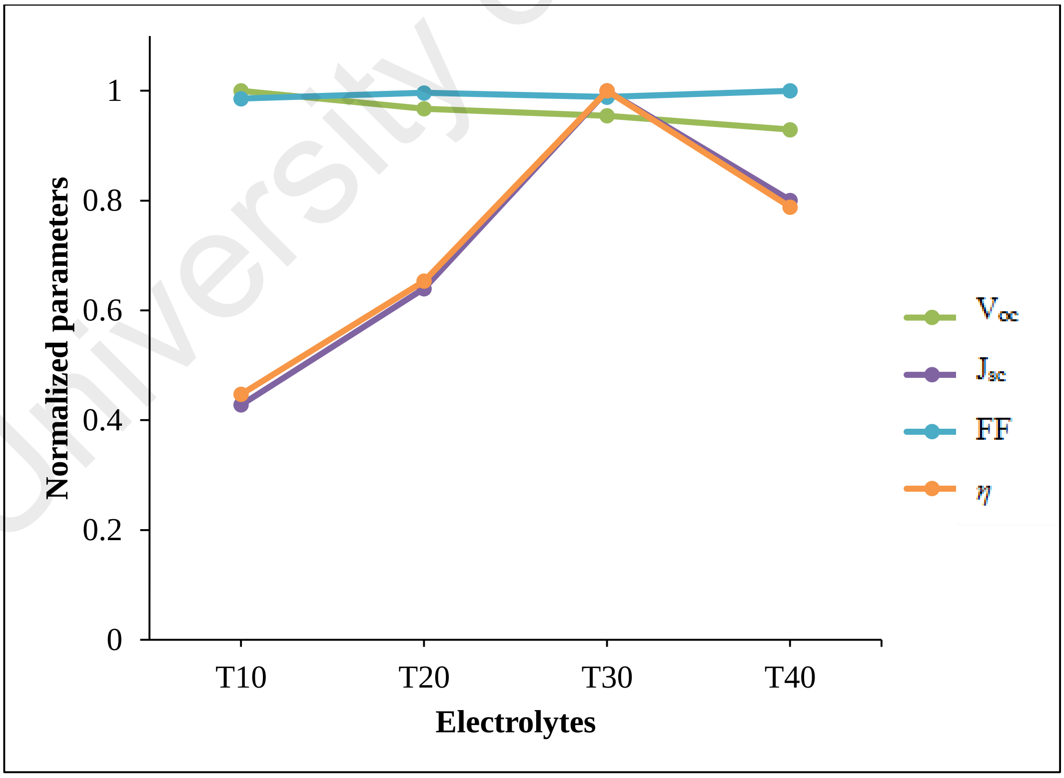

Figure 4.36: The normalization curves of the various performance parameters of the DSSCs fabricated with different P(VP-co-VAc)-TPAI GPE samples.

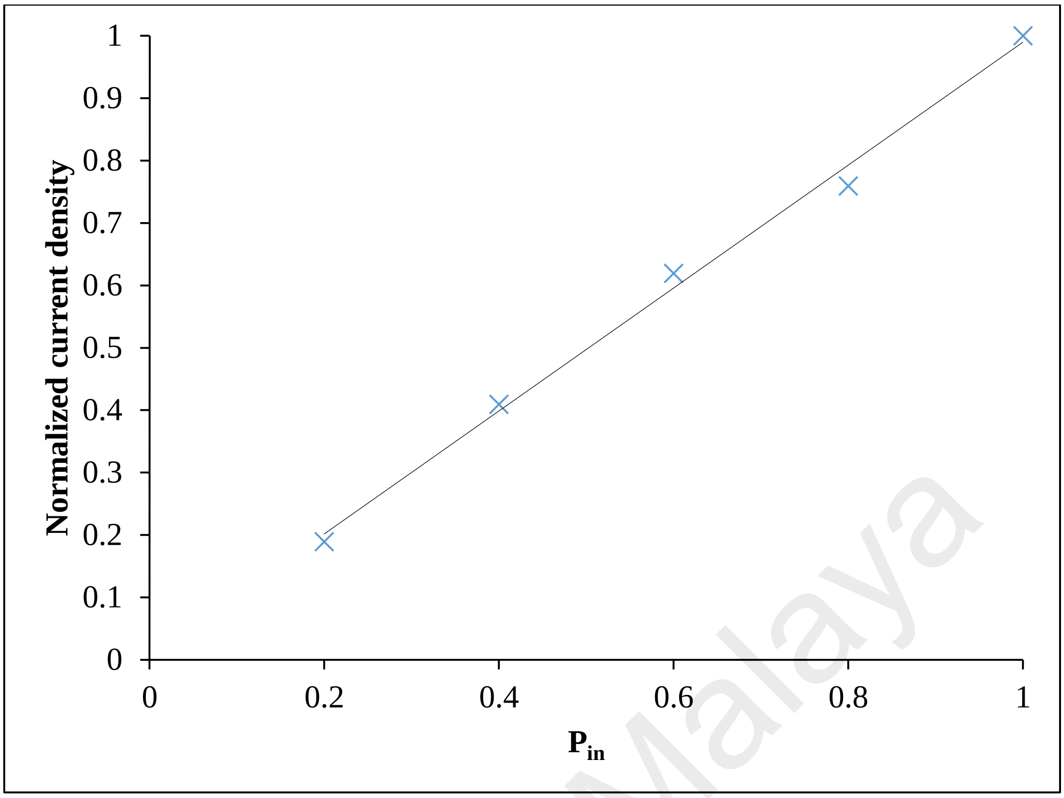

Figure 4.37: Normalized J_{sc} values plotted as a function of different light intensities (P_{in}) for sample T30.

Table 4.10: Photovoltaic parameters of the GPE samples consisted of different weight percentages of TPAI.

Electrolytes	**V_{oc} (V)**	**J_{sc} (mA cm^{-2})**	**FF (%)**	**η (%)**
T10	0.76	2.94	0.61	1.37
T20	0.74	4.39	0.62	2.01
T30	0.73	6.86	0.62	3.07
T40	0.70	5.49	0.62	2.42

4.3.8 EIS studies for DSSCs

Figure 4.38 shown the data obtained for the EIS studies of the DSSCs from the gel polymer electrolytes of the P(VP-co-VAc)-TPAI system. The data was fitted with the equivalent circuit shown in *Figure 4.19* and shown as line charts in *Figure 4.38*. All the parameters obtained from the fitted data were then tabulated in *Table 4.11*. As seen in *Figure 4.38*, the EIS spectra were actually made up from two semicircles which seems to be overlapping to each other. A clearer image of the two semicircles would be shown in *Figure 4.40* for sample T30. Then, there would be a spike occurring at the very low frequency of the DSSCs of the P(VP-co-VAc)-TPAI system. The first and second semicircle from the left were labeled as R_{ct1} and R_{ct2} (Hieu et al., 2014) and the intersection of the first semicircle with the x-axis is labeled as the R_s (Ke et al., 2014). The explanation for R_{ct1}, R_{ct2} and R_s were explained previously in the *section 4.2.8*.

In this system, it seems that the R_{ct2} decreases with the increase of TPAI concentration in the gel polymer electrolytes. This is probably due to the bulkier cations of the TPA^+ able to suppress the recombination reaction between the free electrons the I_3^- must better compare to the small KI salt (Sharma et al., 2013). This result agrees well with the open circuit voltage, V_{oc} value of the DSSCs and the relation between the R_{ct2} and V_{oc} is shown in *Figure 4.41*.

Figure 4.39 shows the Bode EIS spectra of the sample. The peak at the middle frequency zone seems shifted to the right with the increase of the TPAI concentration showing that the electron lifetime decreases with more TPAI added into the gel polymer electrolytes. It agrees well with the previous studies where there was a decrease in the charge recombination rate with an increase of TPA^+ cation concentration (Hoshikawa et al., 2006).

From the Tafel polarization studies and by using the *equation 4.8*, we determined the electrocatalytic properties of the gel polymer electrolytes of the P(VP-co-VAc)-TPAI system. From the equation, it shows that larger value J_{lim} would give us a larger diffusion coefficient (D_n) value and with higher D_n value, it means that the electrocatalytic properties of certain samples would be higher. The extracted J_{lim} value has an order of sample T30>T40>T20>T10. This could explain the increase of PCE of the gel polymer electrolyte samples of this studies (Mingkui Wang et al., 2009).

Meanwhile, as explained previously in *section 4.2.8*, the larger slope in the anodic or cathodic branch indicates a higher exchange current density (J_0). Considering that the pure Tafel region is not observable, therefore the low field region is used to assess J_0 variation. The extracted J_0 has an order of sample T40>T30>T20>T10. J_0 which is inversely proportional to R_{ct2} where it can be associated in the *equation 4.9*. Apparently, the trend of the J_0 matches the order of the R_{ct2} of the samples in the EIS studies (C. Wu et al., 2012).

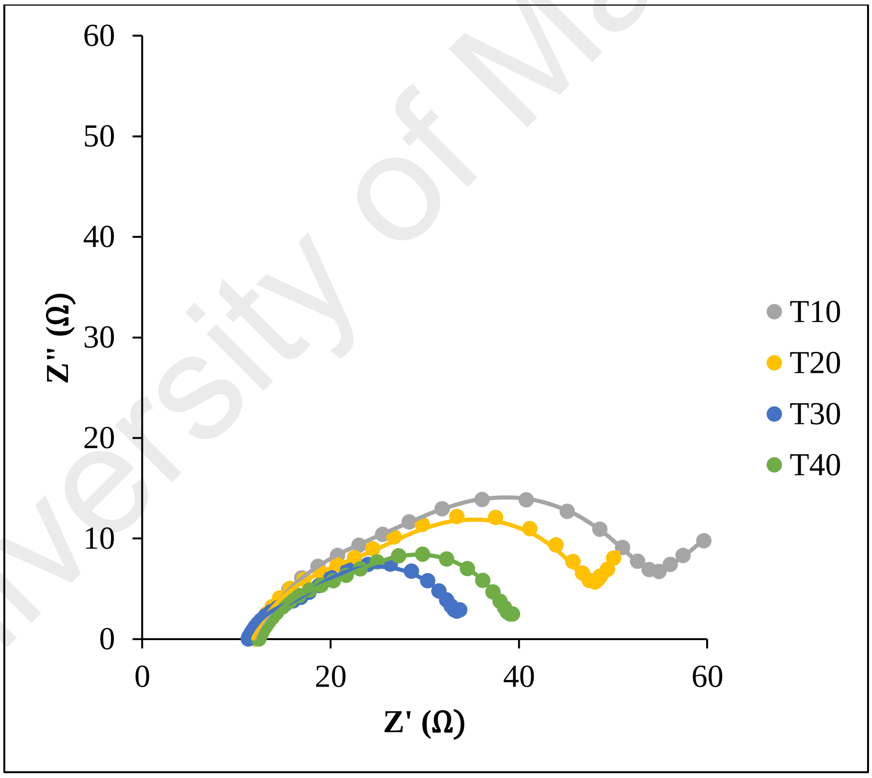

Figure 4.38: The electrochemical impedance spectra of DSSCs assembled with P(VP-co-VAc)-TPAI GPE samples in the forms of Nyquist plots under 100 mW cm^{-2} illuminated sunlight.

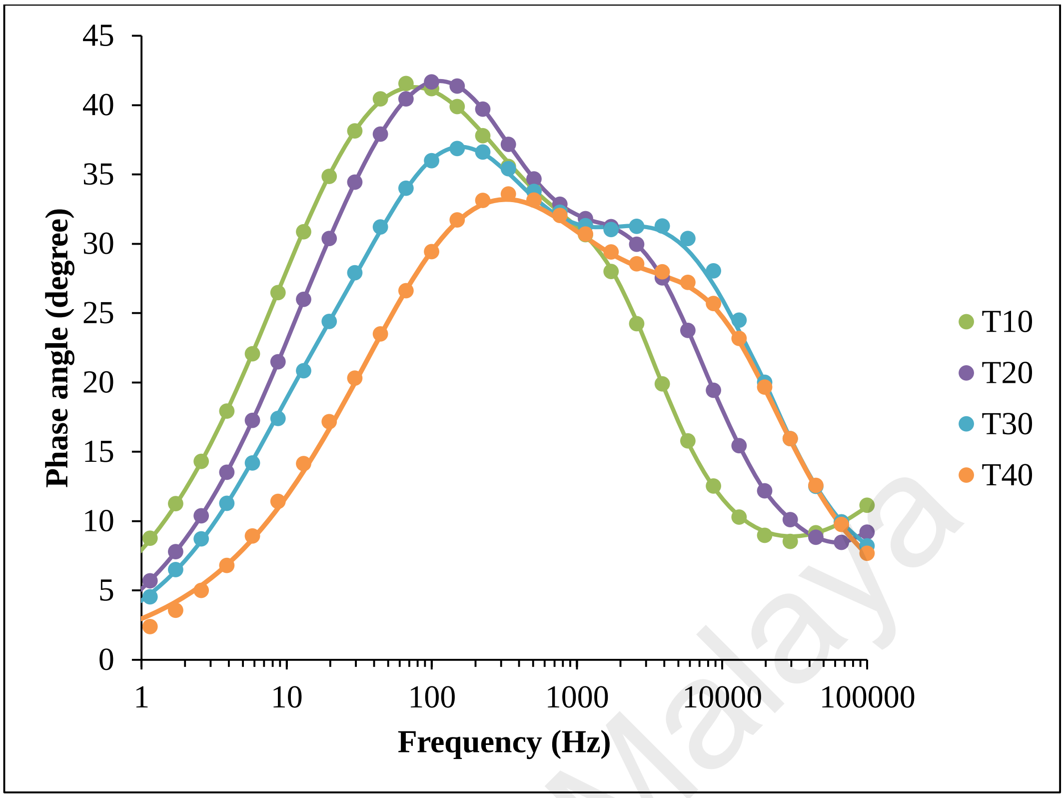

Figure 4.39: The electrochemical impedance spectra of DSSCs assembled with P(VP-co-VAc)-TPAI GPE samples in the forms of Bode phase plots under 100 mW cm^{-2} illuminated sunlight.

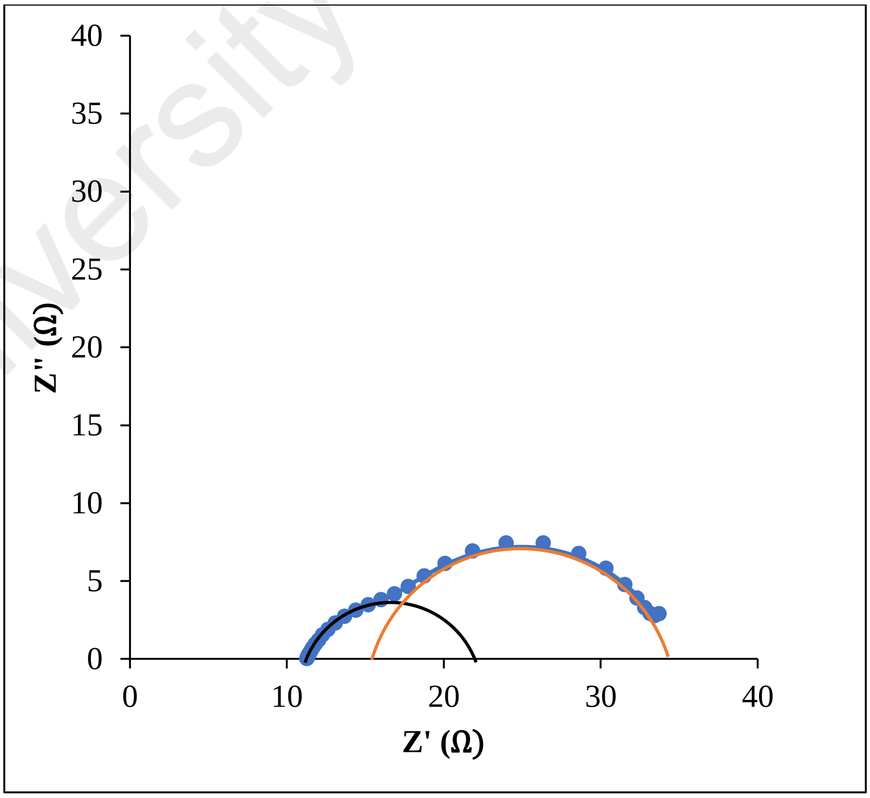

Figure 4.40: EIS spectrum of DSSC containing T30.

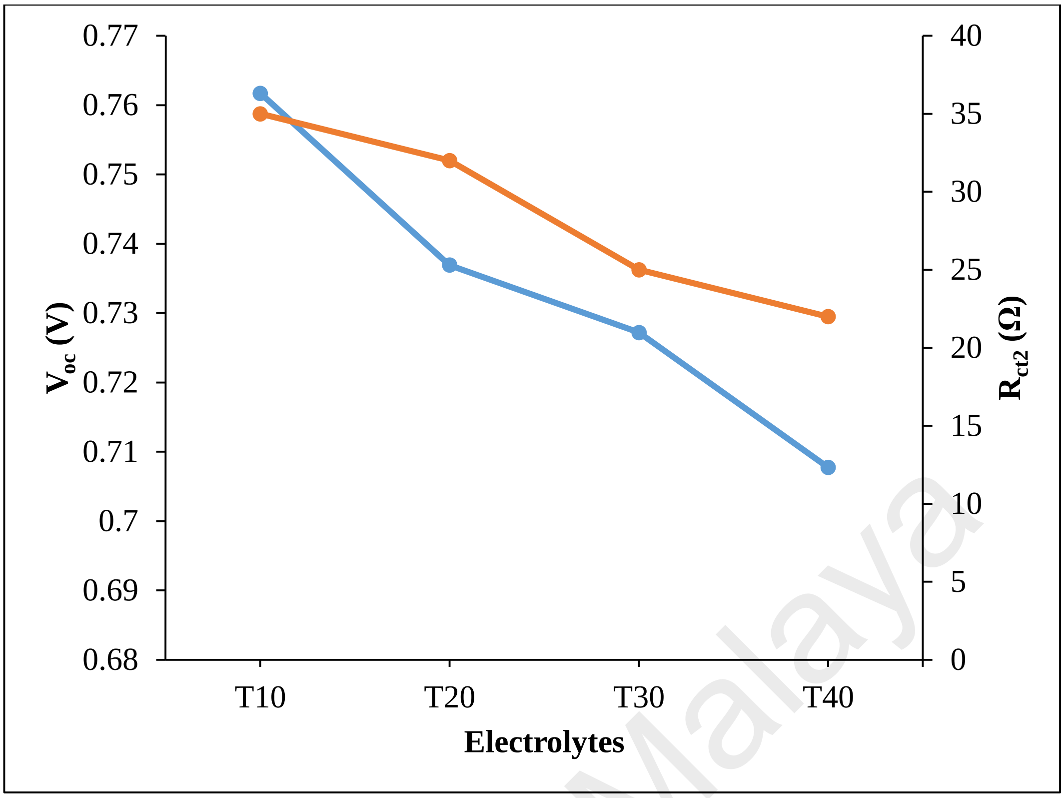

Figure 4.41: The open circuit voltage,V_{oc} and R_{ct2} with the respect of different TPAI concentration in P(VP-co-VAc)-TPAI GPE samples.

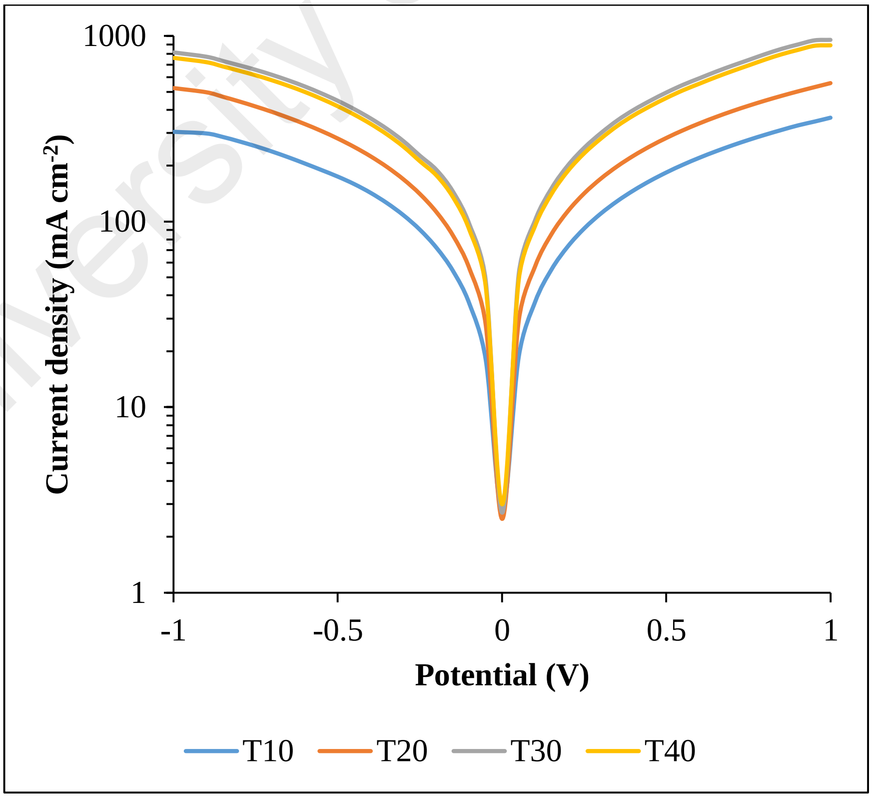

Figure 4.42: Tafel polarization curves of symmetric Pt cells with P(VP-co-VAc)-TPAI gel polymer electrolytes samples

Table 4.11: The parameters of the equivalent circuits used to fit the EIS impedance data of the P(VP-co-VAc)-TPAI based DSSCs.

Electrolytes	R_s (Ω)	R_{ct1}(Ω)	R_{ct2}(Ω)	W($S^{1/2}\ \Omega^{-1}$)	τ (ms)
T10	16.0	16.0	24.7	0.72	120.4
T20	17.5	8.6	22.9	0.74	104.3
T30	16.4	12.0	22.2	0.31	97.5
T40	14.2	16.4	21.9	0.69	91.4

4.4 P(VP-co-VAc)-KI-MPII Gel Polymer Electrolytes

4.4.1 Ambient Temperature-Ionic Conductivities Studies

Figure 4.43 shows the impedance plots of all gel polymer electrolytes sample for this system (KM5-KM20). A single spike can be seen in all of the samples. This implies that the current carriers in the system are the mobile ions that were controlling the entire total electrical conductivity of these electrolytes and there was good contact at the interface of the electrodes and the polymer electrolytes. (Sengwa & Choudhary, 2014).

The compatibility and effect on the ionic conductivity of the GPE samples after the addition of MPII were studied and the results are shown in *Table 4.12* and *Figure 4.44*. As seen in the figure, there is an increase in ionic conductivity right after 5 wt.% of MPII was added into sample K30. This could show that the MPII was compatible to be used in the system. The ionic conductivity increases up to 3.13×10^{-3} S cm^{-1} at 15 wt.% of the MPII added before it starts to decrease at KM20. The increase in the ionic conductivity was caused by production of large amount of mobile charge carriers from MPII that provides the $MPIm^+$ and I^- ions (P. K. Singh, Kim, Park, & Rhee, 2008). The high concentrations of these new charge carriers also help to improve the dissociation of KI where it helps to reduce the solvation of the K^+ cations and eventually promoting the decoupling of the ions due to its high self-dissociating, high ionic hopping properties and high initiation of the ionic transportation within the polymer segments. Hence, it improves the ionic conductivity (Ramesh et al., 2011). The ionic liquids is also well known for plasticizing effect as well where it could soften the polymer backbone and improves the polymer segmental mobility and ionic transportation by providing more conducting pathways for the charge carriers to move around more easier. This also increases the amorphous nature of the polymer electrolytes thus improving the ionic conductivity (Sekhon, Krishnan, Singh, Yamada, & Kim, 2006). As observed in *Table 4.12*, the highest ionic conductivity was obtained at 15 wt.% of MPII which is 3.13 × 10^{-3} S cm^{-1}. The charge carriers' concentration is at the maximum percolation threshold at this level causes the decrease in ionic conductivity with further addition of ionic liquids. This is normally due to the agglomeration of the extra mobile ions that leads to the formation of ion pairs (Liang, Wang, & Chen, 2008). The ion pairs basically restrict the mobility of the free charge carriers and prevent the passage of ions in the polymer matrix.

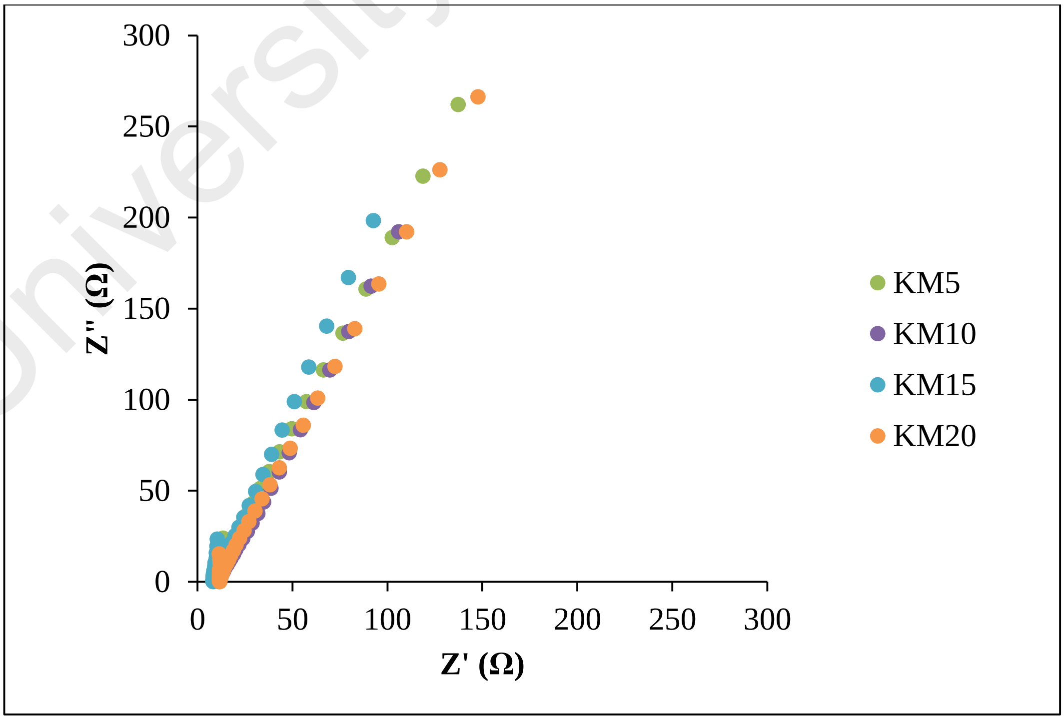

Figure 4.43: Typical complex impedance plot of P(VP-co-VAc)-KI-MPII GPE samples at room temperature.

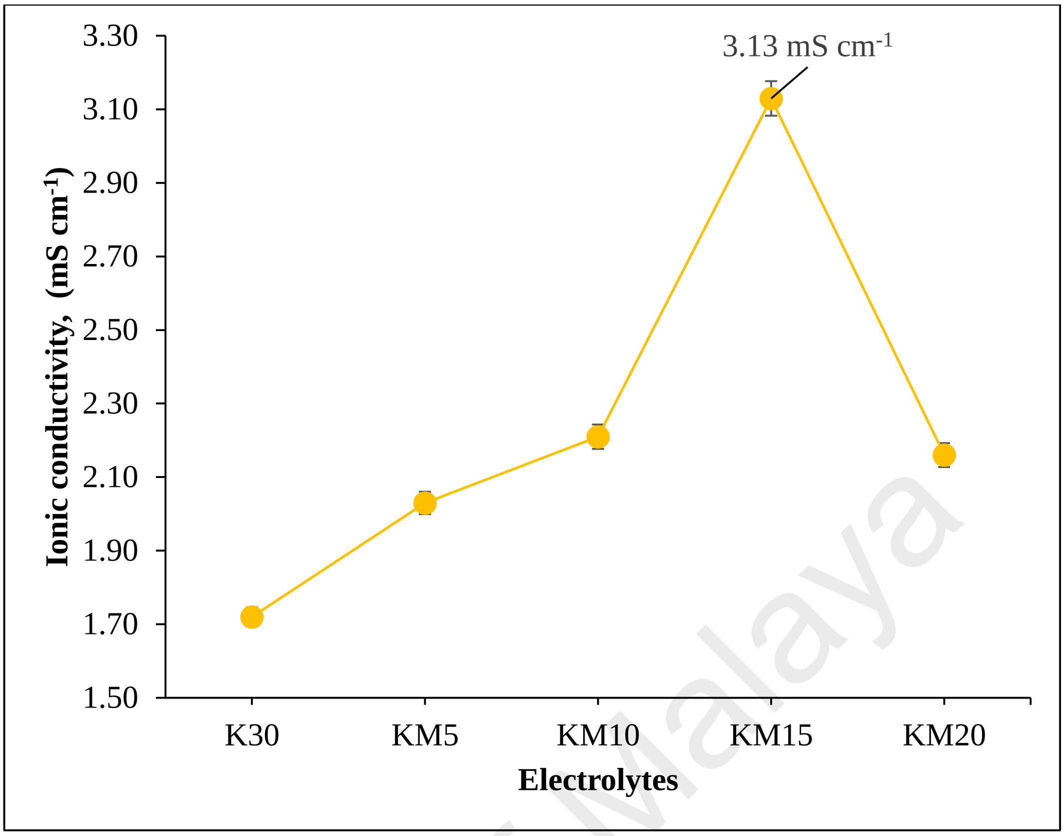

Figure 4.44: Variation of ionic conductivity of the GPE samples with different MPII concentration at room temperature.

Table 4.12: Ionic conductivity values for the P(VP-co-VAc)-KI-MPII GPE samples at room temperature.

Electrolytes	**Ionic Conductivity (mS cm^{-1})**
K30	1.72
KM5	2.03
KM10	2.21
KM15	3.13
KM20	2.16

4.4.2 Temperature dependence-Ionic conductivity studies

The ion transport mechanism of the P(VP-co-VAc)-KI-MPII GPEs was evaluated by measuring ionic conductivity over the temperature range of 30 - 100°C, as represented by the Arrhenius plot in *Figure 4.45*. The temperature dependent variation appears to be linear with an average regression value of ~0.992, revealing that the ionic conduction mechanism is also obeying the Arrhenius theory after the addition of ionic liquid, MPII into the single salt system. This shows that the changes of the occurrence of the ion hopping into the neighboring vacant site is expected to increase with the increase in temperature due to the high energy of the ions upon being heated. The increase in ionic conductivity was observed to increase with the rise in temperature due to the ionic conductivity being very dependent on the mobility of charge carriers in amorphous phase (Ramesh, Ng, Shanti, & Ramesh, 2013).

By calculating the slope of each respective graph, the activation energy (E_a) for each GPE can be determined. The activation energy is the minimum energy that is required by the ions to hop from one coordination to another coordination. Thus, GPEs with lower E_a value would be expected to have higher ion transport mobility and thus, it exhibits higher ionic conductivity (Yang, Yang, & Wu, 2009). The calculated E_a value for the samples with different wt.% of the MPII are summarized and tabulated in *Table 4.13*. *Figure 4.46* shows the variation of the ionic conductivity and the E_a of the GPE samples and sample KM15 was found to have lowest activation energy followed by KM20, KM10 and then KM5.

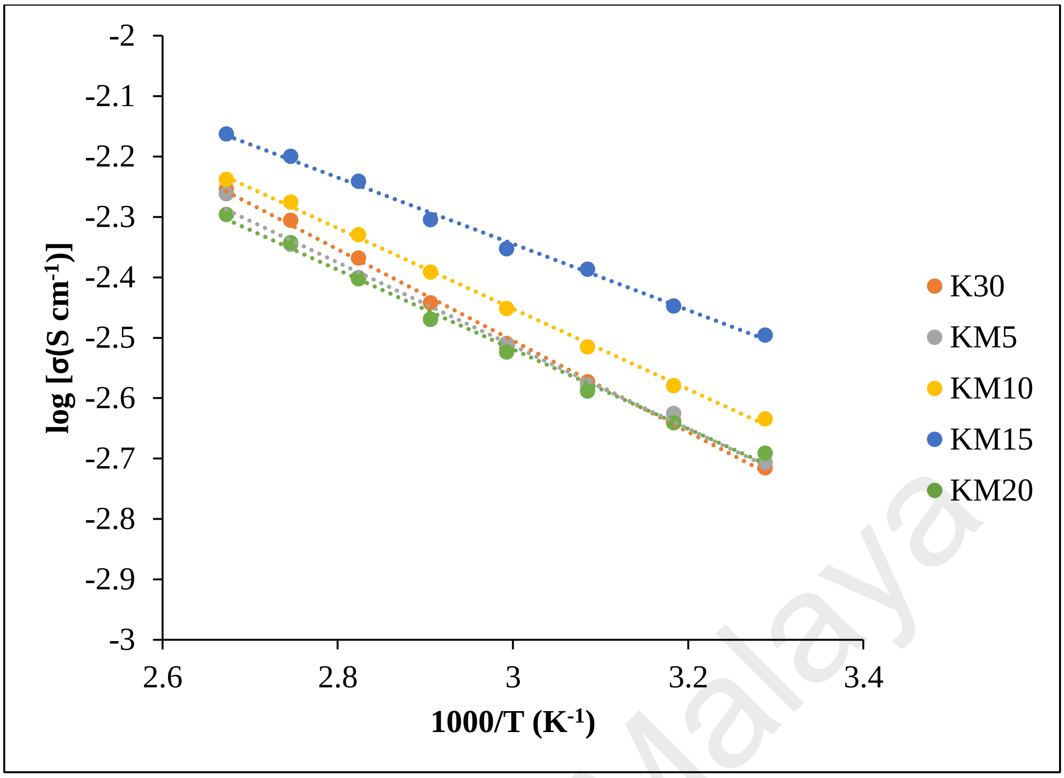

Figure 4.45: Arrhenius plots for the conductivity of the GPE samples with different concentration of MPII.

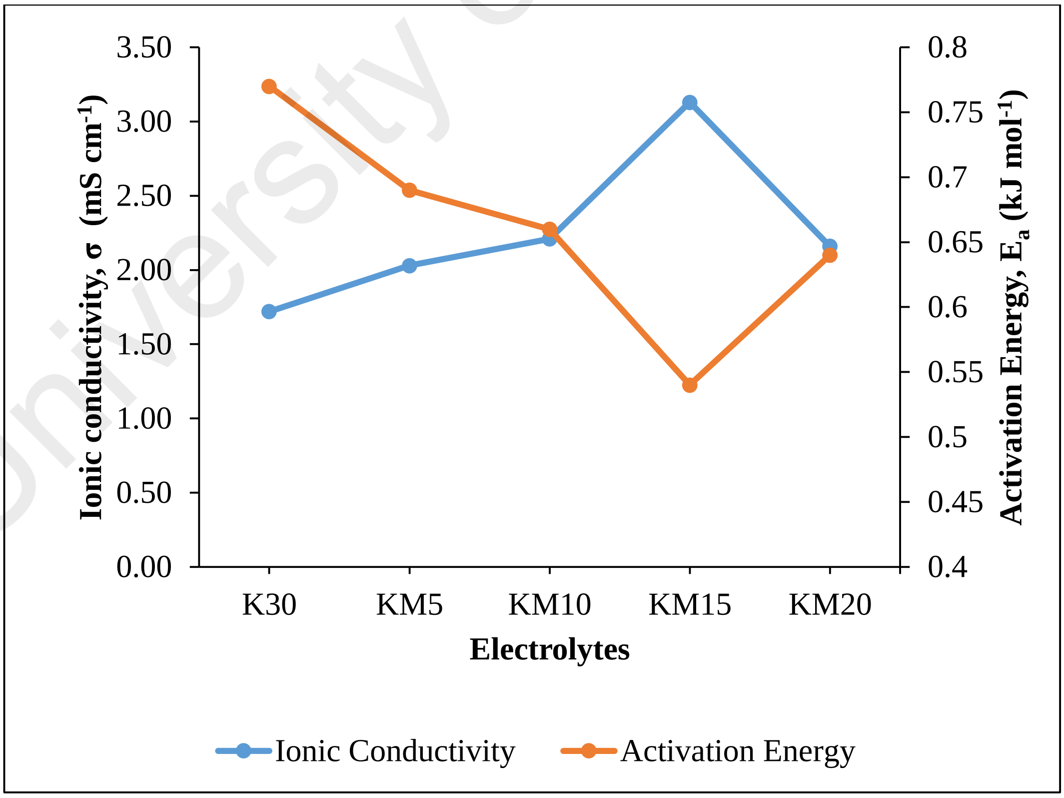

Figure 4.46: Variation of ionic conductivity and the activation energy of the P(VP-co-VAc)-KI-MPII GPE samples with different MPII concentration at room temperature.

Table 4.13: The activation energy of the GPEs sample with different concentration of MPII

Electrolytes	**Activation Energy, Ea (kJ mol^{-1})**
K30	0.77
KM5	0.69
KM10	0.66
KM15	0.54
KM20	0.64

4.4.3 Dielectric Studies

4.4.3.1 Conductivity-frequency studies

The relaxation processes of the salt system based P(VP-co-VAc) gel polymer electrolytes has been studied and the relaxation process of the P(VP-co-VAc)-KI gel polymer electrolytes with the addition of the ionic liquid, MPII were studied. This study is done in order to monitor if there is any changes happening to the relaxation process after the addition of the ionic liquid in the P(VP-co-VAc) based gel polymer electrolytes. The ionic liquid, MPII was added to the best conducting sample of the P(VP-co-VAc)-KI system and the variation of the ionic conductivity with different frequencies was shown in *Figure 4.47*. It is shown that, even after the addition of MPII up to 20 wt.%, there was not much changes can be observed in the graph. This shows that the addition of MPII does not change the types of relaxation process occurring in the P(VP-co-VAc) based gel polymer electrolytes. It means that the nature variation of the ionic conductivity of the MPII added P(VP-co-VAc)-KI based gel polymer electrolytes is still similar with the universal dynamic responses which is explained previously where at higher frequencies, the chances of the mobile ions to hop back into the initial sites are much higher compare to the lower frequency region which leading to higher ionic conductivity (Dillip et al., 2009).

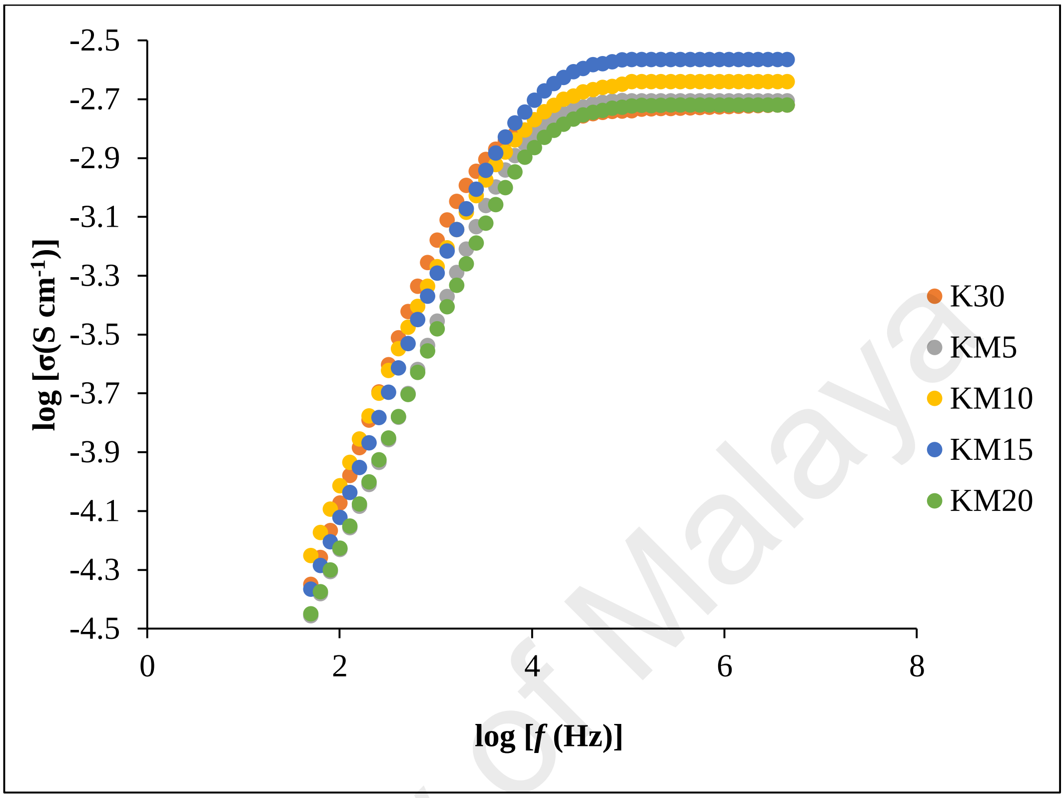

Figure 4.47: Frequency-dependent conductivity at various MPII concentration of P(VP-co-VAc)-KI-MPII gel polymer electrolytes samples.

4.4.3.2 Dielectric Relaxation Studies

As mentioned previously, the polarization effect of the GPEs at the electrode and electrolyte interface as well as the correlation between ionic relaxation time with conductivity are very important in order to know more about the dielectric properties of our samples. This is why the relative permittivity studies were also done on the single salt GPE samples that have been added with MPII ionic liquids.

The dielectric constant *ε' and* dielectric loss, *ε''* versus log *f* plots of the K30, KM5, KM10, KM15 and KM20 samples were shown in *Figure* 4.48 and *Figure 4.49*, respectively. As seen in the figure, the GPE samples which added with ionic liquids can be observed having similar spectra compared to the P(VP-co-VAc)-KI GPE samples (K30). This tells us that similar phenomenon is happening inside the polymer matrix in between the samples with and without ionic liquids. At low frequency, the dispersion value of *ε'* is still high because of the dielectric polarization which is due tothe high charge density caused by the accumulated trapped ions (Raghu, Kilarkaje, Sanjeev, Nagaraja, & Devendrappa, 2014). Meanwhile at higher frequency, the dielectric constant is becoming frequency independent as well causes by the periodic reversal of the electric field that are occurred very fast (Abo El Ata et al., 2004).

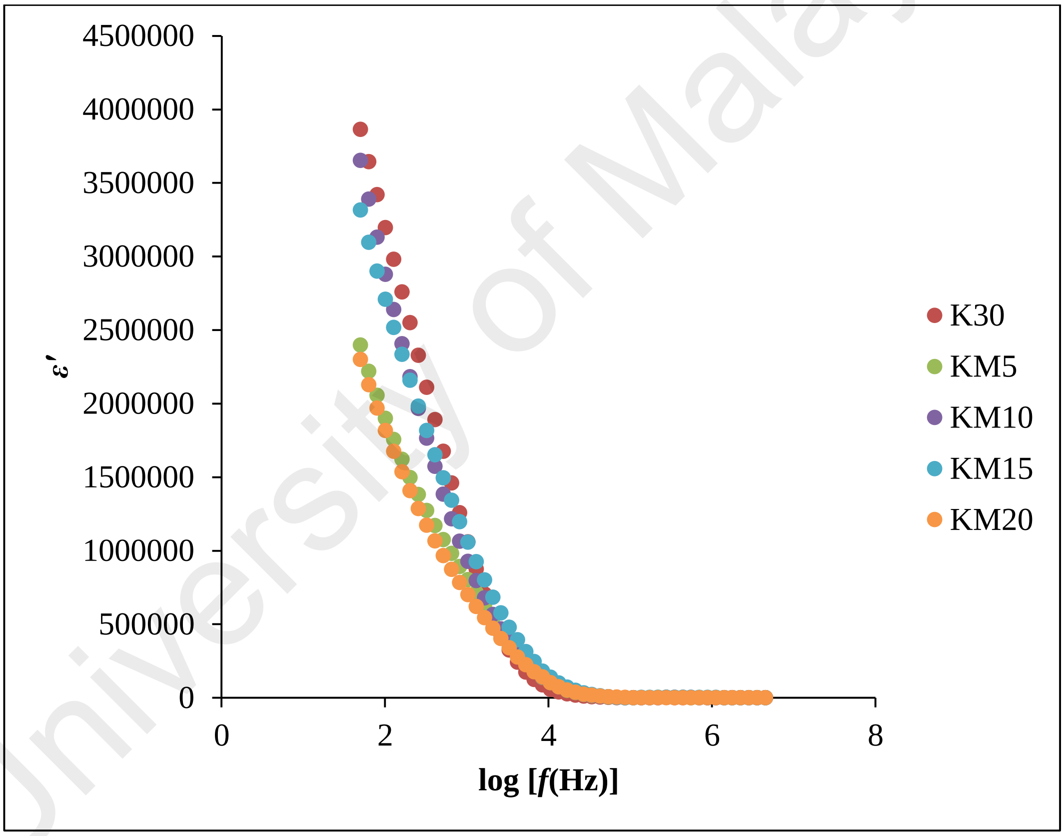

Figure 4.48: Variation of real part of dielectric constant, ε' with frequency for sample K30, KM5, KM10, KM15, and KM20.

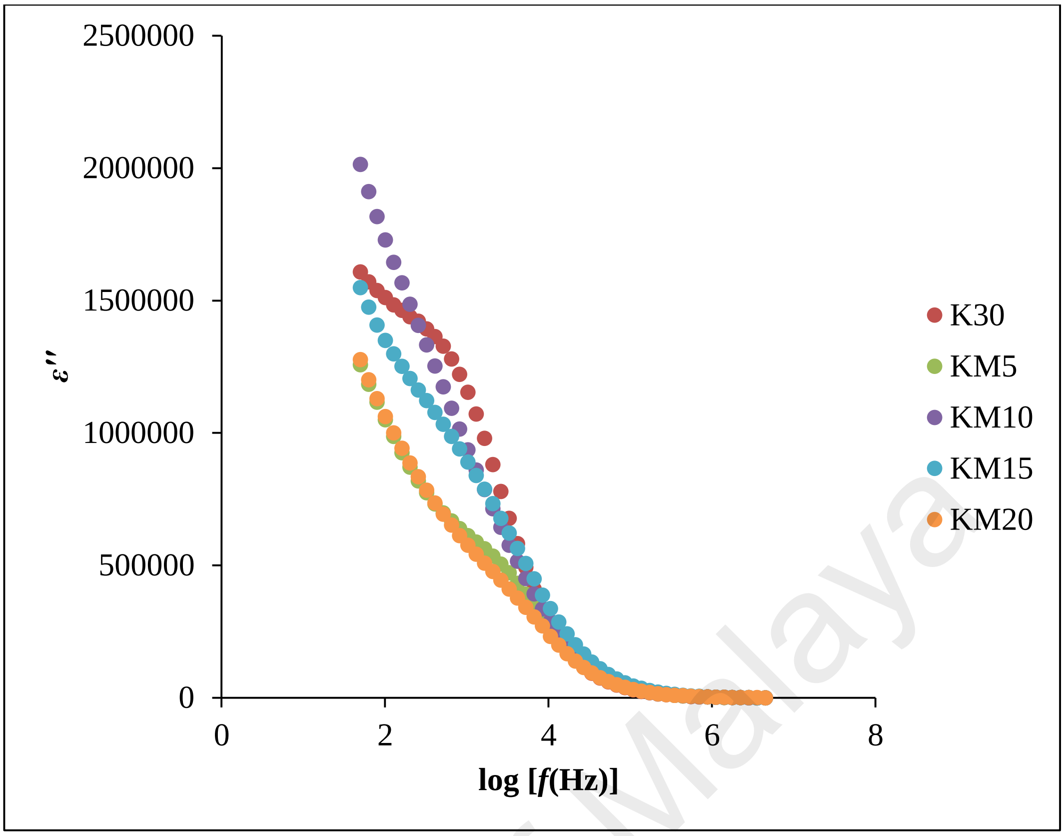

Figure 4.49: Variation of real part of dielectric loss, ε'' with frequency for sample K30, KM5, KM10, KM15, and KM20

4.4.3.3 Modulus Studies

Figure 4.50 and *Figure 4.51* shows the plots of the variation of real (M') and imaginary (M'') parts of the modulus as a function of frequency for all the samples for this system. Upon addition of ionic liquid, similar variation can be observed as it can observed there would be dispersion of M' occurring at the high frequency regions and it approaches to almost nothing when it reaches low frequency region (Ramya et al., 2008). This shows that there is no changes in the masking of the electrode polarization effects which occurs at the electrode-electrolyte interface. The loss of the peaks were because of higher frequency which could not be applied due to the limitation of the machine. However, the trend of the peaks still can be predicted from dispersion parts of the dielectric modulus which can be seen in the insets of *Figure 4.50* and *Figure 4.51*. By looking at the dispersion parts, the peaks were assumed to be shifted towards the higher region of the frequency with the increase of the MPII concentration (Ramesh & Ng, 2009).

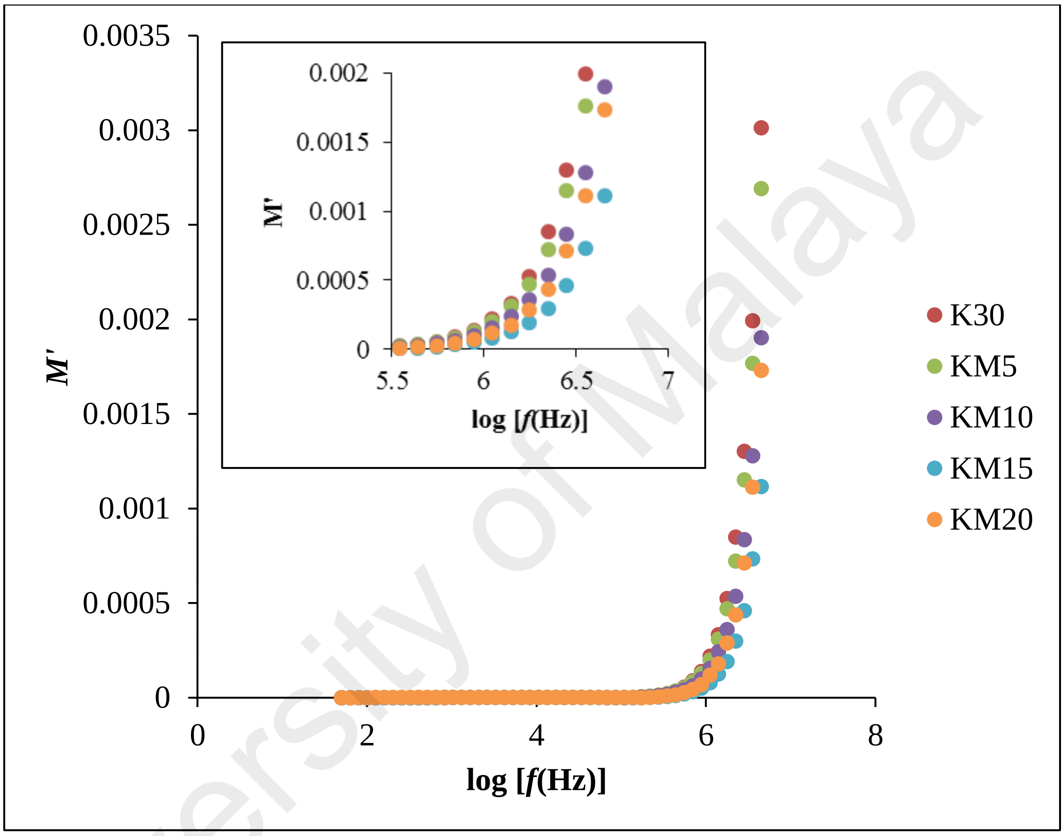

Figure 4.50: The real part of modulus, M' as a function of frequency for sample K30, KM5, KM10, KM15, and KM20.

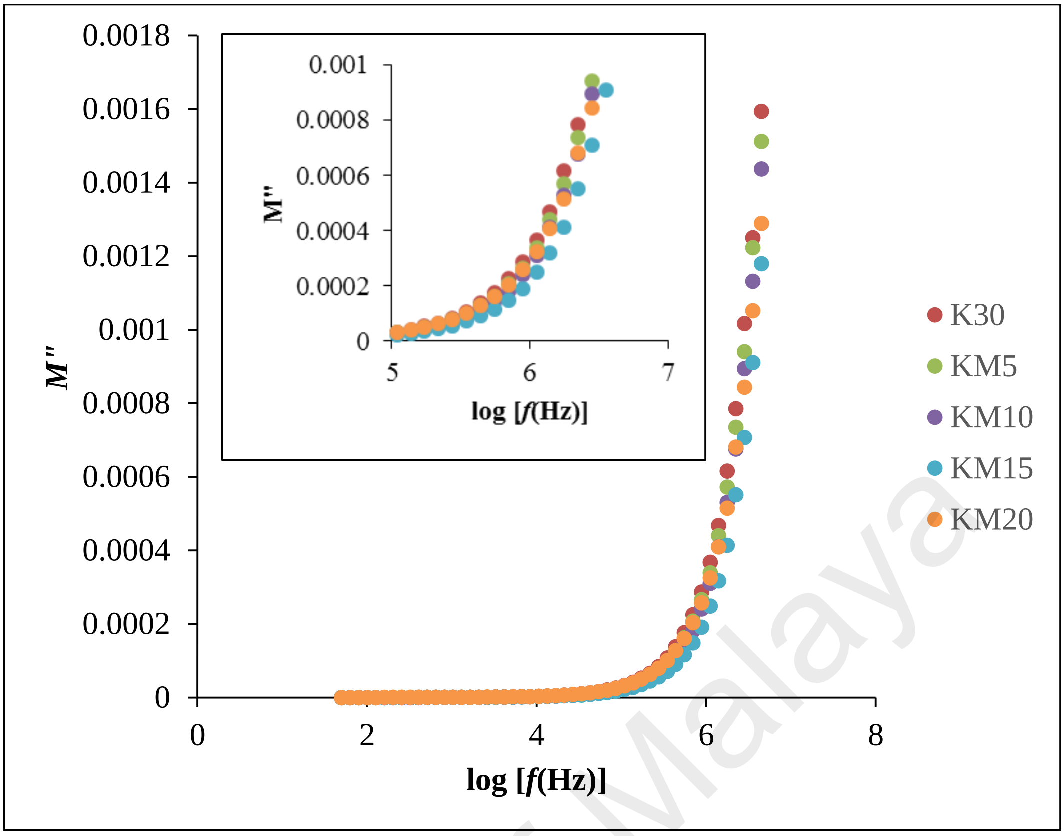

Figure 4.51: The imaginary part of modulus, M" as a function of frequency for sample K30, KM5, KM10, KM15, and KM20.

4.4.4 FTIR studies

Figure 4.52 shows the FTIR spectra of pure P(VP-co-VAc), pure KI, pure MPII, sample K30 and the P(VP-co-VAc)-KI-MPII GPE samples. The appearance of strong bands in the spectrum in the region of 1750 cm^{-1} to 1710 cm^{-1} and 1700 cm^{-1} to 1630 cm^{-1} which is shown in *Figure 4.53* was corresponded to C=O stretching of PVAc and PVP, respectively. After the addition of MPII, the bands of all samples were shifted to higher wavenumbers. The observed shift indicates the formation of complexes. The shifts are also indicating increase of the basicity of the PVP carbonyl group after the addition of MPII. It implies that the C=O group is able to act as a strong electron donor to interact with MPIm^{+} ions (Wieczorek & Stevens, 1997). The appearance of the band at 1247 cm^{-1} corresponding to C-N stretching frequency of sample K30, shifted to lower wavenumbers after the addition of MPII. This was due to the interaction of I⁻ ion from MPII with the N atom of C-N. The strong withdrawing character of the N atom in the PVP chain attracts the I⁻ ion (Ramya et al., 2007). Due to the changes in the intensity and the shifting in peaks, the complexation between P(VP-co-VAc), KI and MPII can be confirmed.

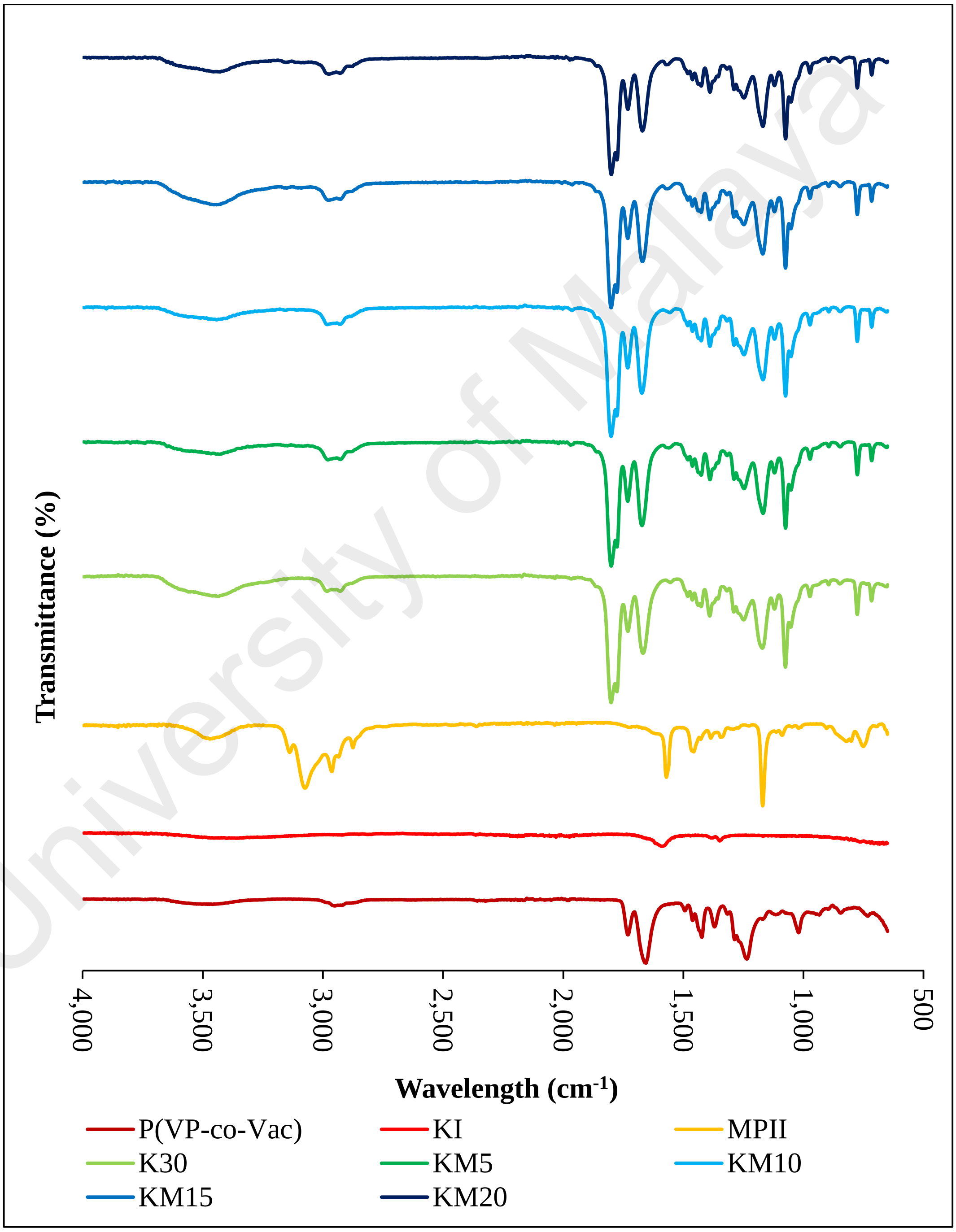

Figure 4.52: FTIR spectra for pure P(VP-co-VAc), pure KI, pure MPII, sample K30 and P(VP-co-VAc)-KI-MPII gel polymer electrolytes.

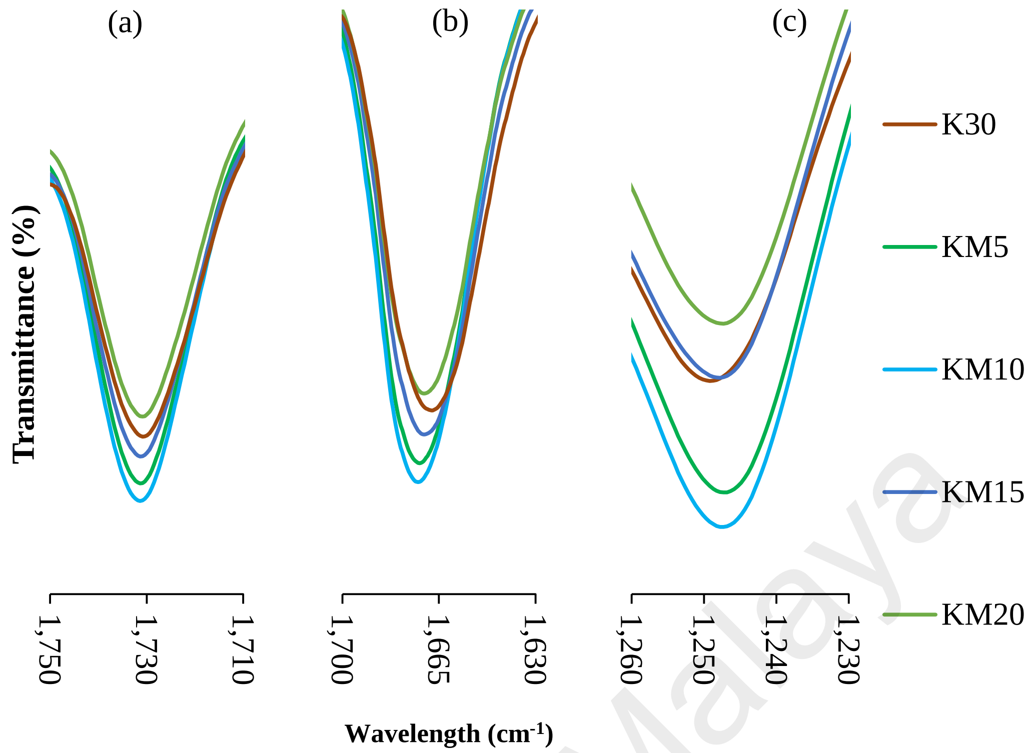

Figure 4.53: FTIR spectra in the region (a) 1750-1710 cm^{-1}, (b) 1700-1630 cm^{-1}, (c) 1260-1230 cm^{-1} for sample K30 and P(VP-co-VAc)-KI-MPII GPE samples.

4.4.5 X-ray diffraction (XRD) studies

XRD studies were performed for the samples of P(VP-co-VAc)-KI-MPII system and the results are shown in Figure 4.54. Previously, the XRD patterns of the system with with KI added into the P(VP-co-VAc) gel polymer electrolytes shows a broad peak. With the liquid characteristic of ionic liquids, the addition of the MPII into the system would have expected to show the same XRD patterns as well. The XRD patterns of all of the P(VP-co-VAc)-KI-MPII system gel polymer electrolytes samples shows only a broad peak at around 2θ = 21.6° for KM5, KM15 and KM20. The XRD patterns were quite similar with the previous system and thus, the only way to prove there were complexation occurring in the polymer matrix between the copolymer, salts and the ionic liquid is through the observation of the changes of the intensity of the peak after the addition of the MPII and the shifting of the main intensity peaks in the XRD pattern (Rajendran et al., 2007).

As seen in *Figure 4.54*, upon addition of MPII, it was observed the peak become much broader and decreases in intensity and the trend goes on up until 15 wt.% of MPII added into the system and slightly increases back in intensity at 20 wt.% of the MPII. This shows the complexation of the copolymer, salts and the ionic liquid in the polymer matrix. It also implies that the addition of the MPII further decreases the crystallinity of the gel polymer electrolytes until the optimum concentration that the GPE can handle. This is probably due to the well-known plasticizers effect of the ionic liquid which could help to soften the backbone of the polymer chains. With the crystallinity actually decreases, the ionic conductivity increases and it fits well with the ionic conductivity results which already been mentioned in *section 4.4.1.* As mentioned previously, the broad peaks of sample K30 were found to be shifted and this is also the indication of the complexation that has been occurred in between the P(VP-co-VAc), KI and MPII (Costa et al., 2007).

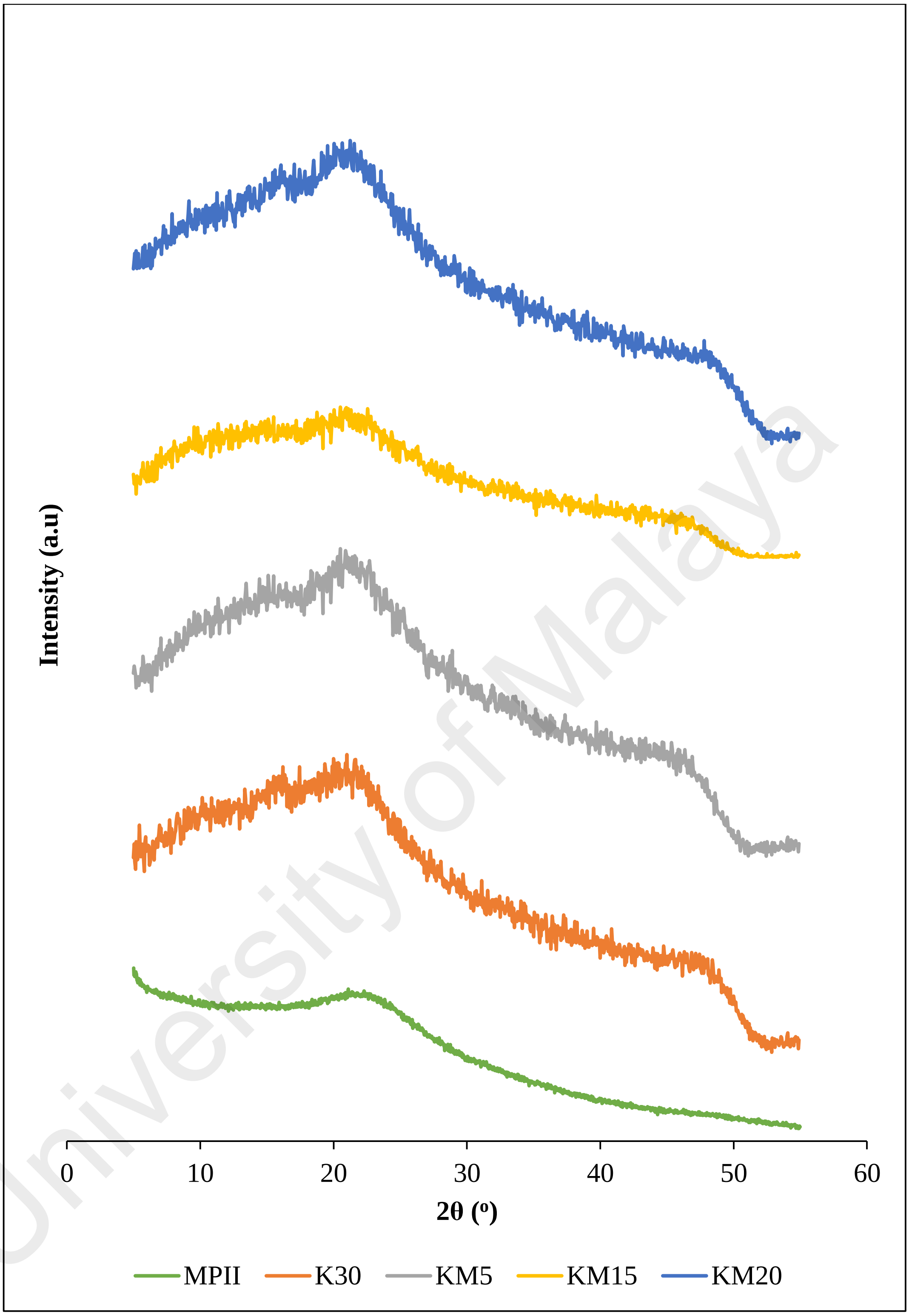

Figure 4.54: XRD patterns of the pure MPII, sample K30, KM5, KM15 and KM20.

4.4.6 Thermogravimetric analysis (TGA)

The thermal stability of the gel polymer electrolytes was evaluated by thermogravimetry (TG) studies. TG profile of the GPE samples is as shown in *Figure 4.55*. Initial weight loss of 2 - 7 wt.% is observed for all P(VP-co-VAc)-KI-MPII GPE samples in the temperature range of 30 – 100 ^oC is presumably due to the evaporation of the low molecular weight substance such as absorbed moisture and minor impurities. Meanwhile, the mass loss that can be observed at the range of 100 – 200 ^oC was attributed to the evaporation of the EC, PC and the small amount of the iodine, I_2 added as explained previously (K.-S. Kim et al., 2005). The summarized degradation temperature of PVP and PVAc region for the pure P(VP-co-VAc) and all of the samples are tabulated previously in *Table 4.14.* The degradation temperature T_{max1} can be seen to decrease initially after the addition of KI salts as explained in previous section but gradually increases after the addition of the MPII ionic liquid into the systems. This implies that the addition of the MPII once again increases the thermal stability of the PVAc region of the gel polymer electrolytes. In contrast, T_{max2} was observed to decrease after the addition of MPII. It indicates that the PVP region of the samples suffers decrease in thermal stability with the addition of ionic liquid into the GPEs system. These two occurrences were due to the different amount of energy that are required to break the interactive bonds in the different region. It is also in agreement with the FTIR studies about complexation between P(VP-co-VAc), KI and MPII. It can be observed that the weight loss for the deacetylation of the PVAc in the samples added with MPII was not abrupt compared to sample K30. This is due to the overlapping of the weight loss of deacetylation of the PVAc and the degradation of the MPII which has been found to start degrade at 260 ^oC (Hao, Lin, Zhang, & Li, 2011). This idea is supported by higher mass loss in this region in the thermogram of the ionic liquid added GPE samples compared to sample K30.

Meanwhile, degradation beyond 600 °C is most likely due to the decomposition of the KI salts in the polymer matrix (Zaccaron et al., 2005).

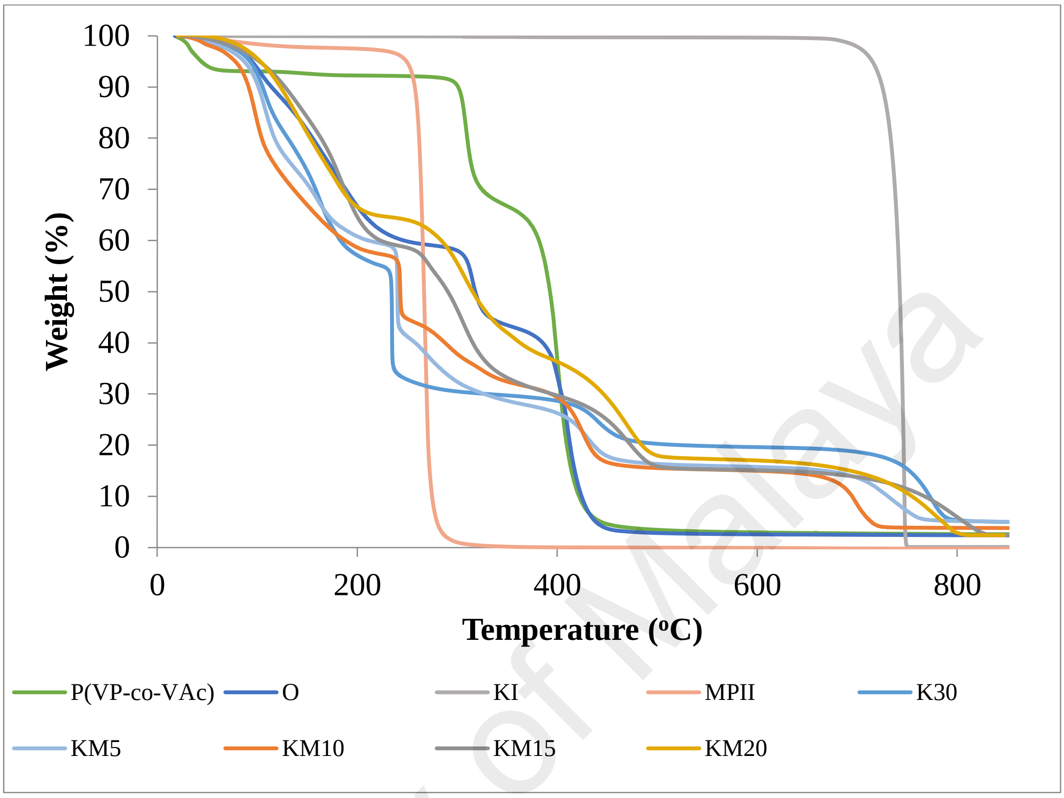

Figure 4.55: Thermogravimetric analysis of pure P(VP-co-VAc) and the P(VP-co-VAc)-KI-MPII GPE samples.

Table 4.14: The degradation temperature of the pure P(VP-co-VAc), sample O, K30 and the P(VP-co-VAc)-KI-MPII GPE samples.

Samples	**T_{max1} (°C)**	**T_{max2} (°C)**
P(VP-co-VAc)	310	385
O	314	411
K30	234	420
KM5	240	416
KM10	242	409
KM15	263	392
KM20	271	389

4.4.7 Photocurrent density-voltage (J-V) Characteristics

The photocurrent density-voltage (J-V) curves for DSSCs that employed the P(VP-co-VAc)-KI-MPII GPE samples are shown in *Figure 4.56* and the values of the open-circuit voltage (V_{oc}), short-circuit current density (J_{sc}), fill factor (FF) and conversion efficiency (η) of these DSSCs are tabulated in *Table 4.15*. Meanwhile, the variation of the normalized parameter of these DSSCs are shown in *Figure 4.57*. As observed in *Figure 4.57*, the variation of the solar cell power conversion efficiency (η) was found to have similar variation as the J_{sc} of the DSSCs. This implies that even after the addition of ionic liquid into the single salt system, the short circuit current density, J_{sc} still plays an important role in the variation of the photovoltaic performances for these GPE samples. The increase of the J_{sc} with the increase of the MPII concentration could be explained in terms of the increment of the iodide ion conductivity also known as the iodide ion transference number from the MPII and the intercalation of the cations into the TiO_2 electrode. Small cation, in this case the K^+, can intercalate into the traps in the layer that happened to be reducing the movement of the electrons through the nano-porous TiO_2 layer in the working electrode (Cha et al., 2010). Then, it will cause positive shifting in the conduction bands thus increasing the charge injection rate and leads to an increase in $J_{sc.}$ Meanwhile, for the bulkier cations, in this case the $MPIm^{+,}$ the positive conduction band shift is much smaller, but it could generate much more iodide (I^-) due to its high ionic dissociation rate. By having two different cations in the system, the iodide ion conductivity of the electrolyte is increased as shown previously in the ionic conductivity studies and also increases the charge injection rate which leads to the improvement of the J_{sc} and thus, the efficiency of the DSSCs (Dissanayake, Rupasinghe, Seneviratne, Thotawatthage, & Senadeera, 2014). In addition, ionic liquid exhibits plasticizing effects. It increases the morphology homogeneity of the polymer electrolyte matrix, reducing the crystallinity and promoting much more contact of the GPEs with the working TiO_2

electrode and the Pt counter electrode (Lin et al., 2014). This basically assists in the increase in the J_{sc} and photovoltaic performances. The highest photovoltaic conversion efficiency that was achieved in this system is 4.67% with j_{sc} of 11.98 mA cm^{-2}, V_{oc} of 0.59 V and fill factor of 66%.

In order to check for possible presence of mass transfer limitation in the P(VP-co-VAc) based GPE under high light intensity, the variation of the normalized current density of the DSSC under different illumination conditions were measured and shown in *Figure 4.58*. The linearity shown confirms that neither I^-/I_3^- transportation in the polymer matrix nor the electron transfer at the Pt/electrolyte interface represents rate-determining steps in the photo-electrochemical process. It also shows that the charge diffusion in the electrolyte does not limit the overall photocurrent density of the cells (Chiappone et al., 2014).

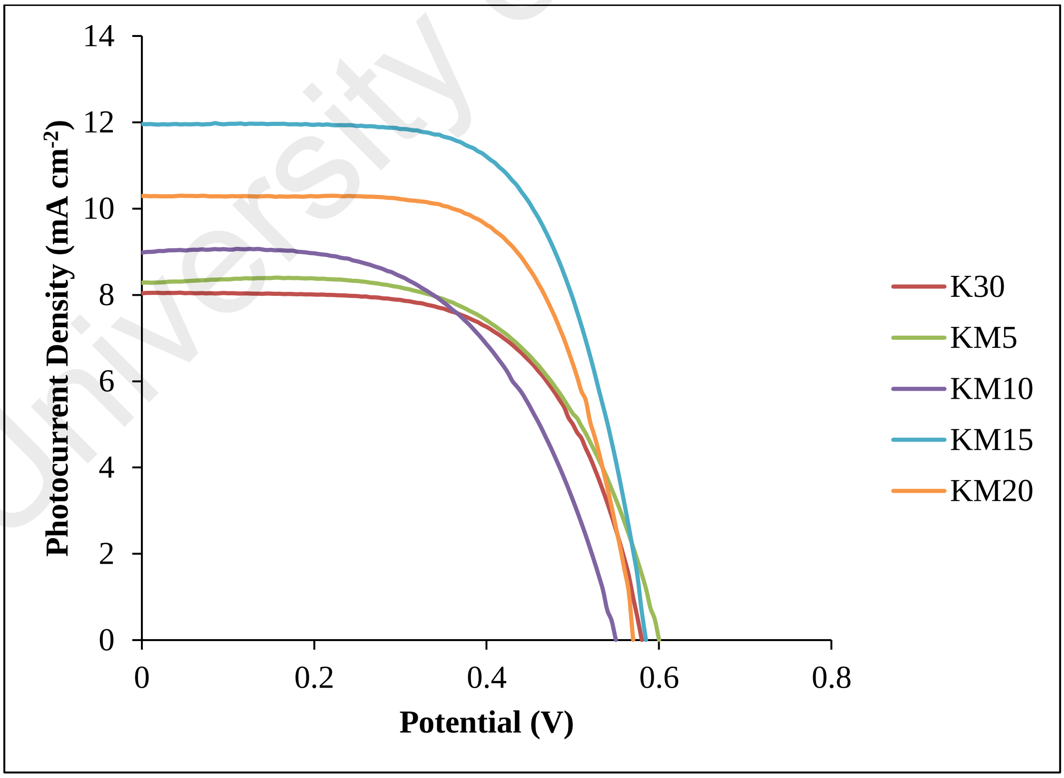

Figure 4.56: The photocurrent-photovoltage (J-V) characteristics of the GPE samples consisting of different weight percentages of MPII.

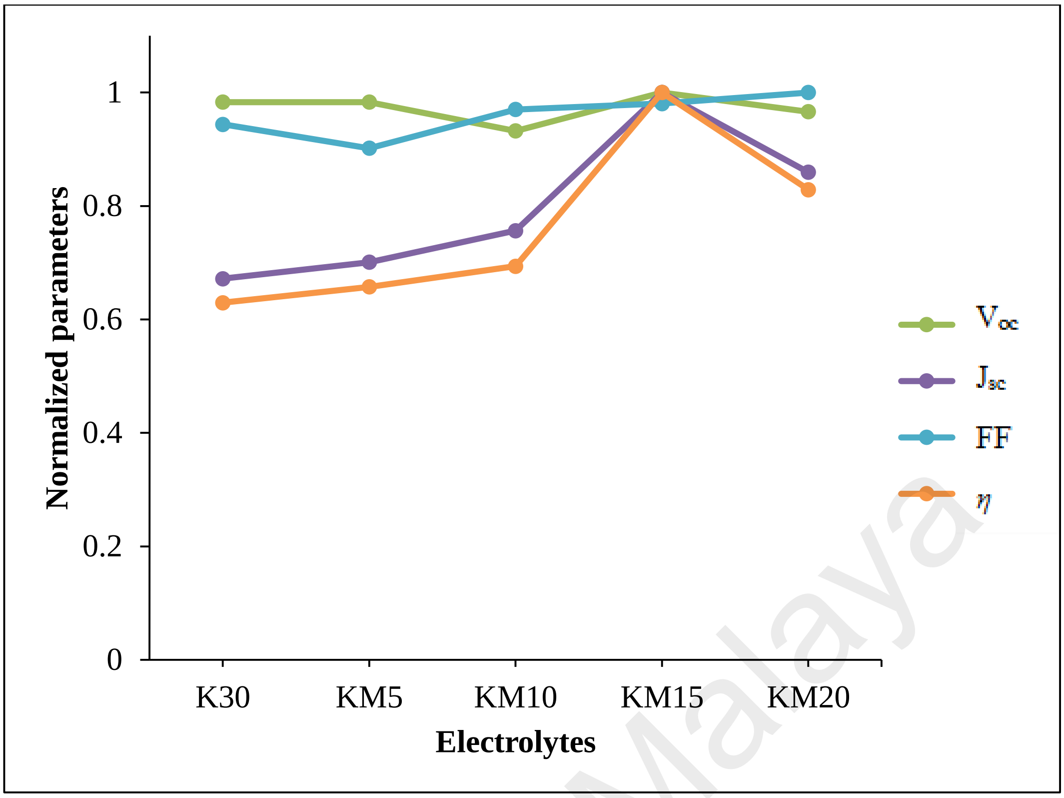

Figure 4.57: The normalization curves of the various performance parameters of the DSSCs fabricated with different P(VP-co-VAc)-KI-MPII GPE samples.

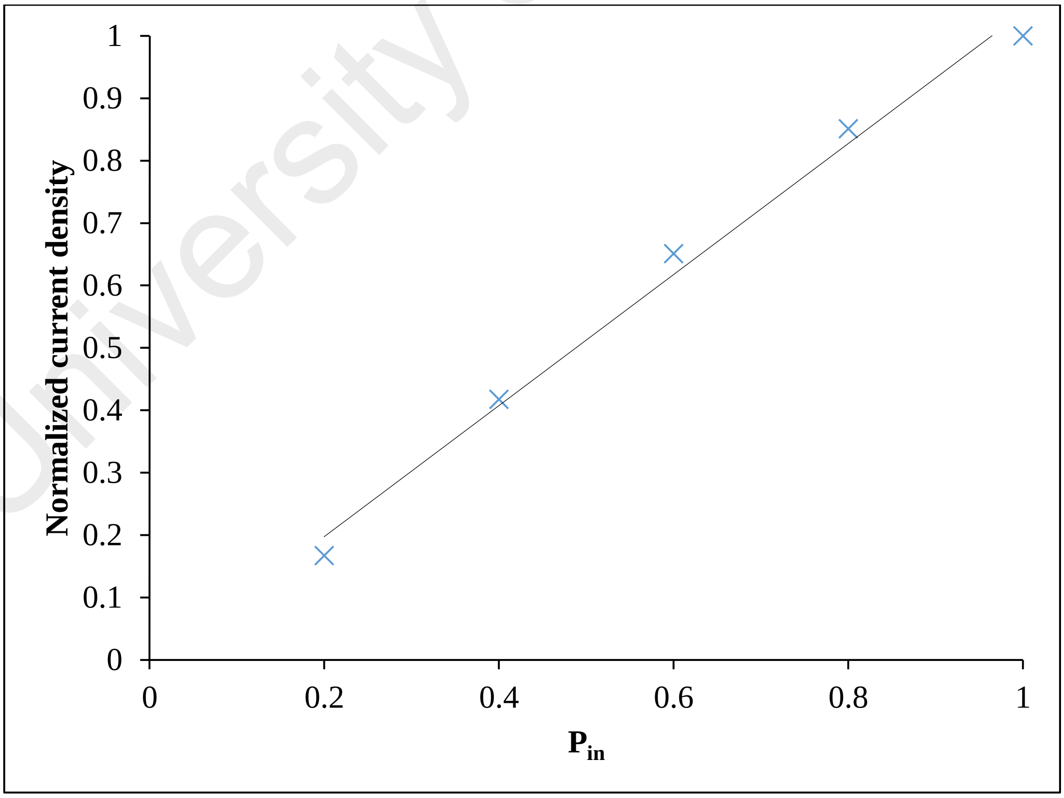

Figure 4.58: Normalized J_{sc} values plotted as a function of different light intensities (P_{in}) for sample KM15.

Table 4.15: Photovoltaic parameters of the GPE samples consisted of different weight percentages of MPII.

Electrolytes	V_{oc} (V)	J_{sc} (mA cm^{-2})	FF (%)	η (%)
K30	0.58	8.05	0.63	2.94
KM5	0.58	8.40	0.60	3.07
KM10	0.55	9.06	0.65	3.24
KM15	0.59	11.98	0.66	4.67
KM20	0.57	10.29	0.67	3.87

4.4.8 EIS studies for DSSCs

In order to investigate the impedance behavior of the fabricated DSSCs, the EIS data of the DSSCs assembled with P(VP-co-VAc)-KI-MPII GPEs was collected, and the results shown in *Figure 4.59(a)*. The data has been fitted with the equivalent circuits shown in *Figure 4.19*. The parameters of the equivalent circuit for both of the DSSCs were tabulated in *Table 4.16*. Two semi-circles in the EIS spectra can be seen in *Figure 4.59(a)*. The semicircle at the high frequency region that was corresponds to the charge transfer resistance at the Pt counter electrode was labelled as R_{ct1}. The middle frequency semicircle that was corresponds to the charge resistance of charge recombination between TiO_2 conduction band and I_3^- ions at TiO_2/dye/electrolyte interface was labelled as $R_{ct2.}$ The impedance at frequency below 5 Hz can be interpreted as the Warburg diffusion (W) process of I_3^-/I^- in the electrolyte, with associated Warburg parameter, Y_0 ($S^{1/2}\ \Omega^{-1}$) (Min Wang et al., 2014). The intersection of high-frequency circle and the x-axis is mainly associated with the sheet resistance of the FTO substrate, which was the ohmic serial resistance (R_s) (C. Wang, Wang, Shi, Zhang, & Ma, 2013). As shown in *Table 4.16*, R_{ct2} value for K30 is 12.4 Ω. High R_{ct2} value will ensure high recombination resistance at the photoanode/electrolyte interface, thus leading to high electron lifetime values. The R_{ct2}

value increases to 15.2 Ω with the incorporation of MPII into the GPE. The addition of MPII was found to be decreasing the charge recombination rate of the GPEs (Ke et al., 2014).

Figure 4.59(b) shows the Bode EIS spectra of the DSSCs of the P(VP-co-VAc)-KI-MPII GPE samples. For the samples, it can be observed that there is a peak in the middle frequency region where the character frequency in this region is inversely proportional to the electron lifetime according to the EIS theory. The electron lifetime value are in agreement with that from the R_{ct2} analysis (Boonsin et al., 2012).

Tafel polarization measurements were performed to explore the electrocatalytic activity and interfacial charge-transfer properties of the I^-/I_3^- redox couples on both of the GPEs. *Figure 4.60* shows the current density (J) as a function of potential (V) for the reduction of I_3^- ions. The limited diffusion current density, J_{lim} which is dependent on the diffusion coefficient (D_n) of the I^-/I_3^- couples in electrolyte can be obtained from the intersection of the cathodic branch with the Y-axis. The diffusion coefficient (D_n) is depicted *equations 4.8*. From the Tafel curves, the J_{lim} of KM15 was found to be higher than the other three samples which show that KM15 would have higher D_n. This suggests that there is enhancement in the diffusion kinetics for I^-/I_3^- redox species which is at the optimum with the addition of 15 wt.% of MPII (S. H. Park et al., 2014). On the other hand, the larger slope for the anodic or cathodic branch of the Tafel curve indicates the exchange current density (j_0). Apparently, the calculated slope for J_0 were having the trend of KM15>KM5>KM20>K10. J_0 can be associated with R_{ct} by equation 4.9 and the variation of V_{oc} and R_{ct2} with the respect of different MPII concentration in P(VP-co-VAc)-KI-MPII GPE samples were shown in *Figure 4.61*. These results show that Tafel polarization studies matches well with the EIS studies (C. Wu et al., 2012).

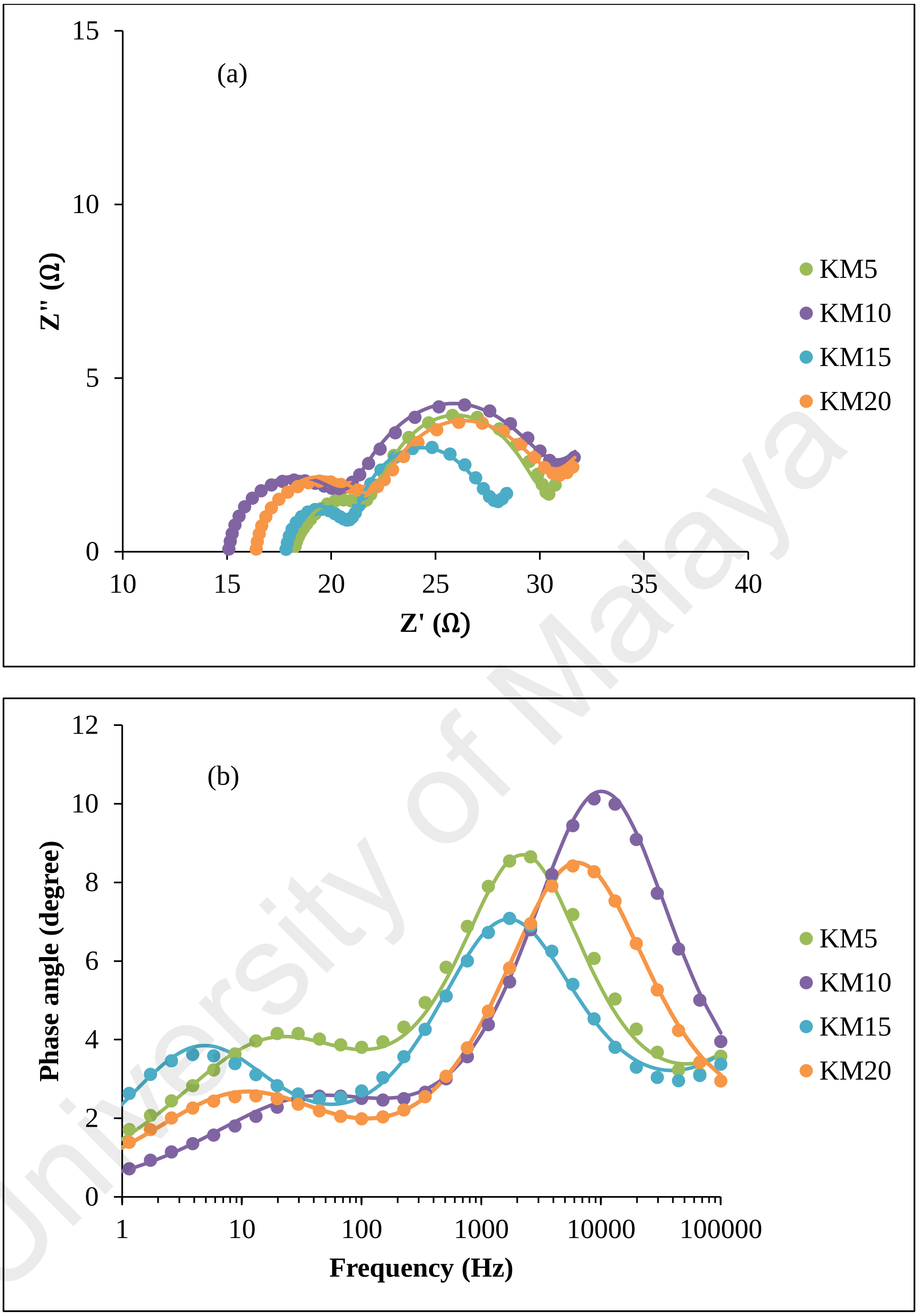

Figure 4.59: The electrochemical impedance spectra of DSSCs assembled with P(VP-co-VAc)-KI-MPII GPE samples in the forms of (a) Nyquist plots and (b) Bode phase plots. The spectra were measured under 100 mW cm^{-2} illuminated sunlight.

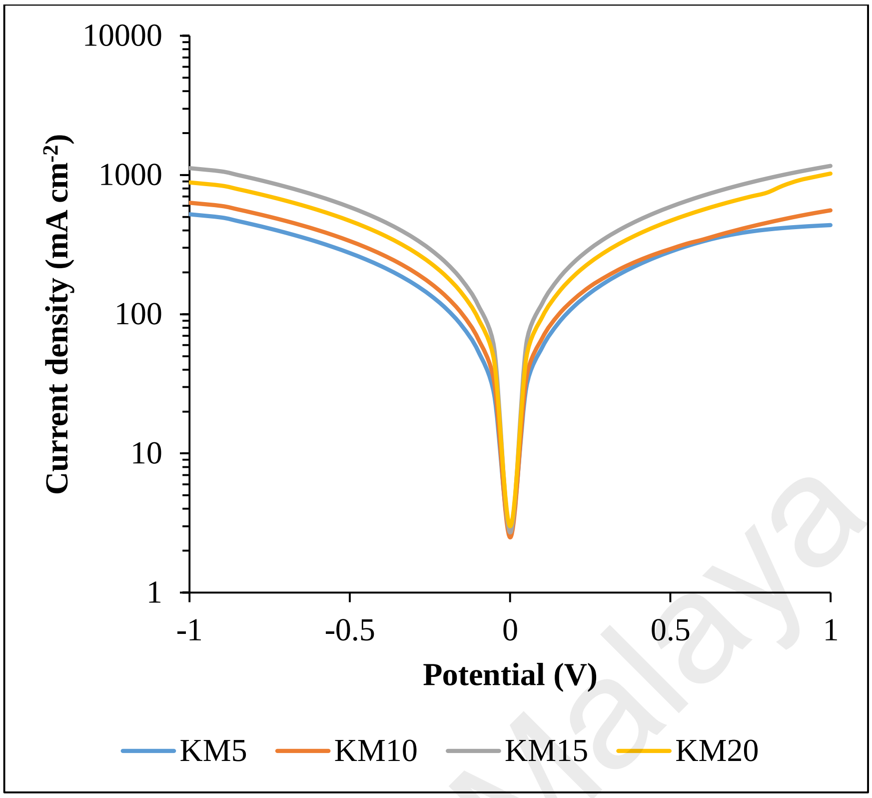

Figure 4.60: Tafel polarization curves of symmetric Pt cells with P(VP-co-VAc)-KI-MPII gel polymer electrolytes samples

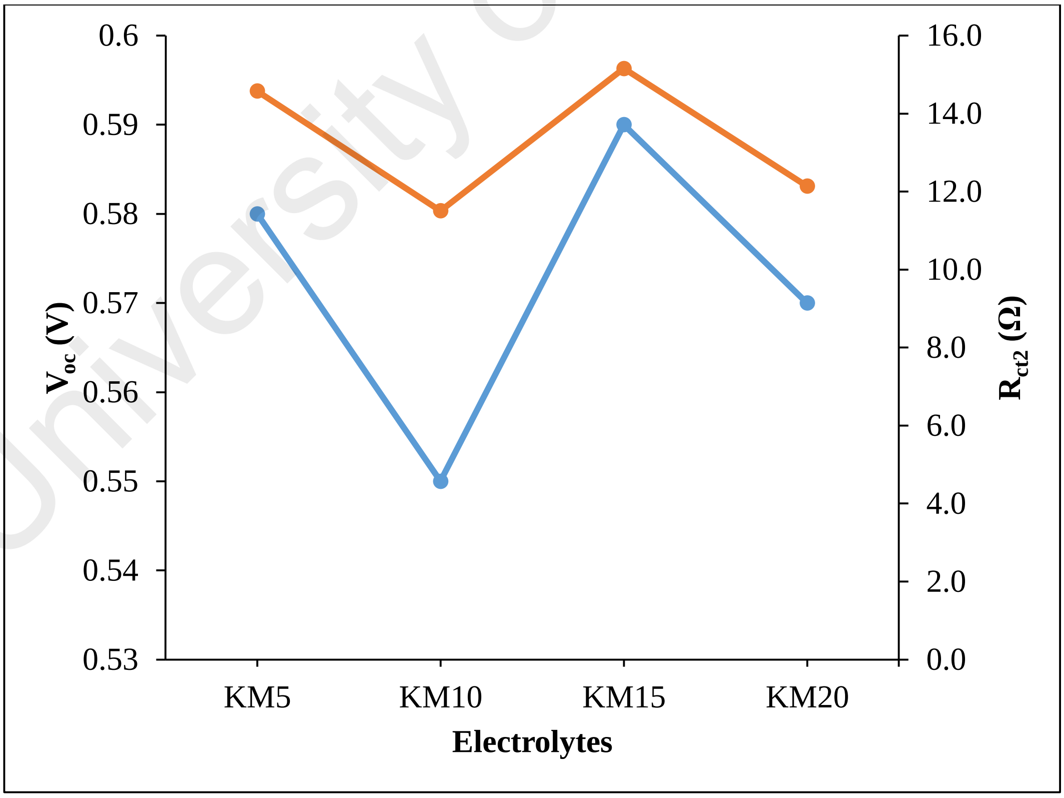

Figure 4.61: The open circuit voltage and R_{ct2} with the respect of different MPII concentration in P(VP-co-VAc)-KI-MPII GPE samples.

Table 4.16: The parameters of the equivalent circuits used to fit the EIS impedance data of the P(VP-co-VAc)-KI-MPII based DSSCs.

Electrolytes	R_s (Ω)	R_{ct1}(Ω)	R_{ct2}(Ω)	W($S^{1/2}$ Ω^{-1})	τ (ms)
K30	18.0	9.2	12.4	0.80	61.7
KM5	13.3	17.3	14.6	0.36	55.4
KM10	15.6	8.2	11.5	0.56	36.3
KM15	13.7	16.6	15.2	0.48	51.3
KM20	16.7	8.9	12.1	0.79	44.1

4.5 P(VP-co-VAc)-KI-TPAI Gel Polymer Electrolytes

4.5.1 Ambient Temperature-Ionic Conductivities Studies

Figure 4.62 shows the impedance plots of the P(VP-co-VAc)-KI-TPAI gel polymer electrolytes samples and only a single spike was observed for all of the samples. These observation shows that the current carriers in the system are the mobile ions that were controlling the entire total electrical conductivity of these electrolytes and there was good contact at the interface of the electrodes and the polymer electrolytes. (Sengwa & Choudhary, 2014).

Figure 4.63 depicts the ionic conductivity of different GPE samples with the variation of different content of KI and TPAI. As seen in the figure, the sample with only KI salt added was having higher ionic conductivity compared to the sample with only TPAI salt. This is due to the K^+ cations were able to move much more freely inside the polymer matrix as they are much more smaller in size and able to dissociate easier compared to the TPAI cations. This could indicates that the total ionic conductivity of the dual salts system would be more dominated by these highly mobile small K^+ cations. However, the I^- anions from both salts are also contributing to the total conductivity of the samples and also an important factor in the photovoltaic performances. Since it is only a single type of anion was being used, thus, there are no comparison can be made in this system (Dissanayake et al., 2014).

As observed in *Table 4.17*, sample with binary salt can be observed having slightly higher ionic conductivity compared to the single salt system of the P(VP-co-VAc)-based GPE samples. Similar occurrence has been reported by Bandara et. al. where this is due to the addition of the bulkier TPA^+ cations could help to enlarge the polymer chains and this could allowe the smaller cations which in this case the K^+, to be able to move in a much efficient way in the polymer matrix. The highest conductivity that could be obtained is 1.96 × 10^{-3} S cm^{-1} which is from sample KT5. This is due to the reason that the content of KI and TPAI has reached an optimum concentration at this point and both of the cations would be able to perform their role effectively inside the polymer matrix (T.M.W.J. Bandara et al., 2014; Dissanayake et al., 2014).

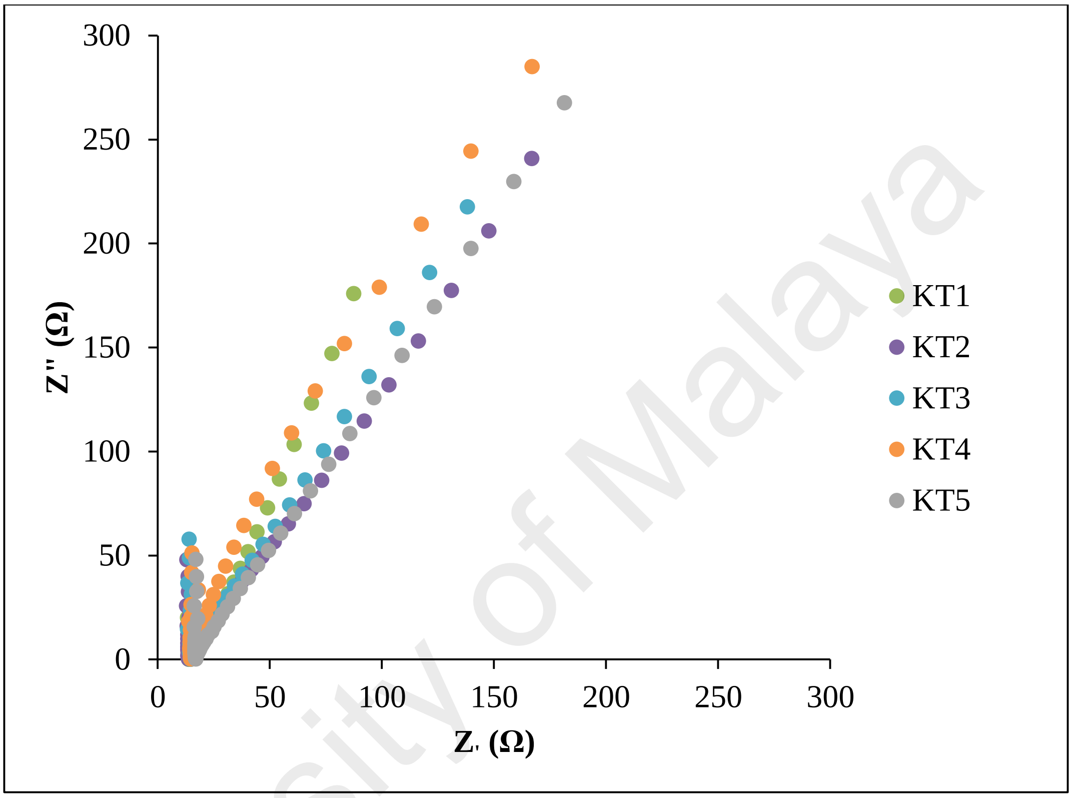

Figure 4.62: Typical complex impedance plot of P(VP-co-VAc)-KI-TPAI GPE samples at room temperature.

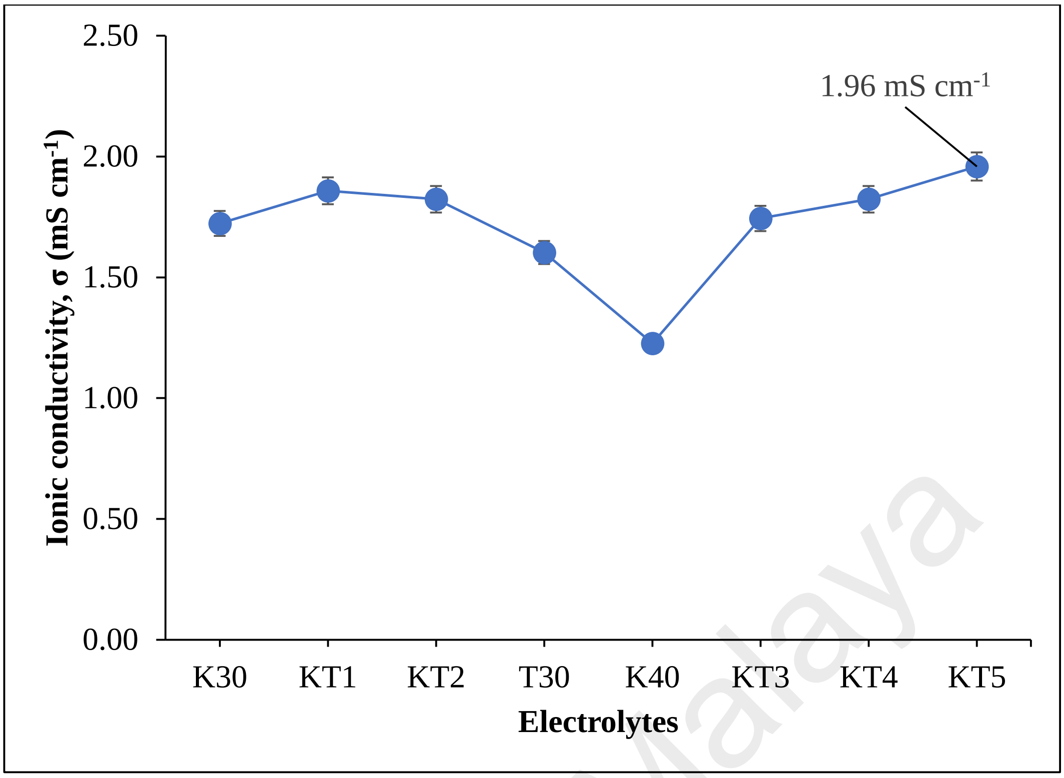

Figure 4.63: Variation of ionic conductivity of the GPE samples with different KI and TPAI ratio concentration at room temperature.

Table 4.17: Ionic conductivity values for the P(VP-co-VAc)-KI-TPAI GPE samples at room temperature.

Electrolytes	**Ionic Conductivity (mS cm^{-1})**
K30	1.72
KT1	1.86
KT2	1.82
T30	1.60
K40	1.23
KT3	1.74
KT4	1.82
KT5	1.96
T40	0.86

4.5.2 Temperature dependence-Ionic conductivity studies

Figure 4.64 shows the ionic conductivity (on log scale) variation with the reciprocal of the absolute temperature for the P(VP-co-VAc)-KI-MPII GPE samples. The linearity of the shape of the graph suggested that the conductivity variation is following the Arrhenius equation. This variation indicates the frequency of the mobile ions in the GPEs to hop from a site to another neighboring site increases when the GPE samples were being heated up by any sources of temperature (Asmara, Kufian, Majid, & Arof, 2011; Sudhakar et al., 2014).

The activation energy (E_a) for each GPE was determined by calculating the slope of each respective graph. *Figure 4.65* shows the variation of the ionic conductivity and the E_a of the P(VP-co-VAc)-KI-TPAI GPE samples. The calculated value of the E_a for all the samples are listed in *Table 4.18*. It is interesting to see that the E_a of the dual salt samples were found to be lower than the samples with only single KI and TPAI salt. This shows that the incorporation of dual salt has lowered the activation energy of the GPE samples. By having lowered activation energy, the energy required by the mobile ions to jump from one coordination to another coordination was lowered as well. Hence, it causes samples with dual salts having mobile ion that could move around slightly faster compare to the single salt system and it would lead to increase the ionic conductivity in a small amount (Yang, Wey, Liou, Li, & Shih, 2012).

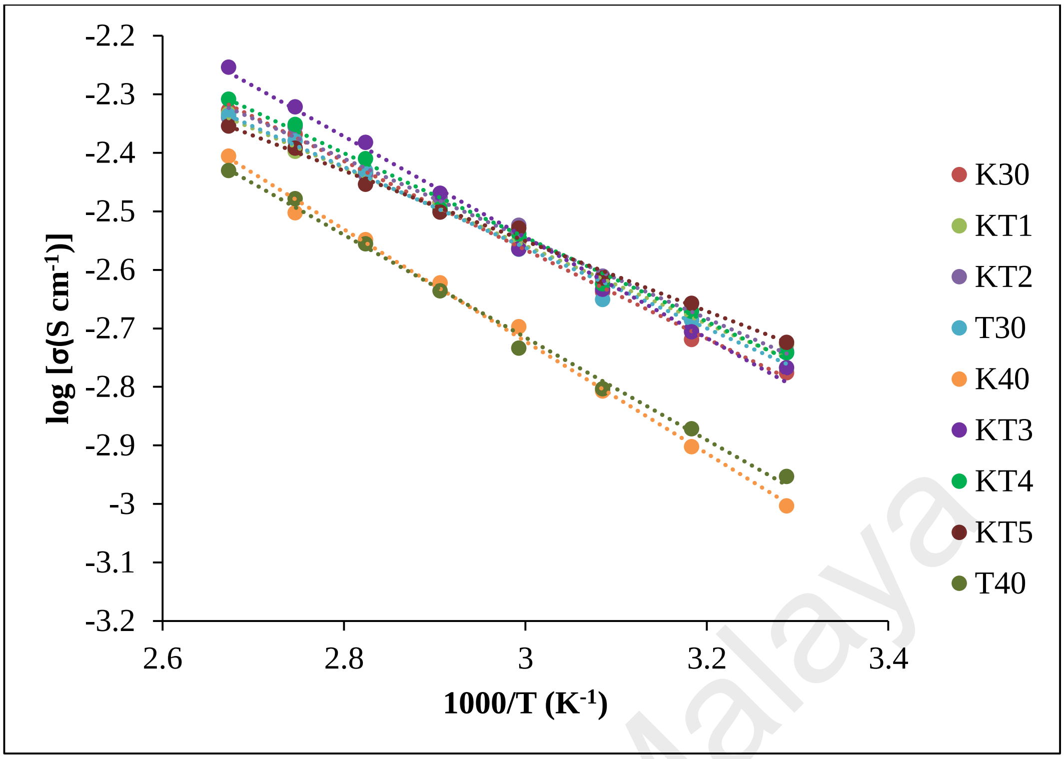

Figure 4.64: Arrhenius plots for the conductivity of the GPE samples with different ratio of concentration of KI and TPAI

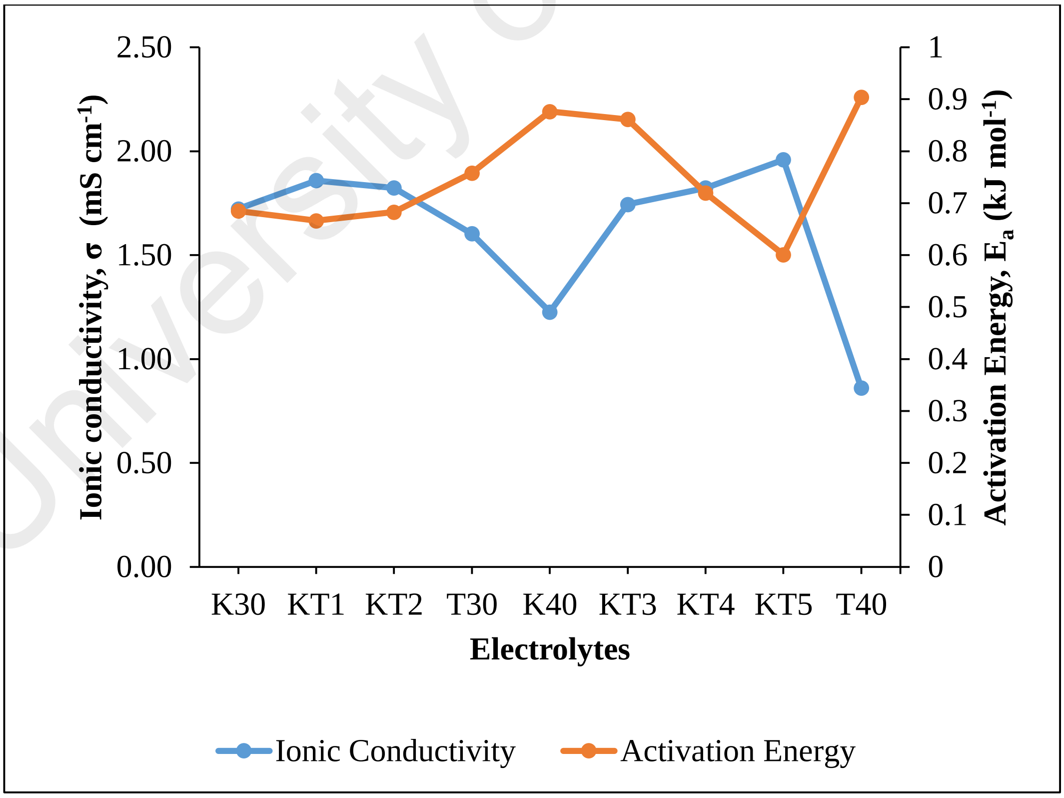

Figure 4.65: Variation of ionic conductivity and the activation energy of the P(VP-co-VAc)-KI-TPAI GPE samples with different KI and TPAI concentration at room temperature.

Table 4.18: The activation energy of the GPEs sample with different ratio of concentration of KI and TPAI.

Electrolytes	Activation Energy, Ea (kJ mol^{-1})
K30	0.69
KT1	0.67
KT2	0.68
T30	0.76
K40	0.88
KT3	0.86
KT4	0.72
KT5	0.60
T40	0.90

4.5.3 Dielectric Studies

4.5.3.1 Conductivity-frequency studies

The conductivity-frequency studies have been done for the binary salt system GPE samples in order to understand more on the relaxation processes of the gel polymer electrolytes which have been added with two different sizes of salts. The variation of the ionic conductivity with the frequency for different KI and TPAI ratio added into the gel polymer electrolyte samples at room temperature were shown in *Figure 4.66*. It is proved that the relaxation processes of the P(VP-co-VAc) based gel polymer electrolytes with binary salt were the same as the single salt system from the variation of the spectra of all of the binary salt systems. The same plateau region can be observed at high frequency region and when it reaches lower frequency it started to deviate from the plateau which is caused by the electrode polarizations. Moreover, with the ionic conductivity for all of the samples can be seen higher at higher frequencies also indicated that the binary salt system also obeying the relaxation model when the high frequency is applied, it would increase the chances for the mobile charge carriers to hop back to their original position leading to high mobility (Woo et al., 2012).

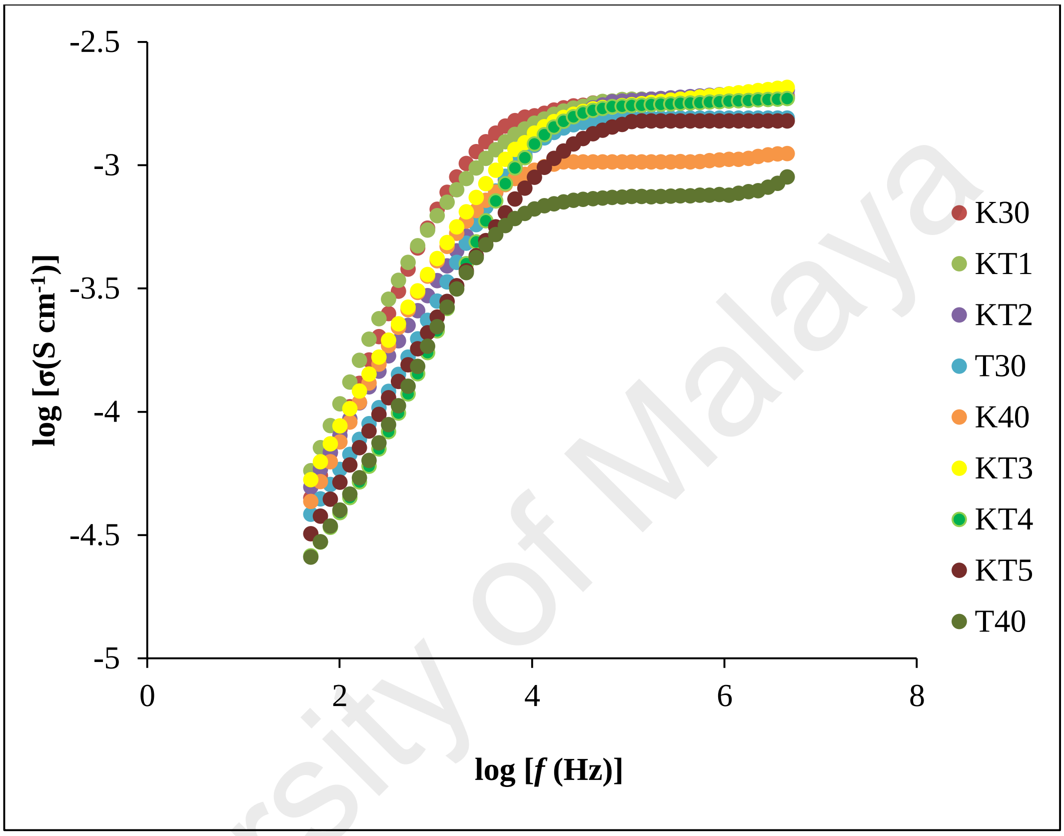

Figure 4.66: Frequency-dependent conductivity at various KI and TPAI concentration of P(VP-co-VAc)-KI-TPAI gel polymer electrolytes samples.

4.5.3.2 Dielectric Relaxation Studies

The study of the relative permittivity, ε_r^* was done to understand the polarization effect that happened at the electrode and electrolyte interface as well as the correlation between the ionic relaxation time with the conductivity of the binary salt systems. The purpose of doing this study is to check whether the addition of the second salt into the system would change the dielectric properties of the P(VP-co-VAc) based gel polymer electrolytes or not.

Figure 4.67 and *Figure 4.68* shows the complex permittivity (real part *ε'* and dielectric loss, *ε'')* spectra of the GPE samples for this systems. It can be seen that even with the usage of two different salts in the P(VP-co-VAc) based GPE samples does not changes the dielectric properties. The trend of the spectrum is still similar while the only thing changes is the value of the dielectric constant and dielectric loss which is due to different conduction properties of the samples. At lower frequency, the *ε'* values of the GPE samples are very large and this is caused by the dielectric polarization which has been explained previous (Raghu et al., 2014). The decrease of the *ε'* values is due to the very fast periodic reversal of the electric field and causes no time for the charges to build up at the interface of the electrodes and electrolytes (Raghu et al., 2013).

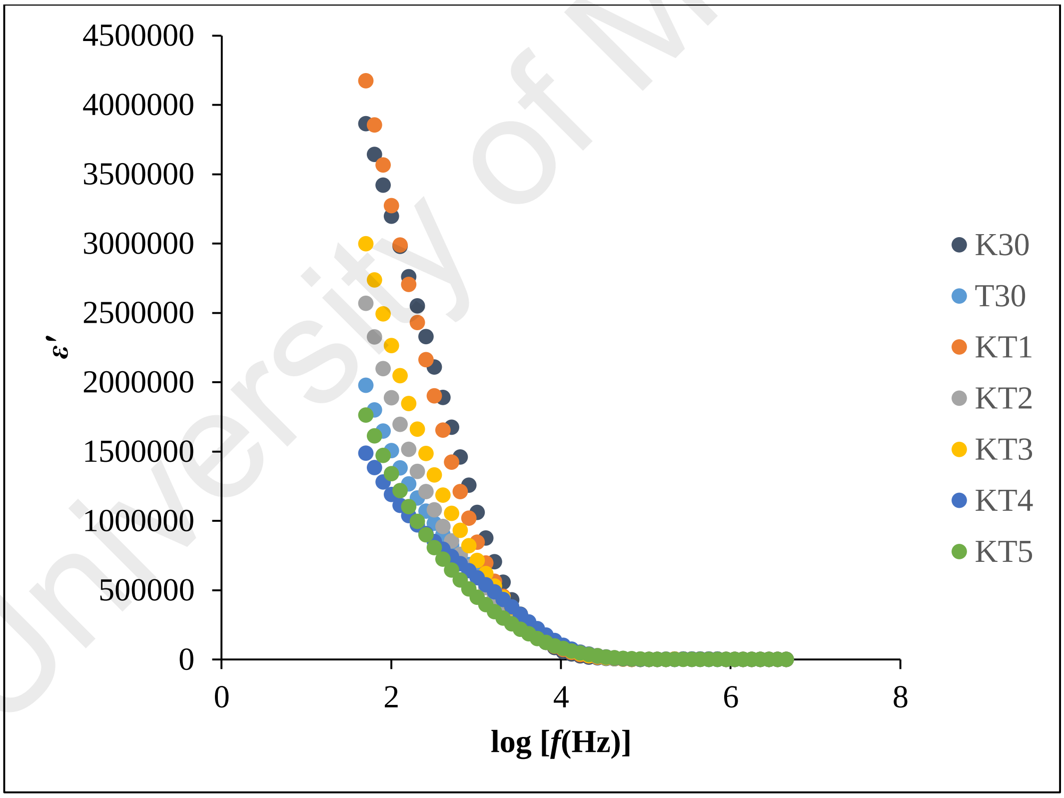

Figure 4.67: Variation of real part of dielectric constant, ε' with frequency for samples of P(VP-co-VAc)-KI-TPAI gel polymer electrolytes.

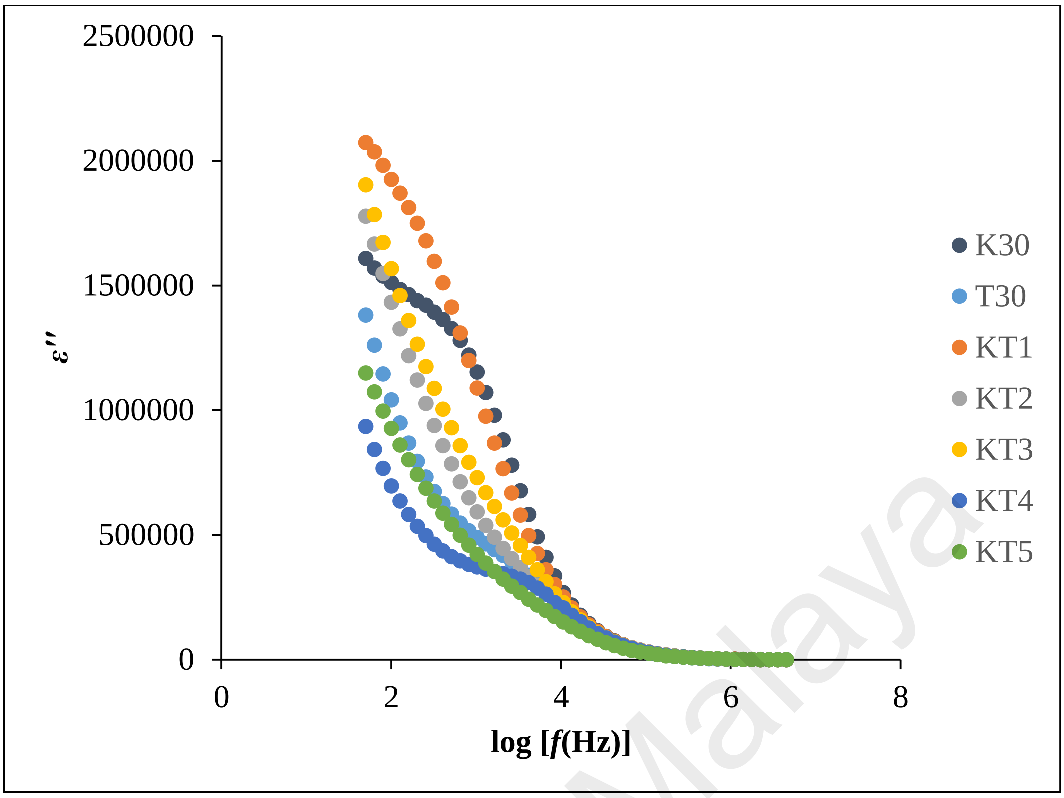

Figure 4.68: Variation of real part of dielectric loss, ε'' with frequency for sample samples of P(VP-co-VAc)-KI-TPAI gel polymer electrolytes.

4.5.3.3 Modulus Studies

The real and imaginary part of modulus (M' and M'') as a function of frequency for all the GPEs for this system were shown in *Figure 4.69* and *Figure 4.70*, respectively. In both figures, there is an appearance of the long tails in all of the samples at low frequency region. It is attributed to the large capacitance that associated with the electrodes. It is also observed that the real and imaginary part of the modulus is decreasing with the decrease of frequency until it approaches zero. This is indicating that the electrode polarization in the GPEs did not contribute anything and it can actually be neglected at that point. As mentioned previously, peaks would be expected to be seen if the sample could be applied with much higher frequencies. Thus, by looking at the trend of the spikes variation of the M' and M'' showing in the inset of both *Figure 4.69* and *Figure 4.70*, respectively, it can be assumed that the peak of the sample KT5 were shifted to the far most left side of the frequency region and was expected to have the shortest relaxation time out of all of the samples. This is in agreement with the ionic conductivity studies which was explained in *section 4.5.1* (Woo et al., 2012).

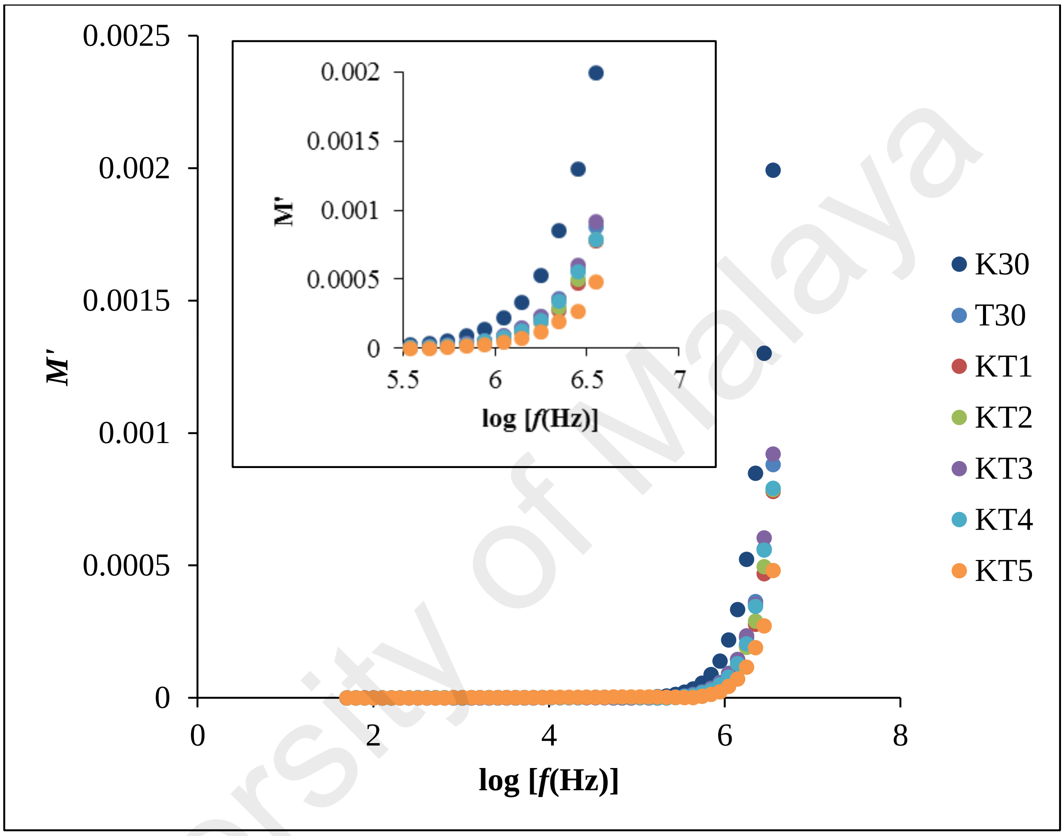

Figure 4.69: The real part of modulus, M' as a function of frequency for samples of P(VP-co-VAc)-KI-TPAI gel polymer electrolytes.

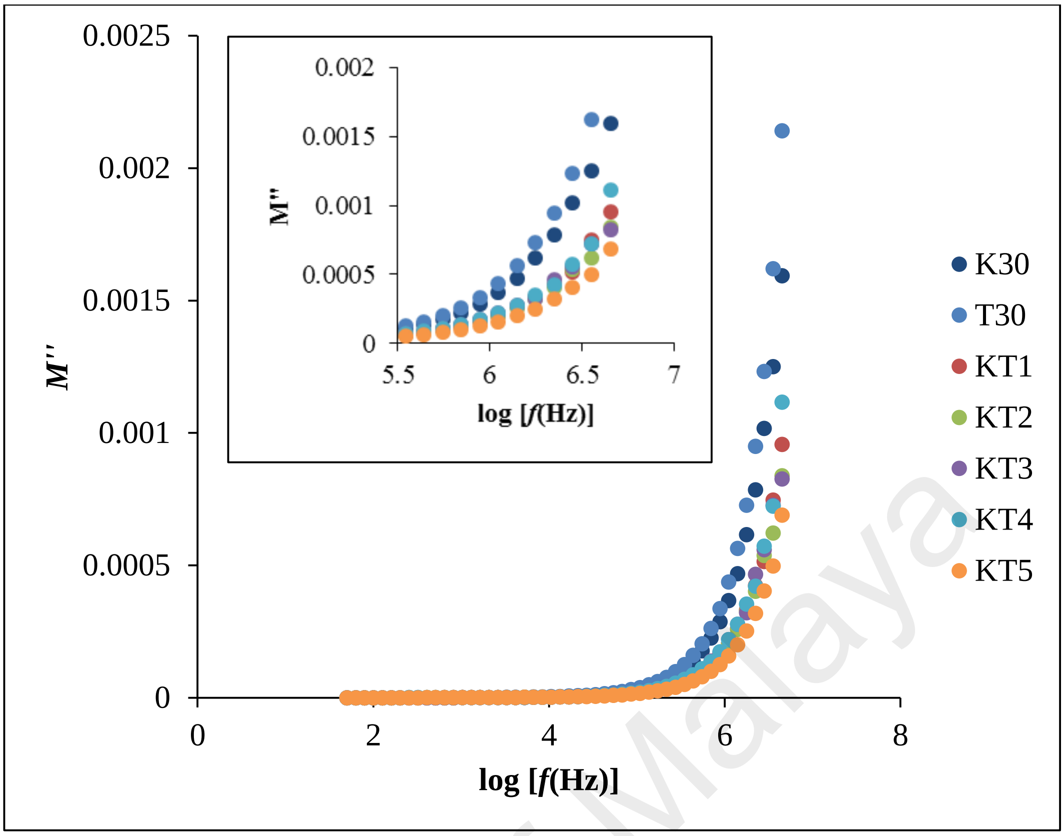

Figure 4.70: The imaginary part of modulus, M" as a function of frequency for samples of P(VP-co-VAc)-KI-TPAI gel polymer electrolytes.

4.5.4 FTIR studies

The interactions between the anions and the cations of KI and TPAI with the GPEs have been discussed previously in *section 4.2.4* and *section 4.3.4*. Thus, in this studies, we are going to look for the interactions occurred with the addition of these two different salts together. The interaction between the materials were investigated by the means of FTIR spectra of pure P(VP-co-VAc), pure TPAI, pure KI, sample K30, T30 and P(VP-co-VAc)-KI-TPAI gel polymer electrolytes samples in *Figure 4.71*.

In order to prove the complexation between the materials occurred in the GPE samples, the observation would be made at the important C=O band which is at 1750 cm^{-1} to 1710 cm^{-1} and 1700 cm^{-1} to 1630 cm^{-1} for the PVAc and PVP region, respectively as well as the wavenumber region at 1230 cm^{-1} to 1260 cm^{-1} for the C=N stretching of P(VP-co-VAc) copolymer. From *Figure 4.72*, it was observed that the peaks at the C=O region of both the PVAc and PVP region were seen to be slightly shifted lower wavenumber indicating that there were complexation occurred at the C=O stretching of both region. The changes in the intensity were another way to prove the complexation as well (Selvasekarapandian et al., 2006). The shifting and the changes in the intensity of the peaks were mostly likely due to the interactions of the K$^+$ and TPA$^+$ anions with the electron donor group C=O which has been explained previously in both sections of the single salt system (Wieczorek & Stevens, 1997).

Meanwhile, the peaks of the P(VP-co-VAc)-KI-TPAI GPE samples at 1230 cm^{-1} to 1260 cm^{-1} region of the C=N stretching were also found to be shifted to lower wavenumber and the intensity of the peaks changes as well. This is the indication of the interaction of the I$^-$ with the C=N stretching group which has been explained previously (Ramya et al., 2007).

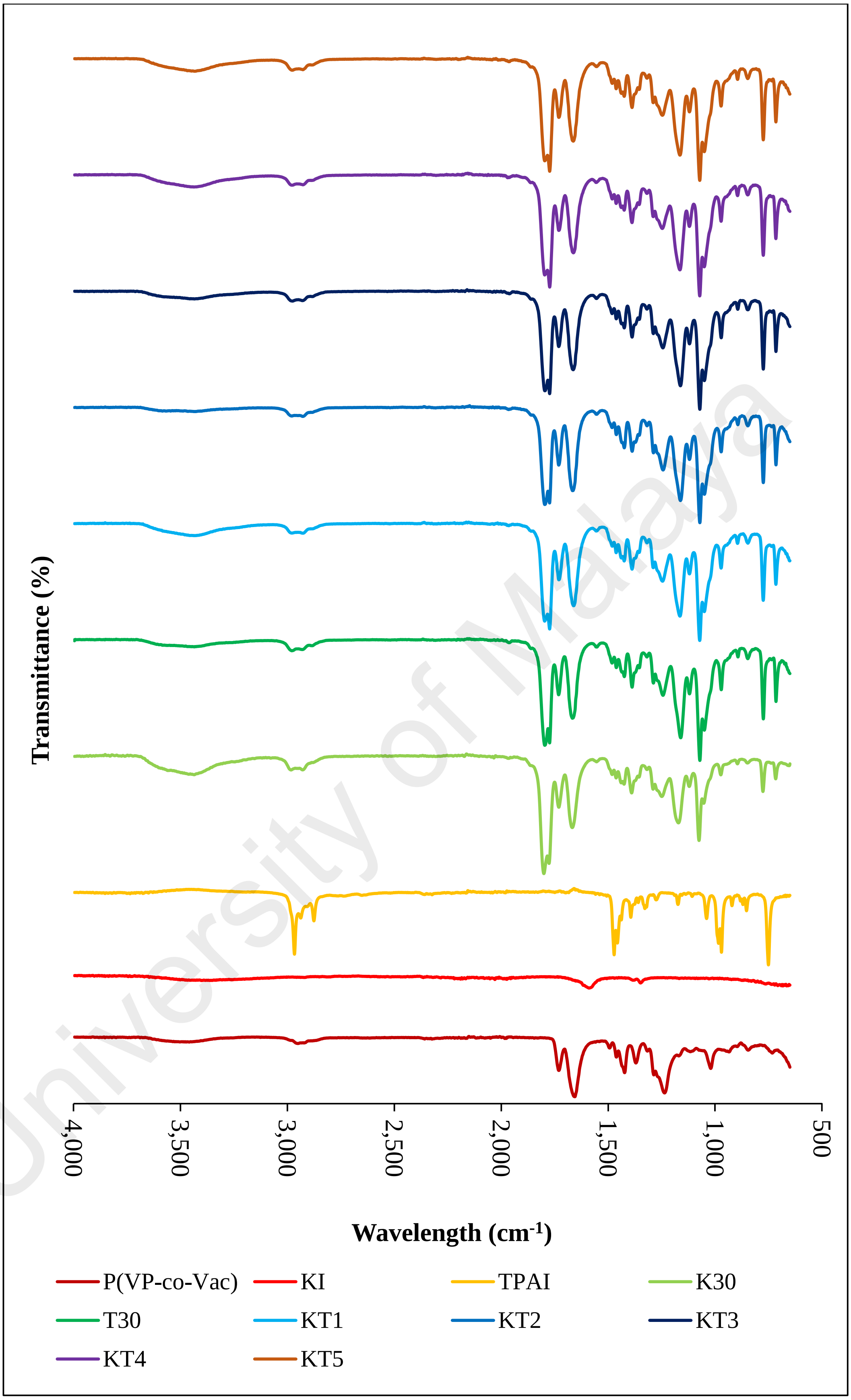

Figure 4.71: FTIR spectra for pure P(VP-co-VAc), pure KI, pure TPAI, sample K30, T30 and P(VP-co-VAc)-KI-TPAI gel polymer electrolytes.

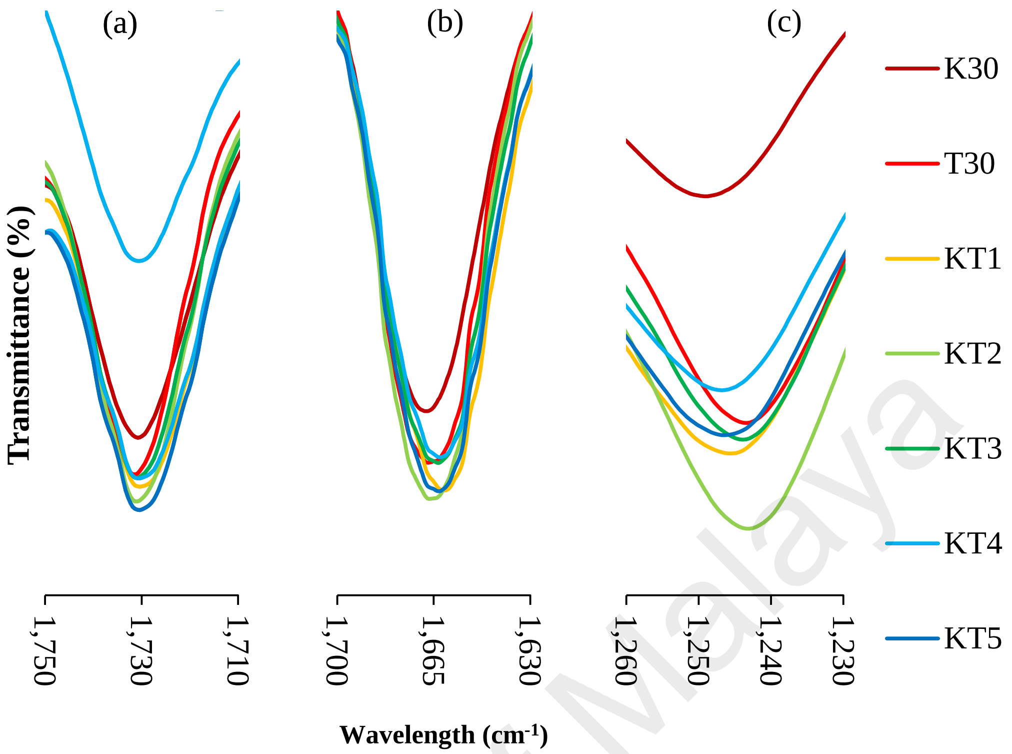

Figure 4.72: FTIR spectra in the region (a) 1750-1710 cm^{-1}, (b) 1700-1630 cm^{-1}, (c) 1260-1230 cm^{-1} for sample K30, T30 and P(VP-co-VAc)-KI-TPAI GPE samples.

4.5.5 X-ray diffraction (XRD) studies

Figure 4.73 shows the XRD patterns of pure P(VP-co-VAc) and all of the samples of the P(VP-co-VAc)-KI-TPAI systems. As explained previously, the XRD patterns of KI and TPAI consist of a number of intense peaks which helps to characterize them as high crystallinity materials (Rajendran et al., 2007). However, the XRD patterns of the P(VP-co-VAc)-KI-TPAI samples show that the crystallinity peaks of the salts disappeared. This simply shows that the salt added into the system undergoes complete dissolution and also prove that the complexation occurred in the polymer matrix (Rajendran et al., 2007). Once again, it proves that the addition of two types of salts did not disturb with the amorphous nature of the gel polymer electrolytes consisting P(VP-co-VAc) only (sample O). The characteristic peaks of the P(VP-co-VAc) copolymer as discussed previously was also found to be shifted to 2θ of 21.9° for KT1, to 21.8° for KT2, to 21.9° for KT3, to 22.1° for KT4 and to 22.2° for KT5 (Costa et al., 2007). The slight shifting of the peak is also another indication of the complexation happened among all of the materials in the polymer matrix. As observed in the figure, sample KT5 was having the lowest crystallinity compared to the other P(VP-co-VAc)-KI-TPAI systems gel polymer electrolytes sample. At this ratio of the KI and TPAI, it might has remarkable disturbed the ordered arrangement of the polymer matrix the most and causing the most drops in crystallinity. This is in agreement with the ionic conductivity studies where sample KT5 with the lower crystallinity is the sample with the highest ionic conductivity. With the changes in the intensity, it also helps to prove the complexation occurs between the copolymer and the salts added into the system (Sivakumar et al., 2006).

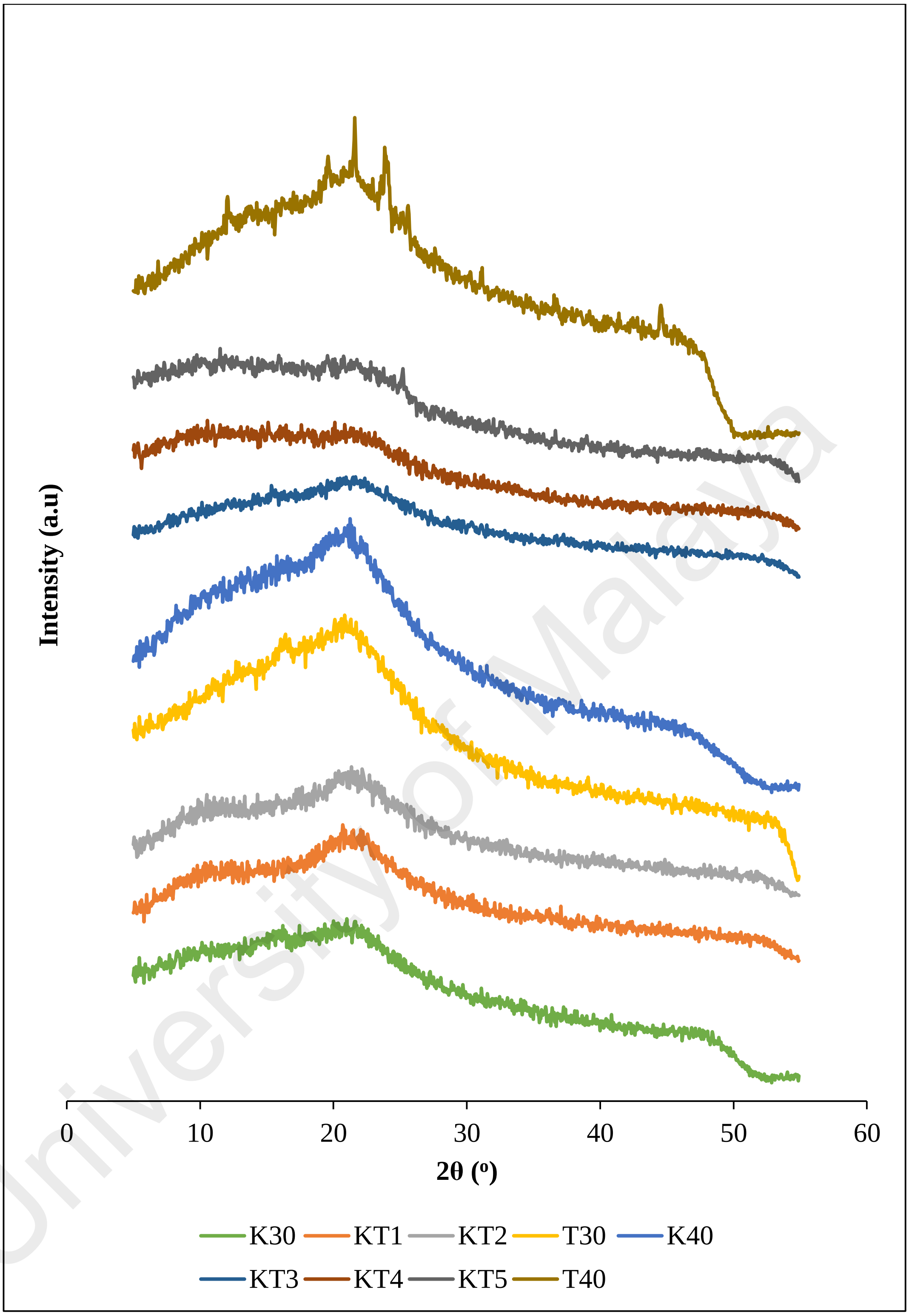

Figure 4.73: XRD patterns of the sample K30, KT1, KT2, T30. K40, KT3, KT4, KT5, and T40.

4.5.6 Thermogravimetric analysis (TGA)

The weight loss of the P(VP-co-VAc)-KI-TPAI gel polymer electrolytes system was evaluated by TGA in nitrogen environment and the results were presented in *Figure 4.74*. The degradation temperature and the weight loss was tabulated in *Table 4.19*. Similar observation as previous system can be observed at temperature around 30 ℃ - 200 ℃ which is due to the weight loss were due to the evaporation of the moisture absorbed, the solvents EC and PC, iodines added as well as some of the minor impurities. With two salts added into the system, it can be observed that the degradation temperature of the PVAc region were further decreased. This might be due to the overlapping reaction comes from both of the salts as the two salts were observed to be reducing the degradation temperature of the PVAc in the previous studies. Thus, when this two salts actually were added together into the P(VP-co-VAc) gel polymer electrolytes, it further decreased the degradation temperature of the PVAc. Meanwhile, the addition of the two salts into the system seems to increase the degradation temperature of the PVP region. This would probably due to the effects from the KI salt as it has been proved previously. It is able to increase the degradation temperature of the PVP region while the addition of the TPAI doesn’t change the degradation temperature of the PVP region. In this system, the TPAI also appeared to be degrade slightly at higher temperature. This might due to some of the complexation occurred in the polymer matrix between the salt and copolymer. On the other hand, the samples with higher ratio of KI were found to have higher weight loss at the PVAc region and lower weight loss at the PVP region. It indicates that the KI salt plays an important role in improving the thermal stability at the PVP region and decreasing the thermal stability at the PVAc region.

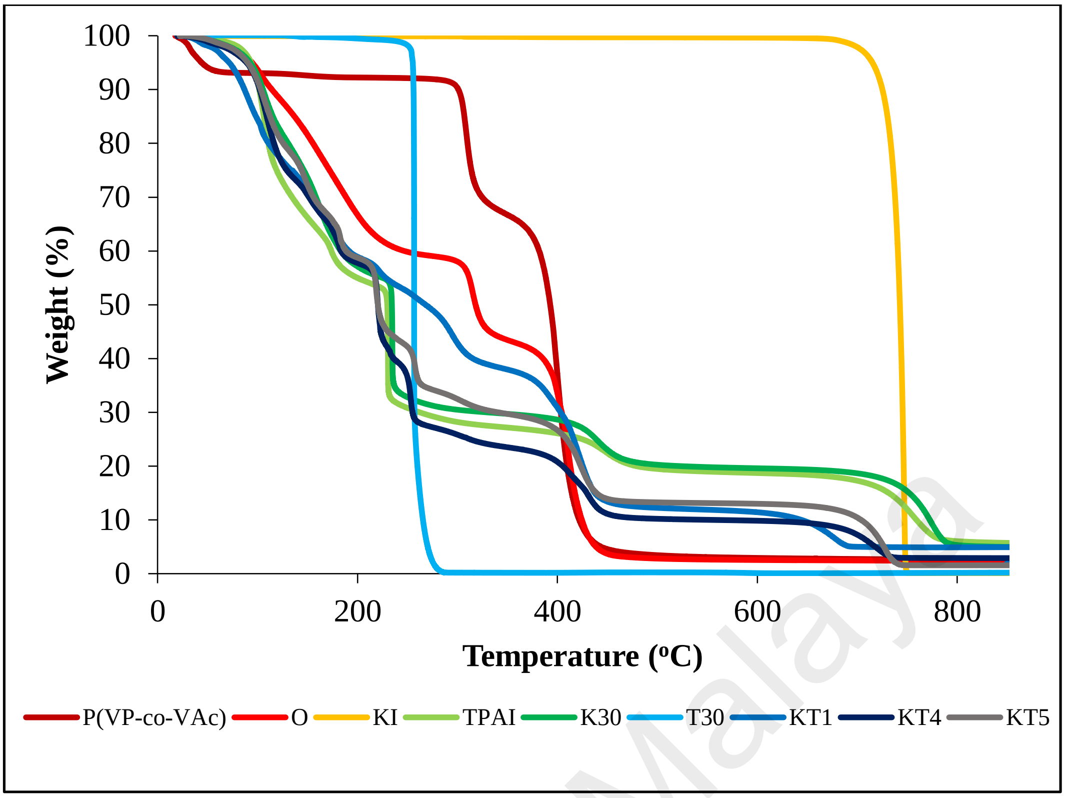

Figure 4.74: Thermogravimetric analysis of pure P(VP-co-VAc) and the P(VP-co-VAc)-KI-TPAI GPE samples.

Table 4.19: The degradation temperature of the sample K30, T30, K40, T40 and the P(VP-co-VAc)-KI-TPAI GPE samples.

Samples	**T_{max1} (ºC)**	**T_{max2} (ºC)**
P(VP-co-VAc)	310	400
O	314	411
K30	234	440
T30	265	412
K40	230	444
T40	245	410
KT2	249	409
KT4	252	408
KT5	256	409

4.5.7 Photocurrent density-voltage (J-V) Characteristics

The dye sensitized solar cells were fabricated using P(VP-co-VAc)-KI-TPAI GPE samples and the values of the open-circuit voltage (V_{oc}), short-circuit current density (J_{sc}), fill factor (FF) and conversion efficiency (η) were obtained, summarized and tabulated in *Table 4.20*. *Figure 4.75* shows the J-V characteristic curves for the solar cells for these GPE samples. Normally, the gel polymer electrolytes with smaller cations would have higher drop in the V_{oc} as there would be a larger downward shift to the conduction band edge which induced by the adsorption of the smaller cations on the surface of nano-sized TiO_2 grain. Similar variation can be seen in our system where the samples with larger amount of KI as they tend to have lower V_{oc} compared to the TPAI system as seen in the table (N. Park, Chang, Lagemaat, Kim, & Frank, 2000; Shi, Wang, Zhang, & Dong, 2011). The fill factor doesn't vary much throughout all of the P(VP-co-VAc)-KI-TPAI GPE samples. Whereas, the J_{sc} varied significantly with the different cation concentration ratio. This indicates that, the power conversion efficiency, η in the binary salt system is also mainly dictated by the J_{sc} of the P(VP-co-VAc) based GPEs. This can be further confirmed by looking at *Figure 4.76* and comparing the trend of the normalized J_{sc} and normalized power conversion efficiency, η where they can be seen having a very similar trend.

The cell efficiencies reached a maximum value of 5.53% for a particular combination of K^+ and TPA^+ (sample KT5). The explanation for these occurrence is that the increase in KI concentrate increases the net iodide ion conductivity and giving a rise in the initial increase of the J_{sc} values. Meanwhile, the ions from the TPAI balanced out the drops of the V_{oc} from the increase of KI salts as seen in *Table 4.20* where sample with huge amount of KI salt was tend to have low V_{oc}. Two of these different cations were balancing each other effectively in the cells and reaching the optimum concentration which could lead to the highest value of the power conversion efficiency of these cells (Dissanayake et al., 2012). As explained previously in the ionic conductivity studies section, the bulkier TPA^+ assist in enlarging the polymer matrix of the GPEs for the fast moving smaller K^+ to effectively move even better. This could improve the mobility of the charges which could lead to increase of J_{sc}. As explained previously, the V_{oc} of the KI system is quite low, in order to balance it out or to get a preferable value for the whole system, the addition of the TPAI has been proven to be able to increase the $V_{oc.}$

The variation of the normalized current density of the cell with highest efficiency under different illumination condition were measured and shown in *Figure 4.77*. This study is done to check for the possible presence of the mass transfer limitation in the P(VP-co-VAc) based GPEs under high light intensity. As seen in the figure, from the linear shapes, it assures that the I^-/I_3^- transportation in the polymer matrix and the electron transfer at all at the Pt/electrolyte interface were not the rate determining steps in the photo electrochemical process. It also shows that the overall photocurrent density of the cells are not limited by the charge diffusion inside the GPE samples (Chiappone et al., 2014; Salvador et al., 2014).

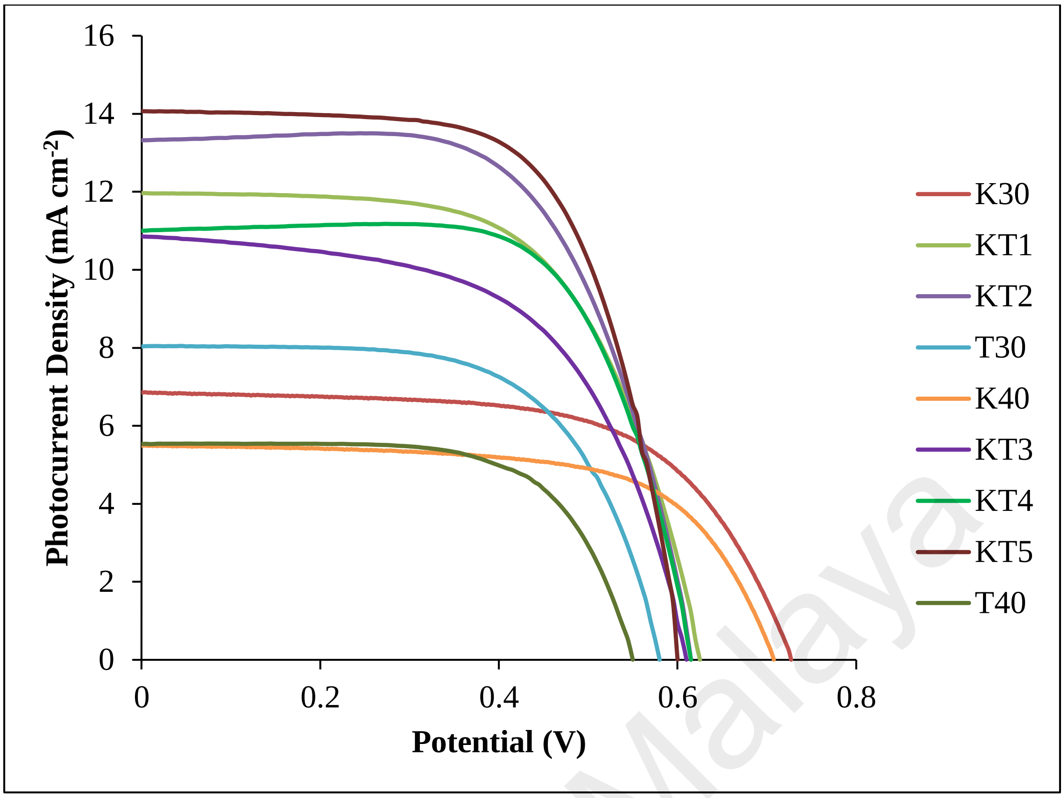

Figure 4.75: The photocurrent-photovoltage (J-V) characteristics of the GPE samples consisting of different ratio weight percentages of KI and TPAI.

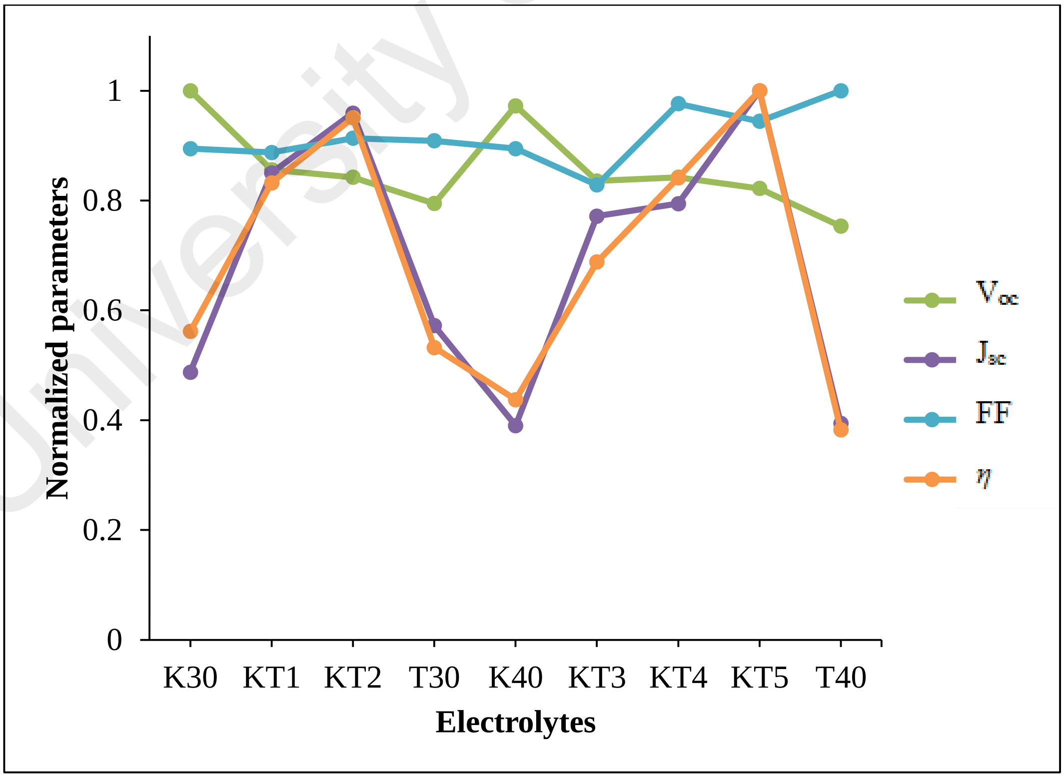

Figure 4.76: The normalization curves of the various performance parameters of the DSSCs fabricated with different P(VP-co-VAc)-KI-TPAI GPE samples.

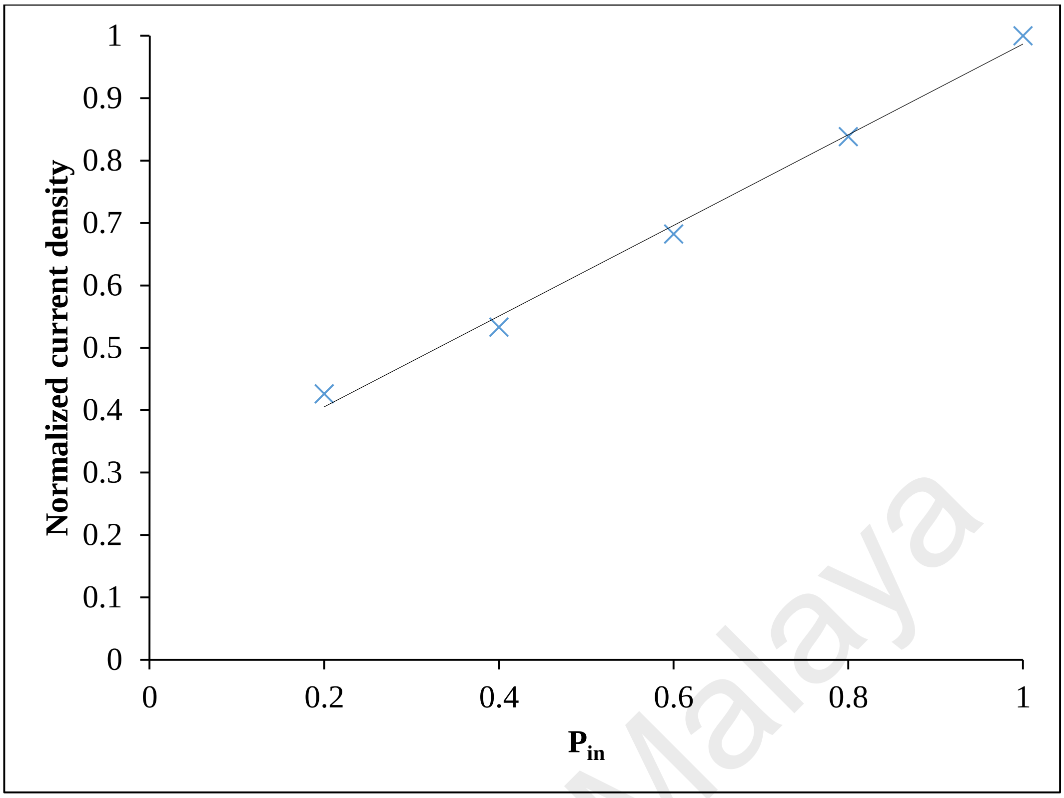

Figure 4.77: Normalized J_{sc} values plotted as a function of different light intensities (P_{in}) for sample KT5.

Table 4.20: Photovoltaic parameters of the GPE samples consisted of different weight percentages of KI.

Electrolytes	**V_{oc} (V)**	**J_{sc} (mA cm^{-2})**	**FF (%)**	**η (%)**
K30	0.58	8.05	0.63	2.94
KT1	0.63	11.97	0.62	4.60
KT2	0.62	13.5	0.63	5.26
T30	0.73	6.86	0.62	3.10
K40	0.55	5.55	0.69	2.11
KT3	0.61	10.86	0.57	3.80
KT4	0.62	11.18	0.68	4.65
KT5	0.6	14.07	0.65	5.53
T40	0.71	5.49	0.62	2.42

4.5.8 EIS studies for DSSCs

In order to correlate the photovoltaic characteristics with the processes of charge transport and interfacial charge transfer, the P(VP-co-VAc)-KI-TPAI GPE based DSSCs were measured using impedance techniques. All of the cells exhibit two distinguish semi-circles. The semi-circle that can be observed at high frequency is due to the charge transfer resistant happening at the Pt counter electrode and it is labeled as R_{ct1}. At middle frequency zone, the observed semi-circle corresponded to the charge resistance of the charge recombination between the TiO_2 conduction band and I_3^- ions at the dye of the mesoporous TiO_2 and the electrolytes interfaces (Cui et al., 2012; Kern, Sastrawan, Ferber, Stangl, & Luther, 2002; Q. Wang, Moser, & Gra, 2005). Apart from these two semicircles, the impedance which can be seen below the frequency of 5 Hz was depicted as the Warburg diffusion (W) process of I_3^-/I^- in the electrolyte which can be associated with the Warburg parameter,$Y_0(S^{1/2}\Omega^{-1})$ (Boonsin et al., 2012). The intersection of the x-axis and the high frequency semi-circle is basically interpreted as the sheet resistance of the FTO substrate and it is known as the ohmic serial resistance (R_s) (C. Wang et al., 2013).

The EIS data obtained were further fitted with Metrohm Nova software and the equivalent circuits were shown in *Figure 4.78*(a). The parameters of the equivalent circuits of the cells are shown in *Table 4.21*. Based on the fitted data, the cell with sample KT5 is having the lowest R_{ct2}. This is due to the reason that the K^+ anion can be easily adsorbed onto the surface of TiO_2. Thus, the conduction band edge of the TiO_2 could easily suffer a positive shift and this has been reported previously as the reason for drop of the $V_{oc.}$ Meanwhile, TPA^+ was added to improve the R_{ct2} as the addition of TPAI could assist to decrease the recombination reactions at the TiO_2/electrolyte interfaces effectively. This result can be attributed to the electrical double layer which suppressed the recombination reaction between the free electron of I_3^-. This result agrees well with the J-V data where slower recombination process will normally result in a higher V_{oc}.(Ke et al., 2014). *Figure 4.79* shows the open circuit voltage, V_{oc} and R_{ct2} with the respect of different KI and TPAI concentration in P(VP-co-VAc)-KI-TPAI GPE samples.

The Bode EIS spectra of the cells for P(VP-co-VAc)-KI-TPAI sample are shown in *Figure 4.78(b).* According to the EIS theory which is shown in *equation 4.7*, the electron lifetime is inversely proportional to the character frequency peak in the higher frequency region of the spectra. (Hoshikawa et al., 2006). Since the f_p for the sample KT5 is higher, it indicates that the electron lifetime of sample KT5 is shorter than the other samples. This result is in agreement with the results obtained in the previous EIS study where normally lower R_{ct2} value means faster charge recombination between TiO_2 and I_3^- in electrolyte and thus, it leads to the deterioration of the V_{oc} of the cells (Lan, Wu, Lin, & Huang, 2010).

Tafel polarization measurements were performed by sandwiching GPE samples in two symmetrical Pt electrodes to study the electrocatalytic activity and interfacial charge-transfer properties of the I^-/I_3^- redox couples. The current density (J) as a function of potential (V) reduction of I_3^- ions are shown in *Figure 4.79*. From this figure, the limited diffusion current density, J_{lim} and the exchange current density (J_0) can be determined. J_{lim} is the dependence on the diffusion coefficient (D_n) of the I^-/I_3^- couples in electrolyte and it can be obtained from the intersection of the cathodic branch with the Y-axis. The equation for D_n is as *equation 4.8* (Mingkui Wang et al., 2009). From the equation, it shows that the J_{lim} would directly affects the diffusion coefficient of the I^-/I_3^- couple. As observed in *Figure 4.80*, sample KT5 shows highest number of J_{lim} and this suggests that the binary salt systems are having higher diffusion coefficient for the I^-/I_3^- redox species compared to the samples with only one salt (S. H. Park et al., 2014).

In the Tafel zone, the intersection of the tangent to the larger slope from the anodic or the cathodic branch with the equilibrium (zero) potential ordinate is the exchange current density (J_0). J_0 can be associated with R_{ct2} by the following *equation 4.9* (C. Wu et al., 2012). In theory, J_0 varies inversely with R_{ct2}. Therefore, in this case, sample KT5 were having the highest exchange current density. This agrees well with R_{ct2} value in the impedance measurement.

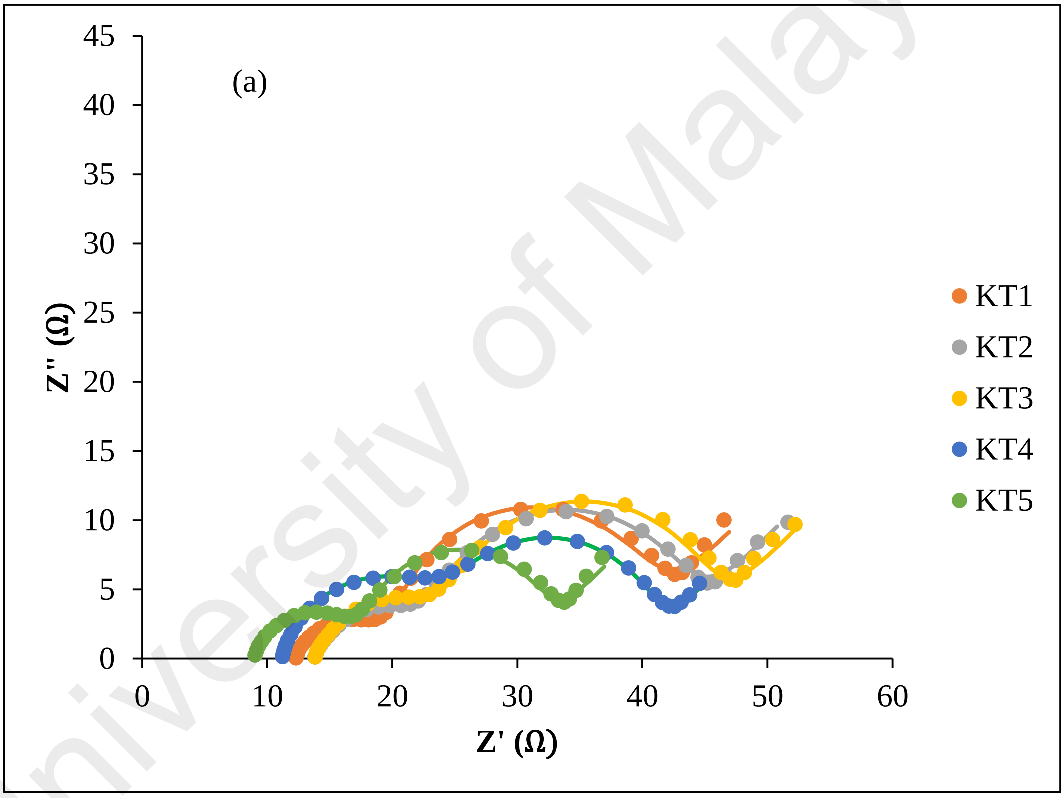

Figure 4.78: The electrochemical impedance spectra of DSSCs assembled with P(VP-co-VAc)-KI-TPAI GPE samples in the forms of (a) Nyquist plots and (b) Bode phase plots. The spectra were measured under 100 mW cm^{-2} illuminated sunlight.

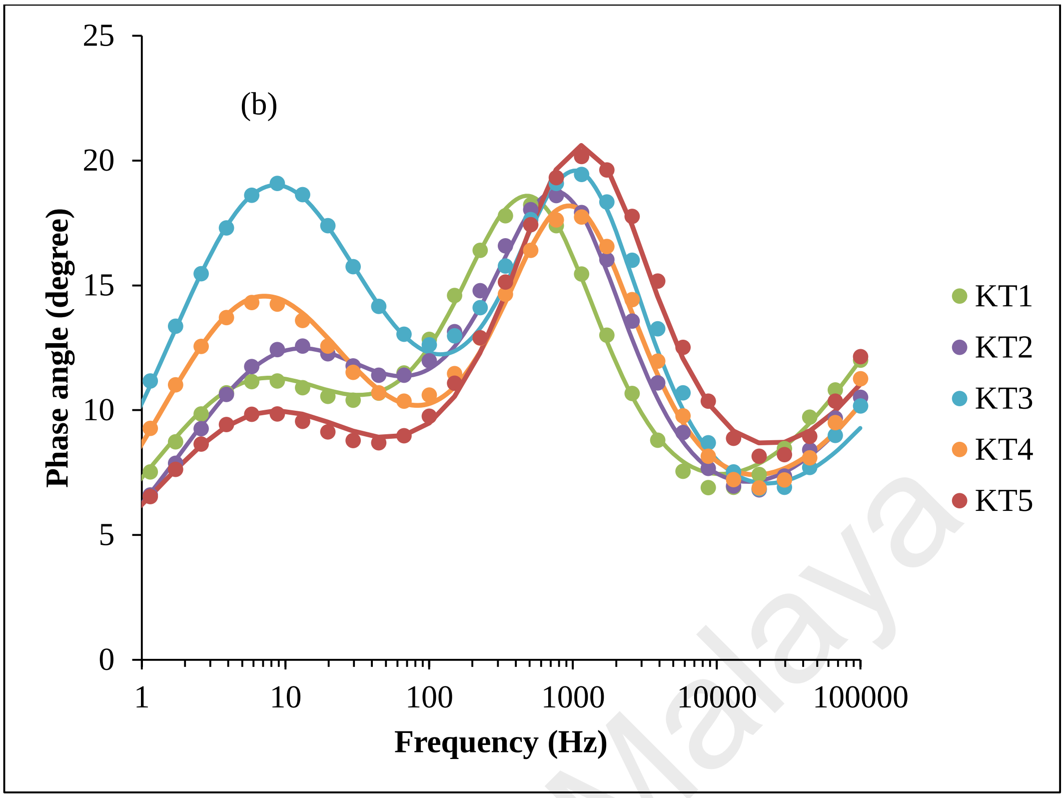

Figure 4.78 (continued): The electrochemical impedance spectra of DSSCs assembled with P(VP-co-VAc)-KI-TPAI GPE samples in the forms of Nyquist plots (a) and Bode phase plots (b). The spectra were measured under 100 mW cm-2 illuminated sunlight.

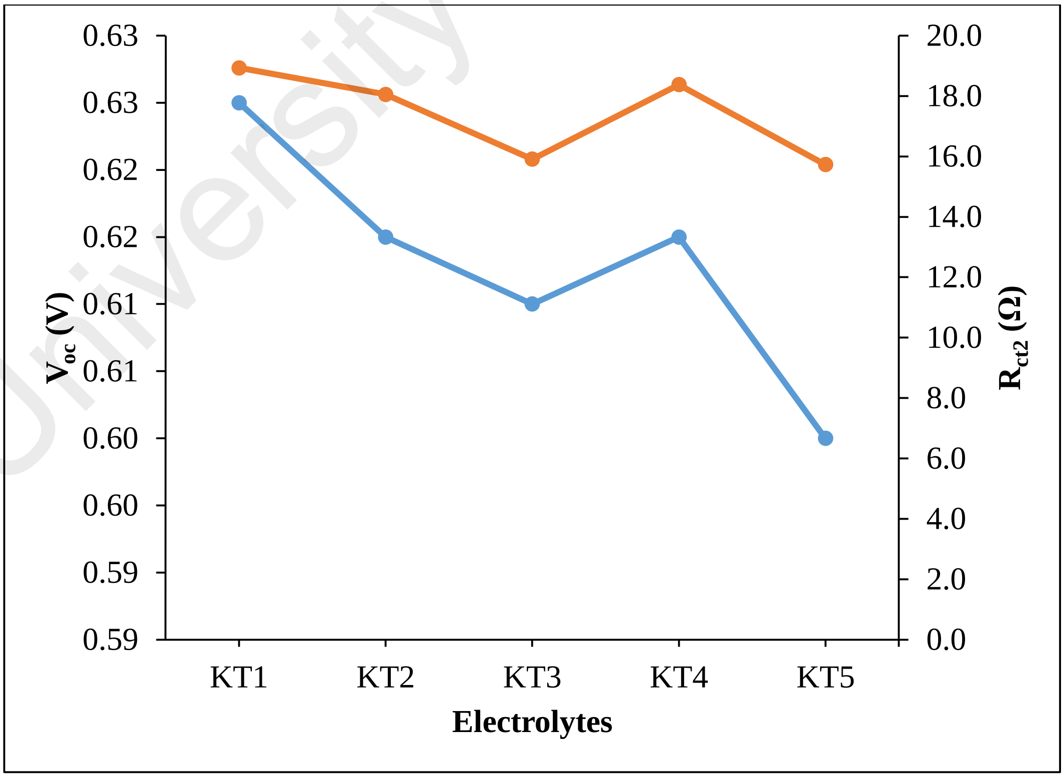

Figure 4.79: The open circuit voltage and R_{ct2} with the respect of different KI and TPAI concentration in P(VP-co-VAc)-KI-TPAI GPE samples.

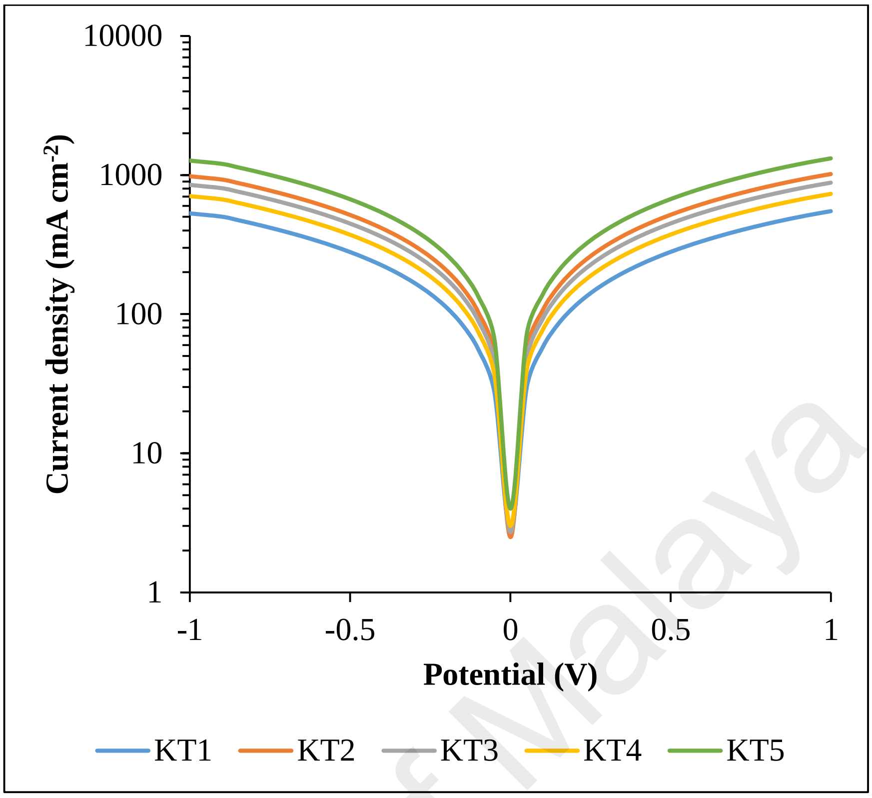

Figure 4.80: Tafel polarization curves of symmetric Pt cells with P(VP-co-VAc)-KI-TPAI gel polymer electrolytes samples.

Table 4.21: The parameters of the equivalent circuits used to fit the EIS impedance data of the P(VP-co-VAc)-KI-TPAI based DSSCs.

Electrolytes	R_s (Ω)	R_{ct1}(Ω)	R_{ct2}(Ω)	W($S^{1/2}$ $Ω^{-1}$)	τ (ms)
KT1	15.1	9.2	18.9	0.66	80.8
KT2	17.7	12.5	18.1	0.35	71.2
KT3	13.2	16.7	15.9	0.56	70.9
KT4	14.9	14.3	18.4	0.31	74.2
KT5	16.2	16.4	15.7	0.52	62.7

4.6 P(VP-co-VAc)-KI-TPAI-MPII Gel Polymer Electrolytes

4.6.1 Ambient Temperature-Ionic Conductivities Studies

There was an attempt made to further enhance the ionic conductivity. The best conducting binary salt system (KT5) was selected and different concentrations of MPII were added to study the variation in performance properties of the samples.

Figure 4.81 shows the impedance plots of the P(VP-co-VAc)-KI-TPAI-MPII gel polymer electrolytes samples. With only a single spike was observed for all of the samples, it shows us that the current carriers in the system are the mobile ions that were controlling the entire total electrical conductivity of these electrolytes and there was good contact at the interface of the electrodes and the polymer electrolytes. (Sengwa & Choudhary, 2014). *Figure 4.82* shows the summarized ionic conductivity at room temperature of the gel polymer electrolytes with best conducting binary salt system sample (KT5) and P(VP-co-VAc)-KI-TPAI GPE samples at room temperature. From the impedance measurement, the gel polymer electrolytes with only single salt as reported previously only exhibits ionic conductivity of 1.60×10^{-3} S cm^{-1} and 1.72×10^{-3} S cm^{-1} for TPAI and KI salt system, respectively. It is also reported that, the GPEs with binary salt system shows slightly higher ionic conductivity (1.90×10^{-3} S cm^{-1}) compared to the single salt system. This is most likely due to the reason that the two cations were working differently inside polymer matrix and balancing out each other advantages properly as mentioned previously. The ionic conductivity was then further improved with the addition of MPII ionic liquid into the binary salt system to the highest value of 4.09×10^{-3} S cm^{-1}. This was due to the addition of MPII that could have helped in the enhancement of the dissociation process of the KI and TPAI salt (Ramesh et al., 2011). Furthermore, ionic liquid such as MPII was well known to have plasticizing effect which could soften the backbone of the host polymer matrix and increase the flow of the mobile charge movement which leads to an increase in ionic conductivity(Sekhon et al., 2006).

The decrease in conductivity after KTM15 was probably due to the reason that the system could accept any extra ionic liquid added into the system. The extra charge carriers from the MPII tends to form neutral pairs again and slowed the movement of the mobile ions in the polymer matrix. Thus, it decreases the ionic conductivity (Liang et al., 2008).

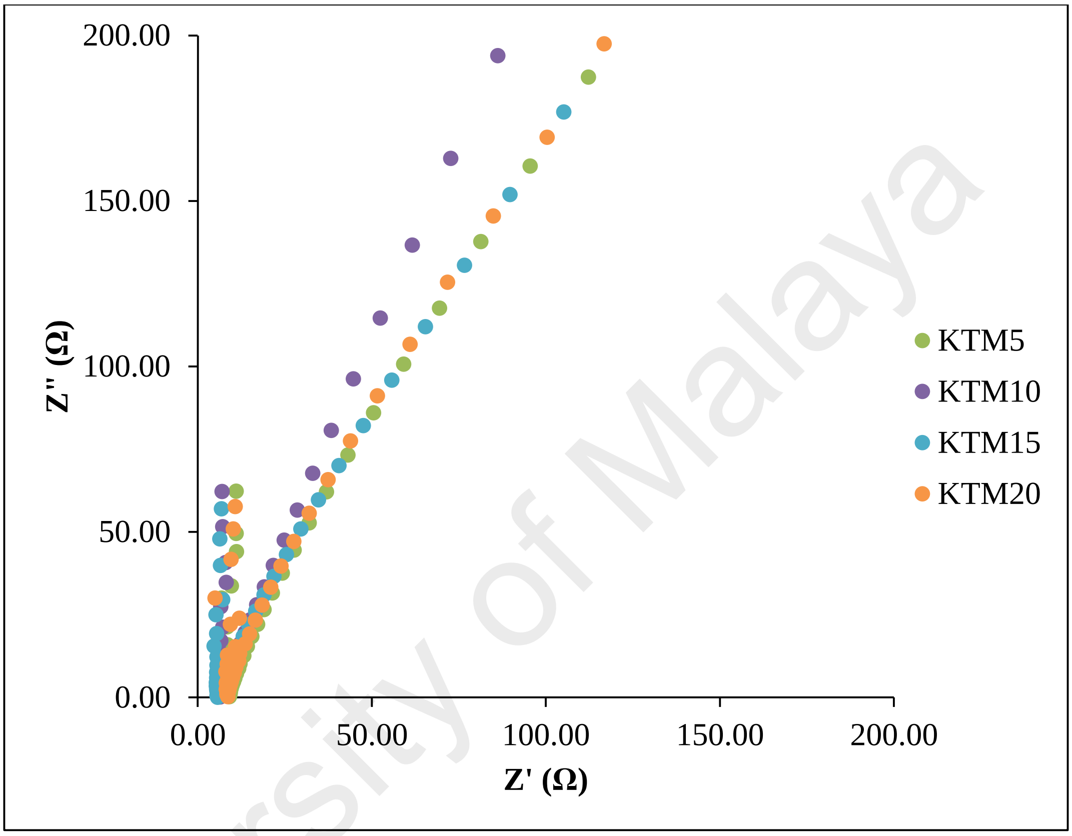

Figure 4.81: Typical complex impedance plot of P(VP-co-VAc)-KI-TPAI GPE samples at room temperature.

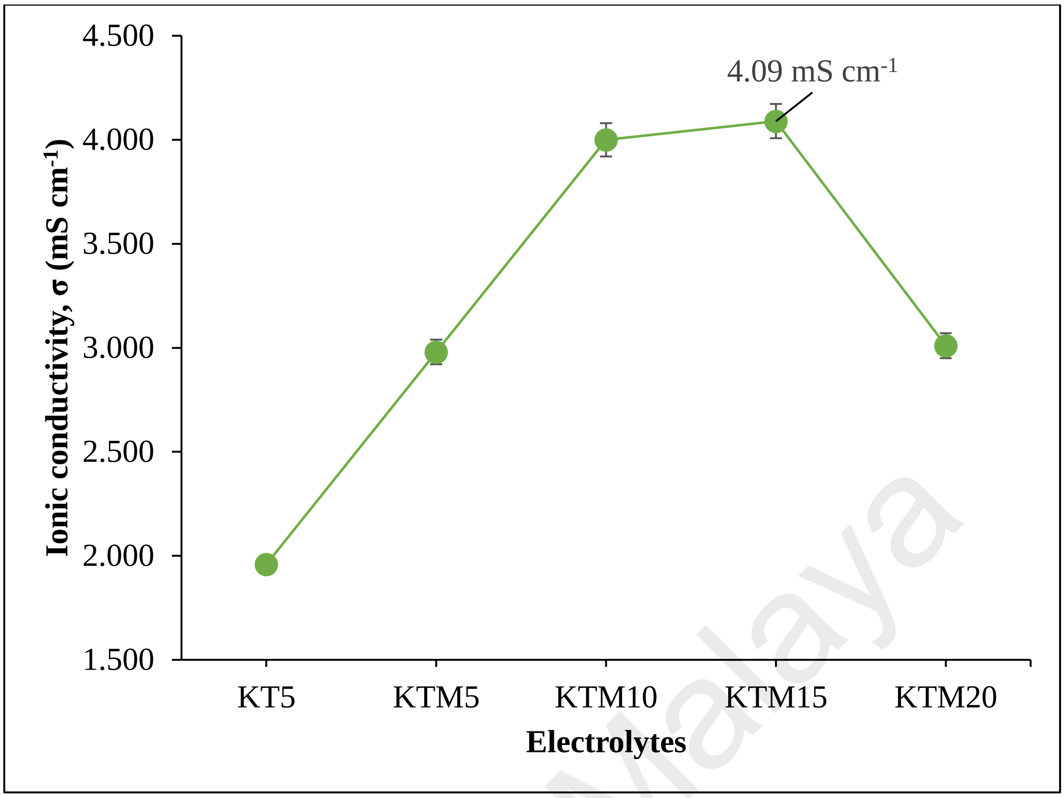

Figure 4.82: Variation of ionic conductivity of the P(VP-co-VAc)-KI-TPAI-MPII GPE samples with different MPII concentration at room temperature.

Table 4.22: Ionic conductivity values for the P(VP-co-VAc)-KI-TPAI-MPII GPE samples at room temperature.

Electrolytes	Ionic Conductivity (mS cm^{-1})
KT5	1.96
KM5	2.98
KM10	4.00
KM15	4.09
KM20	3.01

4.6.2 Temperature dependence-Ionic conductivity studies

The conductivity-temperature (σ-T) relationships for the P(VP-co-VAc)-KI-TPAI-MPII gel polymer electrolytes samples are shown in *Figure 4.83*. From the figure, it can be seen that the conductivity increased with the increase of temperature and the log(σ) versus 1000/T plots is almost linear for every P(VP-co-VAc)-KI-TPAI-MPII GPE samples showing that they obey the Arrhenius behavior (Ramesh et al., 2013).

Table 4.23 shows the activation energy calculated from the slope from *Figure 4.83*. *Figure 4.84* shows the variation of the ionic conductivity and the E_a of the (VP-co-VAc)-KI-MPII-TPAI GPE samples. As observed in the table, sample KTM15 is having the lower E_a compared to other samples. This indicates that there were faster ions transportation rate in the polymer matrix of sample KTM15 over the other samples. Normally, when an ionic transport process involves intermolecular ion hopping, the conductivity is determined by the thermal hopping frequency, which in turn is proportional to the $exp(-E_a/kT)$, and this leads to an Arrhenius conductivity-temperature relationship. The ion hopping increases with an increase of temperature, which enhances the conductivity of the system as activation energy is the minimum energy require for mobile ions in the polymer electrolytes to get excited and starts hopping around inside the polymer matrix. The lower the energy means that it is easier for the mobile ions to move around within the polymer matrix and it increases the mobility of the mobile ions which leads to increase in the ionic conductivity of the polymer electrolytes (Yang et al., 2009). This is in agreement with the ionic conductivity studies showed previously. The decreased E_a and increased ionic conductivity are expected to significantly enhance the reaction kinetics of the DSSCs.

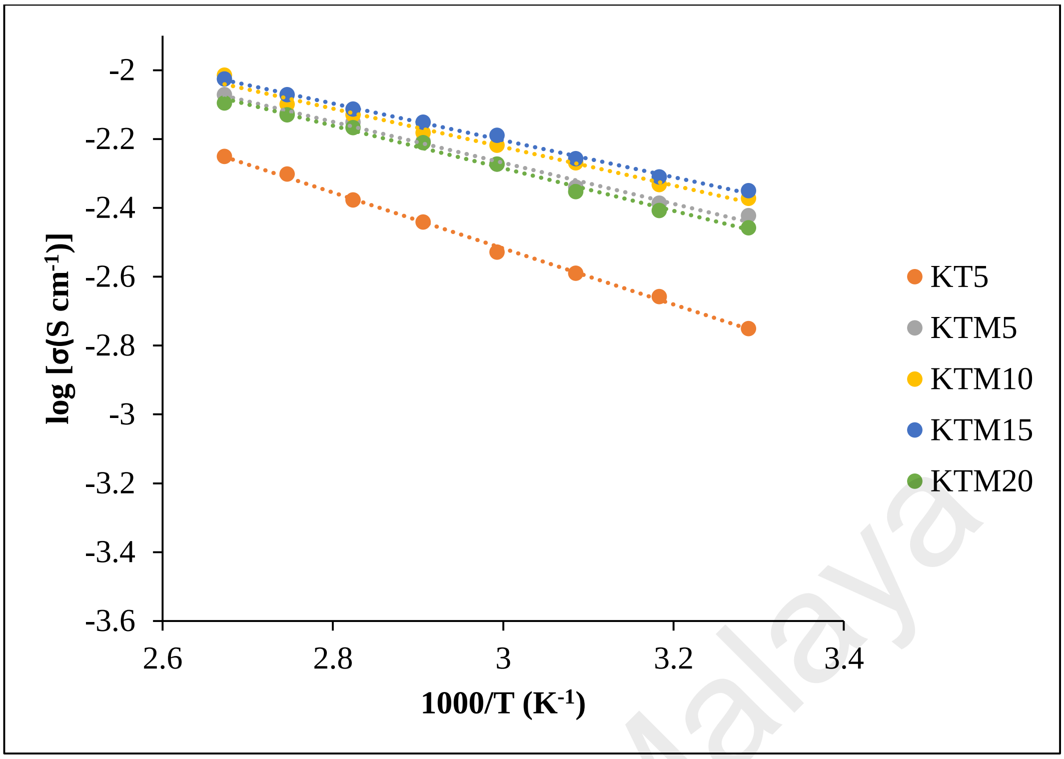

Figure 4.83: Arrhenius plots for the conductivity of the P(VP-co-VAc)-KI-TPAI-MPII GPE samples with different concentration of MPII.

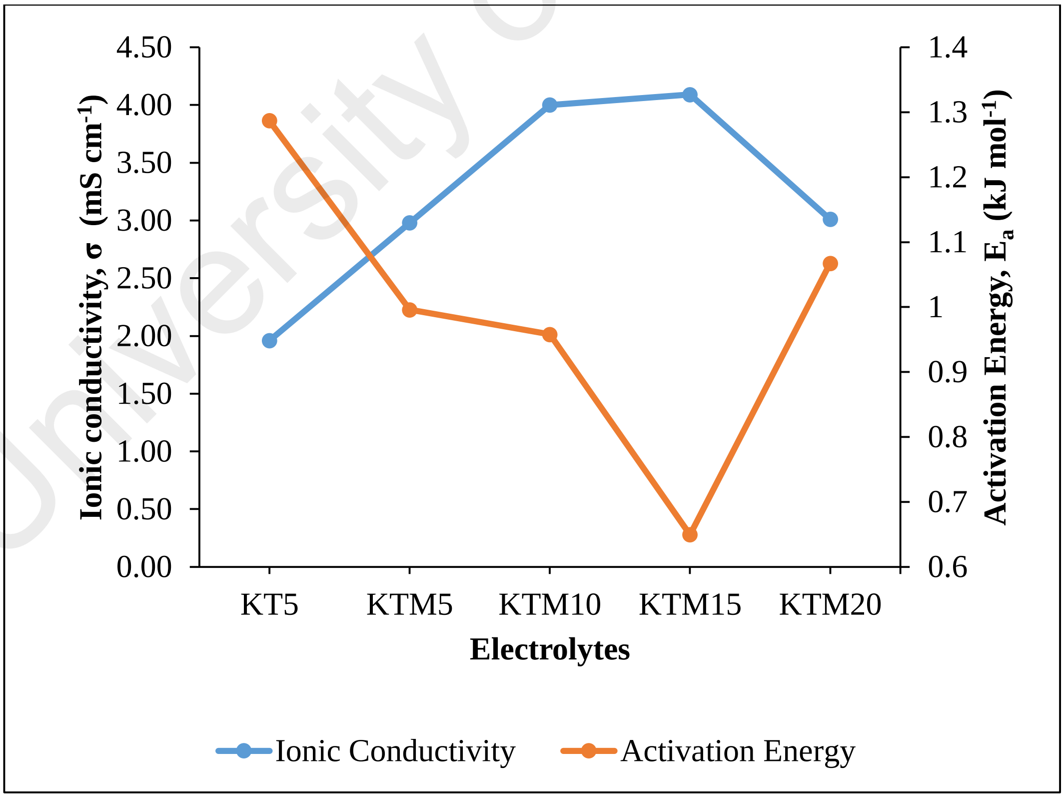

Figure 4.84: Variation of ionic conductivity and the activation energy of the P(VP-co-VAc)-KI-TPAI-MPII GPE samples with different MPII concentration at room temperature.

Table 4.23: The activation energy of the P(VP-co-VAc)-KI-TPAI-MPII GPE samples with different concentration of MPII.

Electrolytes	**Activation Energy, Ea (kJ mol^{-1})**
KT5	0.60
KTM5	0.59
KTM10	0.56
KTM15	0.55
KTM20	0.64

4.6.3 Dielectric Studies

4.6.3.1 Conductivity-frequency studies

The ionic conductivity of the samples for this system (KTM5, KTM10, KTM15, and KTM20) together with sample KT5 were analyzed with the respect of the frequency in order to observe the relaxation processes of this last system. From *Figure 4.85* prospects, there are similar trend observed. It started with a plateau at higher frequency applied to the samples and then it started to deviate with the frequency applied is getting lower. This is basically because of the significant effect of the electrode polarization and it also shows that the samples are still having the natural variation of the ionic conductivity which almost the same with the similar universal dynamic responses. As expected as well, the ionic conductivity tend to be lower when the frequency applied is low and then it started to increase when higher frequency applied. This phenomenon has been explained previously where it is mainly causes by the increment of the chances for the mobile ions to hop back to initial sites when higher frequency is applied (Woo et al., 2012).

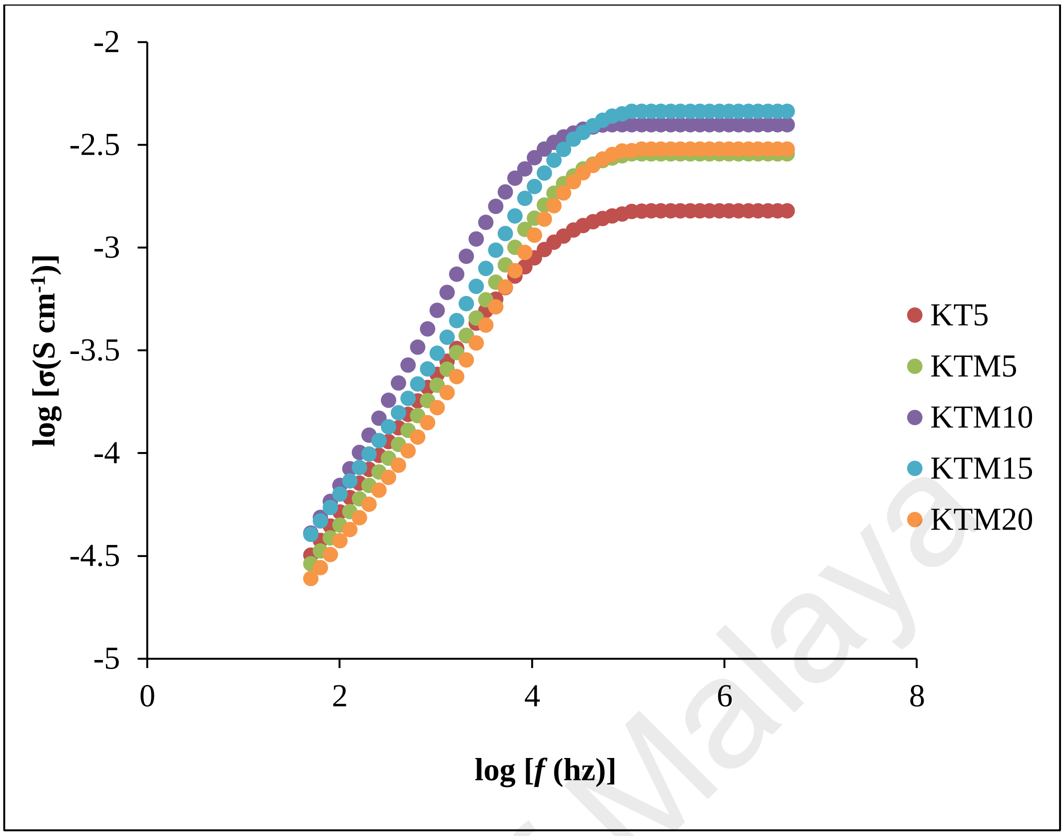

Figure 4.85: Frequency-dependent conductivity at various MPII concentration of P(VP-co-VAc)-KI-TPAI-MPII GPE samples.

4.6.3.2 Dielectric Relaxation Studies

As mentioned previously, this system provides the best conducting sample in the whole research and this is why the study of the relative permittivity, ε_r^* needed to be done to know more about the polarization effect occurring in between the GPEs and the electrodes. The dielectric constant, *ε'* and dielectric loss, *ε''* spectra were shown in *Figure 4.86* and *Figure 4.87*, respectively. Very similar trend can be observed which shows that P(VP-co-VAc) based gel polymer electrolytes doesn't change their dielectric properties even after the addition of two different types of salts (KI and TPAI) and also the ionic liquid, MPII.

The research is started with only a single salt added into the P(VP-co-VAc) based gel polymer electrolytes. Then eventually the binary salt system and the addition of ionic liquid is introduced into the P(VP-co-VAc) based gel polymer electrolytes. The relative permittivity studies of all these samples has been studied and it shows that there is not much changes can be observed even with all those new materials that have been added into the P(VP-co-VAc) based gel polymer electrolytes. The *ε'* and *ε''* values values of all the GPE samples are very large at low frequency which causes by the dielectric polarization that has been explained previously (Raghu et al., 2014). Meanwhile, when all of the samples were gradually applied with higher frequency, it can be observed the *ε'* and *ε''* values decreased up until it is closed to zero. This is due to the quick periodic reversal of the electric field which causes that there were not even any time for any charges to build up at the moment (Raghu et al., 2013).

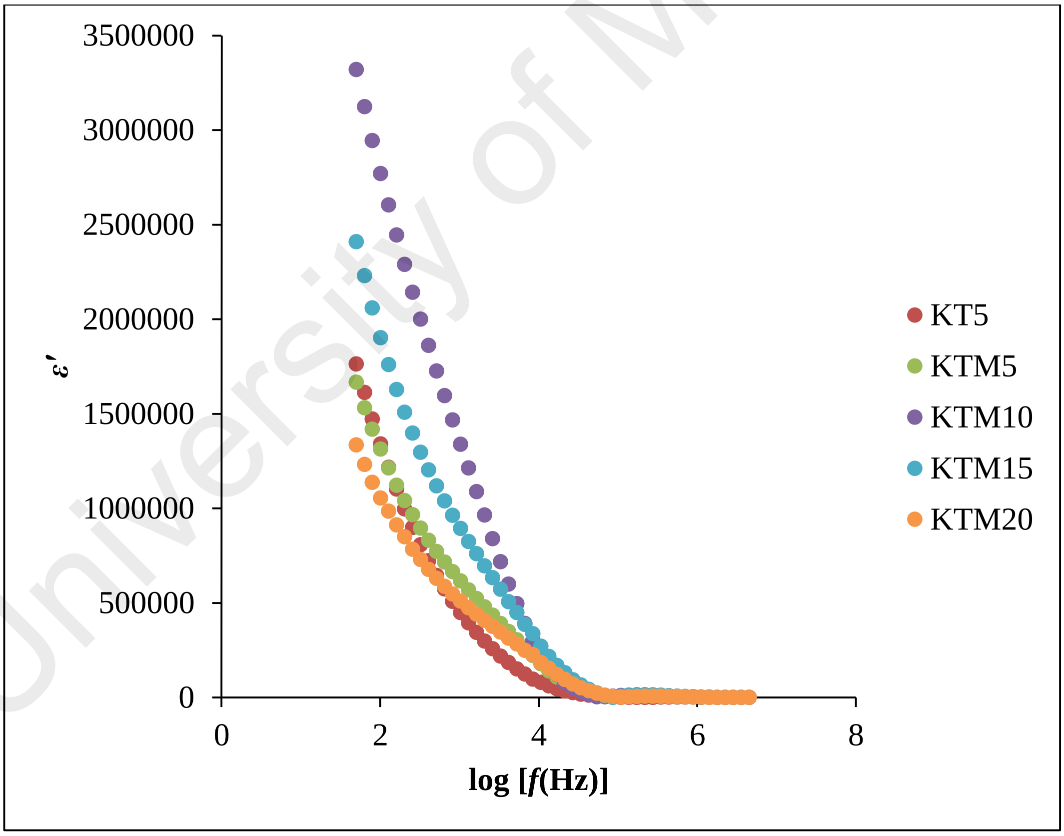

Figure 4.86: Variation of real part of dielectric constant, ε' with frequency for sample KT5, KTM5, KTM10, KTM15, and KTM20.

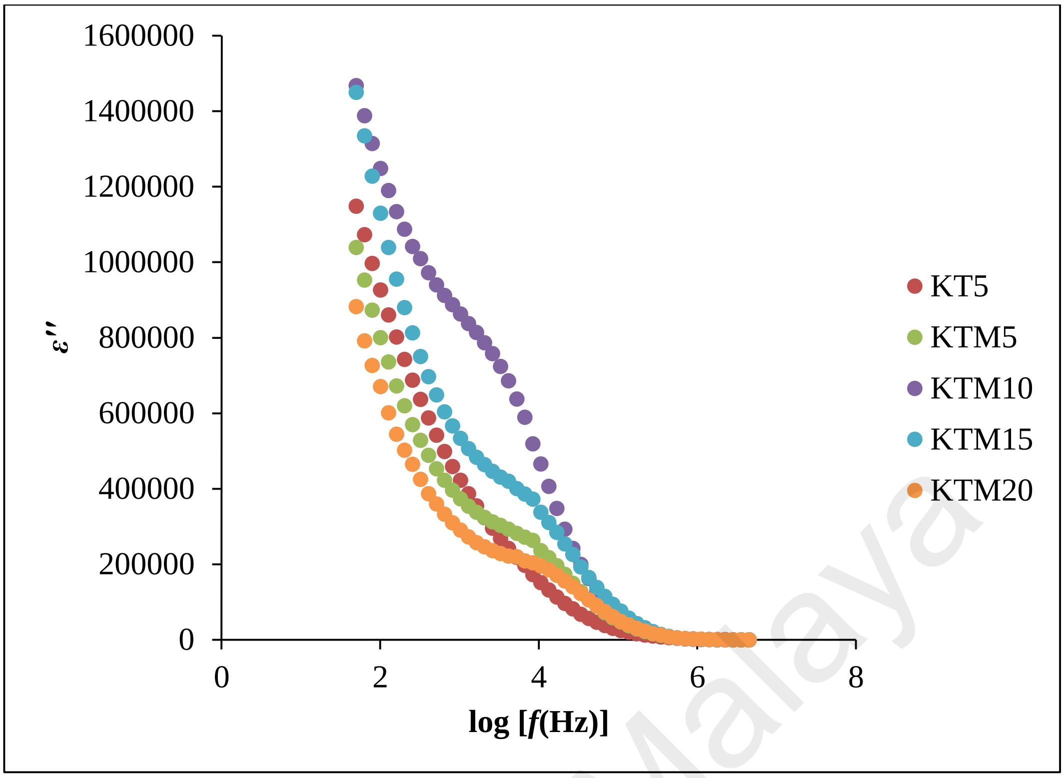

Figure 4.87: Variation of real part of dielectric loss, ε'' with frequency for sample KT5, KTM5, KTM10, KTM15, and KTM20

4.6.3.3 Modulus Studies

Figure 4.88 and *Figure 4.89* shows the real and imaginary part of modulus (M' and M") as a function of frequency for all the GPEs for this system, respectively. By comparing the spectra of all systems studied in this work, not much changes can be observed. This proves that even with the addition of double salt and ionic liquid into the P(VP-co-VAc) based gel polymer electrolytes, there is not much changes in the modulus studies. The electrode polarization still did not contributes anything and actually can be neglected at low frequency and the samples with higher ionic conduction properties would have a peak shifted to much more higher frequency even though the peaks cannot be seen but it could be assumed by the trend of the spike in the insets of both the figures. In this case, the peak of sample KTM15 were expected to be shifted to the most left side of the spectrum (Ramya et al., 2008).

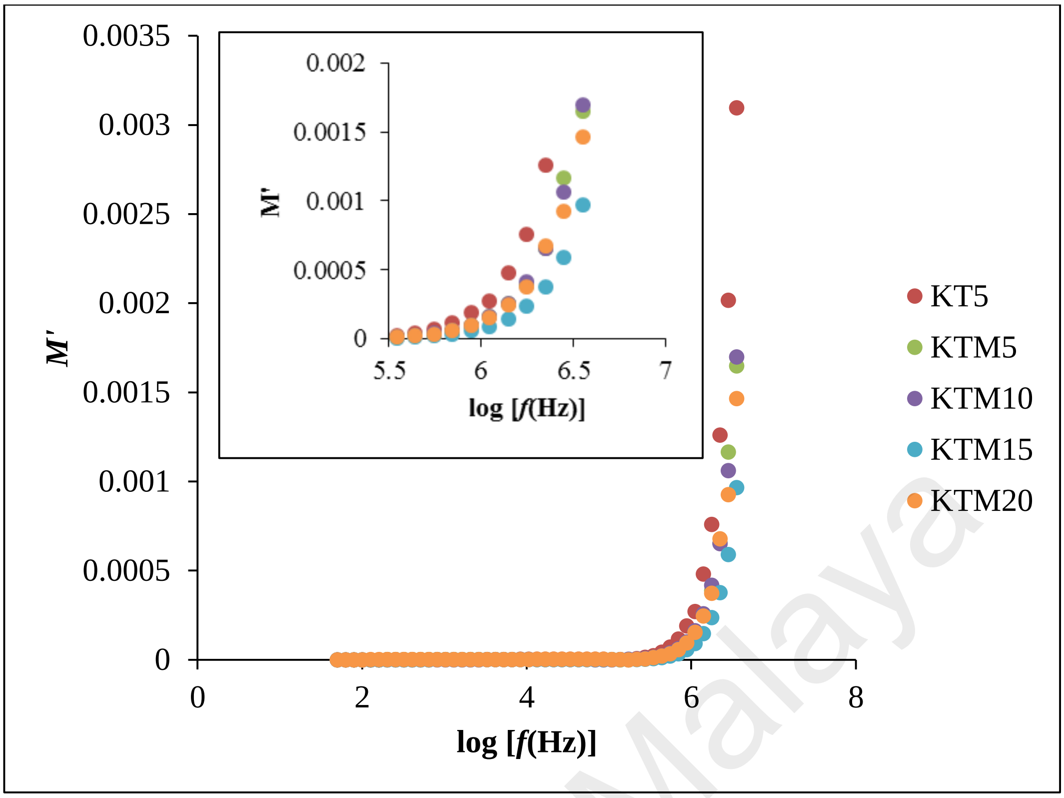

Figure 4.88: The real part of modulus, M' as a function of frequency for sample KT5, KTM5, KTM10, KTM15, and KTM20.

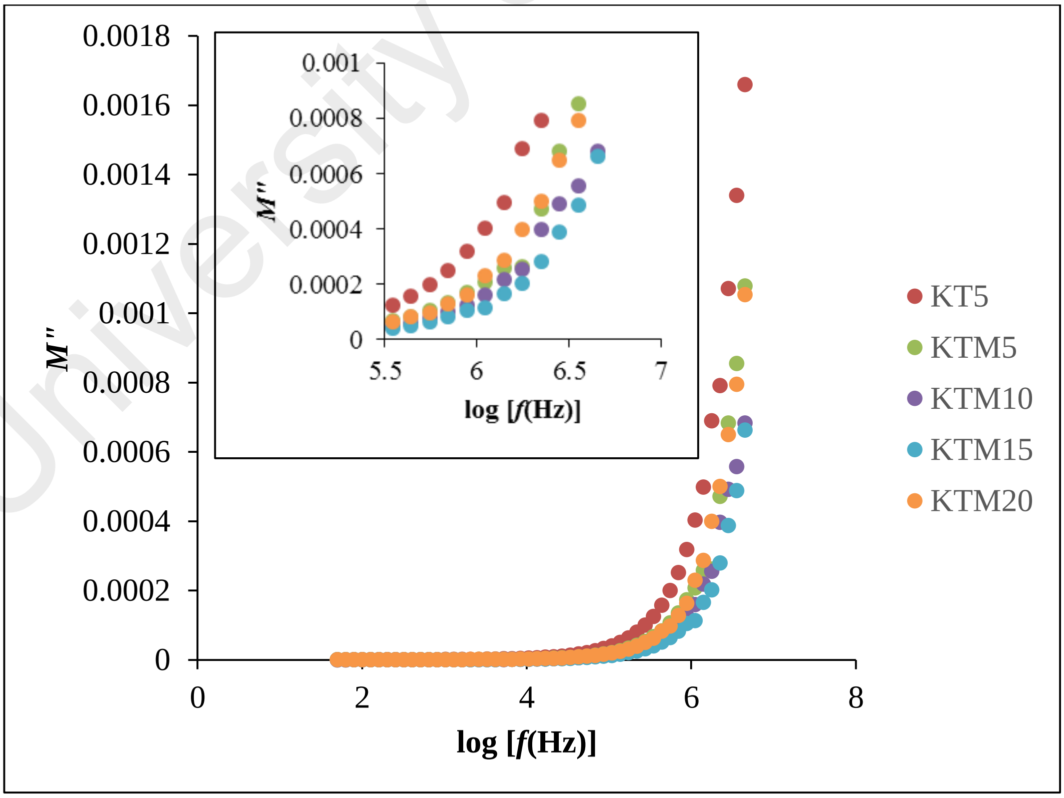

Figure 4.89: The imaginary part of modulus, M" as a function of frequency for sample KT5, KTM5, KTM10, KTM15, and KTM20.

4.6.4 FTIR studies

The FTIR spectra of KTM5, KTM10, KTM15, and KTM20 were shown in *Figure 4.90* in transmittance mode. With complexation of the binary salt system has been studied, we then moved on to investigate the changes in the coordination and complexation of the P(VP-co-VAc)-KI-TPAI system with the MPII ionic liquid.

There are no new appearance or disappearance of peaks can be seen in all of the samples after the addition of the MPII into the binary salt system. Thus, in order to prove the complexation of the MPII with the P(VP-co-VAc)-KI-TPAI system, we were going to look into the changes of the important peaks of the systems. As seen in the spectra *Figure 4.91,* the peaks at region 1710 cm^{-1} to 1750 cm^{-1} of the C=O stretching of PVAc have been shifted to higher wavenumbers in all of the samples together with a decrease of intensities after the addition of MPII into KT5. It can also be observed that the peaks for the C=O stretching of PVP were having similar occurrence but instead the peaks ware shifted to lower wavenumbers. These changes in intensities and shifting peaks show that there were interaction with the newly added $MPIm^+$ ions with C=O stretching of the P(VP-co-VAc) as well as some complexation occurred as well (Wieczorek & Stevens, 1997).

Meanwhile, the C=N stretching peaks of the P(VP-co-VAc) at 1230 cm^{-1} to 1260 cm^{-1} of the P(VP-co-VAc)-KI-TPAI-MPII gel polymer electrolytes samples were also found to decrease in its intensities and the peaks shifted to higher wavenumber. This is the indication of the strong withdrawing character of the N atom of the C-N in the PVP chain of the copolymer reacted with newly added cations from the MPII ionic liquid (Ramya et al., 2007).

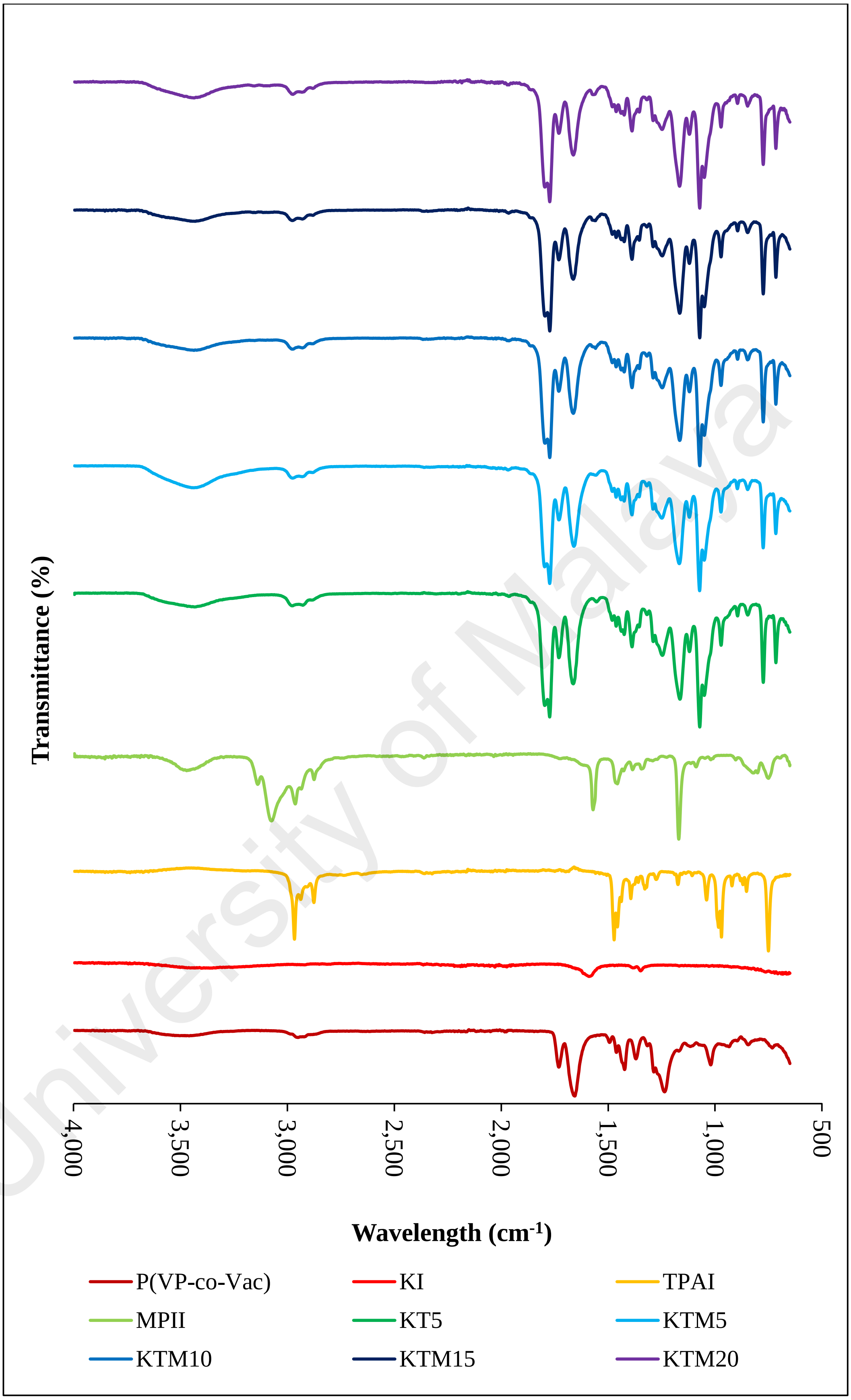

Figure 4.90: FTIR spectra for pure P(VP-co-VAc), pure KI, pure TPAI, pure MPII, sample KT5 and P(VP-co-VAc)-KI-TPAI-MPII gel polymer electrolytes.

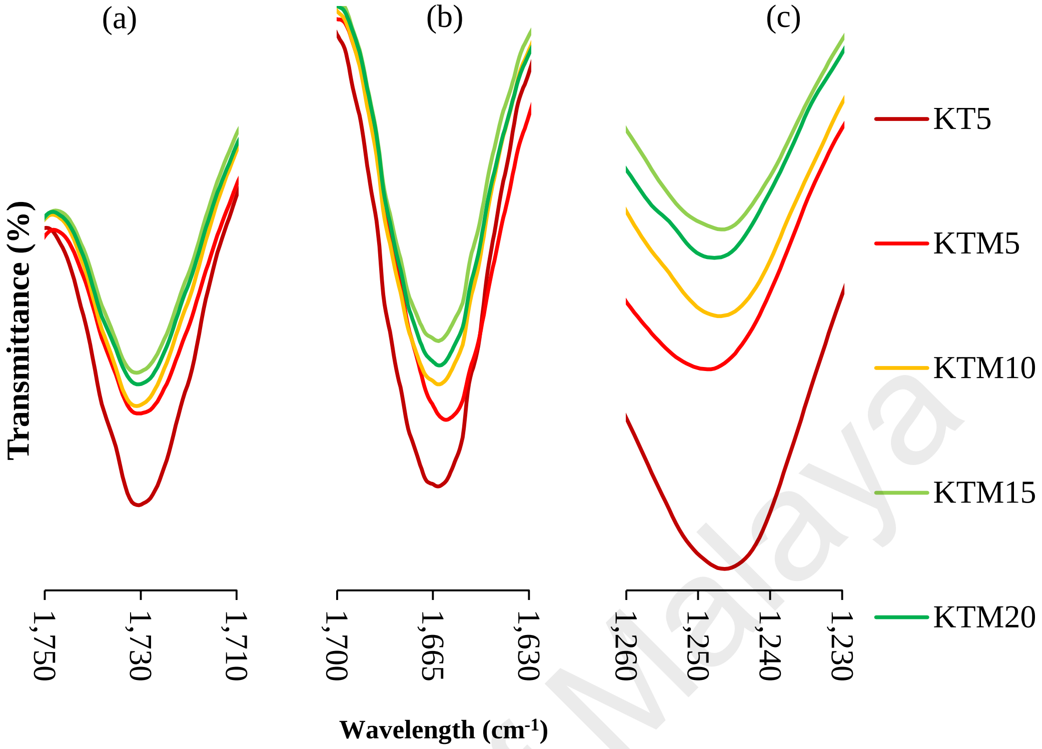

Figure 4.91: FTIR spectra in the region (a) 1750-1710 cm^{-1}, (b) 1700-1630 cm^{-1}, (c) 1260-1230 cm^{-1} for sample K30 and P(VP-co-VAc)-KI-MPII GPE samples.

4.6.5 X-ray diffraction (XRD) studies

XRD analysis has been performed, and their respective diffraction patterns of the pure materials and the KTM5, KTM10, KTM15, and KTM20 are show in *Figure 4.92*. Shifting of peaks can be observed upon the addition of MPII into the sample KT5. Peak at 2θ of 22.2° of the KT5 can be seen shifted to 2θ of 22.0° for KTM5, to 22.5° for KTM15, and to 22.4° for KTM20. This is the indication of the new complexation occurred in the polymer matrix after the addition of MPII into the binary salt system sample KT5 (Rajendran et al., 2007).

On the other hand, the changes of the intensity of the broad peaks were also the indication of the complexation as well. The intensity of peaks was seen to be reducing after the initial addition of MPII (KTM5) and further decreased in KTM15 and then slightly increased at KTM20. The decrease in the intensity of the peaks after the addition of the MPII into sample KT5 is probably due to the deterioration of the ordered arrangement of the polymer matrix due to the plasticizing effect of the MPII ionic liquid. It also helps to promote the segmental mobility of the polymer chain and favors the ionic transportation as discussed in the ionic conductivity studies (Costa et al., 2007). This is well in agreement with the ionic conductivity studies of the P(VP-co-VAc)-KI-TPAI-MPII gel polymer electrolytes in *section 4.6.1*.

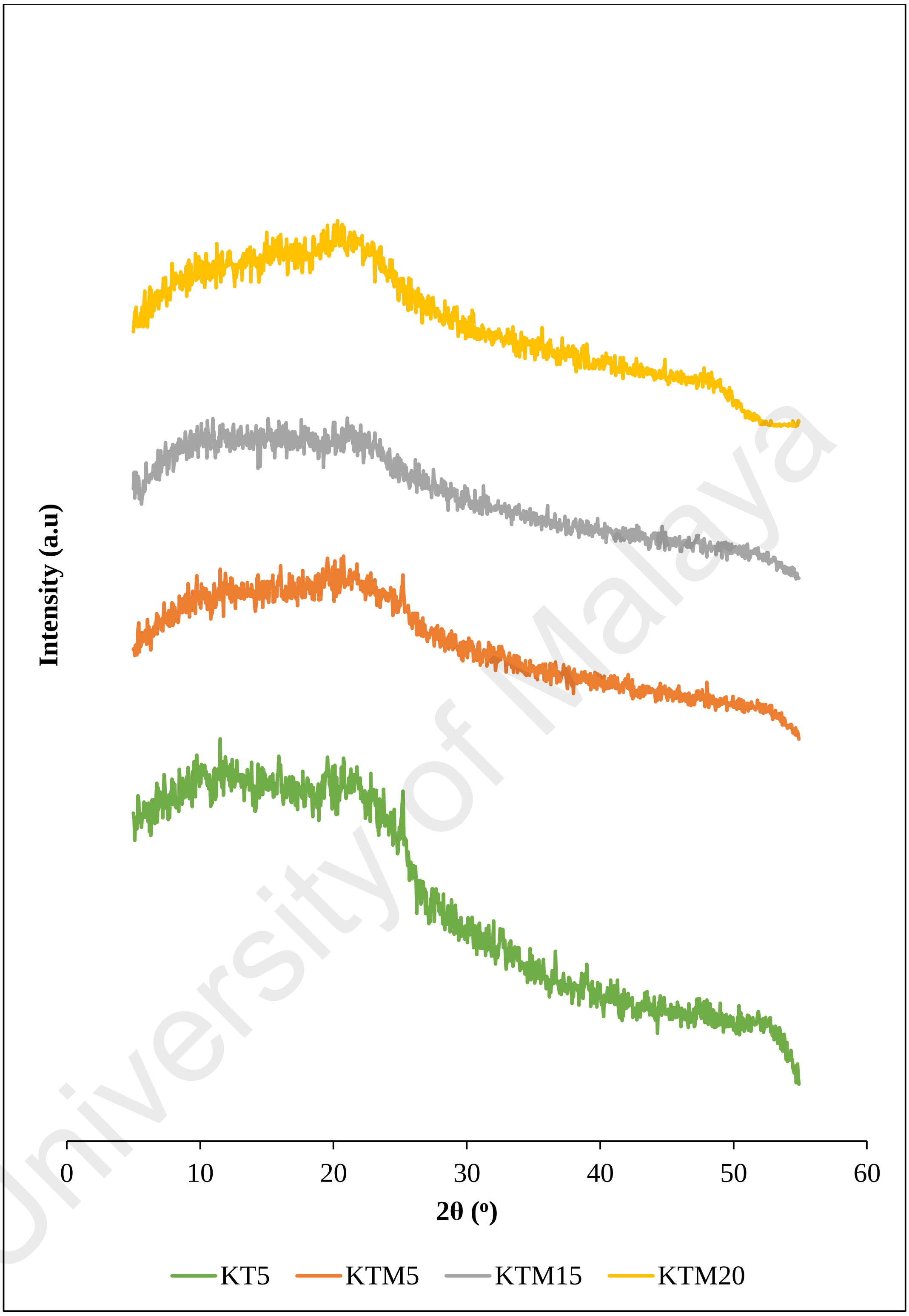

Figure 4.92: XRD patterns of the sample KT5, KTM5, KTM15 and KTM20.

4.6.6 Thermogravimetric analysis (TGA)

Figure 4.95 depicts the thermal gravimetric analysis (TGA) thermograms of gel polymer electrolytes with different MPII concentration added into the previously best performing P(VP-co-VAc)-KI-TPAI sample, KT5. Similar trend of weight loss can be observed at temperature around 30 ℃ - 200 ℃ and this has been explained previously, it was due to the evaporation of moisture, solvents, iodines and some other impurities.

As seen in *Table 4.24*, the degradation temperature of the PVAc region is found to be increase after the addition of MPII into sample KT5 indicating that the incorporation of MPII at this level has slightly improved the thermal stability of the PVAc region of the P(VP-co-VAc)-KI-TPAI-MPII samples. Meanwhile, the degradation temperature of the PVP region is found to have slightly increased after the addition of MPII into sample KT5 showing slight increase in the thermal stability of the PVP region as well. Both of these occurrences were due to the different amount of energy that are required to break the interactive bonds in the different region as well as complexation between P(VP-co-VAc), TPAI, KI and MPII which has been shown in the with the FTIR studies. The higher mass loss after T_{max1} in all of the samples were due to the overlapping of the weight loss of deacetylation of the PVAc and the degradation of the MPII. Meanwhile, the degradation of the TPAI were found to be increase s reported previously in the thermogram of P(VP-co-VAc)-TPAI which is most likely due to more energy needed to overcome the complexation that has occurred between the TPAI and the polymer matrix as already shown in the FTIR spectra.

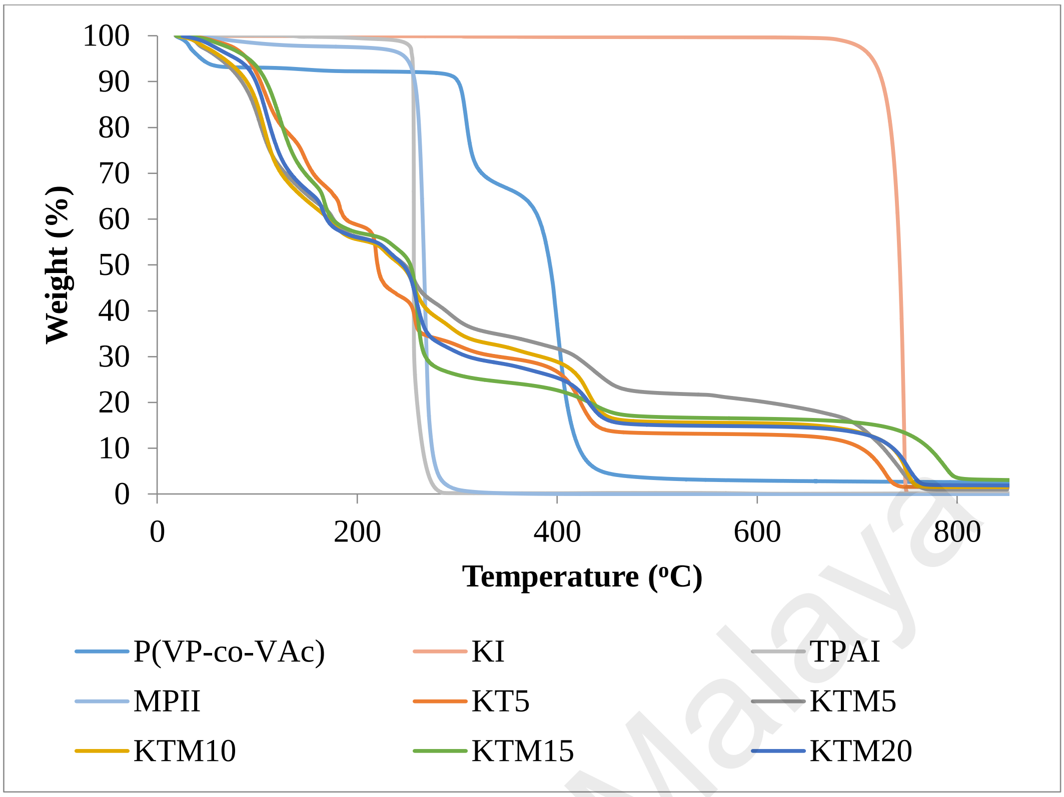

Figure 4.93: Thermogravimetric analysis of pure P(VP-co-VAc) and the P(VP-co-VAc)-KI-TPAI-MPII GPE samples.

Table 4.24: The degradation temperature of the pure P(VP-co-VAc), sample O, KT5, KTM5, KTM10, KTM15 and KTM20.

Samples	**T_{max1} (°C)**	**T_{max2} (°C)**
P(VP-co-VAc)	310	385
O	314	411
KT5	217	423
KTM5	255	444
KTM10	256	431
KTM15	258	432
KTM20	258	437

4.6.7 Photocurrent density-voltage (J-V) Characteristics

The photovoltaic performance of the DSSCs fabricated with the gel polymer electrolytes added with binary salt (KT5) and different MPII concentration under the simulated solar light of 100 mW cm^{-2} (AM 1.5) was evaluated, and the J-V characteristic curves were shown in *Figure 4.94*. The photovoltaic parameters of the cells were listed in *Table 4.25*. The normalized value of parameters of the DSSCs were shown in *Figure 4.95*. Initially, the GPEs with only single salt were having power conversion efficiencies of 3.10 % and 2.94 % for TPAI and KI salts system respectively as seen in previous sections. However, when these two salts were added into the system, the power conversion efficiency could increase up to 5.53% as observed in *section 4.5.7*.

Upon the addition of MPII into the binary salt system, the power conversion efficiency observed to be increased to 5.94% in which is mostly due to the slight increase in V_{oc} and J_{sc} of the system. As mentioned previous, bulkier cations would have lower downward shift to the conduction band edge which causing it to have higher V_{oc} and with the bulky cation from MPII added into the system it slightly increases the V_{oc} (N. Park et al., 2000; Shi et al., 2011). Meanwhile, the slight improvement of the J_{sc} could be due to the increase in the iodide ionic conductivity from the MPII. It might also due to the plasticizing effect that could have decreased the viscosity of the GPEs which could lead to increase in the flow of the mobility of the iodide ion in the polymer matrix (Lin et al., 2014). It is observed that there were a slight drop in the fill factor of the P(VP-co-VAc)-KI-TPAI sample.

The variation of the normalized current density of the DSSC under different illumination condition were measured and shown in *Figure 4.96*. The linear shape of the curve shows that there are no mobile ions and electron transport occurring at the Pt and electrode interface that could represent the rate-determining steps in the photo-electrochemical process (Chiappone et al., 2014).

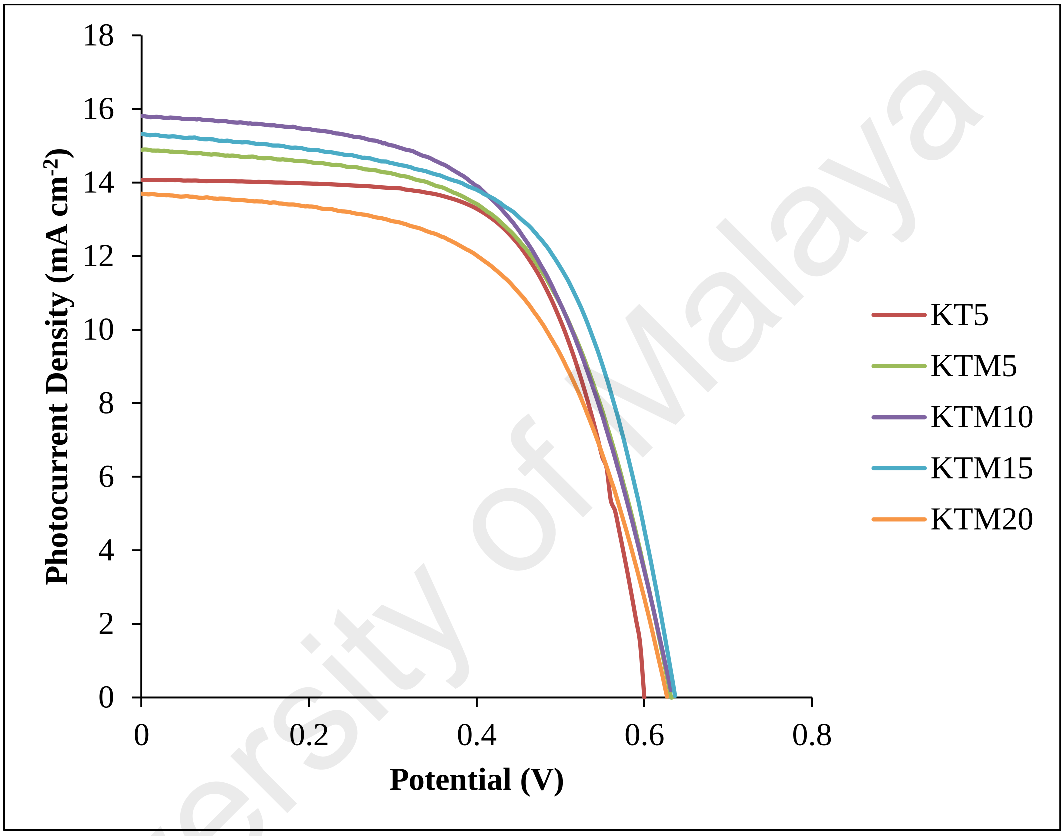

Figure 4.94: The photocurrent-photovoltage (J-V) characteristics of the P(VP-co-VAc)-KI-TPAI-MPII GPE samples consisting of different weight percentages of MPII.

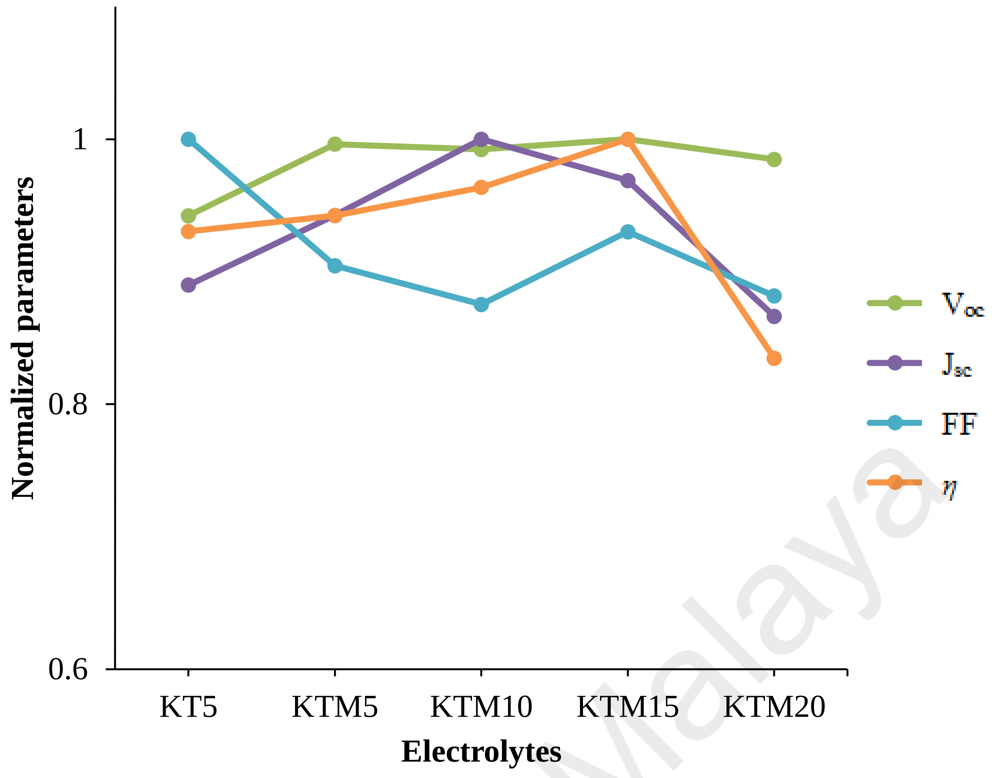

Figure 4.95: The normalization curves of the various performance parameters of the DSSCs fabricated with different P(VP-co-VAc)-KI-TPAI-MPII GPE samples.

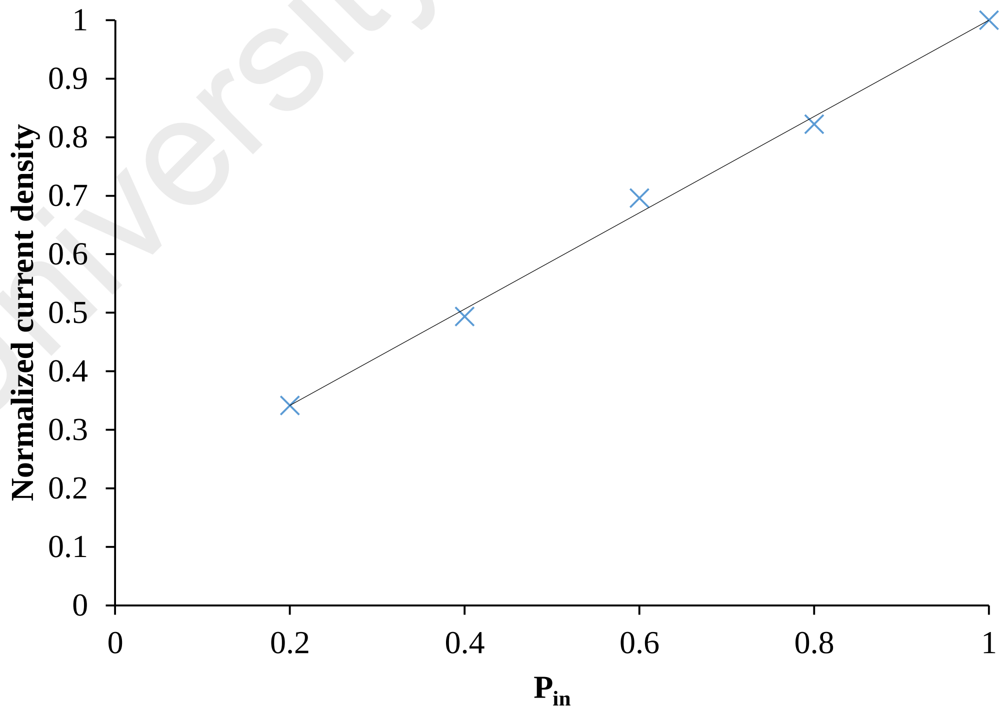

Figure 4.96: Normalized J_{sc} values plotted as a function of different light intensities (P_{in}) for sample KTM15.

Table 4.25: Photovoltaic parameters of the P(VP-co-VAc)-KI-TPAI-MPII GPE samples consisted of different weight percentages of MPII.

Electrolytes	V_{oc} (V)	J_{sc} (mA cm^{-2})	FF (%)	η (%)
KT5	0.60	14.07	0.65	5.53
KTM5	0.63	14.90	0.59	5.60
KTM10	0.63	15.81	0.57	5.72
KTM15	0.64	15.32	0.61	5.94
KTM20	0.63	13.70	0.58	4.96

4.6.8 EIS studies for DSSCs

Figure 4.97(a) presents the Nyquist plots of the P(VP-co-VAc)-KI-TPAI-MPII gel polymer electrolytes and sample KT5 at 100 mW/cm^2 illuminations. As observed in the figure, each plot consists of two distinctive semi-circles at two different frequency range and another spike at the low frequency range. These semi-circles were denoted as R_{ct1}, R_{ct2} and W. R_{ct1} can be observed at high frequency region and it is due to the charge transfer resistance happening at the Pt counter electrode. Meanwhile, R_{ct2} was found in medium frequency region and it is corresponded to the charge resistance of the charge recombination between the TiO_2 conduction band and I_3^- ions at the dye of the mesoporous TiO_2 and the electrolytes interface. The spike can be attributed to the Warburg diffusion (W) (C. Wang et al., 2013). The intersection of the x-axis and the high frequency semi-circle is basically interpreted as R_s (Min Wang et al., 2014).

The plots obtained were then fitted with Metrohm Nova software and the equivalent circuits are shown in *Figure 4.97(a)*. The parameters used to fit the curves were listed in *Table 4.26*. R_{ct2} is an important parameter that could explain the variation of the PCE of the cells. The higher value in R_{ct} indicates that resistant between the working electrode and the electrolytes interface were increasing and the charge recombination rate between the TiO_2 and the I_3^- in the electrolytes were becoming lower leading to longer electron lifetime. As seen in *Table 4.26*, the R_{ct2} was increasing upon the addition of the MPII into sample KT5. The increase in R_{ct2} is consistent with our explanation for the increased V_{oc} where the reduction of the combination rate is normally responsible for the higher V_{oc} exhibited by the TiO_2 photoanode-based cells. *Figure 4.98* shows the open circuit voltage, V_{oc} and R_{ct2} with the respect of different MPII concentration in P(VP-co-VAc)-KI-TPAI-MPII GPE samples.

In the Bode plots in *Figure 4.97(b)*, the peaks corresponding to the TiO_2 and electrolyte interface in the middle frequency range are shifted in an order of sample KTM15>sample KTM10>sample KTM20>sample KTM, indicating that samples are having decrease in electron lifetime in that order. The electron lifetime is inversely proportional to the character frequency peak in the higher frequency region of the spectra. Thus, the data collected are in consistent with the R_{ct2} obtained (Boonsin et al., 2012).

Tafel-polarization plots were recorded to determine the electrocatalytic activity of the P(VP-co-VAc)-KI-TPAI-MPII gel polymer electrolyte are shown in *Figure 4.99*. A larger slope in the anodic or cathodic branch indicates a higher exchange current density (J_0). Considering that the pure Tafel region is not observable, therefore the low field region is used to assess J_0 variation. The extracted J_0 has an order of sample KTM15>sample KTM10>sample KTM20>sample KTM5. J_0 which is inversely proportional to R_{ct2} where it can be associated in *equation 4.9*. Apparently, the trend of the J_0 matches the order of the samples in the EIS studies. Additionally, the intersection of the cathodic branch with the Y-axis can be determined as the limiting diffusion current density (J_{lim}), a parameter that depends on the diffusion coefficient (D_n) of I^-/I_3^- redox couple at the counter electrode and electrolyte interface. J_{lim} is in proportion to D_n which is shown in *equation 4.8* (S. H. Park et al., 2014). Apparently, both J_{lim} and D_n have a sequence of sample KTM15>sample KTM10>sample KTM5>sample TM20 indicating that the D_n is in consistent with that from the EIS studies. This could explain the increase of PCE of the gel polymer electrolyte samples of these system (C. Wu et al., 2012).

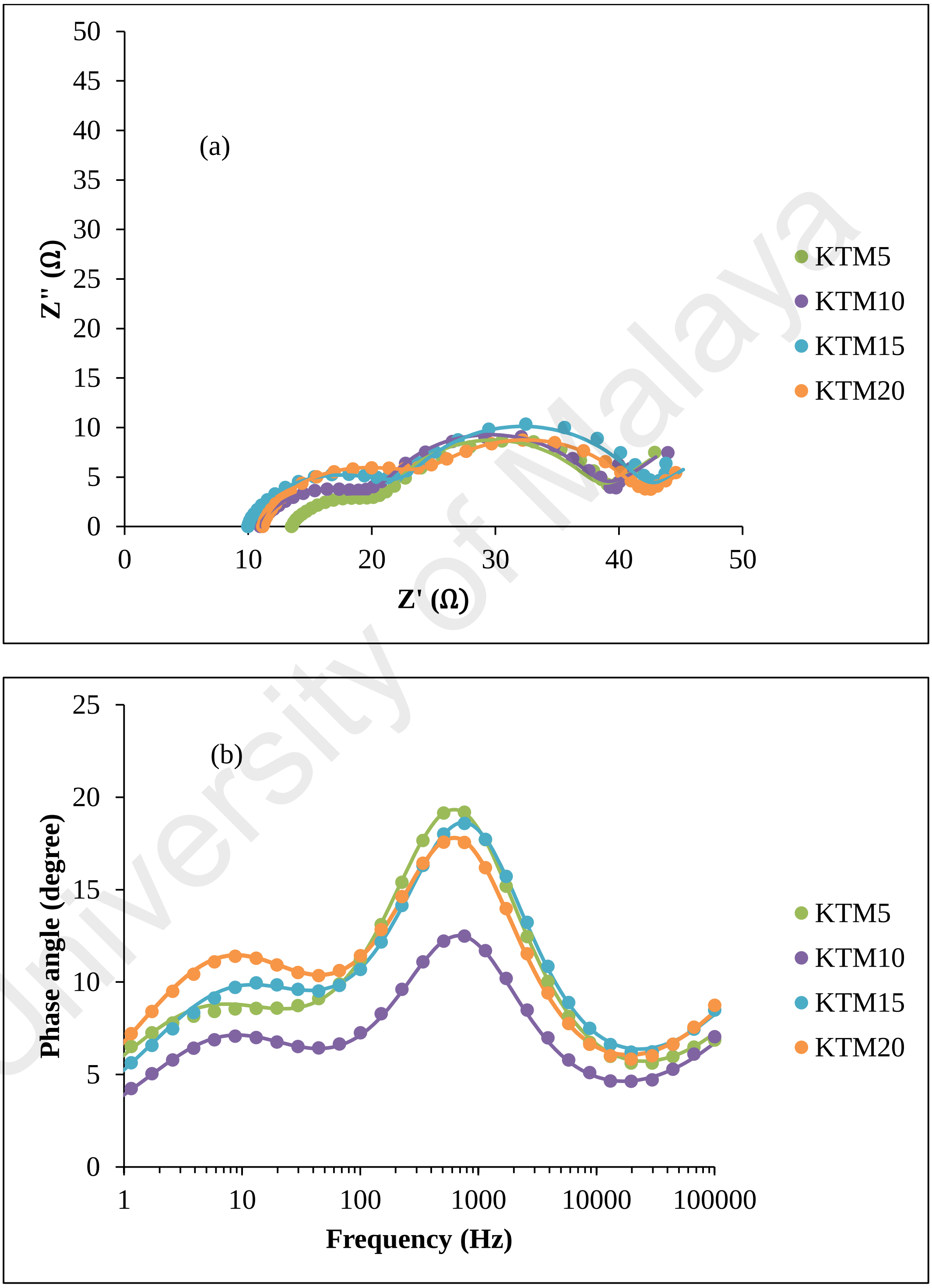

Figure 4.97: The electrochemical impedance spectra of DSSCs assembled with P(VP-co-VAc)-KI-TPAI-MPII GPE samples in the forms of (a) Nyquist plots and (b) Bode phase plots. The spectra were measured under 100 mW cm^{-2} illuminated sunlight.

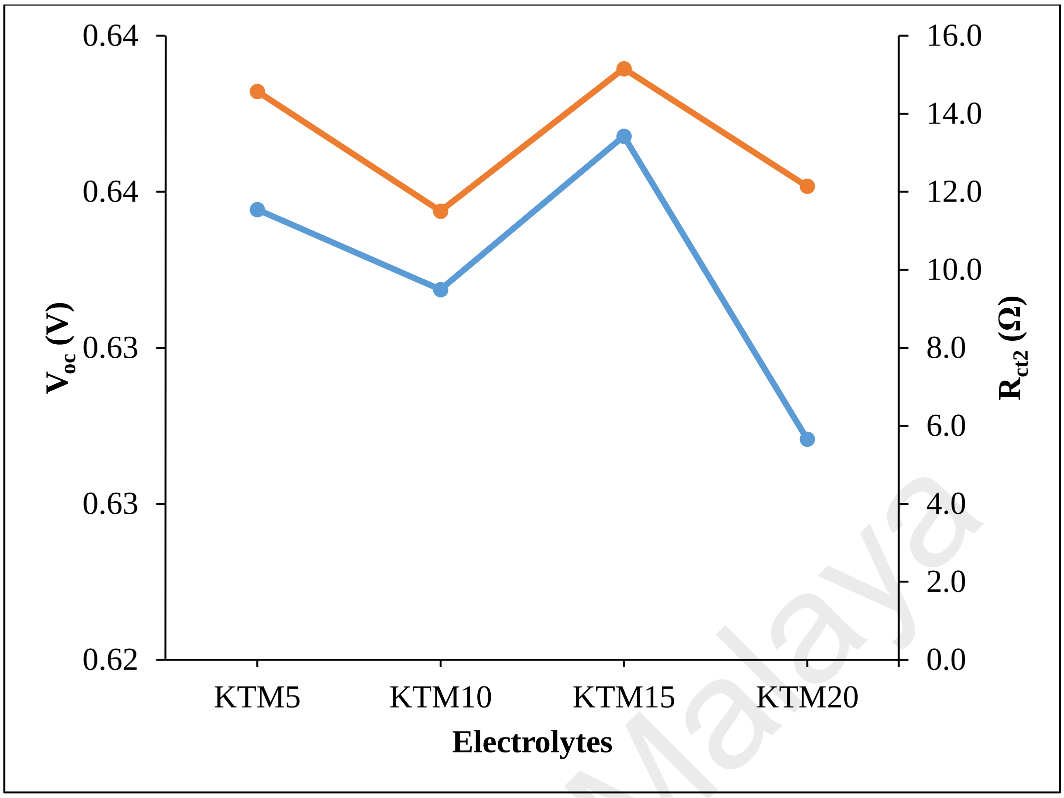

Figure 4.98: The open circuit voltage and R_{ct2} with the respect of different MPII concentration in P(VP-co-VAc)-KI-TPAI-MPII GPE samples.

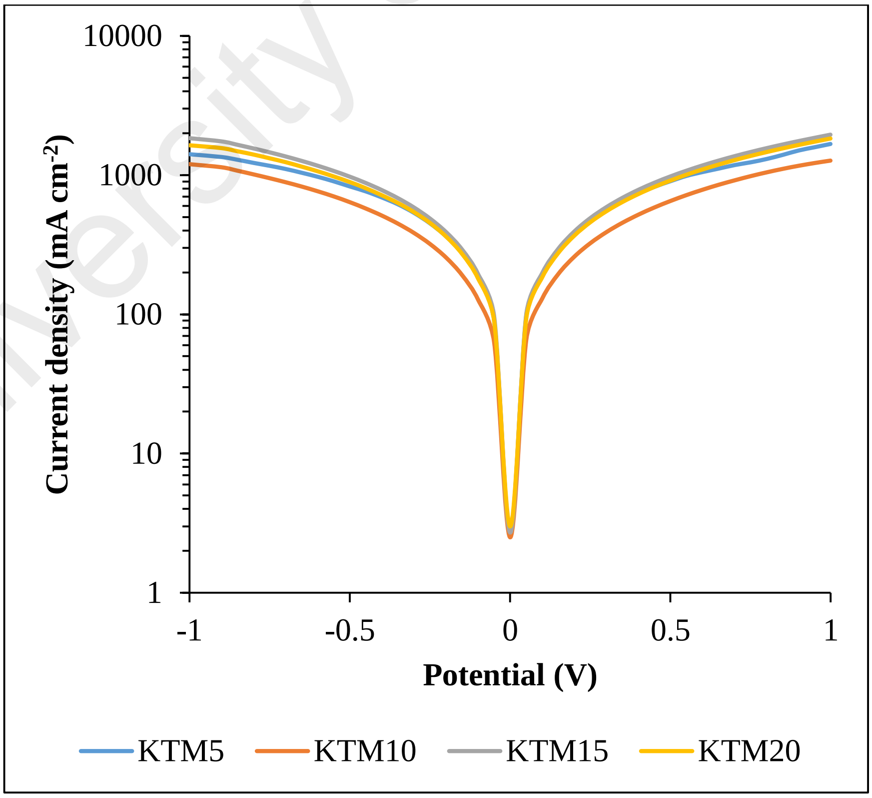

Figure 4.99: Tafel polarization curves of symmetric Pt cells with P(VP-co-VAc)-KI-TPAI-PMII gel polymer electrolytes samples.

Table 4.26: The parameters of the equivalent circuits used to fit the EIS impedance data of the P(VP-co-VAc)-KI-TPAI-MPII based DSSCs.

Electrolytes	R_s (Ω)	R_{ct1}(Ω)	R_{ct2}(Ω)	W($S^{1/2}\ \Omega^{-1}$)	τ (ms)
KTM5	15.7	16.4	19.3	0.60	85.3
KTM10	13.9	19.3	19.1	0.53	83.9
KTM15	16.2	6.9	21.0	0.64	88.8
KTM20	14.8	12.8	19.1	0.50	84.1

4.7 Summarize of the chapter

The P(VP-co-VAc) based GPEs were successfully prepared and fabricated into DSSCs. KTM15 and its DSSC was found to be giving the highest ionic conductivity and power conversion efficiency with the value of 4.09×10^{-3} S cm^{-1} and 5.94%, respectively. All of the P(VP-co-VAc) based GPEs sample was found to be obeying the Arrhenius behavior. The complexation of materials used was confirmed by using FTIR and XRD techniques. Meanwhile, the thermal properties of the samples have been done by using TGA. The EIS studies of the DSSCs have also been done to learn more on the electrical characterization of the DSSCs.

CHAPTER 5: CONCLUSIONS

5.1 Conclusions

A total of five gel polymer electrolyte systems was prepared aimed at optimizing the DSSCs using three different strategies: the use of co-polymer with the addition of single salt, the combination of two different sizes of salts and the addition of the ionic liquid into the gel polymer electrolytes. As discussed in the respective sections, valuable information has been collected and reported in this thesis.

P(VP-co-VAc) was used as host polymer with KI and TPAI as doping salts and MPII was used as the ionic liquid in this research. Usage of P(VP-co-VAc) shows promising results as the highest ionic conductivity be obtained was 1.72×10^{-3} S cm^{-1} and 1.60×10^{-3} S cm^{-1} for P(VP-co-VAc) based gel polymer electrolytes added with KI and TPAI salt, respectively. With the combination of these two salts, in the best ratio, the ionic conductivity increased to 1.96×10^{-3} S cm^{-1} showing that the strategy of using binary salt was successful in increasing the ionic conduction properties of the P(VP-co-VAc) based gel polymer electrolytes. The suitability of the ionic liquid with the P(VP-co-VAc) based gel polymer electrolytes was tested on the P(VP-co-VAc)-KI system and a perfect gel polymer electrolyte could be formed. The ionic conductivity of this P(VP-co-VAc)-KI-MPII system reached 3.13×10^{-3} S cm^{-1} and with the good result, it has motivated us to incorporate it into the binary salt system. With the addition of the MPII into the P(VP-co-VAc)-KI-TPAI system, the ambient temperature-ionic conductivity reaches a maximum value of 4.09×10^{-3} S cm^{-1} upon addition of 15 wt.% of MPII and was the best P(VP-co-VAc) based gel polymer electrolyte prepared in the whole research.

The ionic conductivity of all the samples were increasing with the increase of temperature. It shows that they were obeying the Arrhenius behavior which further shows that they were having the ion hopping mechanism occurring inside the polymer matrix of the samples. The dielectric studies were done to further understand more on the dielectric properties of the studies. It was also found that, there were no changes in the dielectric properties in all of the system after all the strategies has been applied on the P(VP-co-VAc) based gel polymer electrolytes.

Furthermore, the FTIR spectroscopy studies has been done and the complexation of the P(VP-co-VAc), KI, TPAI and MPII has been proven through the changes in the peak shifting, intensity, shape and formation of new peaks. The K^+ and TPA^+ ions were found to be interacting strongly with the strong electron donor C=O group of both PVP and PVAc region of the P(VP-co-VAc) copolymer and the I^- ion were found to be interacting with the strong withdrawing N atom of the C-N stretching in the PVP chain.

X-ray diffraction (XRD) studies have been done and it is found that the higher degree of amorphous nature of the gel polymer electrolytes increased the ionic conductivity of the samples by disturbing the ordered arrangement of the polymer matrix, causing the most drop in crystallinity and thus increasing the mobility of the ions inside the polymer matrix. Thermogravimetric studies (TGA) studies have been done to understand more on the thermal properties of the P(VP-co-VAc) based gel polymer electrolytes.

On the other side, all of the samples from different systems have been used to fabricate the DSSCs and all of them were successful. The KI and TPAI system have shown the highest power conversion efficiency of 2.94 % and 3.07 %, respectively for their own system. However, by mixing these salts together and at the best ratio, the power conversion efficiency increased to the highest value of 5.53 % with the ration 30:10 wt.% of KI:TPAI salt. Then, by further adding MPII ionic liquid into the binary salt system, the power conversion efficiency increases to 5.94 % at 15 wt.% of the MPII added with open circuit voltage (V_{oc}) at 640 mV, short circuit current density (Jsc) of 15.32 mA cm^{-2} and fill factor at 61 %. This sample is denoted as KTM15 and it was the best sample that provides the best power conversion efficiency in this research. To further understand more on these DSSCs, the EIS of the DSSCs has been studied and it was found that all of the samples can be fitted with the electronic circuit shown in *Figure 4.19*. Samples with higher R_{ct2} were found to have slower charge recombination rate which causes higher electron lifetime and this sample has higher V_{oc} as well. The Tafel polarization studies show that the samples with higher electrocatalytic activity would have higher power conversion efficiency.

5.2 Future work

Further investigation could still be carried out to improve the performances of these P(VP-co-VAc) gel polymer electrolytes and its DSSCs. Some of the work that can be done is listed below:

1. Substitute the solvent used in this research to a higher dielectric constant organic compounds. This may enhance the ionic conductivity of the GPEs which could also lead to an increase in the short circuit current density of the DSSCs. Hence, enhancing the PCE of the DSSCs.
2. Add electrochemically inert nano-scale fillers such as TiO_2 to the highest conducting sample. This may enhance the ionic conductivity by decreasing the degree of crystallinity and introduction of new pathways for ion conduction.
3. Newer and better techniques of electrode preparation could be introduced to improve the photovoltaic performances of the P(VP-co-VAc) based GPEs as the electrode preparation techniques that was used in this research was the basic conventional techniques.

REFERENCES

Abo El Ata, a. M., Attia, S. M., & Meaz, T. M. (2004). AC conductivity and dielectric behavior of $CoAl_xFe_{2-x}O_4$. *Solid State Sciences*, *6*(1), 61–69.

Abraham, K. M. (1996a). A Polymer Electrolyte-Based Rechargeable Lithium/Oxygen Battery. *Journal of The Electrochemical Society*, *143*(1), 1.

Abraham, K. M. (1996b). A Polymer Electrolyte-Based Rechargeable Lithium/Oxygen Battery. *Journal of The Electrochemical Society*, *143*(1), 1.

Agarwala, S., Thummalakunta, L. N. S. a., Cook, C. a., Peh, C. K. N., Wong, a. S. W., Ke, L., & Ho, G. W. (2011). Co-existence of LiI and KI in filler-free, quasi-solid-state electrolyte for efficient and stable dye-sensitized solar cell. *Journal of Power Sources*, *196*(3), 1651–1656.

Aravindan, V., & Vickraman, P. (2007). Polyvinylidenefluoride–hexafluoropropylene based nanocomposite polymer electrolytes (NCPE) complexed with $LiPF_3(CF_3CF_2)_3$. *European Polymer Journal*, *43*(12), 5121–5127.

Asmara, S. N., Kufian, M. Z., Majid, S. R., & Arof, a. K. (2011). Preparation and characterization of magnesium ion gel polymer electrolytes for application in electrical double layer capacitors. *Electrochimica Acta*, *57*, 91–97.

Avakian, P., Starkweather, H. W., & Kampert, W. G. (2002). Dielectric analysis of polymers. *Handbook of Thermal Analysis and Calorimetry*, *3*(1), 147–165.

Bandara, T. M. W. J., Jayasundara, W. J. M. J. S. R., Dissanayake, M. a. K. L., Fernando, H. D. N. S., Furlani, M., Albinsson, I., & Mellander, B.-E. (2014). Quasi solid state polymer electrolyte with binary iodide salts for photo-electrochemical solar cells. *International Journal of Hydrogen Energy*, *39*(6), 2997–3004.

Bandara, T. M. W. J., Svensson, T., Dissanayake, M. A. K. L., & Furlani, M. (2012). Tetrahexylammonium Iodide Containing Solid and Gel Polymer Electrolytes for Dye Sensitized Solar Cells. *Energy Procedia*, *14*(2011), 1.

Baskaran, R., Selvasekarapandian, S., Kuwata, N., Kawamura, J., & Hattori, T. (2006). Conductivity and thermal studies of blend polymer electrolytes based on PVAc–PMMA. *Solid State Ionics*, *177*(26-32), 2679–2682.

Bella, F., Ozzello, E. D., Sacco, A., Bianco, S., & Bongiovanni, R. (2014). Polymer electrolytes for dye-sensitized solar cells prepared by photopolymerization of PEG-based oligomers. *International Journal of Hydrogen Energy*, *39*(6), 3036–3045.

Bella, F., Sacco, A., Pugliese, D., Laurenti, M., & Bianco, S. (2014). Additives and salts for dye-sensitized solar cells electrolytes: what is the best choice? *Journal of Power Sources*, *264*, 333–343.

Bianco, G., Soldi, M. S., Pinheiro, E. a., Pires, a. T. N., Gehlen, M. H., & Soldi, V. (2003). Thermal stability of poly(N-vinyl-2-pyrrolidone-co-methacrylic acid) copolymers in inert atmosphere. *Polymer Degradation and Stability*, *80*(3), 567–574.

Boonsin, R., Sudchanham, J., Panusophon, N., Sae-Heng, P., Sae-Kung, C., & Pakawatpanurut, P. (2012). Dye-sensitized solar cell with poly(acrylic acid-co-acrylonitrile)-based gel polymer electrolyte. *Materials Chemistry and Physics*, *132*(2-3), 993–998.

Cha, S. Y., Lee, Y.-G., Kang, M.-S., & Kang, Y. S. (2010). Correlation between ionic conductivity and cell performance in solid-state dye-sensitized solar cells employing polymer electrolyte. *Journal of Photochemistry and Photobiology A: Chemistry*, *211*(2-3), 193–196.

Chen, C.-L., Chang, T.-W., Su, S.-C., Teng, H., & Lee, Y.-L. (2014). High performance solid-state dye-sensitized solar cells based on poly(acrylonitrile-co-vinyl acetate)/TiO2 nanoparticles redox electrolytes. *Journal of Power Sources*, *247*, 406–411.

Chiappone, A., Bella, F., Nair, J. R., Meligrana, G., Bongiovanni, R., & Gerbaldi, C. (2014). Structure-Performance Correlation of Nanocellulose-Based Polymer Electrolytes for Efficient Quasi-solid DSSCs. *ChemElectroChem*, *1*(8), 1350–1358.

Costa, L. T., Lavall, R. L., Borges, R. S., Rieumont, J., Silva, G. G., & Ribeiro, M. C. C. (2007). Polymer electrolytes based on poly(ethylene glycol) dimethyl ether and the ionic liquid 1-butyl-3-methylimidazolium hexafluorophosphate: Preparation, physico-chemical characterization, and theoretical study. *Electrochimica Acta*, *53*(4), 1568–1574.

Cui, Y., Zhang, J., Wang, P. lifetime in dssc, Zhang, X., Zheng, J., Sun, Q., Zhu, Y. (2012). Improved performance using a plasticized polymer electrolyte for quasi-solid state dye-sensitized solar cells. *Electrochimica Acta*, *74*, 194–200.

Dissanayake, M. a. K. L., Rupasinghe, W. N. S., Seneviratne, V. a., Thotawatthage, C. a., & Senadeera, G. K. R. (2014). Optimization of iodide ion conductivity and nano filler effect for efficiency enhancement in polyethylene oxide (PEO) based dye sensitized solar cells. *Electrochimica Acta*, *145*, 319–326.

Dissanayake, M. a. K. L., Thotawatthage, C. a., Senadeera, G. K. R., Bandara, T. M. W. J., Jayasundera, W. J. M. J. S. R., & Mellander, B.-E. (2012). Efficiency enhancement by mixed cation effect in dye-sensitized solar cells with PAN based gel polymer electrolyte. *Journal of Photochemistry and Photobiology A: Chemistry*, *246*, 29–35.

Fenton, D. E., Parker, J. M., & Wright, P. V. (1973). Complexes of alkali metal ions with poly(ethylene oxide). *Polymer*, *14*(11), 589.

Franck, E. U. (1960). *Electrolyte Solutions, von R. A. Robinson und R. H. Stokes. — The Measurement and Interpretation of Conductance, Chemical Potential and Diffusion in Solutions of Simple Electrolytes. Butterworths Scientific Publication, London 1959. 2. Aufl., XV, 559 S., . Angewandte Chemie* (Vol. 72, p. 426). WILEY-VCH Verlag GmbH.

Hallinan, D. T., & Balsara, N. P. (2013). Polymer Electrolytes. *Annual Review of Materials Research, 43*(1), 503–525.

Hao, F., Lin, H., Zhang, J., & Li, J. (2011). Balance between the physical diffusion and the exchange reaction on binary ionic liquid electrolyte for dye-sensitized solar cells. *Journal of Power Sources*, *196*(3), 1645–1650.

Hieu, N. T., Baik, S. J., Jun, Y., Lee, M., Chung, O. H., & Park, J. S. (2014). Electrospun coaxial titanium dioxide/carbon nanofibers for use in anodes of dye-sensitized solar cells. *Electrochimica Acta*, *142*, 144–151.

Hoshikawa, T., Ikebe, T., Kikuchi, R., & Eguchi, K. (2006). Effects of electrolyte in dye-sensitized solar cells and evaluation by impedance spectroscopy. *Electrochimica Acta*, *51*(25), 5286–5294.

Howell, S., & Bose, R. A. (2007). Electrical Relaxation in a Glass-Forming Molten Salt. *J. Phys. Chem*, *78*(72), 639–648.

Jayathilaka, P. A. R. D., Dissanayake, M. A. K. L., Albinsson, I., & Mellander, B. (2003). Dielectric relaxation , ionic conductivity and thermal studies of the gel polymer electrolyte system PAN / EC / PC / LiTFSI, *156*, 179–195.

K. Nazeeruddin, M., Pechy, P., & Gratzel, M. (1997). Efficient panchromatic sensitization of nanocrystalline TiO2 films by a black dye based on a trithiocyanato-ruthenium complex. *Chem. Commun.*, (18), 1705–1706.

Ke, W., Fang, G., Lei, H., Qin, P., Tao, H., Zeng, W., Zhao, X. (2014). An efficient and transparent copper sulfide nanosheet film counter electrode for bifacial quantum dot-sensitized solar cells. *Journal of Power Sources*, *248*, 809–815.

Kern, R., Sastrawan, R., Ferber, J., Stangl, R., & Luther, J. (2002). Modeling and interpretation of electrical impedance spectra of dye solar cells operated under open-circuit conditions. *Electrochimica Acta*, *47*(26), 4213–4225.

Kim, C. S., & Oh, S. M. (2000). Importance of donor number in determining solvating ability of polymers and transport properties in gel-type polymer electrolytes. *Electrochimica Acta*, *45*(13), 2101–2109.

Kim, K.-S., Park, S.-Y., Yeon, S.-H., & Lee, H. (2005). N-Butyl-N-methylmorpholinium bis(trifluoromethanesulfonyl)imide–PVdF(HFP) gel electrolytes. *Electrochimica Acta*, *50*(28), 5673–5678.

Kumar, D. A., Selvasekarapandian, S., Baskaran, R., Savitha, T., & Nithya, H. (2012). Thermal, vibrational and Ac impedance studies on proton conducting polymer electrolytes based on poly(vinyl acetate). *Journal of Non-Crystalline Solids*, *358*(3), 531–536.

Lan, Z., Wu, J., Lin, J., & Huang, M. (2010). Quasi-solid-state dye-sensitized solar cell based on a polymer gel electrolyte with in situ synthesized ionic conductors. *Comptes Rendus Chimie*, *13*(11), 1401–1405.

Lan, Z., Wu, J., Lin, J., Huang, M., Li, P., & Li, Q. (2008). Influence of ionic additives NaI/I2 on the properties of polymer gel electrolyte and performance of quasi-solid-state dye-sensitized solar cells. *Electrochimica Acta*, *53*(5), 2296–2301.

Lauter, U., Meyer, W. H., & Wegner, G. (1997). Molecular Composites from Rigid-Rod Poly(p -phenylene)s with Oligo(oxyethylene) Side Chains as Novel Polymer Electrolytes. *Macromolecules*, *30*(7), 2092–2101.

Lee, C.-P., Lin, L.-Y., Vittal, R., & Ho, K.-C. (2011). Favorable effects of titanium nitride or its thermally treated version in a gel electrolyte for a quasi-solid-state dye-sensitized solar cell. *Journal of Power Sources*, *196*(3), 1665–1670.

Li, B., Wang, L., Kang, B., Wang, P., & Qiu, Y. (2006). Review of recent progress in solid-state dye-sensitized solar cells. *Solar Energy Materials and Solar Cells, 90*(5), 549–573.

Li, P. J., Wu, J. H., Huang, M. L., Hao, S. C., Lan, Z., Li, Q., & Kang, S. (2007). The application of P(MMA-co-MAA)/PEG polyblend gel electrolyte in quasi-solid state dye-sensitized solar cell at higher temperature. *Electrochimica Acta*, *53*(2), 903–908.

Liang, Y.-H., Wang, C.-C., & Chen, C.-Y. (2008). Synthesis and characterization of a new network polymer electrolyte containing polyether in the main chains and side chains. *European Polymer Journal*, *44*(7), 2376–2384.

Liew, C.-W., Ramesh, S., & Arof, a. K. (2014). Characterization of ionic liquid added poly(vinyl alcohol)-based proton conducting polymer electrolytes and electrochemical studies on the supercapacitors. *International Journal of Hydrogen Energy*, 1–11.

Lin, B., Shang, H., Chu, F., Ren, Y., Yuan, N., Jia, B., Ding, J. (2014). Ionic liquid-tethered Graphene Oxide/Ionic Liquid Electrolytes for Highly Efficient Dye Sensitized Solar Cells. *Electrochimica Acta*.

Manuel Stephan, a., & Nahm, K. S. (2006). Review on composite polymer electrolytes for lithium batteries. *Polymer*, *47*(16), 5952–5964.

Marinado, T. (2009). *Photoelectrochemical studies of dye-sensitized solar cells using organic dyes*.

McNeill, I. C., Ahmed, S., & Memetea, L. (1995). Thermal degradation of vinyl acetate-methacrylic acid copolymer and the homopolymers. II. Thermal analysis studies. *Polymer Degradation and Stability*, *48*(1), 89–97.

Md. K. Nazeeruddin, *, S. M. Zakeeruddin, R. Humphry-Baker, M. Jirousek, P. Liska, N. Vlachopoulos, … and M. Grätzel*. (1999). Acid−Base Equilibria of (2,2‘-Bipyridyl-4,4‘-dicarboxylic acid)ruthenium(II) Complexes and the Effect of Protonation on Charge-Transfer Sensitization of Nanocrystalline Titania. *Inorganic Chemistry, 38*(26), 6298–6305.

Meyer, W. H. (1998). Polymer electrolytes for lithium-ion batteries. *Advanced Materials (Deerfield Beach, Fla.), 10*(6), 439–48.

Miao, R., Liu, B., Zhu, Z., Liu, Y., Li, J., Wang, X., & Li, Q. (2008). PVDF-HFP-based porous polymer electrolyte membranes for lithium-ion batteries. *Journal of Power Sources, 184*(2), 420–426.

Mishra, R., & Rao, K. J. (1998). Electrical conductivity studies of poly(ethyleneoxide)-poly(vinylalcohol) blends. *Solid State Ionics*, *106*(1–2), 113–127.

Nath, a. K., & Kumar, a. (2014). Scaling of AC conductivity, electrochemical and thermal properties of ionic liquid based polymer nanocomposite electrolytes. *Electrochimica Acta*, *129*, 177–186.

Nazeeruddin, M. K., Kay, a., Rodicio, I., Humphry-Baker, R., Mueller, E., Liska, P., … Graetzel, M. (1993). Conversion of light to electricity by cis-X2bis(2,2'-bipyridyl-4,4'-dicarboxylate)ruthenium(II) charge-transfer sensitizers (X = Cl-, Br-, I-, CN-, and SCN-) on nanocrystalline titanium dioxide electrodes. *Journal of the American Chemical Society*, *115*(14), 6382–6390.

National Renewable Energy Laboratory (NREL). (n.d.). Retrieved September 7, 2015, from http://www.nrel.gov/

O'Regan, B., & Grätzel, M. (1991). A low-cost, high-efficiency solar cell based on dye-sensitized colloidal TiO_2 films. *Nature*, *353*(6346), 737–740.

Park, N., Chang, S., Lagemaat, J. Van De, Kim, K., & Frank, A. J. (2000). Effect of Cations on the Open-Circuit Photovoltage and the Charge-Injection Efficiency of Dye-Sensitized Nanocrystalline Rutile TiO 2 Films, *21*(10), 985–988.

Park, S. H., Kim, O.-H., Kang, J. S., Lee, K. J., Choi, J.-W., Cho, Y.-H., & Sung, Y.-E. (2014). Poly(3,4-Ethylenedioxythiophene) Inverse Opal Electrode Fabricated from Poly(3,4-Ethylenedioxythiophene):Poly(Styrene Sulfonate)-Filled Polystyrene Template for Dye-Sensitized Solar Cells. *Electrochimica Acta*, *137*, 661–667.

Prasanth, R., Shubha, N., Hng, H. H., & Srinivasan, M. (2012). Effect of nano-clay on ionic conductivity and electrochemical properties of poly(vinylidene fluoride) based nanocomposite porous polymer membranes and their application as polymer electrolyte in lithium ion batteries. *European Polymer Journal*, 1–12.

Raghu, S., Kilarkaje, S., Sanjeev, G., & Devendrappa, H. (2013). Electron beam induced modifications in conductivity and dielectric property of polymer electrolyte film. *Radiation Measurements*, *53-54*, 56–64.

Raghu, S., Kilarkaje, S., Sanjeev, G., Nagaraja, G. K., & Devendrappa, H. (2014). Effect of electron beam irradiation on polymer electrolytes: Change in morphology, crystallinity, dielectric constant and AC conductivity with dose. *Radiation Physics and Chemistry*, *98*, 124–131.

Rajendran, S., Babu, R. S., & Sivakumar, P. (2007). Effect of salt concentration on poly (vinyl chloride)/poly (acrylonitrile) based hybrid polymer electrolytes. *Journal of Power Sources*, *170*(2), 460–464.

Ramesh, S., Liew, C.-W., & Arof, a. K. (2011). Ion conducting corn starch biopolymer electrolytes doped with ionic liquid 1-butyl-3-methylimidazolium hexafluorophosphate. *Journal of Non-Crystalline Solids*, *357*(21), 3654–3660.

Ramesh, S., Ng, H. M., Shanti, R., & Ramesh, K. (2013). Studies on the Influence of Titania Content on the Properties of Poly(vinyl chloride) - Poly (acrylonitrile)-Based

Polymer Electrolytes. *Polymer-Plastics Technology and Engineering*, *52*(14), 1474–1481.

Ramesh, S., & Ng, K. Y. (2009). Characterization of polymer electrolytes based on high molecular weight PVC and Li_2SO_4. *Current Applied Physics*, *9*(2), 329–332.

Ramesh, S., Yahaya, A. H., & Arof, A. K. (2002). Dielectric behaviour of PVC-based polymer electrolytes, *153*, 291–294.

Ramya, C. S., Selvasekarapandian, S., Hirankumar, G., Savitha, T., & Angelo, P. C. (2008). Investigation on dielectric relaxations of PVP–NH_4SCN polymer electrolyte. *Journal of Non-Crystalline Solids*, *354*(14), 1494–1502.

Ramya, C. S., Selvasekarapandian, S., Savitha, T., Hirankumar, G., & Angelo, P. C. (2007). Vibrational and impedance spectroscopic study on PVP–NH4SCN based polymer electrolytes. *Physica B: Condensed Matter*, *393*(1-2), 11–17.

Ravi, M., Bhavani, S., Kiran Kumar, K., & Narasimaha Rao, V. V. R. (2013). Investigations on electrical properties of PVP:KIO_4 polymer electrolyte films. *Solid State Sciences*, *19*, 85–93.

Ravi, M., Kiran Kumar, K., Madhu Mohan, V., & Narasimha Rao, V. V. R. (2014). Effect of nano TiO_2 filler on the structural and electrical properties of PVP based polymer electrolyte films. *Polymer Testing*, *33*, 152–160.

Ravi, M., Pavani, Y., Kiran Kumar, K., Bhavani, S., Sharma, a. K., & Narasimha Rao, V. V. R. (2011). Studies on electrical and dielectric properties of PVP:$KBrO_4$ complexed polymer electrolyte films. *Materials Chemistry and Physics*, *130*(1-2), 442–448.

Rhee, Y. H., Ahn, D. J., Ko, M. J., Jin, H.-Y., Jin, J.-H., & Min, N. K. (2014). Enhanced electrocatalytic activity of plasma functionalized multi-walled carbon nanotube-entrapped poly(3,4-ethylendioxythiophene):poly(styrene sulfonate) photocathode. *Electrochimica Acta*, *146*, 68–72.

Salvador, G. P., Pugliese, D., Bella, F., Chiappone, A., Sacco, A., Bianco, S., & Quaglio, M. (2014). New insights in long-term photovoltaic performance characterization of cellulose-based gel electrolytes for stable dye-sensitized solar cells. *Electrochimica Acta*, *146*, 44–51.

Sekhon, S. S., Krishnan, P., Singh, B., Yamada, K., & Kim, C. S. (2006). Proton conducting membrane containing room temperature ionic liquid. *Electrochimica Acta*, *52*(4), 1639–1644.

Selvasekarapandian, S., Baskaran, R., Kamishima, O., Kawamura, J., & Hattori, T. (2006). Laser Raman and FTIR studies on Li^+ interaction in PVAc-LiClO4 polymer electrolytes. *Spectrochimica Acta. Part A, Molecular and Biomolecular Spectroscopy*, *65*(5), 1234–40.

Sengwa, R. J., & Choudhary, S. (2014). Dielectric properties and fluctuating relaxation processes of poly(methyl methacrylate) based polymeric nanocomposite electrolytes. *Journal of Physics and Chemistry of Solids*, *75*(6), 765–774.

Sharma, G. D., Daphnomili, D., Angaridis, P. a., Biswas, S., & Coutsolelos, a. G. (2013). Effect of thiourea incorporation in the electrolyte on the photovoltaic performance of the DSSC sensitized with pyridyl functionalized porphyrin. *Electrochimica Acta*, *102*, 459–465.

Shi, Y., Wang, Y., Zhang, M., & Dong, X. (2011). Influences of cation charge density on the photovoltaic performance of dye-sensitized solar cells: lithium, sodium, potassium, and dimethylimidazolium. *Physical Chemistry Chemical Physics : PCCP*, *13*(32), 14590–7.

Singh, B., Kumar, R., & Sekhon, S. S. (2005). Conductivity and viscosity behaviour of PMMA based gels and nano dispersed gels: Role of dielectric constant of the solvent. *Solid State Ionics*, *176*(17-18), 1577–1583.

Singh, P. K., Kim, K.-W., Park, N.-G., & Rhee, H.-W. (2008). Mesoporous nanocrystalline TiO_2 electrode with ionic liquid-based solid polymer electrolyte for dye-sensitized solar cell application. *Synthetic Metals*, *158*(14), 590–593.

Sivakumar, M., Subadevi, R., Rajendran, S., Wu, H.-C., & Wu, N.-L. (2007). Compositional effect of PVdF–PEMA blend gel polymer electrolytes for lithium polymer batteries. *European Polymer Journal*, *43*(10), 4466–4473.

Sivakumar, M., Subadevi, R., Rajendran, S., Wu, N.-L., & Lee, J.-Y. (2006). Electrochemical studies on [(1−x)PVA–xPMMA] solid polymer blend electrolytes complexed with LiBF4. *Materials Chemistry and Physics*, *97*(2-3), 330–336.

Stephan, A., & Thirunakaran, R. (1999). A study on polymer blend electrolyte based on PVC/PMMA with lithium salt. *Journal of Power …*, *89*, 2000. Retrieved from http://www.sciencedirect.com/science/article/pii/S0378775399001482

Sudhakar, Y. N., Selvakumar, M., & Bhat, D. K. (2014). Tubular array, dielectric, conductivity and electrochemical properties of biodegradable gel polymer electrolyte. *Materials Science and Engineering: B*, *180*, 12–19.

Suryanarayanan, V., Lee, K.-M., Ho, W.-H., Chen, H.-C., & Ho, K.-C. (2007). A comparative study of gel polymer electrolytes based on PVDF-HFP and liquid electrolytes, containing imidazolinium ionic liquids of different carbon chain lengths in DSSCs. *Solar Energy Materials and Solar Cells*, *91*(15-16), 1467–1471.

Tang, Z., Wu, J., Liu, Q., Zheng, M., Tang, Q., Lan, Z., & Lin, J. (2012). Preparation of poly(acrylic acid)/gelatin/polyaniline gel-electrolyte and its application in quasi-solid-state dye-sensitized solar cells. *Journal of Power Sources*, *203*, 282–287.

Ulaganathan, M., Nithya, R., Rajendran, S., & Raghu, S. (2012). Li-ion conduction on nanofiller incorporated PVdF-co-HFP based composite polymer blend electrolytes for flexible battery applications. *Solid State Ionics*, *218*, 7–12.

Wang, C., Wang, L., Shi, Y., Zhang, H., & Ma, T. (2013). Printable electrolytes for highly efficient quasi-solid-state dye-sensitized solar cells. *Electrochimica Acta*, *91*, 302–306.

Wang, M., Anghel, A. M., Marsan, B., Cevey Ha, N.-L., Pootrakulchote, N., Zakeeruddin, S. M., & Grätzel, M. (2009). CoS supersedes Pt as efficient electrocatalyst for triiodide reduction in dye-sensitized solar cells. *Journal of the American Chemical Society*, *131*(44), 15976–7.

Wang, M., Tang, Q., Xu, P., He, B., Lin, L., & Chen, H. (2014). Counter electrodes from polyaniline−graphene complex/graphene oxide multilayers for dye−sensitized solar cells. *Electrochimica Acta*, *137*, 175–182.

Wang, M., Xiao, X., Zhou, X., Li, X., & Lin, Y. (2007). Investigation of PEO-imidazole ionic liquid oligomer electrolytes for dye-sensitized solar cells. *Solar Energy Materials and Solar Cells*, *91*(9), 785–790.

Wang, Q., Moser, J., & Gra, M. (2005). Electrochemical Impedance Spectroscopic Analysis of Dye-Sensitized Solar Cells. *J. Phys. Chem. B*, *109*, 14945–14953.

Wang, Y. (2009). Recent research progress on polymer electrolytes for dye-sensitized solar cells. *Solar Energy Materials and Solar Cells*, *93*(8), 1167–1175.

Wei, Z. (2011). *Fabrication of dye sensitized solar cells with enhanced energy conversion efficiency*.

Wenger, S. (2010). *Strategies to Optimizing Dye-Sensitized Solar Cells : Organic Sensitizers , Tandem Device Structures , and Numerical Device Modeling*.

Wieczorek, W., & Stevens, J. R. (1997). Impedance Spectroscopy and Phase Structure of Polyether - Poly (methyl methacrylate) - $LiCF_3SO_3$ Blend-Based Electrolytes. *J. Phys. Chem. B*, *101*(9), 1529–1534.

William, A. V. L., Cesar, A. Q. S., & Johann, S. H. A. (1991). The Chemistry and Physics of Dye-Sensitized Solar Cells. In *Solar Cells – Dye-Sensitized Devices* (pp. 399–418).

Woo, H. J., Majid, S. R., & Arof, a. K. (2012). Dielectric properties and morphology of polymer electrolyte based on poly(ε-caprolactone) and ammonium thiocyanate. *Materials Chemistry and Physics*, *134*(2-3), 755–761.

Wu, C., Gong, Y., Han, S., Jin, T., Chi, B., Pu, J., & Jian, L. (2012). Electrochemical characterization of a novel iodine-free electrolyte for dye-sensitized solar cell. *Electrochimica Acta*, *71*, 33–38.

Wu, J., Lan, Z., Lin, J., Huang, M., Hao, S., & Fang, L. (2007). Influence of solvent on the poly (acrylic acid)-oligo-(ethylene glycol) polymer gel electrolyte and the performance of quasi-solid-state dye-sensitized solar cells. *Electrochimica Acta*, *52*(24), 7128–7135.

Wu, J., Lan, Z., Wang, D., Hao, S., Lin, J., Huang, Y., Sato, T. (2006). Gel polymer electrolyte based on poly(acrylonitrile-co-styrene) and a novel organic iodide salt for quasi-solid state dye-sensitized solar cell. *Electrochimica Acta*, *51*(20), 4243–4249.

Xu, P., Tang, Q., He, B., Li, Q., & Chen, H. (2014). Transmission booster from SiO2 incorporated TiO2 crystallites: Enhanced conversion efficiency in dye-sensitized solar cells. *Electrochimica Acta*, *134*, 281–286.

Yang, C.-C., Wey, J.-Y., Liou, T.-H., Li, Y. J., & Shih, J.-Y. (2012). A quasi solid state dye-sensitized solar cell based on poly(vinylidenefluoride-co-hexafluoropropylene)/SBA-15 nanocomposite membrane. *Materials Chemistry and Physics*, *132*(2-3), 431–437.

Yang, C.-C., Yang, J. M., & Wu, C.-Y. (2009). Poly(vinyl alcohol)/poly(vinyl chloride) composite polymer membranes for secondary zinc electrodes. *Journal of Power Sources*, *191*(2), 669–677.

Ye, M., Wen, X., Wang, M., Iocozzia, J., Zhang, N., Lin, C., & Lin, Z. (2014). Recent advances in dye-sensitized solar cells: from photoanodes, sensitizers and electrolytes to counter electrodes. *Materials Today*, *18*(3), 155–162.

Zaccaron, C. M., Oliveira, R. V. B., Guiotoku, M., Pires, A. T. N., & Soldi, V. (2005). Blends of hydroxypropyl methylcellulose and poly(1-vinylpyrrolidone-co-vinyl acetate): Miscibility and thermal stability. *Polymer Degradation and Stability*, *90*(1), 21–27.

Zhang, J., Yang, Y., Wu, S., Xu, S., Zhou, C., Hu, H., … Zhao, X. (2008). Improved photovoltage and performance by aminosilane-modified PEO/P(VDF-HFP) composite polymer electrolyte dye-sensitized solar cells. *Electrochimica Acta*, *53*(16), 5415–5422.